SOME EFFECTS OF NON-LINEAR STRESS/STRAIN RELATIONS IN ROTATIONALLY SYMMETRIC THIN SHELLS AND OTHER ENGINEERING COMPONENTS

by

A. C. Mackenzie

T H E S I S

submitted

to

The UNIVERSITY of GLASGOW

for the degree of

Doctor of Philosophy

September, 1965.

ProQuest LLC.
789 East Eisenhower Parkway
P.O. Box 1346
Ann Arbor, MI 48106 – 1346

Some Effects of Non-linear Stress/Strain Relations in Rotationally Symmetric Thin Shells and other Engineering Components

by

A. C. Mackenzie

S U M M A R Y

This thesis is mainly concerned with rotationally symmetric thin shells made of materials obeying non-linear stress/strain laws, in particular an n-power law relating effective stress and effective strain. To formulate boundary value problems in such shells, it is convenient to have relations between edge forces and moments and mid-surface deformations. With the usual assumptions of thin shell theory, these relations can be obtained as integral expressions in the thickness co-ordinate, but the integrations cannot be performed analytically for all values of the index n. Simple approximate relations are thus suggested for thin shells which are rotationally symmetric both in geometry and loading; the approximate relations are compared with the exact relations computed numerically for the particular

condition in which one curvature change of the mid-surface is zero. This condition applies in the analysis of circular cylindrical shells.

The approximate relations are used to formulate boundary value problems in cylindrical shells, and a method of solution using an analogue computer is described. Solutions are given for a long, fixed end cylinder under uniform radial loading and under internal pressure. A feature of these solutions, in the form presented, is the small variation in the maximum values of important variables with the index n. This suggests that the linear elastic (n = 1) solution may be used to make reasonable estimates of these maximum values for a range of values of n.

As a preliminary to the work on shells, an examination was made of solutions obtained with an n-power law for deformations in a number of other engineering components. A simple method, based on the linear elastic solution, was devised for estimating deformations and is described in the present work. The method makes direct use of the stress/strain curve without need for determining material constants. Although it was derived for an n-power law, physical explanations for the method suggest that it might give

reasonable estimates of deformations for non-linear laws other than the n-power law. Some available experimental results are given in support of this suggestion.

ACKNOWLEDGEMENTS

The writer is grateful for the facilities made available by the University of Glasgow for the performance of this work, and is particularly grateful to his supervisor, Professor G.D.S. MacLellan for help and encouragement at times when it was most needed.

The writer also wishes to express his thanks to Dr. C. Kuo and Miss J. Robb for help in communicating with the Deuce, and latterly the K.D.F.9. computer: to Dr. C.N. Kerr for an introduction to analogue computation: and to Dr. J. Orr and Mr. V.R. Paling for a number of helpful suggestions.

C O N T E N T S

LIST OF SYMBOLS

A ... ... internal radius of cylinder and sphere.

A_1, A_2 ... ... constants.

B ... ... material constant.

C, C_1, C_2 ... ... constants.

D ... ... constant.

F_1 ... ... function of ϵ_{m1}, ϵ_{m2}, K_1, K_2, and γ.

F_2 ... ... function of e_1, e_2, k_1, k_2 and ρ.

F_3 ... ... function of e_1, e_2, k_1, k_2 (and e_x, e_θ, k_x, k_θ).

F_4 ... ... function of w, $\frac{du}{dx}$ and $\frac{d^2w}{dx^2}$.

F_T ... ... part of surface on which forces are prescribed.

G_1 ... ... function of w and $\frac{d^2w}{dx^2}$.

G_2 ... ... function of $\frac{du}{dx}$, w and $\frac{d^2w}{dx^2}$.

G_3, G_4, G_5 ... ... functions of $\frac{w}{0.7}$ and $\frac{\frac{d^2w}{d\gamma^2}}{0.05}$.

G_6 ... ... function of $\frac{w}{0.7}$, $\frac{du}{d\tau}$ and $\frac{\frac{d^2w}{d\tau^2}}{0.05}$

H ... ... half thickness of cylinder, sphere and flat plate.

J ... ... function of n.

K ... ... curvature of neutral axis of beam (K_1 for n = 1).

K_1, K_2, K_x, K_θ .. ... mid-surface curvature changes of shell element.

L ... ... length of beam.

M ... ... bending moment in beam.

M_1, M_2, M_x, M_θ . ... edge bending moments on shell element.

P ... ... internal pressure.

P_x ... ... radial loading in cylinder.

Q_x ... ... transverse edge shear force on element of cylinder.

R_i ... ... internal radius of thick cylinder.

R_o ... ... external radius of thick cylinder.

T ... ... non-dimensional axial load per unit circumference of cylinder.

T_1, T_2, T_x, T_θ . ... in-plane edge forces on shell element.

T_i ... ... prescribed forces.

U.... ... ... axial displacement in cylinder; potential of internal forces.

V ... ... volume.

W ... ... applied load; radial displacement in cylinder.

X ... ... axial co-ordinate in cylinder.

a ... ... distance to point load on beam.

b ... ... breadth of beam; function of e_1, e_2, k_1, k_2.

c ... ... function of e_1 and e_2.

d ... ... depth of beam.

e_1, e_2, e_x, e_θ ... ... non-d. mid-surface strains in shell element.

f_1, f_2 ... ... functions of n.

k_1, k_2, k_x, k_θ ... non-d. mid-surface curvature changes in shell element.

l ... ... non-d. length of cylinder.

m_1, m_2, m_x, m_θ ... non-d. edge moments in shell element.

n ... ... index in stress/strain law.

p_x ... ... non-d. radial loading in cylinder.

p ... ... uniform non-d. radial loading in cylinder.

q_1, q_2 ... ... parameters.

q_x ... ... non-d. edge shear force in cylinder.

r ... ... radius to point in thick cylinder.

t_1, t_2, t_x, t_θ ... non-d. in-plane forces in shell element.

u ... ... non-d. axial displacement in cylinder.

u_i ... ... displacements associated with prescribed forces.

v ... ... deflection co-ordinate for beams

w ... ... uniformly distributed load on beam and plate.

x ... ... non-d. axial co-ordinate in cylinder and beam.

y ... ... distance from neutral axis in beam.

z ... ... thickness co-ordinate.

α ... ... { radius ratio in thick cylinder; constant; proportionality factor.

α_1, α_2 ... ... proportionality factors.

β ... ... { proportionality factor; fractional error.

$\gamma_1(n)$ to $\gamma_8(n)$ ... functions of n.

δ ... ... { displacement at point in structure; small increase in n.

ϵ ... ... direct strain.

ϵ_o ... ... reference strain.

$\bar{\epsilon}$ ... ... effective strain.

ϵ_{m1}, ϵ_{m2}, ϵ_{mx}, $\epsilon_{m\theta}$	mid-surface strains in shell element.
ζ	non-d. thickness co-ordinate.
θ	angular co-ordinate.
λ_0	factor proportional to end bending moment in cylinder.
λ_1, λ_3	functions of loading, dimensions of structure and σ_0.
λ_2, λ_4	functions of n.
Π	potential function.
σ	direct stress.
σ_0	reference stress.
$\bar{\sigma}$	effective stress.
τ	time.
ψ	non-d. function of e_1, e_2, k_1, and k_2 (exact).
$\psi_{APP.}$, $\psi_{APP2.}$, ψ_{APP3}	non-d. functions of e_1, e_2, k_1 and k_2 (approximate).
Ω	factor relating curvature and bending moment for beam.

CHAPTER 1

INTRODUCTION

Much is known about the behaviour of structures made of materials which have linear relations between stress and strain, and in recent years this knowledge has been extended to behaviour under conditions of non-work-hardening plastic flow. Less attention has been given to structures of materials which have intermediate, non-linear stress/strain relations.

Many light alloys and polymeric materials, which are being used increasingly as structural components, show little or no linear elasticity; design of these components should take account of the non-linear behaviour. Also, more and more structures are being designed to operate at temperatures and stress levels at which significant creep occurs, and in most materials the creep strain rate bears a non-linear relationship to stress.

In the past, the difficulties in studying structures made of such materials have arisen mainly from the complex stress/strain relations necessary to describe the material behaviour accurately, and from inability to cope with such relations in analysis. As modern computing techniques have developed, it has become possible, with numerical

methods of analysis, to deal with increasingly complex material characteristics. There is a tendency, however, for too much emphasis to be placed on the development of involved computer programmes, and too little attention given to obtaining solutions leading to a better understanding of the behaviour of structures. There is some advantage in selecting a family of simple non-linear relations, which only approximate to material behaviour but by way of relatively simple analysis may be used to explore some features of the behaviour of structures. They may also suggest approximate methods of analysis applicable with other non-linear laws.

A family of stress/strain relations which may be used in problems involving a single stress variable is

$$\epsilon = B\sigma^{n} \qquad (1.1)$$

where ϵ and σ are uniaxial strain and stress respectively, and B and n are constants. With $n = 1$, equation 1.1 is a statement of linear elasticity and for $n \to \infty$, written in appropriate non-dimensional form, it represents a rigid-non-work-hardening material.[1] It has been used with other values of n to approximate to the behaviour of some metals in their plastic range. Written in the form expressing strain rate as a function of stress, i.e.

$$\dot{\epsilon} = B\sigma^{n} \qquad (1.2)$$

it is commonly used to describe the steady state creep behaviour of metals.

For problems involving multiaxial states of stress, further assumptions have to be made about material behaviour. One assumption which has found wide acceptance for simple loading paths is that the root mean square of the principal shear strains is a function of the root mean square of the principal shear stresses (usually termed the effective strain and stress and denoted $\bar{\epsilon}$ and $\bar{\sigma}$ respectively). Experiments made by many investigators have shown this to be a reasonable assumption for the plastic flow of metals, whether under short-term loading or under longer term creep conditions, when it is found that the effective strain rate is a function of the effective stress. Since it is well established that plastic flow in metals is a shear phenomenon, it is not surprising that approximate relations should exist between simple statistical measures of shear stress and shear strain "intensity". It has been found recently[2] that these concepts are useful also in describing the behaviour of some polymeric materials.

The functional relationship between $\bar{\epsilon}$ and $\bar{\sigma}$ of which equation 1.1 is a special case is

$$\bar{\epsilon} = B\bar{\sigma}^n \tag{1.3}$$

while equation 1.2 is a special case of

$$\dot{\bar{\epsilon}} = B\bar{\sigma}^n \tag{1.4}$$

At this stage it is relevant to mention Hoff's analogy[1] between solutions to structural problems obtained with equation 1.3 and those obtained with equation 1.4. For a given loading, the stresses throughout a structure are the same in the two cases, deformations obtained with equation 1.3 becoming deformation rates with equation 1.4. Solutions to non-time-dependent problems with equation 1.3 can thus be used for steady state creep problems obeying equation 1.4 and vice versa.

It is as an equation of steady state creep that the n-power law has been most widely applied in structural analysis, and solutions to many problems with a single stress variable are easily obtained. A number of problems involving multiaxial states of stress have also been solved with equation 1.4. Among these are the thick-wall cylinder and sphere under internal pressure, the rotating disc, and the circular flat plate under rotationally symmetric loading. The most important of the results have been gathered by Finnie and Heller[3], and also by Odqvist and Hult.[4]

A bound method for analysis of structures in steady state creep obeying equation 1.4 has been suggested by Calladine and Drucker.[5],[6] It is based on surfaces of constant energy dissipation rate, and the bounds are

obtained from the linear elastic ($n = 1$) and the rigid-non-work-hardening plastic ($n \to \infty$) solutions. The method is useful when the solution for $n \to \infty$ is readily obtainable and the bounds are reasonably close. In many structures, the solution for $n \to \infty$ is as difficult to obtain as the solution for an intermediate value of n. Calladine has applied bound methods to a number of structures[7],[8] and has also recently suggested a method for estimating the greatest stress in a structure subject to creep.[9]

As part of the present work, an examination was made of some of the existing solutions for deformations in simple structures obtained with the n-power law. It was found that when the solution for n = 1 was factored out, the rest of the solution could be made relatively insensitive to the value of n if a non-dimensional group, dependent on the dimensions of the structure and on the loading, was given a particular value. This suggested a method for predicting deformations which used the linear elastic solution and did not require evaluation of the material constants B and n in equations 1.3 or 1.4, the stress/strain (or strain rate) curve being used directly. Furthermore, physical explanations for the method suggested that it might give reasonable estimates of deformations for non-linear laws other than the n-power

law. Some available experimental results supported this suggestion.

The method is reported here and results are given for a number of structures. No apology is made for the relatively simple examples which have been considered. They are frequently met in the design of engineering components, and a ready, if only approximate, method of predicting deformations is all that is required, particularly in the early stages of developing a design. The use of the n-power solutions as normally presented requires determination of the material constants. As few materials obey an n-power law exactly, it is usually difficult to decide on values for the constants which best fit the test data.

In recent years a growing need has developed for an understanding of the behaviour of rotationally symmetric thin shells made of materials with non-linear stress/strain relations. Such shells are widely used as pressure vessels and are now frequently made of light alloys and polymeric materials. Pressure vessels of more conventional materials are also being required to operate at temperatures at which significant creep occurs.

Several attempts have been made with the n-power law to obtain solutions to such thin shell problems. Only limited progress has been made with even the simplest

of rotationally symmetric shells. One difficulty lies in obtaining relations between forces and moments on an element of the shell and the associated mid-surface deformations. This requires integration of the non-linear stress/strain relations through the shell thickness and the integrations cannot be performed analytically. There is also coupling between in-plane and bending actions which does not occur in the corresponding linear relations.

In an early attempt to obtain these relations, Onat and Yuksel[10] avoided the difficulty of integrating stresses through the shell thickness by considering a sandwich construction. Two identical thin layers of material were considered to be separated by a central core, the only other function of which was to withstand shear stresses associated with changing bending moments in the shell. Further simplifying assumptions were introduced by the use of a steady state creep law based on a relationship between maximum shear stress and maximum shear strain rate (analogous to the Tresca condition in the theory of plasticity). The analysis could be applied if the outer layers of the shell were assumed to obey relations between effective stress and effective strain rate as in equation 1.4, but it is difficult to see that it gives anything but a very crude approximation to the behaviour of shells having uniform properties through the thickness.

Bieniek and Freudenthal[11], in performing an analysis of secondary creep in thin cylinders, made drastic simplifying assumptions which removed the coupling between in-plane and bending actions. They applied extremum principles to obtain solutions to the problem of the thin cylinder with fixed ends under internal pressure, but the moment distributions which they obtained show very unlikely trends.

The first attempt to use a reasonable set of approximate relations was made by Calladine[12]. He postulated semi-empirical relations based on an ellipsoidal interaction surface between the forces and moments on a shell element, and used the relations to establish a governing differential equation for secondary creep in a cylindrical shell. By casting the equation into finite difference form, he obtained a numerical solution to a boundary value problem in a shell with edge shear force and bending moment for a value of the index $n = 3$.

One object of the present work was to propose a rational basis for the suggestion of approximate relations between forces and moments and mid-surface deformations, and for comparison with "exact" relations computed numerically. It was noted that the exact relations can be derived from a function which, in steady state

creep, is the energy dissipation rate. An approximate form of the function, based on an n-power law, was obtained for an element of a shell rotationally symmetric both in geometry and loading, and led to approximate relations simple enough to be useful in further analysis. The relations were compared with the exact relations for a cylindrical shell and showed favourable agreement.

After these approximate relations had been obtained, the writer became aware of relations suggested by Rozenblium[13]. The latter are based on an approximate expression for the rate of energy dissipation in steady state creep of a shell element, and can be shown to be the same as those obtained here. Rozenblium based his approximate expression for the rate of energy dissipation on a yield surface suggested originally by Ilyushin,[14] and developed it in load space. In the present work, the energy function and the approximate relations are developed in deformation space, the advantage of this being the ease with which comparison can be made with the exact relations.

Rozenblium has included in his relations the in-plane edge shear forces and the twisting moments which arise in a shell not rotationally symmetric in geometry and/or loading. In the writer's opinion, it is premature to attempt to deal with this general case before the relations are tried and proved for the simpler, but

important, practical examples of rotationally symmetric shells. Illustrating the use of the relations, Rozenblium used variational principles to obtain approximate solutions to the problem of an infinite cylinder with a circumferential line loading.

In the present work, the approximate relations have been used to formulate the problem of a cylindrical shell under rotationally symmetric loading. It was found that the resulting fourth order system of two simultaneous, non-linear differential equations could conveniently be solved on an analogue computer. Solutions were obtained for a number of boundary value problems in semi-infinite cylinders and, in particular, for the long cylinder with fixed ends under internal pressure. The results indicate that it may be possible in many problems to make reasonable estimates of forces and moments at boundary restraints and of deformations in the shell, from the linear elastic solution.

To summarise, the objects of the present study are

(i) to examine solutions obtained with an n-power law for the deformations in some simple structures, and to suggest approximate methods for predicting deformations which may be applicable with other non-linear laws;

(ii) to suggest approximate relations between forces and moments and mid-surface deformations, based

on an n-power law and suitable for analysis of thin shells which are rotationally symmetric both in geometry and loading;

(iii) to demonstrate the use of these approximate relations in obtaining solutions to boundary value problems in cylindrical shells.

CHAPTER 2

SOME DEFINITIONS AND ASSUMPTIONS

2.1 The uniaxial stress/strain law

A typical stress/strain curve of the family defined by equation 1.1 i.e.

$$\epsilon = B\sigma^n$$

is shown in Fig. 2.1 for $n > 1$ (With $n < 1$ equation 1.1 defines a material behaviour which is not commonly met, and in what follows values of $n < 1$ are not considered.)

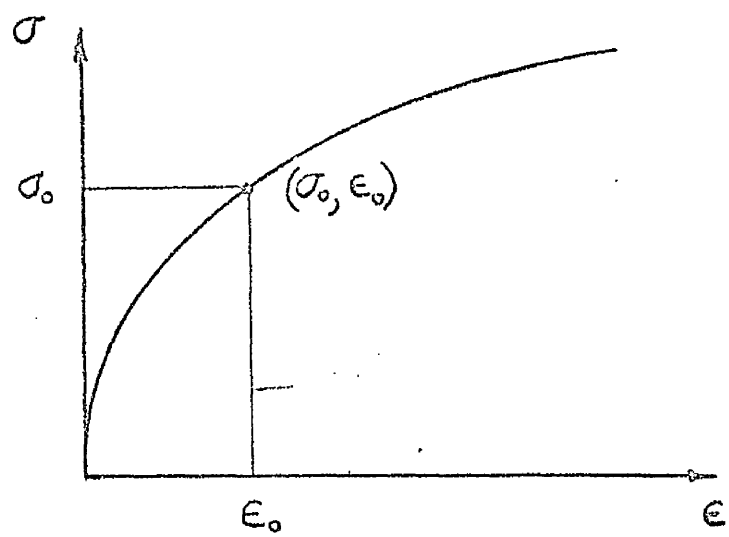

FIG. 2.1

As suggested by Calladine and Drucker[5] the constant B may be expressed in terms of the co-ordinates (σ_o, ϵ_o) of an arbitrary point on the stress/strain curve, i.e.

$$B = \frac{\epsilon_o}{\sigma_o^n}$$

and equation 1.1 may be written in the non-dimensional form

$$\frac{\epsilon}{\epsilon_o} = \left(\frac{\sigma}{\sigma_o}\right)^n \qquad (2.1)$$

Equation 2.1 is plotted for different values of n in Fig. 2.2.* Written in this form, it is seen to represent a rigid/non-work-hardening material for $n \to \infty$.

The material behaviour is assumed to be the same in tension and compression, and this can lead to difficulty in using equation 2.1 when n is even. The difficulty is avoided, however, if the equation is used in the forms

$$\frac{\epsilon}{\epsilon_o} = (\text{sign}\,\sigma)\left(\frac{|\sigma|}{\sigma_o}\right)^n \qquad (2.2a)$$

or

$$\frac{\sigma}{\sigma_o} = (\text{sign}\,\epsilon)\left(\frac{|\epsilon|}{\epsilon_o}\right)^{1/n} \qquad (2.2b)$$

2.2 Stress/strain relations for complex states of stress

In defining stress/strain relations for complex states of stress, the following assumptions are made:

(a) The material is homogeneous and isotropic.

(b) No change in volume occurs during deformation.

(c) The material is initially unstressed and the stresses increase monotonically from zero in a

* Where not included in the text all figures are to be found at the ends of the relevant chapters.

constant ratio. (Loads applied to a structure must therefore increase monotonically from zero in a constant ratio.)

(d) Deformation is governed by the flow rule

$$\frac{\epsilon_1-\epsilon_2}{\sigma_1-\sigma_2} = \frac{\epsilon_2-\epsilon_3}{\sigma_2-\sigma_3} = \frac{\epsilon_3-\epsilon_1}{\sigma_3-\sigma_1} = \frac{3}{2}\,\frac{\bar{\epsilon}}{\bar{\sigma}} \qquad (2.3)$$

where

$$\left.\begin{aligned} \bar{\epsilon} &= \frac{\sqrt{2}}{3}\left[(\epsilon_1-\epsilon_2)^2+(\epsilon_2-\epsilon_3)^2+(\epsilon_3-\epsilon_1)^2\right]^{1/2} \\ \bar{\sigma} &= \frac{1}{\sqrt{2}}\left[(\sigma_1-\sigma_2)^2+(\sigma_2-\sigma_3)^2+(\sigma_3-\sigma_1)^2\right]^{1/2} \end{aligned}\right\} \qquad (2.4)$$

In these equations σ_1, σ_2, σ_3 are principal stresses and ϵ_1, ϵ_2, ϵ_3 are principal strains. (Assumption (c) allows the flow rule to be written in terms of total rather than incremental strains.)

(e) The equivalent stress and strain $\bar{\sigma}$ and $\bar{\epsilon}$ are related by the equation

$$\bar{\epsilon} = B\,\bar{\sigma}^{\,n} \qquad (2.5)$$

or, in non-dimensional form,

$$\frac{\bar{\epsilon}}{\epsilon_o} = \left(\frac{\bar{\sigma}}{\sigma_o}\right)^n \qquad (2.6)$$

With the assumptions (a) to (e), the following stress/strain relations are obtained in Appendix 2.1:

$$\left.\begin{aligned}
\epsilon_1 &= B\bar{\sigma}^{n-1}\left[\sigma_1 - \tfrac{1}{2}(\sigma_2+\sigma_3)\right] \\
\epsilon_2 &= B\bar{\sigma}^{n-1}\left[\sigma_2 - \tfrac{1}{2}(\sigma_3+\sigma_1)\right] \\
\epsilon_3 &= B\bar{\sigma}^{n-1}\left[\sigma_3 - \tfrac{1}{2}(\sigma_1+\sigma_2)\right]
\end{aligned}\right\} \qquad (2.7)$$

In developing relations between forces and moments and mid-surface deformations, suitable for the analysis of thin shells, a state of plane stress ($\sigma_3 = 0$) is assumed. With this assumption, expressions for σ_1 and σ_2 in terms of ϵ_1 and ϵ_2 are obtained as follows:

From equation 2.3, with $\sigma_3 = 0$

$$\left.\begin{aligned}
\sigma_1 &= \tfrac{2}{3}\,\frac{\bar{\sigma}}{\bar{\epsilon}}\,(\epsilon_1 - \epsilon_3) \\
\sigma_2 &= \tfrac{2}{3}\,\frac{\bar{\sigma}}{\bar{\epsilon}}\,(\epsilon_2 - \epsilon_3)
\end{aligned}\right\} \qquad (2.8)$$

With

$\epsilon_1 + \epsilon_2 + \epsilon_3 = 0$ (for constant volume),

$$\bar{\sigma} = \left(\frac{\bar{\epsilon}}{B}\right)^{1/n} ,$$

$$\bar{\epsilon} = \frac{2}{\sqrt{3}}\left(\epsilon_1^2 + \epsilon_1\epsilon_2 + \epsilon_2^2\right)^{1/2} ,$$

equations 2.8 become finally

$$\left.\begin{aligned}
\sigma_1 &= \frac{1}{B^{1/n}}\left(\frac{4}{3}\right)^{\frac{n+1}{2n}}\left(\epsilon_1^2+\epsilon_1\epsilon_2+\epsilon_2^2\right)^{\frac{1-n}{2n}}\left(\epsilon_1+\tfrac{1}{2}\epsilon_2\right) \\
\sigma_2 &= \frac{1}{B^{1/n}}\left(\frac{4}{3}\right)^{\frac{n+1}{2n}}\left(\epsilon_1^2+\epsilon_1\epsilon_2+\epsilon_2^2\right)^{\frac{1-n}{2n}}\left(\epsilon_2+\tfrac{1}{2}\epsilon_1\right)
\end{aligned}\right\} \qquad (2.9)$$

No difficulty arises in using these relations, whether n is odd or even. The term $(\epsilon_1^2 + \epsilon_1\epsilon_2 + \epsilon_2^2)$ can be written $\left[\left(\epsilon_1 + \frac{1}{2}\epsilon_2\right)^2 + \frac{3}{4}\epsilon_2^2 \right]$ and is always positive.

2.3 Limitations on strains and displacements

Non-linearities arise in the analysis of structures from changes in geometry as well as from the stress/strain relations. The equilibrium equations are normally obtained for an element in the undeformed structure. If substantial deformation and/or rotation of the element occurs, the equilibrium equations must be established for the deformed state and non-linear terms are thereby introduced. The strain/displacement relations also become non-linear when rotations are taken into account.

As discussed, for example, by Novozhilov,[15] the non-linearities associated with physical and geometric sources can occur independently. In the present study it is assumed that non-linearities arising from geometry changes can be disregarded. This implies a limitation on displacements and strains in the structure. It is not possible to define these limits. They will depend on the nature of the problem and the required accuracy of solution, and are perhaps best established from individual experiments.

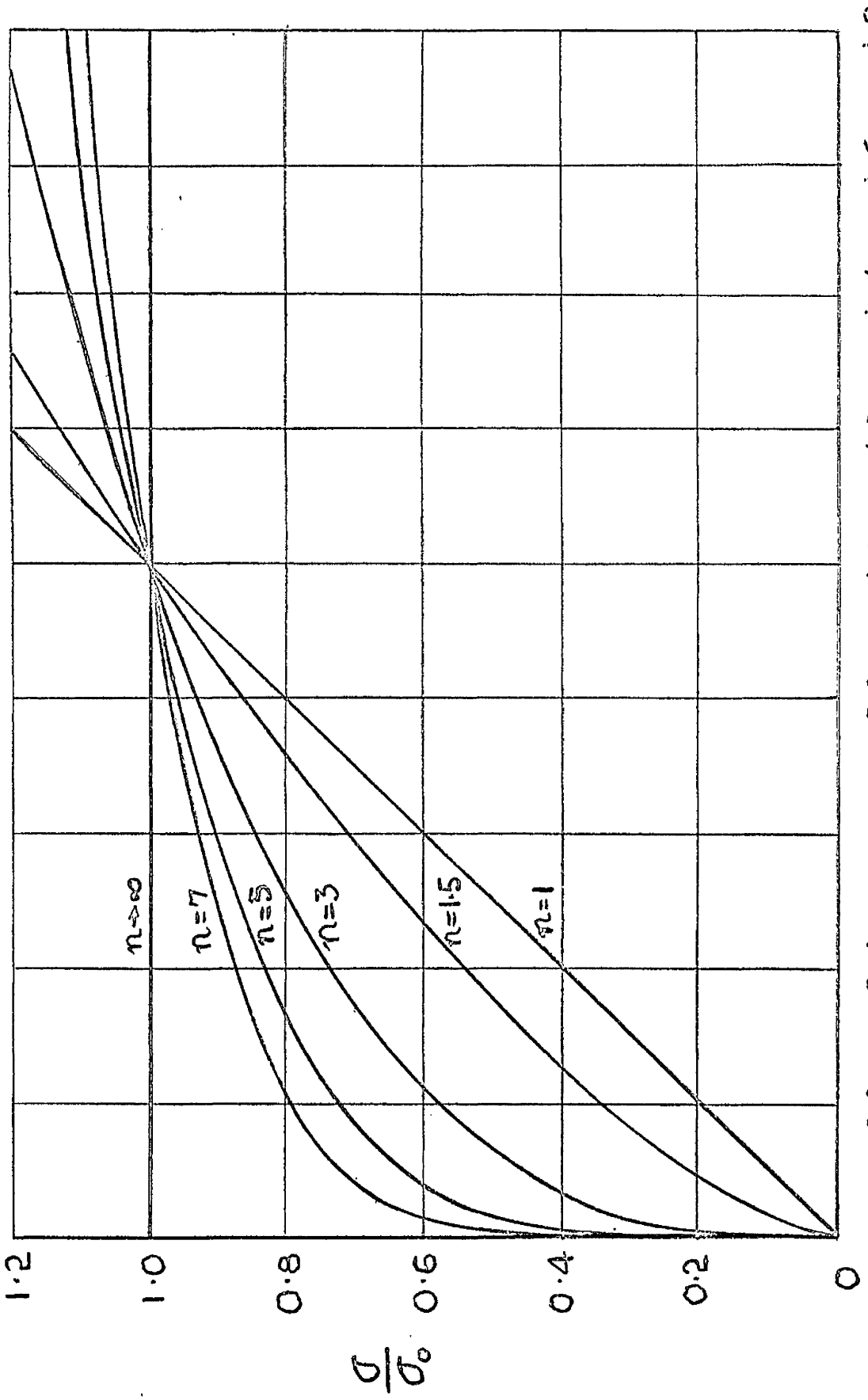

FIG. 2.2 THE STRESS / STRAIN FAMILY $\left(\frac{\epsilon}{\epsilon_0}\right) = \left(\frac{\sigma}{\sigma_0}\right)^n$

CHAPTER 3

AN APPROXIMATE METHOD FOR PREDICTING DEFORMATIONS IN SOME SIMPLE STRUCTURES WITH NON-LINEAR STRESS/STRAIN RELATIONS

3.1 Illustration of method with reference to beams in uniform bending

A method for predicting deformations in simple structures obeying non-linear stress/strain relations is illustrated for a beam of rectangular cross-section in uniform bending.

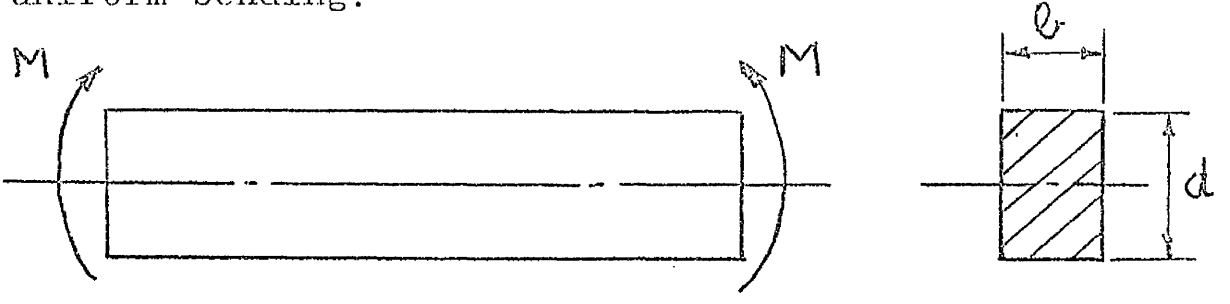

For a material obeying equation 2.1, i.e.

$$\frac{\epsilon}{\epsilon_o} = \left(\frac{\sigma}{\sigma_o}\right)^n$$

the relationship between the applied moment M and the curvature K to which the central axis of the beam bends is obtained in Appendix 3.1 (a) as

$$K = \left(\frac{2n+1}{n}\right)^n 2^{n+1} \left(\frac{\epsilon_o}{\sigma_o^n b^n d^{2n+1}}\right) M^n \qquad (3.1)$$

With $n = 1$, this reduces to the familiar expression for a linear elastic beam

$$K_1 = \frac{12\,M}{(\sigma_0/\epsilon_0)\,b\,d^3} \tag{3.2}$$

Factoring K_1 from the right hand side of equation 3.1 leads to

$$K = K_1\left(\frac{M}{\sigma_0 b d^2}\right)^{n-1} \frac{2}{3}^{n-1} \left(\frac{2n+1}{n}\right)^n \tag{3.3}$$

Thus for $n > 1$

$$K = K_1$$

if

$$\left(\frac{M}{\sigma_0 b d^2}\right)^{n-1} \frac{2}{3}^{n-1} \left(\frac{2n+1}{n}\right)^n = 1$$

or

$$\frac{M}{\sigma_0 b d^2} = \frac{3}{2}^{\frac{1}{n-1}} \left(\frac{n}{2n+1}\right)^{\frac{n}{n-1}}$$

$$= \gamma_1(n), \text{ SAY} \tag{3.4}$$

Table 3.1 shows that $\gamma_1(n)$ does not vary greatly for $1.1 \leq n \leq 7$.

[NOTE: It is shown in Appendix 3.2 that

$$\lim_{n \to 1} \gamma_1(n) = \frac{1}{6} e^{1/3} = 0.2326$$

Equation 3.3 is not violated with $\frac{M}{\sigma_0 b d^2} = 0.2326$ for $n \to 1$, since $\frac{M}{\sigma_0 b d^2}$ is raised to the power $n - 1$ Similar remarks apply to all the examples of structures considered in this Chapter.]

n	$\gamma_1(n)$
1.1	0.233
1.5	0.237
2.0	0.240
3 0	0.243
4.0	0.244
5.0	0.245
7.0	0.247

Table 3.1

It is thus possible to select a value for the non-dimensional group $\frac{M}{\sigma_0 b d^2}$ which will make K approximately equal to K_1 for a range of values of n. The error incurred can be assessed as follows:

From equation 3.3

$$\frac{K}{K_1} = \left(\frac{M}{\sigma_0 b d^2}\right)^{n-1} \frac{2^{n-1}}{3} \left(\frac{2n+1}{n}\right)^n \qquad (3.5)$$

Selecting from Table 3.1 the value

$$\frac{M}{\sigma_0 b d^2} = 0.245$$

gives

$$\frac{K}{K_1} = (0.245)^{n-1} \frac{2^{n-1}}{3} \left(\frac{2n+1}{n}\right)^n \qquad (3.6)$$

The ratio $\frac{K}{K_1}$ is given for different values of n in Table 3.2. It differs from unity by less than $\pm$ 5% for $1.1 \leq n \leq 7$

n	$\frac{K}{K_1}$
1.1	1.005
1.5	1.016
2.0	1.021
3.0	1.020
4.0	1.005
5.0	1.000
7.0	0.959

Table 3.2

The result suggests the following method for predicting curvatures in beams in uniform bending, obeying an n-power law:

(a) For a given value of M and dimensions of beam obtain σ_0 from

$$\frac{M}{\sigma_0 b d^2} = 0.245$$

or

$$\sigma_0 = \frac{M}{0.245 b d^2}$$

(b) Read this value of σ_o into the stress/strain curve to obtain ϵ_o.

(c) Use these values of σ_o and ϵ_o to calculate K_1 from the linear elastic solution, equation 3.2, i.e.

$$K_1 = \frac{12M}{(\sigma_o/\epsilon_o)bd^3}$$

The actual curvature K will not differ from K_1 by more than $\pm$ 5% for $1.1 \leq n \leq 7$.

Fig 3.1 gives a physical explanation for the method. The bending stress is plotted in convenient non-dimensional form over half the depth of the beam for different values of n, the moment M being the same in each case. The curves for $1.1 \leq n \leq 7$ intersect the curve for n = 1 at approximately the same distance from the neutral axis of the beam. If the stress at the intersection "point" is taken to be σ_o, the strain at this point, and hence the curvature of the beam, will be the same for members of the family of stress/strain curves in Fig. 2.2.

If the value of $\frac{\sigma_o bd^2}{M}$ at the intersection "point" is taken to be

$$\frac{\sigma_o bd^2}{M} = 4.1$$

then

$$\sigma_o = \frac{M}{0.244\, bd^2}$$

This compares with the value for σ_o obtained above.

For other non-linear laws which are reasonably close to the n-power family, the stress distributions will not be very different from those in Fig. 3.1, and intersection with the linear distribution will occur at approximately the same point. Thus it may be expected that the method will give reasonable estimates of curvature for other non-linear laws. Examination of some experimental results for beams in bending supports this claim.

Gill[16] conducted uniform bending tests on magnesium alloy beams of different cross-sections. The stress/strain curve for the material (a mean of curves obtained in tension and compression) is reproduced in Fig. 3.2. Moment/curvature results for a beam of rectangular cross-section are reproduced in Fig. 3.3, and the curvatures predicted from the stress/strain curve by the method described above are plotted for comparison. The maximum curvature represents a 6% strain at the extreme fibres, and there is good agreement between the experimental and predicted curvatures over the whole range.

The stress/strain curve of Fig. 3.2 is plotted logarithmically in Fig. 3.4 for strains up to 6%. It shows that the material does not obey an n-power law over this range, the slope of the curve increasing from

1 (in the elastic range) to approximately 3.2. This is an illustration of the difficulty, mentioned in Chapter 1, of using the n-power solutions in their usual form. It would be difficult to decide on values for the constants B and n from Fig. 3.4.

The method can be applied to other cross-sections and is applied to an I-beam in Appendix 3.1(b). The results are compared in Fig. 3.5 with experimental results for an I-beam tested by Gill. Again there is good agreement between the experimental and estimated curvatures.

3.2 Other Applications

(a) Beams in non-uniform bending

The example considered is a beam of rectangular cross-section, simply supported at its ends and centrally loaded.

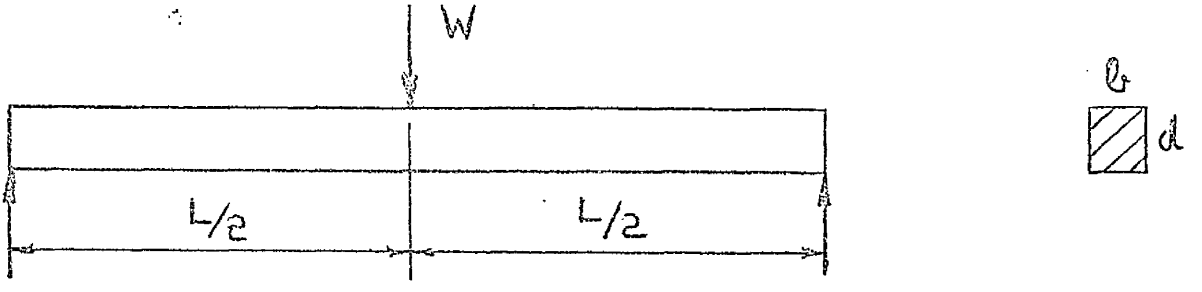

If the effects of shear stresses associated with shear forces in the beam are disregarded, and only small deflections considered, the central deflection δ is shown in Appendix 3.3 to be

$$\delta = \frac{W^n}{b^n} \frac{L^{n+2}}{d^{2n+1}} \frac{\epsilon_0}{\sigma_0^n} \left(\frac{2n+1}{n}\right)^n \frac{1}{2^{n+1}(n+2)} \qquad (3.7)$$

and

$$\delta_1 = \frac{WL^3}{b d^3} \frac{\epsilon_0}{\sigma_0} \cdot \frac{1}{4}$$

Equation 3.7 can then be written

$$\delta = \delta_1 \left(\frac{WL}{\sigma_0 b d^2}\right)^{n-1} \left(\frac{2n+1}{n}\right)^n \frac{2^{1-n}}{n+2}$$

and

$$\delta = \delta_1$$

if

$$\frac{WL}{\sigma_0 b d^2} = \left(\frac{n}{2n+1}\right)^{\frac{n}{n-1}} (n+2)^{\frac{1}{n-1}} \cdot 2$$
$$= \gamma_2(n) \quad , \text{ SAY}$$

Table 3.3 shows values of $\gamma_2(n)$.

n	$\gamma_2(n)$
1.1	1.30
1.5	1.29
2.0	1.28
3.0	1.26
4.0	1.23
5.0	1.22
6.0	1.20
7.0	1.19

Table 3.3

Again there is not a strong dependence on n, and a suitable value may be chosen for the non-dimensional

group $\frac{WL}{\sigma_0 b d^2}$. For example, with

$$\frac{WL}{\sigma_0 b d^2} = 1.20$$

or

$$\sigma_0 = 0.833 \frac{WL}{b d^2}$$

the values of $\frac{\delta}{\delta_1}$ given in Table 3.4 are obtained, and show that, for $1.1 \leq n \leq 7$

$$\delta = \delta_1 \pm \text{approx. } 10\%.$$

Other values can be chosen for $\frac{WL}{\sigma_0 b d^2}$ to give a better approximation for a smaller range of n.

n	$\frac{\delta}{\delta_1}$ for $\frac{WL}{\sigma_0 b d^2} = 1.20$
1.1	1.020
1.5	0.964
2.0	0.937
3.0	0.914
4.0	0.923
5.0	0.937
6.0	1.002
7.0	1.055

Table 3.4

Although the central deflection can be made the same for different values of n, the deflected shapes are not the same. This is illustrated in Fig. 3.6, in which

the deflected shapes are plotted for the same central deflection and different values of n. In most applications, however, it is the deflection under the load, and not the exact deflected shape, that is important.

Results for three further examples of beams of rectangular cross-section in non-uniform bending are given below. The results are derived in Appendix 3.4.

(i)

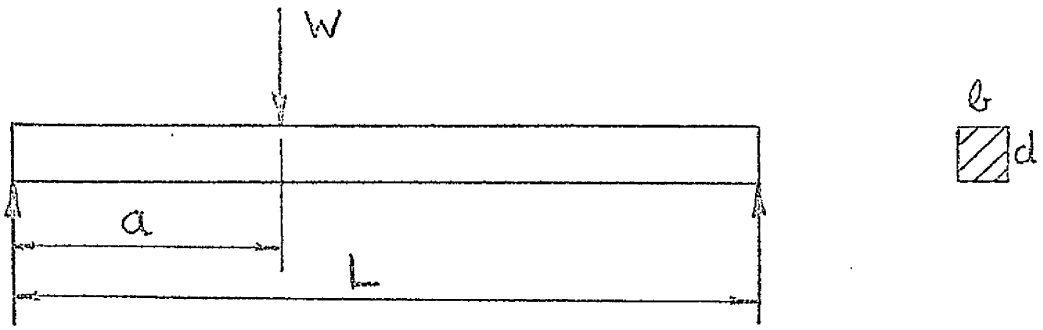

Simply supported beam of rectangular cross-section with non-central point load.

Deflection under load $\delta = \delta_1 \pm 10\%$ for $1.1 \leq n \leq 7$ if

$$\frac{Wa}{\sigma_0 b d^2}\left(1 - \frac{a}{L}\right) = 0.300$$

or

$$\sigma_0 = 3.33 \frac{Wa}{b d^2}\left(1 - \frac{a}{L}\right)$$

(ii)

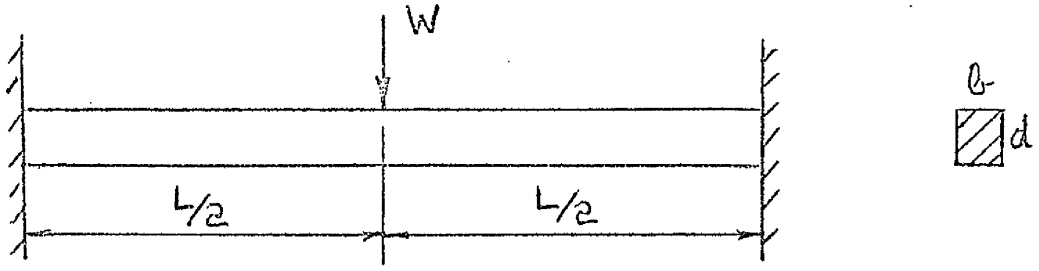

Beam of rectangular cross-section with built-in ends and central point load.

Deflection under load $\delta = \delta_1 \pm 10\%$ for $1.1 \leq n \leq 7$ if

$$\frac{WL}{\sigma_0 b d^2} = 2.4$$

or

$$\sigma_0 = 0.417 \frac{WL}{b d^2}$$

(iii)

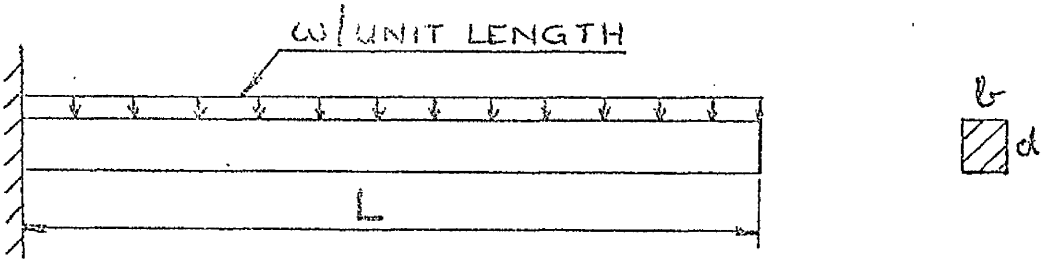

Cantilever of rectangular cross-section with uniformly distributed load.

End deflection $\delta = \delta_1 \pm 15\%$ for $1.1 \leq n \leq 7$ if

$$\frac{\omega L^2}{\sigma_0 b d^2} = 0.635$$

or

$$\sigma_0 = 1.575 \frac{\omega L^2}{b d^2}$$

(b) <u>The thin wall cylinder with closed ends under internal pressure</u>

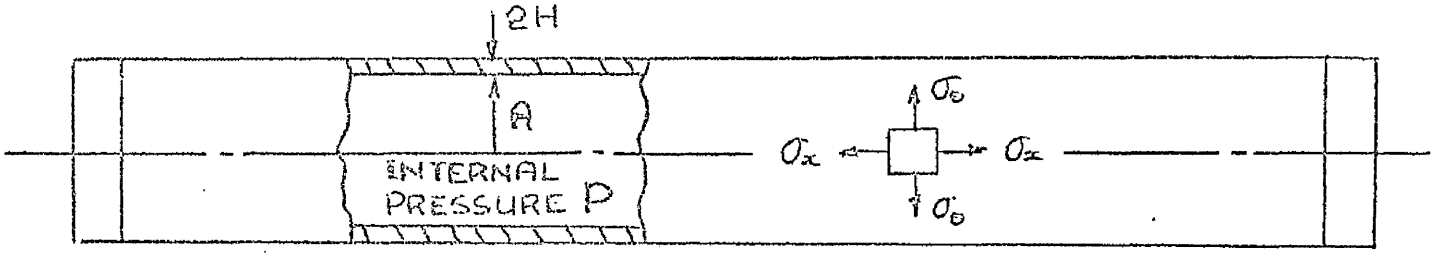

Away from the ends, the circumferential and longitudinal stresses, σ_θ and σ_x respectively, are approximately

$$\sigma_\theta = \frac{PA}{2H} \quad ; \quad \sigma_x = \frac{PA}{4H}$$

It can be shown with equations 2.7 that the circumferential strain ϵ_θ is

$$\epsilon_\theta = \frac{\epsilon_o}{\sigma_o^n} \left(\frac{PA}{2H}\right)^n \left(\frac{3}{4}\right)^{\frac{n+1}{2}} \tag{3.8}$$

For n = 1

$$\epsilon_{\theta 1} = \frac{3}{4}\left(\frac{PA}{2H}\right) \frac{1}{(\sigma_o/\epsilon_o)}$$

and

$$\epsilon_\theta = \epsilon_{\theta 1} \left(\frac{PA}{2H\sigma_o}\right)^{n-1} \left(\frac{3}{4}\right)^{\frac{n-1}{2}}$$

Thus, for all values of n,

$$\epsilon_\theta = \epsilon_{\theta 1}$$

if

$$\frac{PA}{2H\sigma_o} = \left(\frac{4}{3}\right)^{1/2} = 1.155$$

or

$$\sigma_o = 0.433 \frac{PA}{H} \tag{3.9}$$

The interpretation of this result is that the reference stress σ_o has been equated to the effective

stress $\bar{\sigma}$ in the cylinder wall. The effective strain $\bar{\epsilon}$ is thus ϵ_o and the same for all values of n in the family of equation 2.6. $\bar{\epsilon}$ is directly proportional to the circumferential strain ϵ_θ, and thus ϵ_θ is the same for all values of n.

(c) Thin wall sphere under internal pressure

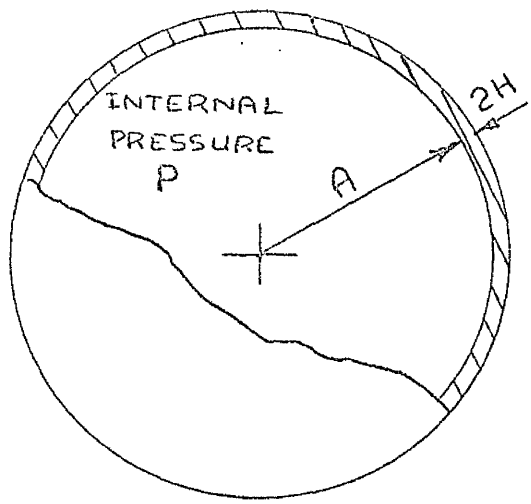

The stress σ in the wall is given approximately by

$$\sigma = \frac{PA}{4H}$$

Again, with equations 2.7, the circumferential strain ϵ_θ is

$$\epsilon_\theta = \frac{\epsilon_o}{\sigma_o^n}\left(\frac{PA}{2H}\right)^n \frac{1}{2^{n+1}} \qquad (3.10)$$

and

$$\epsilon_{\theta 1} = \frac{1}{4}\ \frac{PA}{2H}\ \frac{1}{(\sigma_o/\epsilon_o)}$$

ϵ_θ can thus be written

$$\epsilon_\theta = \epsilon_{\theta 1} \left(\frac{PA}{2H\sigma_o}\right)^{n-1} \frac{1}{2^{n-1}}$$

and $\epsilon_\theta = \epsilon_{\theta 1}$ if

$$\frac{PA}{2H\sigma_o} = \frac{1}{2}$$

or

$$\sigma_o = \frac{PA}{H}$$

This value for σ_o is again the effective stress $\bar{\sigma}$.

(d) <u>The thick-wall cylinder with closed ends under internal pressure</u>

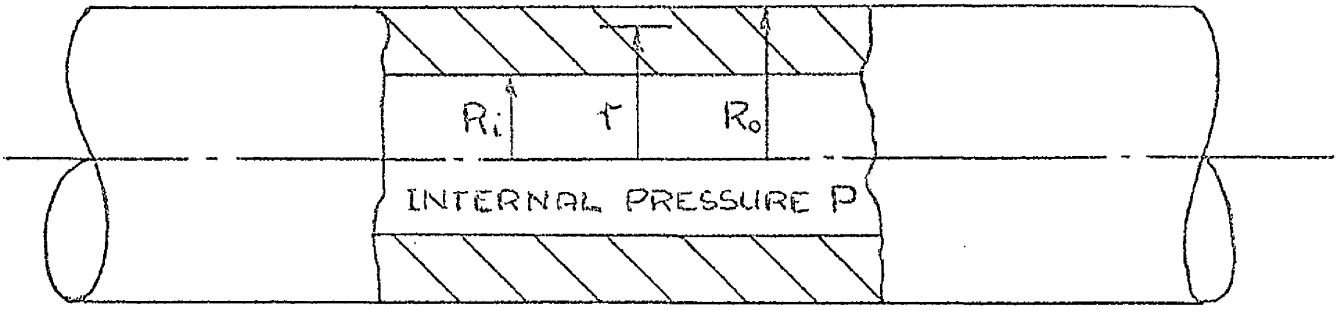

A solution, originally obtained by Bailey[17] for steady state creep, and based on equations 2.7, gives the circumferential strain ϵ_θ at any radius r in the cylinder wall as

$$\epsilon_\theta = \left(\frac{3}{4}\right)^{\frac{n+1}{2}} \frac{\epsilon_o}{\sigma_o^n} \left(\frac{R_o}{r}\right)^2 \left[\frac{2}{n} \frac{P}{\alpha^{2/n} - 1}\right]^n \qquad (3.11)$$

where

$$\alpha = \frac{\text{outer radius}}{\text{inner radius}} = \frac{R_o}{R_i}$$

For n = 1

$$\epsilon_{\theta 1} = \frac{3}{4} \frac{1}{\sigma_o/\epsilon_o} \left(\frac{R_o}{r}\right)^2 \left(\frac{2P}{\alpha^2 - 1}\right)$$

and

$$\epsilon_\theta = \epsilon_{\theta 1} \left(\frac{P}{\sigma_o}\right)^{n-1} \frac{3^{\frac{n-1}{2}}}{n^n} \frac{\alpha^2 - 1}{\left(\alpha^{2/n} - 1\right)^n}$$

The condition for $\epsilon_\theta = \epsilon_{\theta 1}$ is

$$\frac{P}{\sigma_o} = \left[\frac{n^n}{3^{\frac{n-1}{2}}} \frac{\left(\alpha^{2/n} - 1\right)^n}{\alpha^2 - 1} \right]^{\frac{1}{n-1}} = \gamma_3(n), \text{ SAY}$$

Table 3.5 gives values of $\gamma_3(n)$ for $\alpha = 4, 2, \frac{4}{3}$ and n values from 1.1 to 7.

n	$\gamma_3(n)$		
	$\alpha = 4$	$\alpha = 2$	$\alpha = \frac{4}{3}$
1.1	1.218	0.739	0.328
1.5	1.323	0.749	0.329
2	1.385	0.771	0.330
3	1.425	0.782	0.331
4	1.485	0.786	0.332
5	1.506	0.790	0.333
6	1.525	0.792	0.334
7	1.538	0.794	0.335

Table 3.5

Even for a very thick wall cylinder ($\alpha = 4$), $\gamma_3(n)$ does not vary greatly with n. If $\frac{P}{\sigma_o}$ is given the value of $\gamma_3(n)$ for n = 5 in each case, i.e.

α	4	2	$4/3$
$\frac{P}{\sigma_o}$	1.506	0.790	0.333

the values for $\left(\frac{\epsilon_\theta}{\epsilon_{\theta 1}}\right)$ shown in Table 3.6 are obtained.

n	$\frac{\epsilon_\theta}{\epsilon_{\theta i}}$		
	$\alpha = 4$	$\alpha = 2$	$\alpha = 4/3$
1.1	1.024	1.007	1.001
1.5	1.067	1.020	1.006
2	1.088	1.027	1.008
3	1.072	1.020	1.008
4	1.039	1.015	1.006
5	1.000	1.000	1.000
6	0.936	0.990	0.995
7	0.880	0.970	0.988

Table 3.6

With these values of $\frac{P}{\sigma_o}$, the circumferential strain at any radius, and hence the radial displacement of any point in the cylinder wall, can be estimated from the linear elastic solution. The accuracy of the estimate is $\pm$ 12% for $\alpha = 4$ and values of n from 1.1 to 7, and it improves greatly for lower values of α .

In Fig 3.7, $\frac{P}{\sigma_o}$ is plotted for values of α from 1 to 4. Also shown is the curve obtained from the following thin cylinder approximation.

From equation 3.9

$$\sigma_o = 0.433 \frac{PA}{H}$$

or

$$\frac{P}{\sigma_o} = 1.155 \frac{2H}{A}$$

But

$$\frac{2H}{A} = \frac{R_o - R_i}{R_i} = \alpha - 1$$

$$\therefore \quad \frac{P}{\sigma_o} = 1.155 (\alpha - 1)$$

(e) Circular flat plates under rotationally symmetric loading

Solutions have been obtained by Malinin[18] for the central deflection in the following four examples of circular flat plates. A summary of the results is given in reference (3).

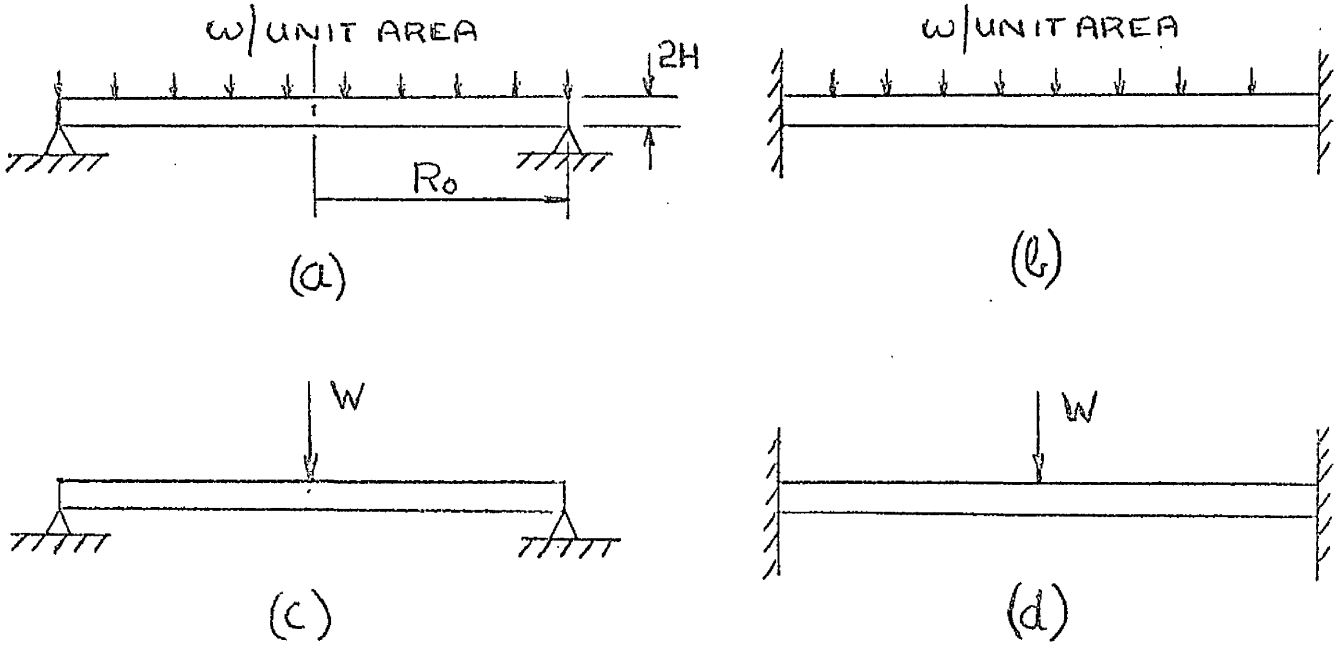

(a) and (b) - uniform load w/unit area distributed over whole area.

(c) and (d) - central load W.

(a) and (c) - simply supported edges.

(b) and (d) - clamped edges.

The solutions were obtained with relations between moments and changes in mid-surface curvatures based on equations 2.7.

If $W = \pi R_o^2 \omega$ in cases (a) and (b), the central deflection δ for all four plates may be written as

$$\delta = C \frac{\epsilon_o}{\sigma_o^n} \left(\frac{D}{J}\right)^n W^n \frac{R_o^2}{(2H)^{2n+1}} 3^{\frac{n+1}{2}} \left(\frac{2n+1}{n}\right)^n \qquad (3.12)$$

where

J is a function of n plotted for the four cases in Fig. 3.8,

C and D are constants having the following values

Case	(a)	(b)	(c)	(d)
C	$11/4$	$1/4$	$7/12$	$1/4$
D	$5/8\pi$	$1/24\pi$	$7/24\pi$	$1/8\pi$

From equation 3.12

$$\delta_1 = C \frac{1}{(\sigma_o/\epsilon_o)} \frac{D}{J_1} W \frac{R_o^2}{(2H)^3} \cdot 9$$

where J_1 is the value of J for n = 1.

The expression for the central deflection may thus be written

$$\delta = \delta_1 \left(\frac{W}{4H^2\sigma_0}\right)^{n-1} \left(\frac{D}{J}\right)^{n-1} \frac{J_1}{J} \frac{1}{9} 3^{\frac{n+1}{2}} \left(\frac{2n+1}{n}\right)^n$$

For $\delta = \delta_1$

$$\frac{W}{4H^2\sigma_0} = \frac{J}{D} \left(\frac{J}{J_1}\right)^{\frac{1}{n-1}} 9^{\frac{1}{n-1}} \frac{1}{3^{\frac{n+1}{2(n-1)}}} \left(\frac{n}{2n+1}\right)^{\frac{n}{n-1}}$$

$$= \gamma_4(n), \quad \text{say.}$$

Values of $\gamma_4(n)$ have been calculated for each example and are given in Table 3.7

n	$\gamma_4(n)$			
	(a)	(b)	(c)	(d)
1.25	4.81	10.44	0.155	0.225
1.5	4.91	10.53	0.165	0.245
2.0	4.97	10.77	0.174	0.266
3.0	5.03	11.10	0.185	0.284
4.0	5.09	11.25	0.189	0.290
5.0	5.15	11.32	0.191	0.295

Table 3.7

Solutions are available only for values of n from 1.25 to 5, but in this range $\gamma_4(n)$ does not depend strongly on n.

In Table 3.8 are shown values of $\frac{\delta}{\delta_1}$ calculated with $\frac{W}{4H^2\sigma_0}$ having the values of $\gamma_4(n)$ for n = 5.

n	$\frac{\delta}{\delta_1}$			
	(a)	(b)	(c)	(d)
1.25	1.018	1.021	1.053	1.070
1.5	1.025	1.036	1.075	1.097
2.0	1.037	1.051	1.098	1.100
3.0	1.050	1.040	1.062	1.079
4.0	1.033	1.021	1.020	1.060
5.0	1.000	1.000	1.000	1.000

Table 3.8

With these values for $\frac{W}{4H^2\sigma_0}$

$$\delta = \delta_1 \pm 10\% \text{ approx for } 1.25 \leq n \leq 5$$

3.3 Summary of Method

For some structures obeying an n-power law, the displacement δ at a particular point can be expressed in the form

$$\delta = \lambda_1 \left(P_i \text{ ---}, L_i \text{ ---}, \sigma_o, \epsilon_o \right) . \lambda_2 (n) \qquad (3.13)$$

where

λ_1 is a non-linear function of the loading P_i, the dimensions of the structure L_i and the co-ordinates σ_o, ϵ_o of an arbitrary point on the stress/strain curve;

λ_2 is a numerical function of n.

Equation 3.13 can be written as

$$\delta = \delta_1 \left[\lambda_3 \right]^{n-1} \lambda_4 (n) \qquad (3.14)$$

where

δ_1 is the displacement for n = 1 (the linear elastic solution with the modulus of elasticity written as $\frac{\sigma_o}{\epsilon_o}$ and Poisson's ratio taken as $\frac{1}{2}$);

λ_3 is a non-dimensional grouping of

P_i, L_i and σ_o;

λ_4 is a new numerical function of n.

The condition for $\delta = \delta_1$ when $n > 1$ is thus

$$\lambda_3 = \left(\frac{1}{\lambda_4} \right)^{\frac{1}{n-1}} \qquad (3.15)$$

The parameter λ_3 can be given a numerical value for each n to satisfy equation 3.15 and hence give $\delta = \delta_1$. It is found, however, that λ_3 is often not strongly dependent on n and may be chosen to give $\delta \doteq \delta_1$ for a range of n.

λ_3 chosen in this way defines σ_o in terms of the loading and the dimensions of the structure, and ϵ_o is obtained from the stress/strain curve. The values of σ_o and ϵ_o are used in the linear elastic solution to evaluate δ_1.

3.4 Discussion

The method suggested for estimating displacements in some structures obeying an n-power law has the advantages that

(a) the linear elastic solution replaces the more complex non-linear one;

(b) the non-linear stress/strain curve can be used directly without evaluating the constants B and n in equations 1.3 and 1.4.

For the structures considered, the reference stress σ_o can be chosen to give estimates of displacements which are within $\pm$ 15% of the exact values for $1.1 \leq n \leq 7$. ($1.25 \leq n \leq 5$ for the circular flat plates). Other values of σ_o will give

better accuracy for a smaller range of n but greater errors are introduced if the range is extended beyond n = 7.

The physical explanation of the method for the beam in uniform bending suggests that it might be useful for non-linear laws besides the n-power law. Similar physical explanations can be obtained for the other structures and also suggest that the method might be more widely applicable. For example, Fig. 3.9 shows the effective stress $\overline{\sigma}$ through the wall of a cylinder having a diameter ratio of 2, for different values of n and the same internal pressure. In Fig. 3.10, the product of the moment and curvature is plotted along a beam of rectangular cross-section, simply supported at its ends and centrally loaded. The central deflection (and thus the area under the curve) is the same for each value of n.

In Figs 3.9 and 3.10, the curves for $1 \leq n \leq 7$ intersect the curve for n = 1 at approximately the same point. Use of the intersection "point" to obtain the results of paragraphs 3.2 (a) and (d) is demonstrated in Appendix 3.5. For other non-linear laws, which are reasonably close to the n-power family for $1 \leq n \leq 7$, intersection with the n = 1 curve may be expected to occur in the same region.

It has been brought to the writer's attention[19] that characteristics of an n-power system similar to those discussed above have been used by Preston[20], in the measurement of fluid flow in circular pipes. The velocity distribution for turbulent flow can be described by an n-power expression where the value of n depends on Reynold's Number. It was found that there is a radius in the pipe at which, for a given mass flow rate, the velocity does not depend strongly on n. Measurement of the velocity at this radius will thus give a measure of mass flow rate which, within limits, is independent of Reynold's Number.

Experiments conducted by Campbell[21] on beams in three point bending provide a more rigorous test of the method than the experiments in uniform bending. Beams of rectangular cross-section 1" depth x $\frac{1}{2}$" width were simply supported over an 18" span, and centrally loaded. Stress/strain curves for beams of annealed copper and brass are given in Fig 3.11, and plotted logarithmically in Fig 3.12. for strains up to 5%.

The experimental load/central deflection curves for deflections up to 1" are reproduced in Figs 3.13 and 3.14. The curves estimated by the method of paragraph 3.2(a) are shown for comparison and there is reasonable agreement with the experimental results.

The maximum fibre strain at a 1" central deflection is approximately 3% for the copper beam and 5% for the brass beam.

One application of the method which may prove to be important is for the prediction of creep rates in simple structures. The method suggests that a uniaxial creep test conducted at one stress level would be sufficient to predict a second stage deformation rate in a structure for one value of the applied load. In studying the creep of uniformly loaded beams of rectangular cross-section, Anderson, Gardner and Hodgkins[22] noted the existence of what they termed a "representative stress," and the possibility of conducting a single creep test at this level.

Furthermore, Marriot and Leckie[23] investigated the stress redistribution which occurs during first stage or primary creep in a number of structures, and observed that the stress at a particular point remained nearly unchanged during the redistribution. They termed this the "skeletal point" in the structure, and for the beam of rectangular cross-section in uniform bending and the thick-wall cylinder under internal pressure, the skeletal point is the same as the intersection point of Figs 3.1 and 3.9. This

suggests that a single uniaxial test might be sufficient to predict the creep behaviour of such simple structures throughout both primary and secondary stages. As discussed by Marriot and Leckie, it also suggests methods of predicting creep deformations when the temperature and/or loads are changing with time. However, these suggestions must be treated with caution until sufficient experimental results are available to put them to test.

Results obtained by King[24] for creep of thick wall cylinders under internal pressure provide an opportunity for checking the method when applied to creep conditions. The experiments were conducted on cylinders of 0.07% Ti Aluminium alloy at 250°C, the diameter ratio of the cylinders being 3.125. Uniaxial tests were performed at six values of tensile stress and the second stage creep rates are given below.

Tensile Stress lbf./in^2	738	980	1134	1290	1493	1750
Minimum Creep rate /hr	5.3 x 10^{-4}	2.6 x 10^{-3}	6.4 x 10^{-3}	1.1 x 10^{-2}	2.9 x 10^{-2}	7.2 x 10^{-2}

Plotted logarithmically these results are close to a straight line and thus obey approximately an n-power

law. King determined the value of n to be 5.8.

A graph of second stage creep rate against internal pressure in the cylinders obtained from the uniaxial results by the approximate method of paragraph 3.2(d) is plotted in Fig 3.15. To cover the required pressure range, it was necessary to extrapolate the tensile data, assuming an n-power law and n = 5.8. This part of the curve has been drawn as a broken line. The minimum creep rates observed by King at four pressures are shown on the graph. While the approximate method gives a reasonable estimate of creep rates at the lower pressures, it is considerably in error at the highest experimental value. One reason for this may be that the cylinder became fully plastic when the highest pressure was applied, and relatively large strains occurred. King achieved an improved theoretical prediction by using the Bailey analysis modified for large strains.

There are very few experimental results available in which deformation rates in structures and the tensile creep data are adequately recorded. A great deal more experimental work will have to be done before a better understanding of the behaviour of structures in creep can be claimed.

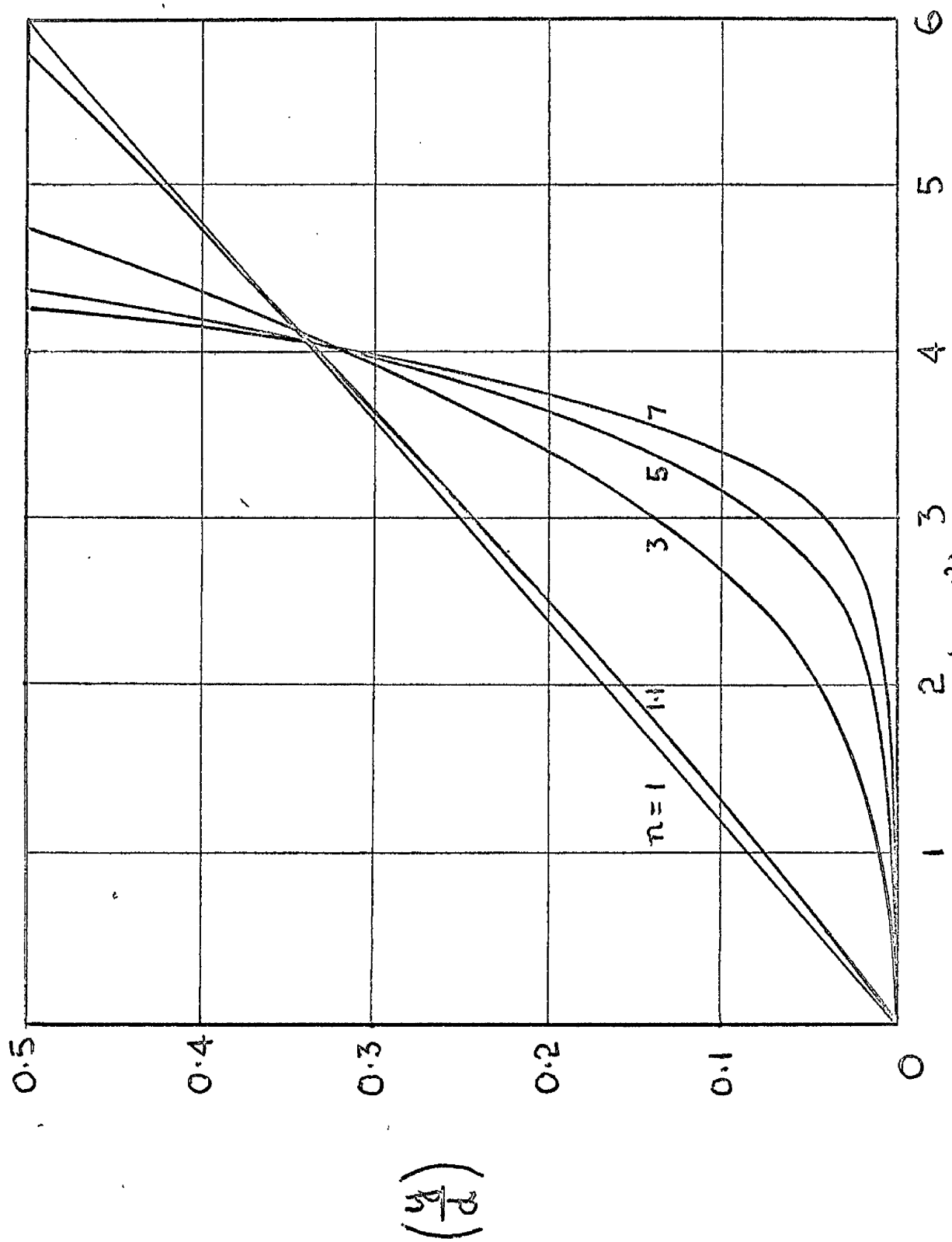

FIG. 3.1 DISTRIBUTION OF BENDING STRESS

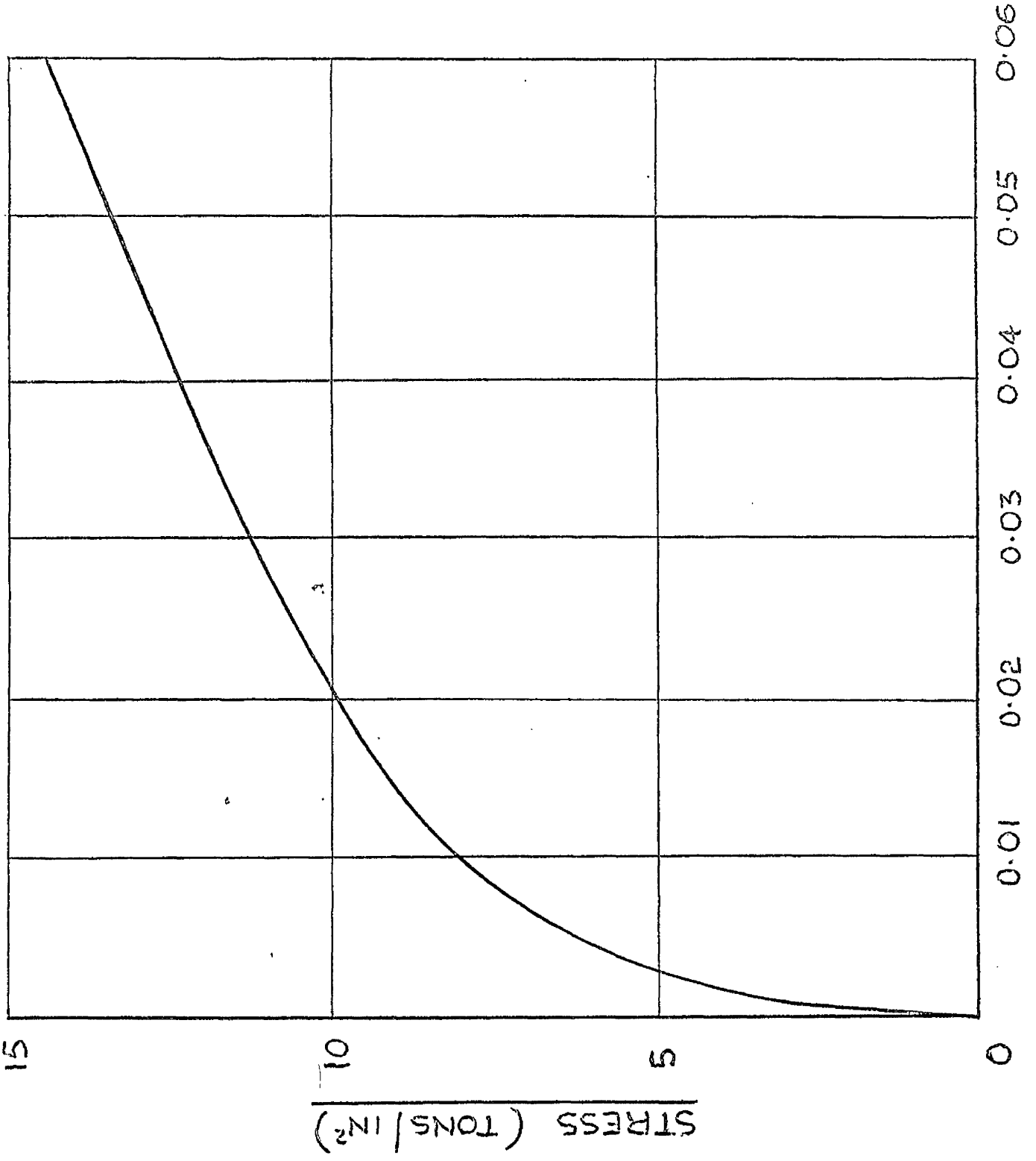

FIG. 3.2 STRESS / STRAIN CURVE FOR CAST MG. ALLOY

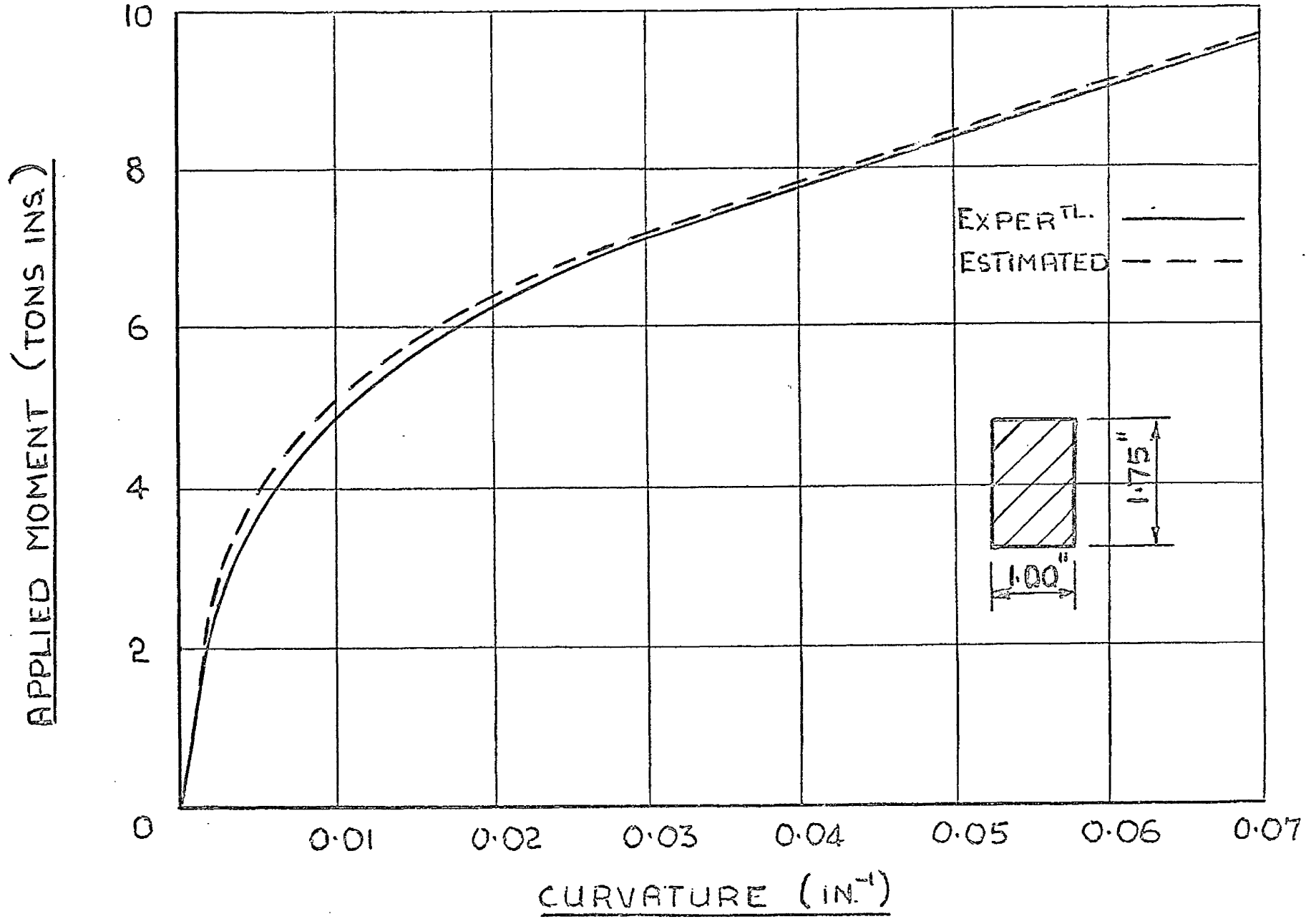

FIG. 3.3

MOMENT/CURVATURE RESULTS FOR BEAM

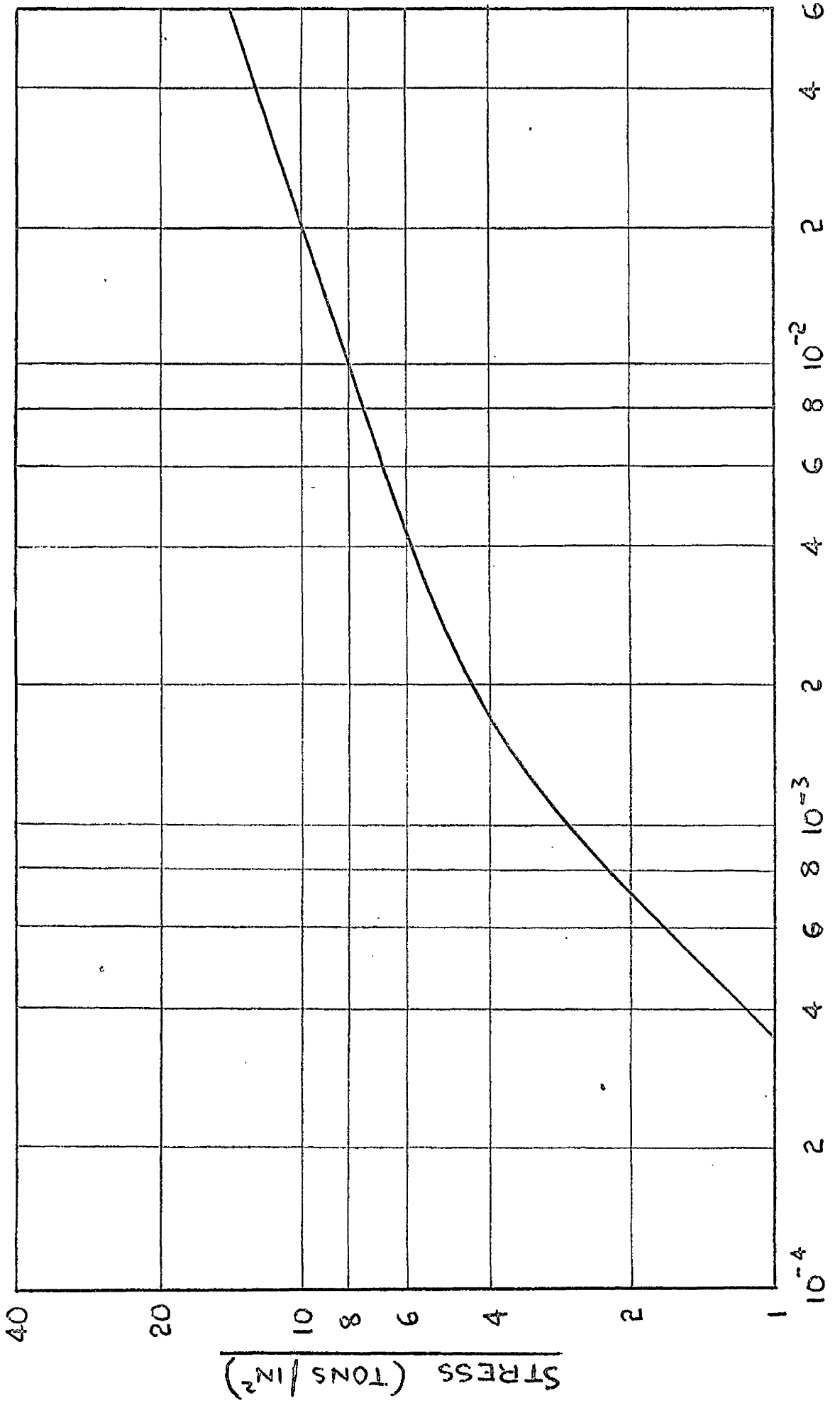

FIG. 3.4 STRESS/STRAIN CURVE FOR CAST MAGNESIUM ALLOY

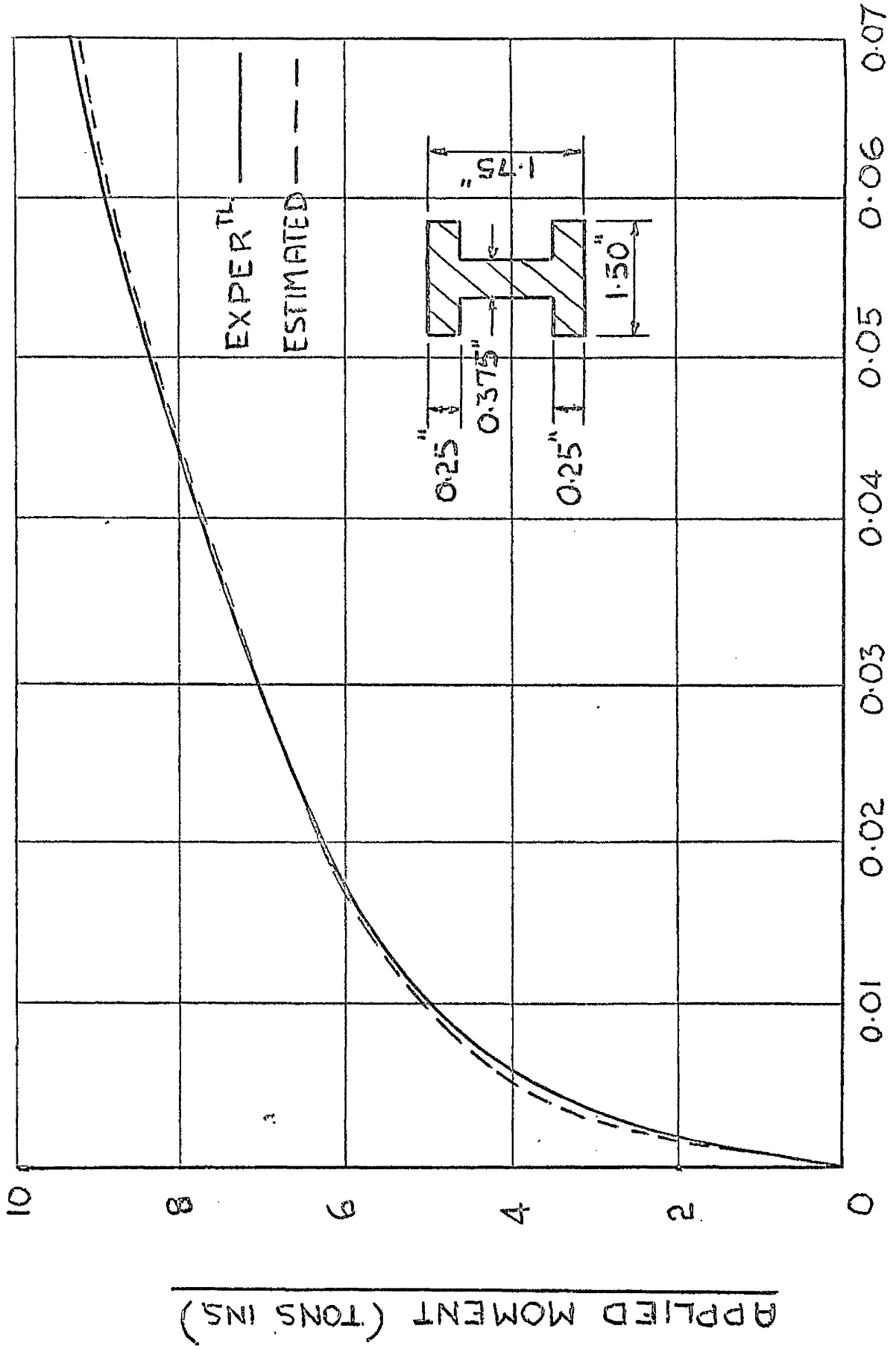

FIG. 3.5 MOMENT / CURVATURE RESULTS FOR I-BEAM

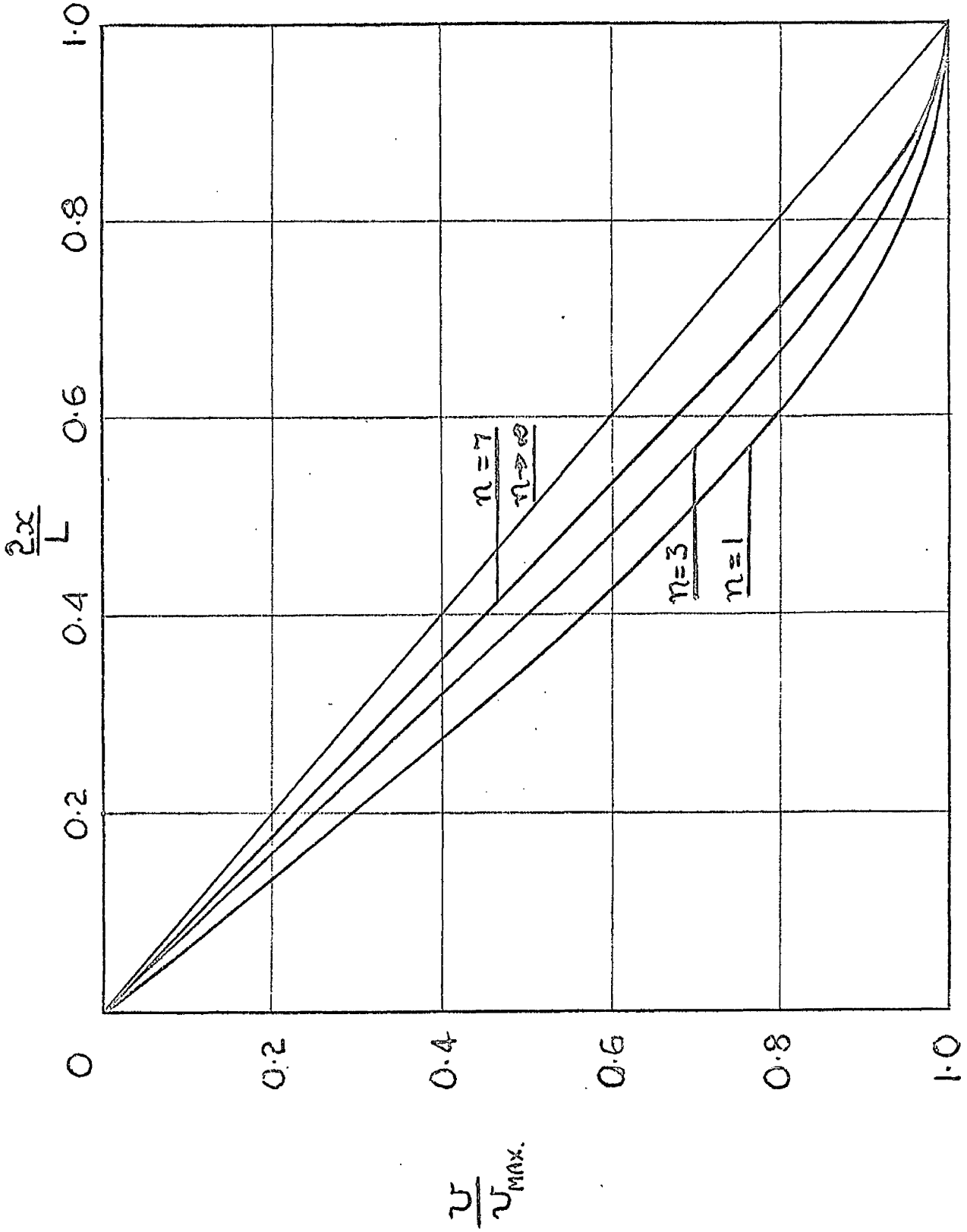

FIG. 3.6 DEFLECTED SHAPES OF S.S. BEAM WITH CENTRAL LOAD

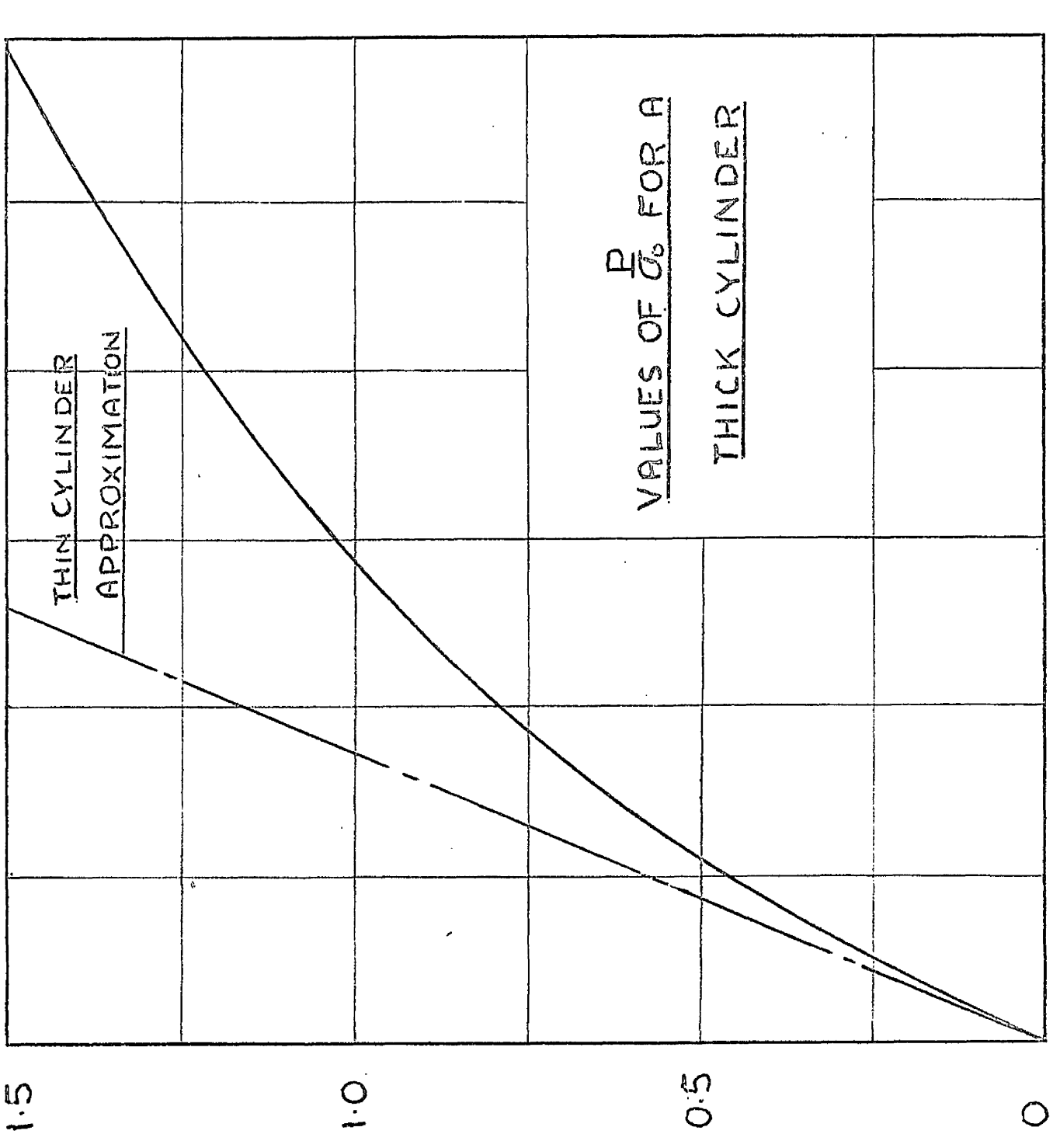
THIN CYLINDER
APPROXIMATION
VALUES OF $\frac{P}{\sigma_0}$ FOR A
THICK CYLINDER
1.5
1.0
0.5
0
P/σ_0
1.0
2.0
3.0
4.0
α

FIG. 3.7

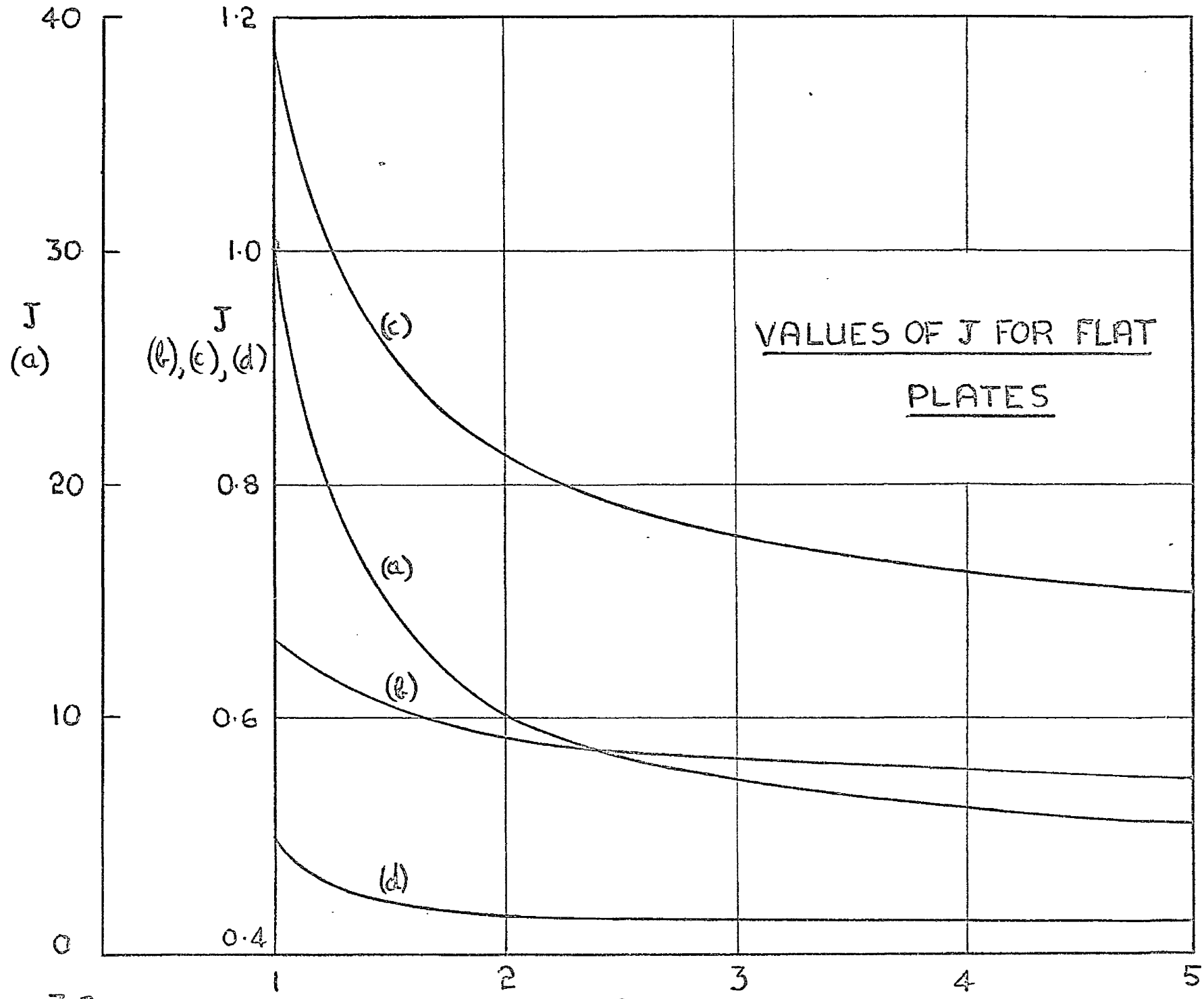
40
30
20
10
0
1·2
1·0
0·8
0·6
0·4
J
(a)
J
(b), (c), (d)
(c)
(a)
(b)
(d)
VALUES OF J FOR FLAT PLATES
1
2
3
4
5

Fig. 3.8

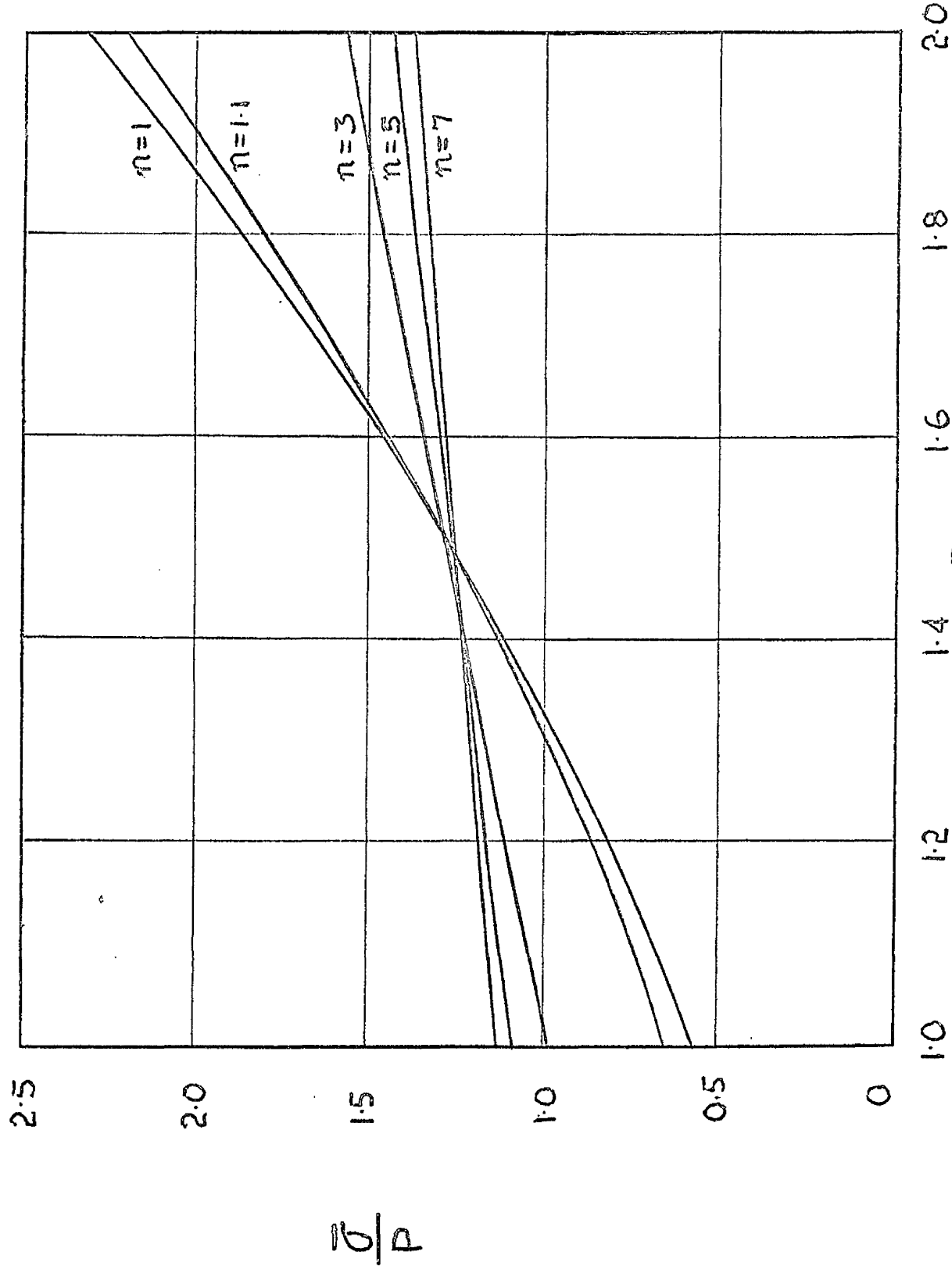

FIG. 3.9 DISTRIBUTION OF $\bar{\sigma}$ IN THICK CYLINDER ($\alpha=2$)

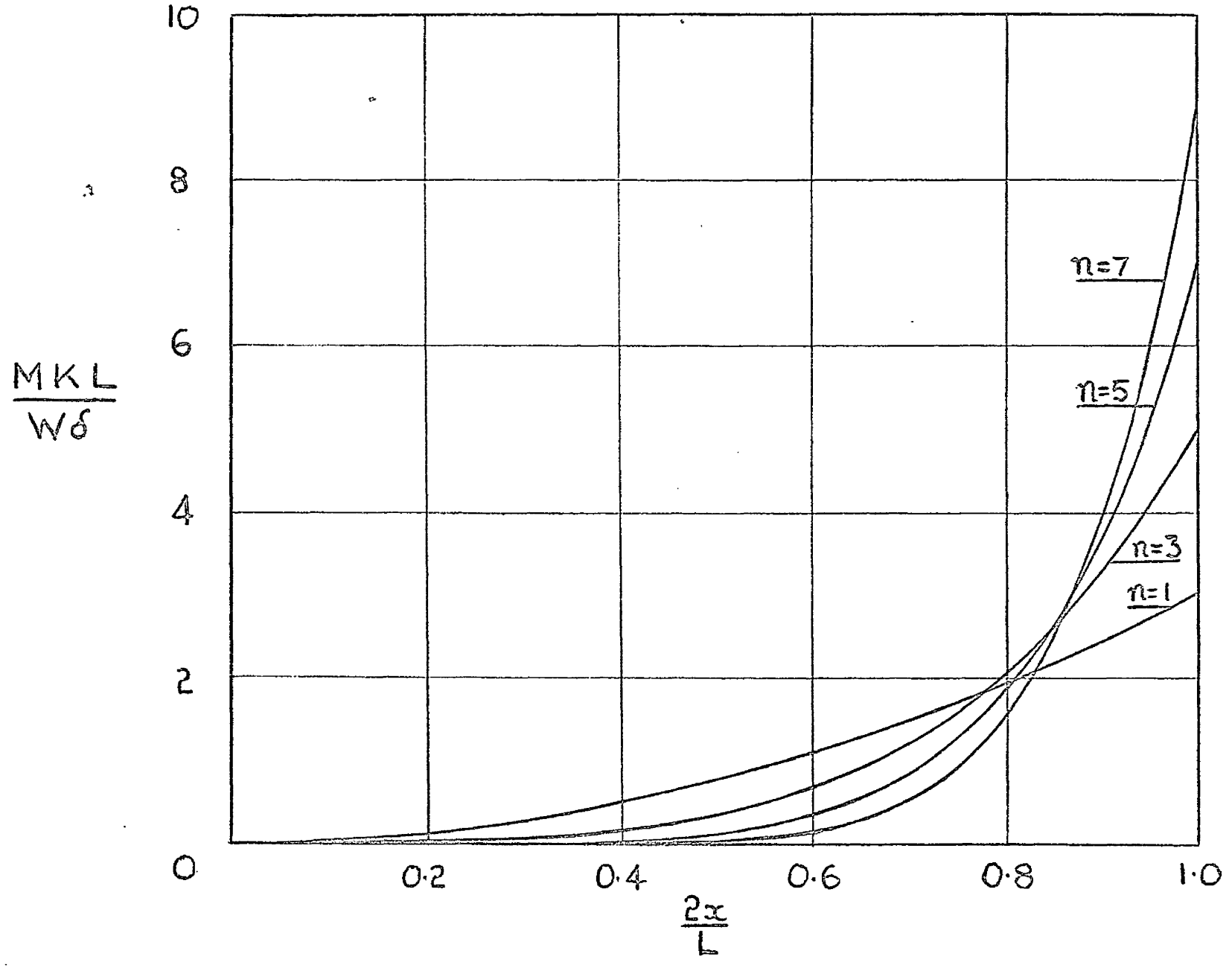

FIG. 3.10 DISTRIBUTION OF M.K FOR S.S. BEAM WITH CENTRAL LOAD.

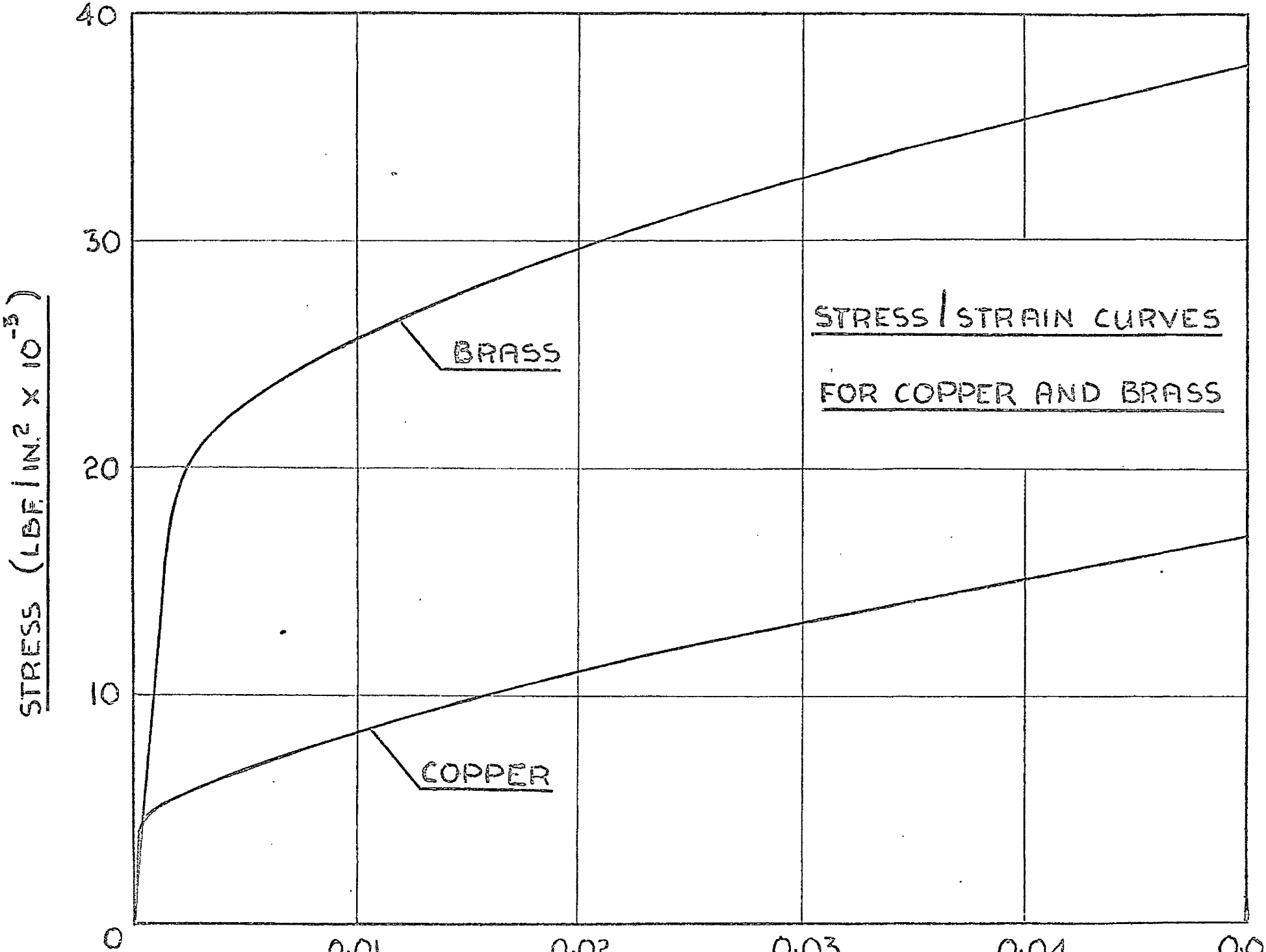
40
30
20
10
0
0·01
0·02
0·03
0·04
0·05
STRESS (LBF./IN.² × 10⁻³)
STRAIN
BRASS
COPPER
STRESS / STRAIN CURVES
FOR COPPER AND BRASS

FIG. 311

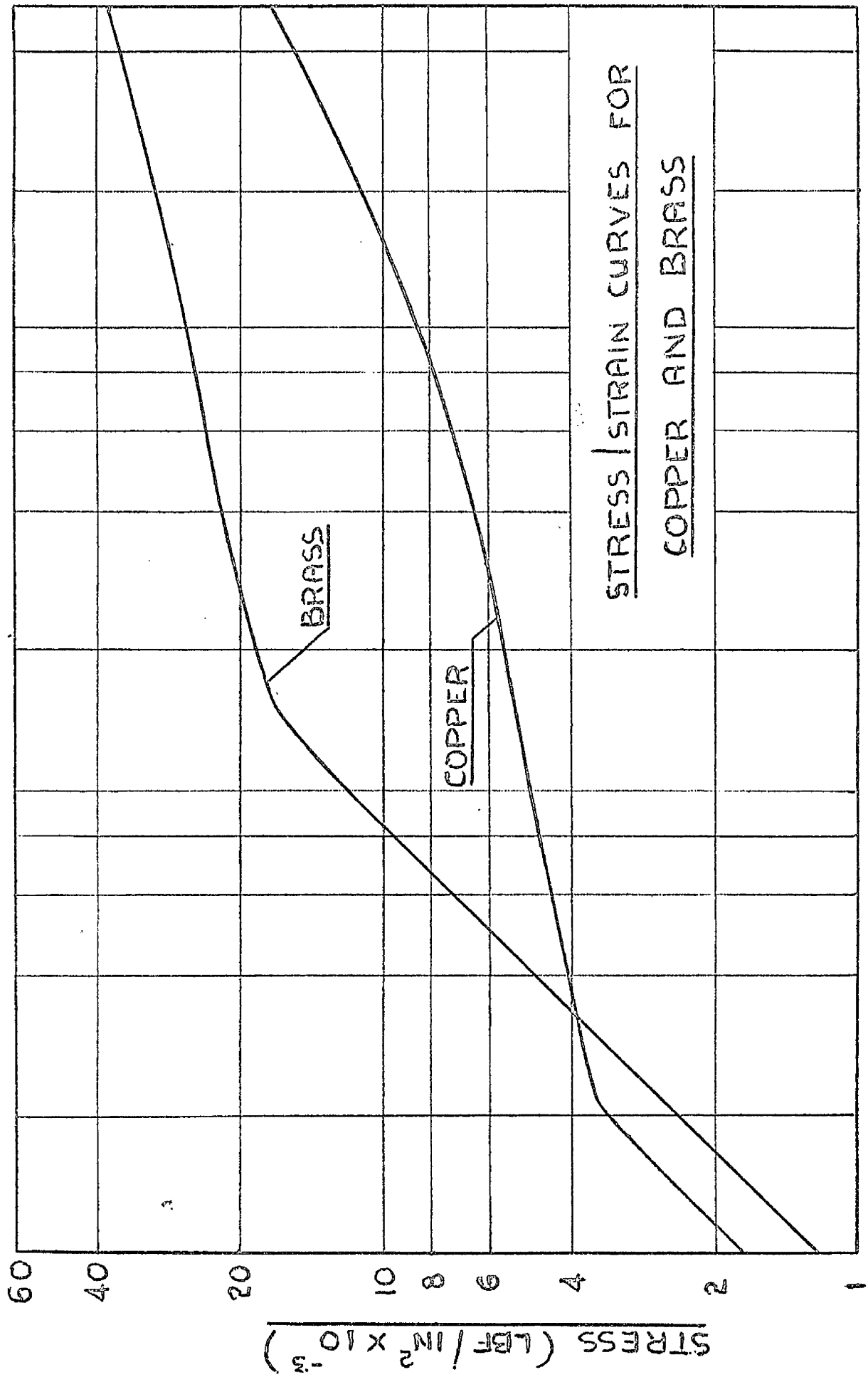
STRESS / STRAIN CURVES FOR
COPPER AND BRASS
BRASS
COPPER
STRESS (LBF/IN² x 10⁻³)
STRAIN
60
40
20
10
8
6
4
2
1
10⁻⁴
2
4
6
8
10⁻³
2
4
6
8
10⁻²
2
4
5

FIG 3.12

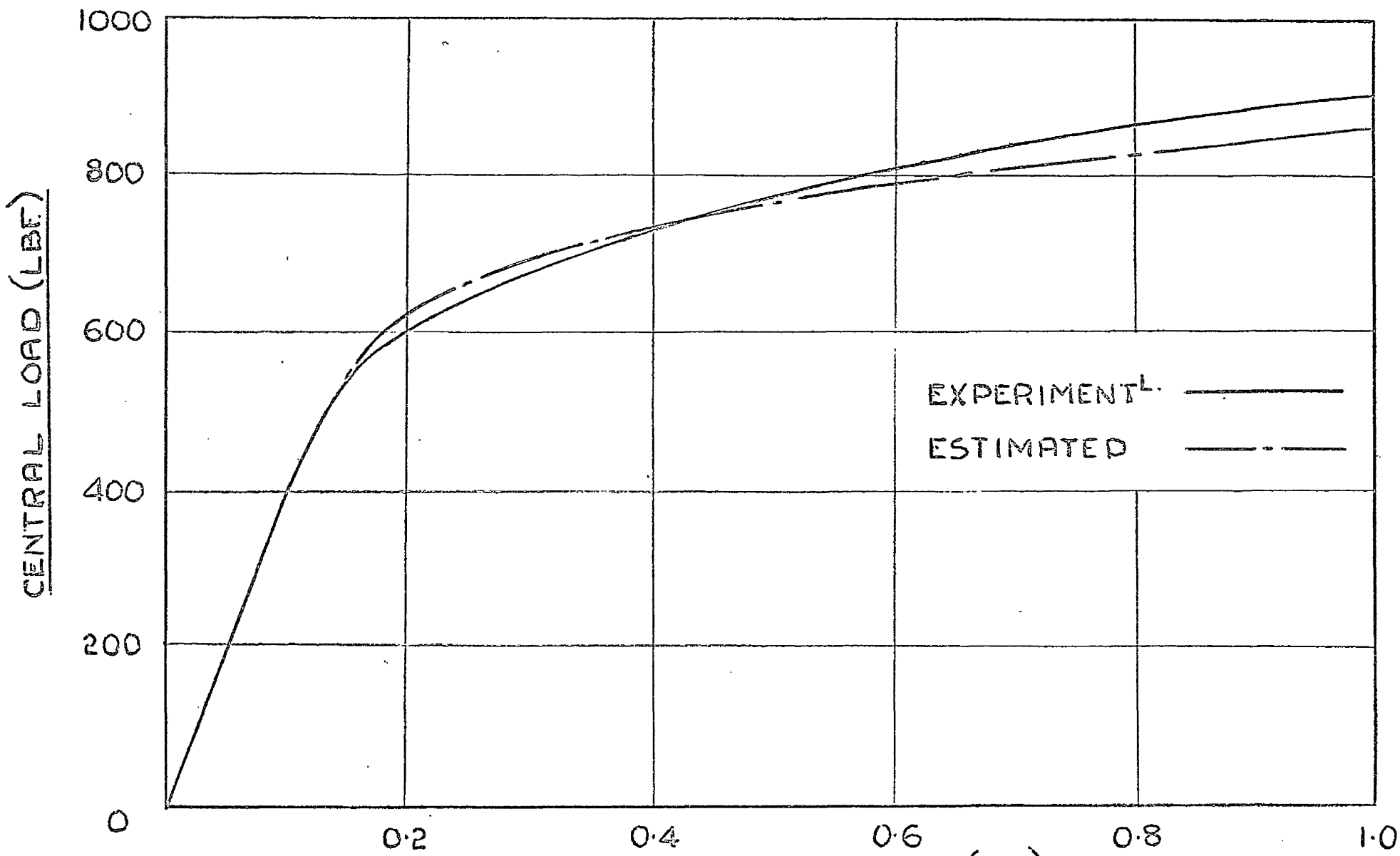

FIG. 3.13 LOAD / DEFLECTION CURVES FOR S.S. BRASS BEAM

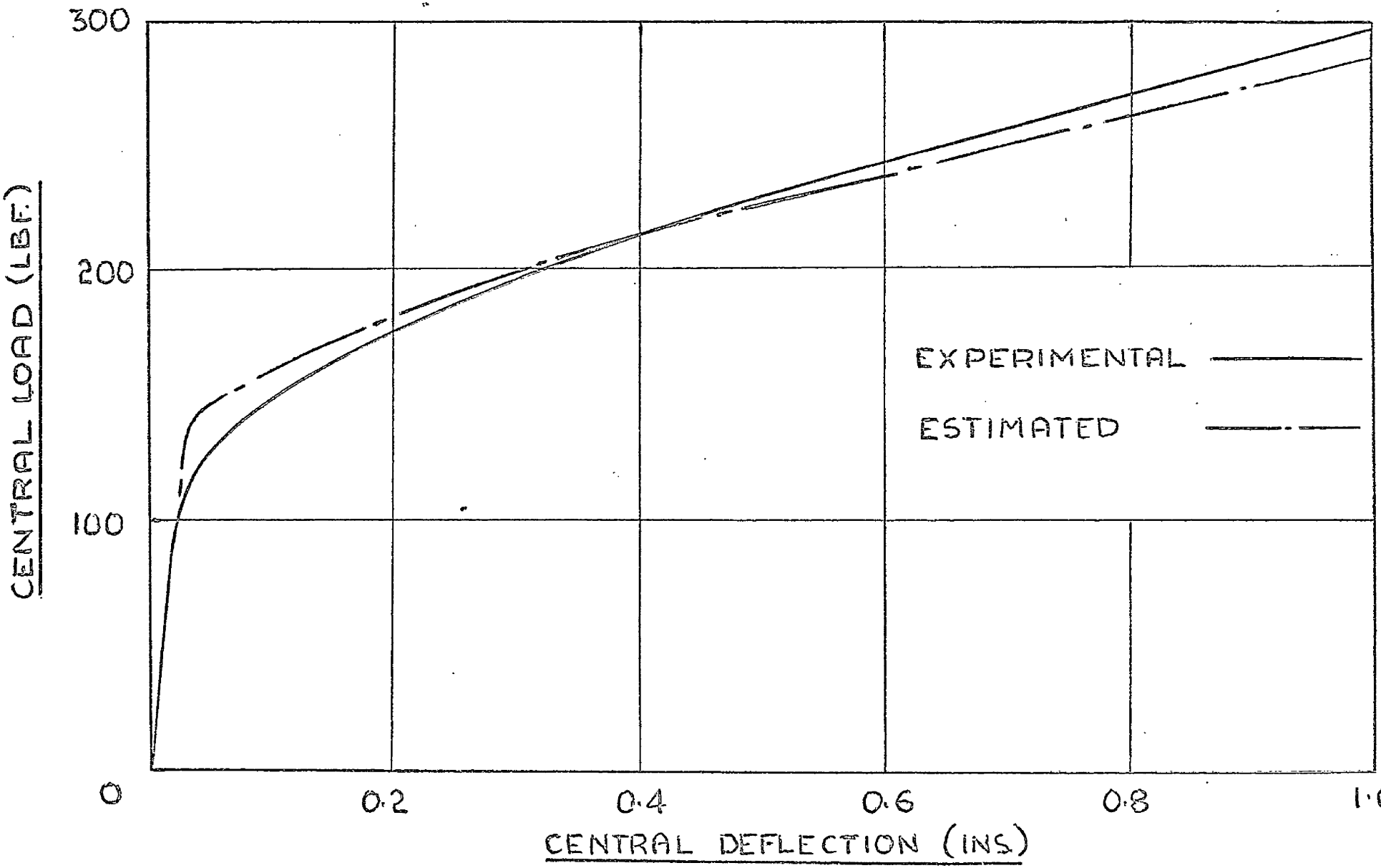

FIG. 3.14 LOAD / DEFLECTION CURVES FOR S.S. GORDER BEAM

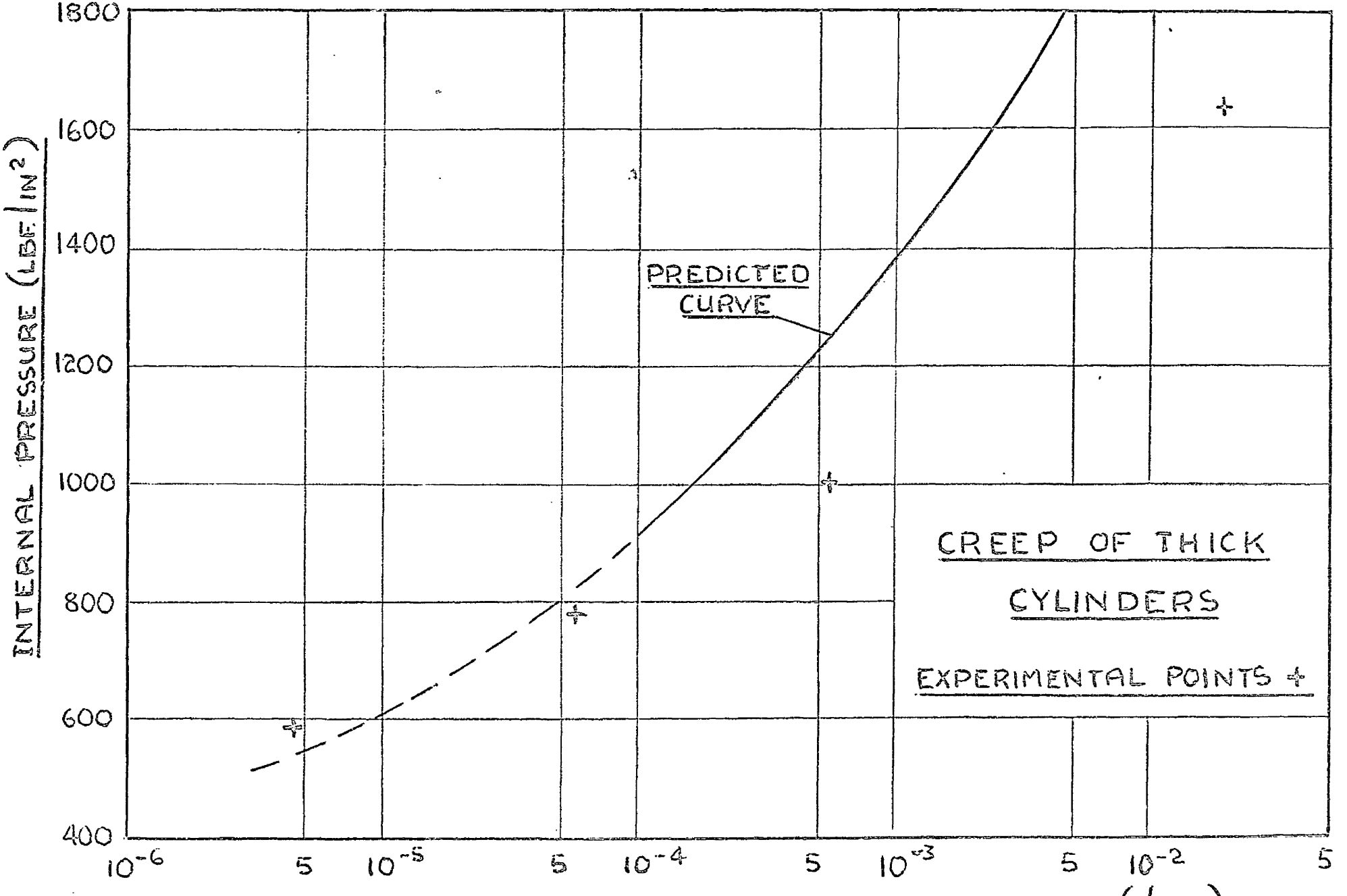
INTERNAL PRESSURE (LBF/IN²)
1800
1600
1400
1200
1000
800
600
400
PREDICTED CURVE
CREEP OF THICK CYLINDERS
EXPERIMENTAL POINTS +
10⁻⁶
5
10⁻⁵
5
10⁻⁴
5
10⁻³
5
10⁻²
5
MINIMUM CREEP RATE OF OUTER DIAMETER (/HR)

FIG. 3.15

CHAPTER 4

RELATIONS BETWEEN FORCES AND MOMENTS AND MID-SURFACE DEFORMATIONS FOR AN ELEMENT OF A ROTATIONALLY SYMMETRIC THIN SHELL

4.1 Preliminary

An element of a thin shell which is rotationally symmetric in geometry and loading is shown in Fig 4.1. The directions 1 and 2 are orthogonal.

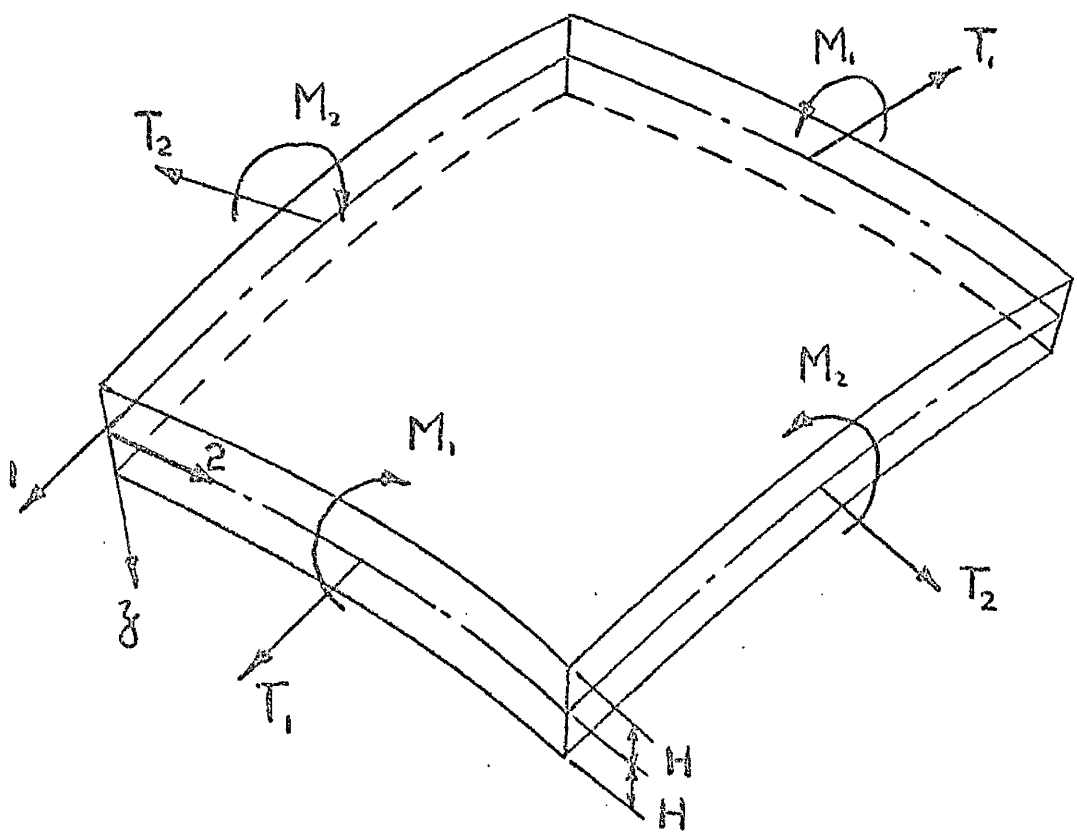

Fig 4.1.

T_1, T_2 and M_1, M_2 are, respectively, normal forces and moments per unit length of mid-surface. ϵ_{m1}, ϵ_{m2} are the corresponding mid-surface strains, and K_1, K_2 the changes in mid-surface curvatures.

It is convenient to have relations between T_1, T_2, M_1, M_2 and ϵ_{m1}, ϵ_{m2}, K_1, K_2 for formulating problems of rotationally symmetric thin shells. If the usual assumptions of thin shell theory are made, these relations may be expressed in integral form for a non-linear material obeying equations 2.9. They are referred to in this form as the exact relations.

As the integrations cannot be performed for all values of n, the exact relations cannot be obtained as closed-form analytical expressions. This difficulty leads in the present chapter to the suggestion of simpler approximate relations. These are compared with the exact relations computed numerically for particular values of n, and with approximate relations used by other investigators.

4.2 The exact relations

In common with the general theory of thin shells, it is assumed that normals to the undeformed middle surface are deformed without change in length into normals to the deformed middle surface. This

assumption leads to the strains ϵ_1, ϵ_2 at z from the mid-surface being expressed in terms of the mid-surface strains ϵ_{m1}, ϵ_{m2} and curvature changes K_1, K_2 by

$$\epsilon_1 = \epsilon_{m1} + z K_1$$
$$\epsilon_2 = \epsilon_{m2} + z K_2 \qquad (4.1)$$

The stresses σ_1 and σ_2 at z from the mid-surface can then be obtained from equations 2.9, i.e.

$$\sigma_1 = \frac{1}{B^{1/n}}\left(\frac{4}{3}\right)^{\frac{n+1}{2n}}\left(\epsilon_1^2 + \epsilon_1\epsilon_2 + \epsilon_2^2\right)^{\frac{1-n}{2n}}\left(\epsilon_1 + \tfrac{1}{2}\epsilon_2\right)$$
$$\sigma_2 = \frac{1}{B^{1/n}}\left(\frac{4}{3}\right)^{\frac{n+1}{2n}}\left(\epsilon_1^2 + \epsilon_1\epsilon_2 + \epsilon_2^2\right)^{\frac{1-n}{2n}}\left(\epsilon_2 + \tfrac{1}{2}\epsilon_1\right)$$

by substituting for ϵ_1 and ϵ_2 from equations 4.1. This gives finally

$$\sigma_1 = \frac{1}{B^{1/n}}\left(\frac{4}{3}\right)^{\frac{n+1}{2n}} F_1^{\frac{1-n}{2n}}\left[\left(\epsilon_{m1} + \tfrac{1}{2}\epsilon_{m2}\right) + z\left(K_1 + \tfrac{1}{2}K_2\right)\right]$$
$$\sigma_2 = \frac{1}{B^{1/n}}\left(\frac{4}{3}\right)^{\frac{n+1}{2n}} F_1^{\frac{1-n}{2n}}\left[\left(\epsilon_{m2} + \tfrac{1}{2}\epsilon_{m1}\right) + z\left(K_2 + \tfrac{1}{2}K_1\right)\right] \qquad (4.2)$$

where

$$F_1 = \left(\epsilon_{m1}^2 + \epsilon_{m1}\epsilon_{m2} + \epsilon_{m2}^2\right)$$
$$+ 2z\left[\epsilon_{m1}\left(K_1 + \tfrac{1}{2}K_2\right) + \epsilon_{m2}\left(K_2 + \tfrac{1}{2}K_1\right)\right] + z^2\left(K_1^2 + K_1K_2 + K_2^2\right)$$

If the ratios of shell thickness to radii of curvature of the mid-surface are small compared to unity, the forces and moments on the edges of the element in Fig 4.1 are

$$T_1 = \int_{-H}^{+H} \sigma_1 \, dz \quad ; \quad T_2 = \int_{-H}^{+H} \sigma_2 \, dz$$
$$M_1 = \int_{-H}^{+H} \sigma_1 z \, dz \quad ; \quad M_2 = \int_{-H}^{+H} \sigma_2 z \, dz \qquad (4.3)$$

where 2 H is the shell thickness.

Substituting from equations 4.2 into equations 4.3 gives

$$T_1 = \frac{1}{B^{1/n}} \left(\frac{4}{3}\right)^{\frac{n+1}{2n}} \int_{-H}^{+H} F_1^{\frac{1-n}{2n}} \left[\left(\epsilon_{m1} + \tfrac{1}{2}\epsilon_{m2}\right) + z\left(K_1 + \tfrac{1}{2}K_2\right)\right] dz$$

$$T_2 = \frac{1}{B^{1/n}} \left(\frac{4}{3}\right)^{\frac{n+1}{2n}} \int_{-H}^{+H} F_1^{\frac{1-n}{2n}} \left[\left(\epsilon_{m2} + \tfrac{1}{2}\epsilon_{m1}\right) + z\left(K_2 + \tfrac{1}{2}K_1\right)\right] dz$$

$$M_1 = \frac{1}{B^{1/n}} \left(\frac{4}{3}\right)^{\frac{n+1}{2n}} \int_{-H}^{+H} F_1^{\frac{1-n}{2n}} \left[\left(\epsilon_{m1} + \tfrac{1}{2}\epsilon_{m2}\right) + z\left(K_1 + \tfrac{1}{2}K_2\right)\right] z \, dz \qquad (4.4)$$

$$M_2 = \frac{1}{B^{1/n}} \left(\frac{4}{3}\right)^{\frac{n+1}{2n}} \int_{-H}^{+H} F_1^{\frac{1-n}{2n}} \left[\left(\epsilon_{m2} + \tfrac{1}{2}\epsilon_{m1}\right) + z\left(K_2 + \tfrac{1}{2}K_1\right)\right] z \, dz$$

This is a convenient stage at which to write the relations in non-dimensional form.

With

$$B = \frac{\epsilon_0}{\sigma_0^n} \quad ; \quad \rho = \frac{z}{H}$$

$$e_1 = \frac{\epsilon_{m1}}{\epsilon_0} \quad ; \quad e_2 = \frac{\epsilon_{m2}}{\epsilon_0}$$

$$k_1 = \frac{HK_1}{2\epsilon_0} \quad ; \quad k_2 = \frac{HK_2}{2\epsilon_0} \qquad (4.5)$$

$$t_1 = \frac{T_1}{2H\sigma_0} \quad ; \quad t_2 = \frac{T_2}{2H\sigma_0}$$

$$m_1 = \frac{M_1}{H^2\sigma_0} \quad ; \quad m_2 = \frac{M_2}{H^2\sigma_0}$$

equations 4.4 become

$$t_1 = \frac{1}{2}\left(\frac{4}{3}\right)^{\frac{n+1}{2n}} \int_{-1}^{+1} F_2^{\frac{1-n}{2n}} \left[(e_1 + \tfrac{1}{2}e_2) + 2\rho(k_1 + \tfrac{1}{2}k_2)\right] d\rho$$

$$t_2 = \frac{1}{2}\left(\frac{4}{3}\right)^{\frac{n+1}{2n}} \int_{-1}^{+1} F_2^{\frac{1-n}{2n}} \left[(e_2 + \tfrac{1}{2}e_1) + 2\rho(k_2 + \tfrac{1}{2}k_1)\right] d\rho \qquad (4.6)$$

$$m_1 = \left(\frac{4}{3}\right)^{\frac{n+1}{2n}} \int_{-1}^{+1} F_2^{\frac{1-n}{2n}} \left[(e_1 + \tfrac{1}{2}e_2) + 2\rho(k_1 + \tfrac{1}{2}k_2)\right] \rho\, d\rho$$

$$m_2 = \left(\frac{4}{3}\right)^{\frac{n+1}{2n}} \int_{-1}^{+1} F_2^{\frac{1-n}{2n}} \left[(e_2 + \tfrac{1}{2}e_1) + 2\rho(k_2 + \tfrac{1}{2}k_1)\right] \rho\, d\rho$$

where

$$F_2 = (e_1^2 + e_1 e_2 + e_2^2) + 4\rho\left[e_1(k_1 + \tfrac{1}{2}k_2) + e_2(k_2 + \tfrac{1}{2}k_1)\right] + 4\rho^2(k_1^2 + k_1 k_2 + k_2^2)$$

Equations 4.6 are referred to as the exact relations.

4.3 Suggestion of approximate relations

In paragraph 4.2 the exact relations were obtained by integration of stresses through the shell thickness. They can also be obtained by applying extremum principles to the shell element.* In Appendix 4.1, it is shown that

$$t_1 = \left(\frac{n}{n+1}\right)\frac{\partial \psi}{\partial e_1} \quad ; \quad t_2 = \left(\frac{n}{n+1}\right)\frac{\partial \psi}{\partial e_2}$$

$$m_1 = \left(\frac{n}{n+1}\right)\frac{\partial \psi}{\partial k_1} \quad ; \quad m_2 = \left(\frac{n}{n+1}\right)\frac{\partial \psi}{\partial k_2} \qquad (4.7)$$

where

*Application of the principles of minimum potential and complementary energy is not restricted to linear elastic stress/strain relations - see, for example, reference (25)

$$\Psi = \frac{1}{2}\left(\frac{4}{3}\right)^{\frac{n+1}{2n}} \int_{-1}^{+1} \left\{ \left(e_1^2 + e_1 e_2 + e_2^2\right) + 4\zeta\left[k_1\left(e_1 + \tfrac{1}{2}e_2\right) + k_2\left(e_2 + \tfrac{1}{2}e_1\right)\right] + 4\zeta^2\left(k_1^2 + k_1 k_2 + k_2^2\right) \right\}^{\frac{n+1}{2n}} d\zeta \qquad (4.8)$$

Equations 4.7 and 4.8 are a statement of the exact relations - equations 4.6.

Ψ is homogeneous of degree $\frac{n+1}{n}$ in e_1, e_2, k_1 and k_2 and Ψ = constant defines a family of surfaces in e_1, e_2, k_1, k_2 space. From equations 4.7 the components of the normal vector to a Ψ- surface in the e_1, e_2, k_1, k_2 directions are proportional to t_1, t_2, m_1, m_2 respectively. Approximate expressions for Ψ can be postulated; these, with equations 4.7, will give relations between e_1, e_2, k_1, k_2 and t_1, t_2, m_1, m_2 which approximate to the exact relations.

Under some conditions equation 4.8 can be integrated to give closed-form analytical expressions and the results give a guide to approximate forms for Ψ:

(a) <u>Linear elasticity; n = 1</u>

$$\Psi_{(a)} = \frac{4}{3}\left[\left(e_1^2 + e_1 e_2 + e_2^2\right) + \frac{4}{3}\left(k_1^2 + k_1 k_2 + k_2^2\right)\right] \qquad (4.9)$$

(b) Plane stress; $k_1 = k_2 = 0$

$$\Psi_{(b)} = \left(\frac{4}{3}\right)^{\frac{n+1}{2n}} \left(e_1^2 + e_1 e_2 + e_2^2\right)^{\frac{n+1}{2n}} \tag{4.10}$$

(c) Pure bending of plate element; $e_1 = e_2 = 0$

$$\Psi_{(c)} = 2^{\frac{n+1}{n}} \left(\frac{n}{2n+1}\right) \left(\frac{4}{3}\right)^{\frac{n+1}{2n}} \left(k_1^2 + k_1 k_2 + k_2^2\right)^{\frac{n+1}{2n}} \tag{4.11}$$

(d) Mid-surface strain and curvature change in one direction suppressed; $e_2 = k_2 = 0$

$$\Psi_{(d)} = \frac{1}{2} \left(\frac{4}{3}\right)^{\frac{n+1}{2n}} \left(\frac{n}{2n+1}\right) \frac{1}{2k_1} \left[(e_1 + 2k_1)^{\frac{2n+1}{n}} - (e_1 - 2k_1)^{\frac{2n+1}{n}} \right] \tag{4.12}$$

(e) Rigid - non - work - hardening plastic material; $n \longrightarrow \infty$.

$$\Psi_{(e)} = \frac{1}{\sqrt{3}} \left\{ \left(\frac{2a+b}{4a}\right) \sqrt{a+b+c} - \left(\frac{-2a+b}{4a}\right) \sqrt{a-b+c} \right.$$

$$\left. + \left(\frac{4ac-b^2}{8a^{3/2}}\right) \log_e \left(\frac{2a+b+2\sqrt{a}\sqrt{a+b+c}}{-2a+b+2\sqrt{a}\sqrt{a-b+c}} \right) \right\} \tag{4.13}$$

where

$$a = 4\left(k_1^2 + k_1 k_2 + k_2^2\right)$$

$$b = 4\left[k_1\left(e_1 + \tfrac{1}{2}e_2\right) + k_2\left(e_2 + \tfrac{1}{2}e_1\right)\right]$$

$$c = \left(e_1^2 + e_1 e_2 + e_2^2\right)$$

Details of the integrations leading to equations 4.12 and 4.13 are given in Appendix 4.2.

Equations 4.12 and 4.13 show what complex expressions would be necessary to obtain a close approximation to ψ for all values of n. Relations between e_1, e_2, k_1, k_2 and t_1, t_2, m_1, m_2 which would result from such expressions would be too complex to be useful in further analysis.

It is desirable that approximate forms for ψ should reduce to equations 4.9, 4.10, 4.11 under conditions (a), (b), (c) respectively. The simplest approximate form which reduces in this manner, and which gives coupling between in-plane and bending actions, is obtained from the combination of $\psi_{(b)}$ and $\psi_{(c)}$

$$\psi_{APP} = \left\{ \left[\psi_{(b)} \right]^{\frac{2n}{n+1}} + \left[\psi_{(c)} \right]^{\frac{2n}{n+1}} \right\}^{\frac{n+1}{2n}}$$

i.e.

$$\psi_{APP} = \left(\frac{4}{3}\right)^{\frac{n+1}{2n}} \left[\left(e_1^2 + e_1 e_2 + e_2^2 \right) + 4\left(\frac{n}{2n+1}\right)^{\frac{2n}{n+1}} \left(k_1^2 + k_1 k_2 + k_2^2 \right) \right]^{\frac{n+1}{2n}} \qquad (4.14)$$

This expression is homogeneous of degree $\left(\frac{n+1}{n}\right)$ in e_1, e_2, k_1, k_2, and with equations 4.7 leads

to the relatively simple relations:

$$
\begin{aligned}
t_1 &= \left(\frac{4}{3}\right)^{\frac{n+1}{2n}} F_3^{\frac{1-n}{2n}} \left(e_1 + \tfrac{1}{2} e_2\right) \\
t_2 &= \left(\frac{4}{3}\right)^{\frac{n+1}{2n}} F_3^{\frac{1-n}{2n}} \left(e_2 + \tfrac{1}{2} e_1\right) \\
m_1 &= \left(\frac{4}{3}\right)^{\frac{n+1}{2n}} F_3^{\frac{1-n}{2n}} 4\left(\frac{n}{2n+1}\right)^{\frac{2n}{n+1}} \left(k_1 + \tfrac{1}{2} k_2\right) \\
m_2 &= \left(\frac{4}{3}\right)^{\frac{n+1}{2n}} F_3^{\frac{1-n}{2n}} 4\left(\frac{n}{2n+1}\right)^{\frac{2n}{n+1}} \left(k_2 + \tfrac{1}{2} k_1\right)
\end{aligned}
\tag{4.15}
$$

where

$$
F_3 = \left[\left(e_1^2 + e_1 e_2 + e_2^2\right) + 4\left(\frac{n}{2n+1}\right)^{\frac{2n}{n+1}} \left(k_1^2 + k_1 k_2 + k_2^2\right)\right]
$$

These are the approximate relations which are investigated in this work and used in the solution of boundary value problems.. They are compared with the exact relations in paragraph 4.4. Other approximate relations are discussed in paragraph 4.5.

4.4. Comparison of exact and approximate relations

A comparison of the exact and approximate relations may be made by comparing the surfaces

$$\psi = \alpha$$

and $$\psi_{APP} = \alpha$$

where α is a constant.

It is convenient to take $\alpha = 1$; the curve of intersection with the plane $k_1 = k_2 = 0$ defined by equation 4.10 is then the same for all values of n.

As the approximate relations are intended in the first instance for the analysis of circular cylindrical shells, the comparison of Ψ- surfaces is made with

$$k_2 = 0$$

(in the circular cylindrical shell the curvature change in the circumferential direction may be disregarded for small displacements).

With $k_2 = 0$, the surfaces $\Psi = 1$ and $\Psi_{APP} = 1$ are reduced to three-dimensional space. From equation 4.8, $\Psi = 1$ becomes

$$\frac{1}{2}\left(\frac{4}{3}\right)^{\frac{n+1}{2n}} \int_{-1}^{+1} \left[\left(e_1^2 + e_1 e_2 + e_2^2\right) + 4\rho k_1\left(e_1 + \tfrac{1}{2}e_2\right) + 4\rho^2 k_1^2\right]^{\frac{n+1}{2n}} d\rho = 1 \qquad (4.16)$$

and, from equation 4.14, $\Psi_{APP} = 1$ becomes

$$\left(\frac{4}{3}\right)\left[\left(e_1^2 + e_1 e_2 + e_2^2\right) + 4\left(\frac{n}{2n+1}\right)^{\frac{2n}{n+1}} k_1^2\right] = 1 \qquad (4.17)$$

The curve of intersection of these surfaces with the plane $k_1 = 0$ is shown in Fig 4.2.

From equation 4.17 it follows that the surfaces $\psi_{APP} = 1$ are symmetrical about the plane $k_1 = 0$. Equation 4.17 is also symmetrical in e_1 and e_2 and it can thus be deduced that the $\psi_{APP} = 1$ surfaces are the same in all four quadrants of Fig 4.3.

That the $\psi = 1$ surfaces are also symmetrical about the plane $k_1 = 0$ can be established from equations 4.2 which, written in non-dimensional form with $k_2 = 0$, are:

$$\frac{\sigma_1}{\sigma_0} = \left(\frac{4}{3}\right)^{\frac{n+1}{2n}} \left[\left(e_1^2 + e_1 e_2 + e_2^2\right) + 4\rho k_1 \left(e_1 + \tfrac{1}{2} e_2\right) + 4\rho^2 k_1^2\right]^{\frac{1-n}{2n}}$$

$$\times \left[\left(e_1 + \tfrac{1}{2} e_2\right) + 2\rho k_1\right]$$

$$\frac{\sigma_2}{\sigma_0} = \left(\frac{4}{3}\right)^{\frac{n+1}{2n}} \left[\left(e_1^2 + e_1 e_2 + e_2^2\right) + 4\rho k_1 \left(e_1 + \tfrac{1}{2} e_2\right) + 4\rho^2 k_1^2\right]^{\frac{1-n}{2n}} \qquad (4.18)$$

$$\times \left[\left(e_2 + \tfrac{1}{2} e_1\right) + \rho k_1\right]$$

The values of $\frac{\sigma_1}{\sigma_0}$ and $\frac{\sigma_2}{\sigma_0}$ at $\rho = +\rho_1$ for the deformation state $(e_1, e_2, +k_1)$ are the same as those at $\rho = -\rho_1$ for the state $(e_1, e_2, -k_1)$. The distributions of $\frac{\sigma_1}{\sigma_0}$ and $\frac{\sigma_2}{\sigma_0}$ through the shell thickness for the two states are shown schematically

in Fig. 4.4. Clearly the values of t_1, t_2, m_1, m_2 to produce the two states differ only in the sense of m_1 and m_2. The $\psi = 1$ surfaces must thus be symmetrical about the plane $k_1 = 0$.

An extension of this argument is used in Appendix 4.3 to show that the $\psi = 1$ surfaces are the same in the diagonal quadrants I, III and II, IV in Fig 4.3. These symmetry properties are also demonstrated mathematically for $n \to \infty$ in Appendix 4.3.

Because of this symmetry, the exact and approximate ψ- surfaces need be compared only in the quadrants I and II. To make the comparison, the intersections of the surfaces with planes $e_2 = \beta e_1$ where $\beta = 1, 0.4$ etc (numbered ① to ⑨ in Fig 4.5) have been computed for $n = 3$, 5 and $n \to \infty$. This computation is straightforward for the $\psi_{APP} = 1$ surfaces, but numerical integration has to be performed for the $\psi = 1$ surfaces. Details are given in Appendix 4.4.

The curves of intersection are plotted for $n = 3$ in Figs 4.6 to 4.10, and for $n \to \infty$ in Figs 4.11 to 4.15. Curves for sections ① and ⑨, ② and ⑧, ③ and ⑦ etc are plotted on the same figure to emphasise the difference in form of the $\psi = 1$ surfaces in quadrants I and II. Similar curves are obtained

for n = 5.

The exact and approximate surfaces are in reasonably close agreement in quadrant II, i.e. between sections (5) and (9), for n = 3 and $n \to \infty$. The surfaces are everywhere identical for n = 1, and it is thus reasonable to conclude that in quadrant II agreement is good for all values of n. In quadrant I, however, agreement is poor, particularly for $n \to \infty$. Agreement is poorest in the region of section (3) ($e_2 = 0$) and Figs 4.16 and 4.17 give further results for this section. Fig 4.16 shows the curves of intersection with the $\psi = 1$ surfaces for n = 1, 1.5, 3, 5 and $n \to \infty$, and Fig 4.17 the corresponding curves for $\psi_{APP} = 1$. Comparison of these two figures shows that agreement improves for smaller values of n.

A direct comparison of the exact and approximate relations at section (3) can be made as follows: from equations 4.6 with $k_2 = e_2 = 0$

$$\frac{t_1}{e_1^{1/n}} = \frac{1}{2}\left(\frac{4}{3}\right)^{\frac{n+1}{2n}} \int_{-1}^{+1} \left[1 + 4\varsigma\left(\frac{k_1}{e_1}\right) + 4\varsigma^2\left(\frac{k_1}{e_1}\right)^2\right]^{\frac{1-n}{2n}} \left[1 + 2\varsigma\left(\frac{k_1}{e_1}\right)\right] d\varsigma$$

$$\frac{t_2}{e_1^{1/n}} = \frac{1}{2}\,\frac{t_1}{e_1^{1/n}}$$

$$\frac{m_1}{k_1^{1/n}} = \left(\frac{4}{3}\right)^{\frac{n+1}{2n}} \left(\frac{e_1}{k_1}\right)^{1/n} \int_{-1}^{+1} \left[1 + 4\varsigma\left(\frac{k_1}{e_1}\right) + 4\varsigma^2\left(\frac{k_1}{e_1}\right)^2\right]^{\frac{1-n}{2n}} \left[1 + 2\varsigma\left(\frac{k_1}{e_1}\right)\right] \varsigma\, d\varsigma \qquad (4.19)$$

$$\frac{m_2}{k_1^{1/n}} = \frac{1}{2}\,\frac{m_1}{k_1^{1/n}}$$

As shown in appendix 4.5, the integrals in equations 4.19 can be evaluated analytically,

and $\frac{t_1}{e_1^{1/n}}$, $\frac{t_2}{e_1^{1/n}}$, $\frac{m_1}{k_1^{1/n}}$, $\frac{m_2}{k_1^{1/n}}$

may be plotted against $\frac{k_1}{e_1}$.

The corresponding approximate relations are from equations 4.15:

$$\frac{t_1}{e_1^{1/n}} = \left(\frac{4}{3}\right)^{\frac{n+1}{2n}} \left[1 + 4\left(\frac{n}{2n+1}\right)^{\frac{2n}{n+1}} \left(\frac{k_1}{e_1}\right)^2\right]^{\frac{1-n}{2n}}$$

$$\frac{t_2}{e_1^{1/n}} = \frac{1}{2} \frac{t_1}{e_1^{1/n}}$$

$$\frac{m_1}{k_1^{1/n}} = \left(\frac{4}{3}\right)^{\frac{n+1}{2n}} \left[1 + 4\left(\frac{n}{2n+1}\right)^{\frac{2n}{n+1}} \left(\frac{k_1}{e_1}\right)^2\right]^{\frac{1-n}{2n}} 4\left(\frac{n}{2n+1}\right)^{\frac{2n}{n+1}} \left(\frac{k_1}{e_1}\right)^{\frac{n-1}{n}} \qquad (4.20)$$

$$\frac{m_2}{k_1^{1/n}} = \frac{1}{2} \frac{m_1}{k_1^{1/n}}$$

Equations 4.19 and 4.20 are plotted in Figs 4.18 to 4.21 for n = 1.5, 3, 5 and $n \to \infty$. To allow comparison for all values of $\frac{k_1}{e_1}$, $\frac{t_1}{e_1^{1/n}}$ and $\frac{m_1}{k_1^{1/n}}$ have been plotted against $\frac{k_1}{e_1}$ from 0 to 1 and against the reciprocal of $\frac{k_1}{e_1}$ from 1 to 0, the two graphs being drawn adjacently. These results give a measure of the divergence of the approximate and exact relations and

confirm that this divergence is reduced for the smaller values of n.

Similar comparison may be made for other sections, but the integrals in the exact relations have to be evaluated numerically. The results for section (7) ($e_1 = 0$) are shown in Figs 4:22 and 4.23 for $n = 3$ and $n \to \infty$ respectively. Section (7) is typical of the region in which there is close agreement between the exact and approximate ψ – surfaces. Although agreement is good for t_2 and m_1 it is poorer for t_1 and m_2. The latter are proportional to the components of the gradient in the e_1 and k_2 directions which are not apparent from Figs 4.8 and 4.13. A similar result is shown in Fig 4.24 for section (5) ($e_2 = - e_1$) with $n = 3$.

Figs 4.25 and 4.26 show the relations for section (6) at which $e_1 = - \frac{1}{2} e_2$. It is shown in Appendix 4.6 that the condition $e_1 = - \frac{1}{2} e_2$ gives $t_1 = 0$, and the relations in Figs 4.25 and 4.26 are those to be used in the analysis of a circular cylindrical shell without axial load. There is reasonable agreement between the exact and approximate relations for $n = 3$ and $n \to \infty$, and similar agreement will exist for all values of $n > 1$.

4.5 Discussion

While a detailed comparison has shown that there are some fundamental differences between the exact relations and the approximate ones suggested in this chapter, there is enough agreement to warrant the use of the approximate relations in the analysis of circular cylindrical shells. The errors incurred will depend on the particular problem and on the value of n. For example, results for a cylinder without axial load would be expected to agree closely for all values of n with the results which would be obtained if the exact relations were used. Other boundary value problems may involve a domain of the ψ-surfaces where agreement with the exact relations is poor, particularly for large values of n.

A convenient approach is to solve particular problems with the approximate relations and then, from the displacements obtained, to determine the domain of the ψ-surfaces in which the solution lies. If necessary, refinements might then be made to the approximate relations to give better local agreement and the solution repeated. For example, the following approximate expression for ψ might be considered:

$$\psi_{APP2} = \left(\frac{4}{3} F\right)^{\frac{n+1}{2n}} \qquad (4.21)$$

where $$F = \left[A_1 (e_1^2 + e_1 e_2 + e_2^2) + A_2 \, 4 \left(\frac{n}{2n+1}\right)^{\frac{2n}{n+1}} (k_1^2 + k_1 k_2 + k_2^2)\right]$$

In paragraph 4.3, A_1 and A_2 were taken as unity to give agreement with ψ when $k_1 = k_2 = 0$ and $e_1 = e_2 = 0$. If either or both of these restrictions is relaxed, better general agreement can be obtained at particular sections.

At section (3) there is a discontinuity in the exact relations for $n \to \infty$ as seen in Fig 4.21. It occurs at $\frac{k_1}{e_1} = 0.5$; for values of $\frac{k_1}{e_1}$ from 0 to 0.5, $m_1 = 0$ and $t_1 =$ constant. This can also be seen from the ψ-surface in Fig 4.13, the gradient to the ψ-surface for $k_1 \leq 0.5\, e_1$ being parallel to the $e_1 - e_2$ plane. An explanation is offered in Appendix 4.7.

In their analysis of a boundary value problem in a thin cylinder, Bieniek and Freudenthal[11] assumed that forces t_1, t_2 are independent of mid-surface curvature changes k_1, k_2 and that moments m_1, m_2 are independent of mid-surface strains e_1, e_2. The relations they used are derived from one of the possible expressions for ψ which reduce to equations 4.9, 4.10 and 4.11, namely

$$\psi_{APP.3} = \psi_{(b)} + \psi_{(c)}$$

or

$$\psi_{APP.3} = \left(\frac{4}{3}\right)^{\frac{n+1}{2n}} \left(e_1^2 + e_1 e_2 + e_2^2\right)^{\frac{n+1}{2n}}$$

$$+ 2^{\frac{n+1}{n}} \left(\frac{n}{2n+1}\right)\left(\frac{4}{3}\right)^{\frac{n+1}{2n}} \left(k_1^2 + k_1 k_2 + k_2^2\right)^{\frac{n+1}{2n}} \qquad (4.22)$$

Although there is no coupling between bending and in-plane actions for n = 1, this assumption is a serious simplification for n > 1.

The approximate relations used by Calladine[12] can be reduced to

$$e_1 = \left[\left(t_1^2 - t_1 t_2 + t_2^2\right) + \frac{1}{16 q_1^2} m_1^2\right]^{\frac{n-1}{2}} \left(t_1 - \tfrac{1}{2} t_2\right)$$

$$e_2 = \left[\left(t_1^2 - t_1 t_2 + t_2^2\right) + \frac{1}{16 q_1^2} m_1^2\right]^{\frac{n-1}{2}} \left(t_2 - \tfrac{1}{2} t_1\right) \qquad (4.23)$$

$$k_1 = \frac{q_2}{16 q_1}\left[\left(t_1^2 - t_1 t_2 + t_2^2\right) + \frac{1}{16 q_1^2} m_1^2\right]^{\frac{n-1}{2}} m_1$$

where q_1 and q_2 were parameters, to which values had to be given depending on the index n and the stress state t_1, t_2, m_1.

Calladine obtained one equation between q_1 and q_2 from the relation between bending moment and curvature, for a shell element in bending with the anticlastic curvature suppressed (equations 4.15 with $e_1 = e_2 = k_2 = 0$). Comparison with the third of equations 4.23 for $t_1 = t_2 = 0$ gave a value for $\frac{q_2}{q_1^2}$. A second equation relating q_1 and q_2 was obtained for a particular set of stress states $t_1 = 0$, when the second and third of equations 4.23 give

$$\frac{e_2}{k_1} = \left(\frac{q_2}{16 q_1}\right)^{-1} \cdot \frac{t_2}{m_1}$$

The ratio $\frac{t_2}{m_1}$ was computed numerically for different values of $\frac{e_2}{k_1}$, and for n = 3, to give values for $\frac{q_2}{q_1}$. The latter did not vary widely over the range of $\frac{e_2}{k_1}$ considered, and Calladine selected a value to give, finally, for n = 3

$$q_1 = 0.308$$

$$q_2 = 3.33$$

With these values for q_1 and q_2,

$$\frac{1}{16 q_1^2} = 0.658$$

$$\frac{q_2}{16 q_1} = 0.676$$

Equations 4.23 can be compared with relations obtained by solving equations 4.15 for e_1, e_2 and k_1

with $k_2 = 0$, i.e.

$$e_1 = \left[\left(t_1^2 - t_1 t_2 + t_2^2\right) + \frac{3}{16}\left(\frac{2n+1}{n}\right)^{\frac{2n}{n-1}} m_1^2\right]^{\frac{n-1}{2}} \left(t_1 - \tfrac{1}{2} t_2\right)$$

$$e_2 = \left[\left(t_1^2 - t_1 t_2 + t_2^2\right) + \frac{3}{16}\left(\frac{2n+1}{n}\right)^{\frac{2n}{n-1}} m_1^2\right]^{\frac{n-1}{2}} \left(t_2 - \tfrac{1}{2} t_1\right) \qquad (4.24)$$

$$k_1 = \frac{3}{16}\left(\frac{2n+1}{n}\right)^{\frac{2n}{n-1}} \left[\left(t_1^2 - t_1 t_2 + t_2^2\right) + \frac{3}{16}\left(\frac{2n+1}{n}\right)^{\frac{2n}{n-1}} m_1^2\right] m_1$$

For n = 3, the coefficients corresponding to $\frac{1}{16 q_1^2}$ and $\frac{q_2^2}{16 q_1}$ in equations 4.23 have a value 0.668.

Thus the relations used by Calladine to solve a particular boundary value problem in a cylindrical shell are very near to those proposed more generally here.

It is noted finally that both the $\psi = 1$ and $\psi_{APP.} = 1$ surfaces as plotted in Figs 4.2 and 4.6 to 4.17 are everywhere convex (or flat) but never concave. This has been shown[26] to be a condition for a stable material. The surfaces also show the nesting property, the existence of which has been proved by Calladine and Drucker[6]. A surface for a given value of n lies inside, or in the limit touches, the surface for any larger value of n.

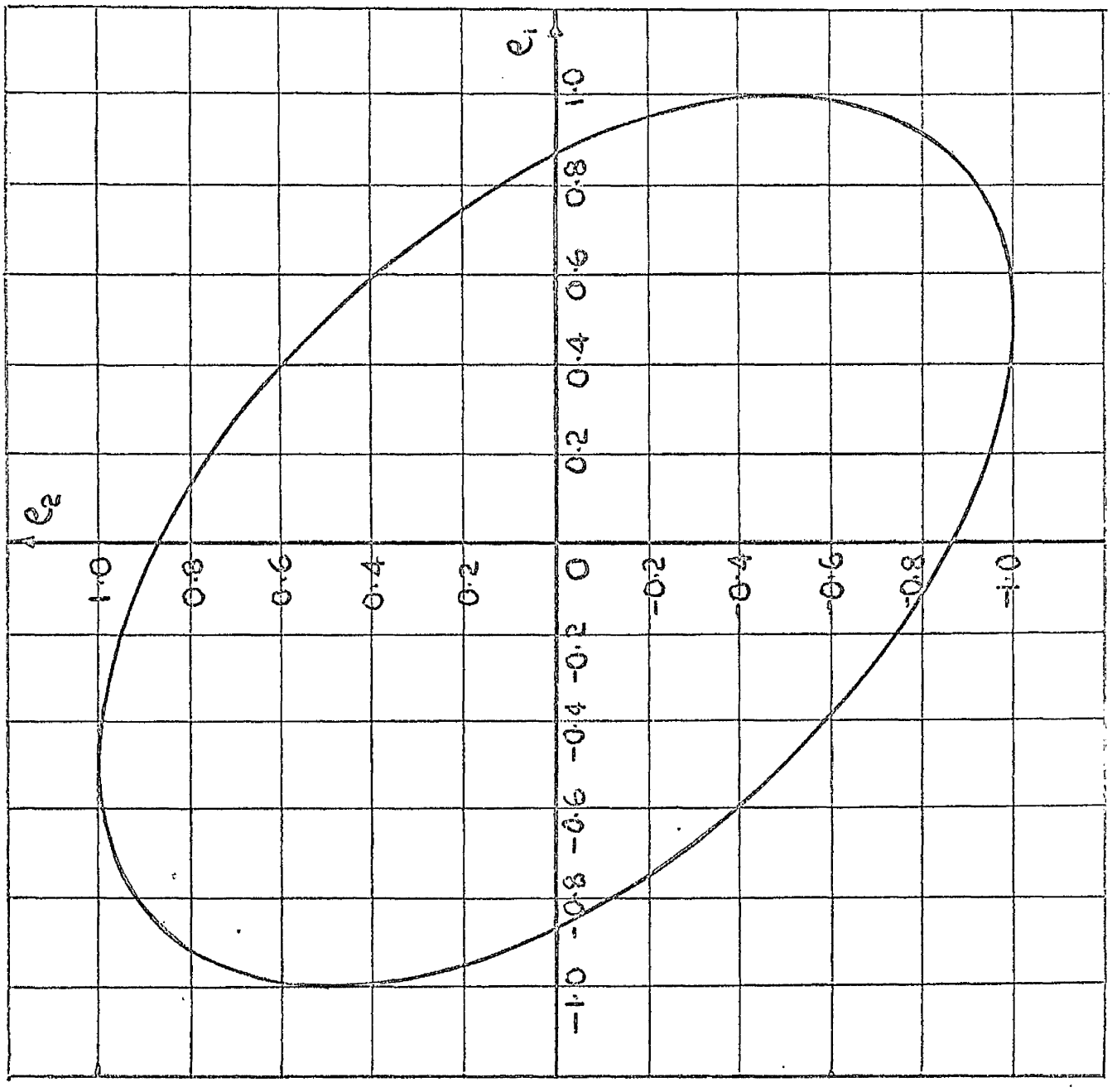

FIG 4.2 INTERSECTION OF ν-SURFACES WITH PLANE $k_3 = 0$

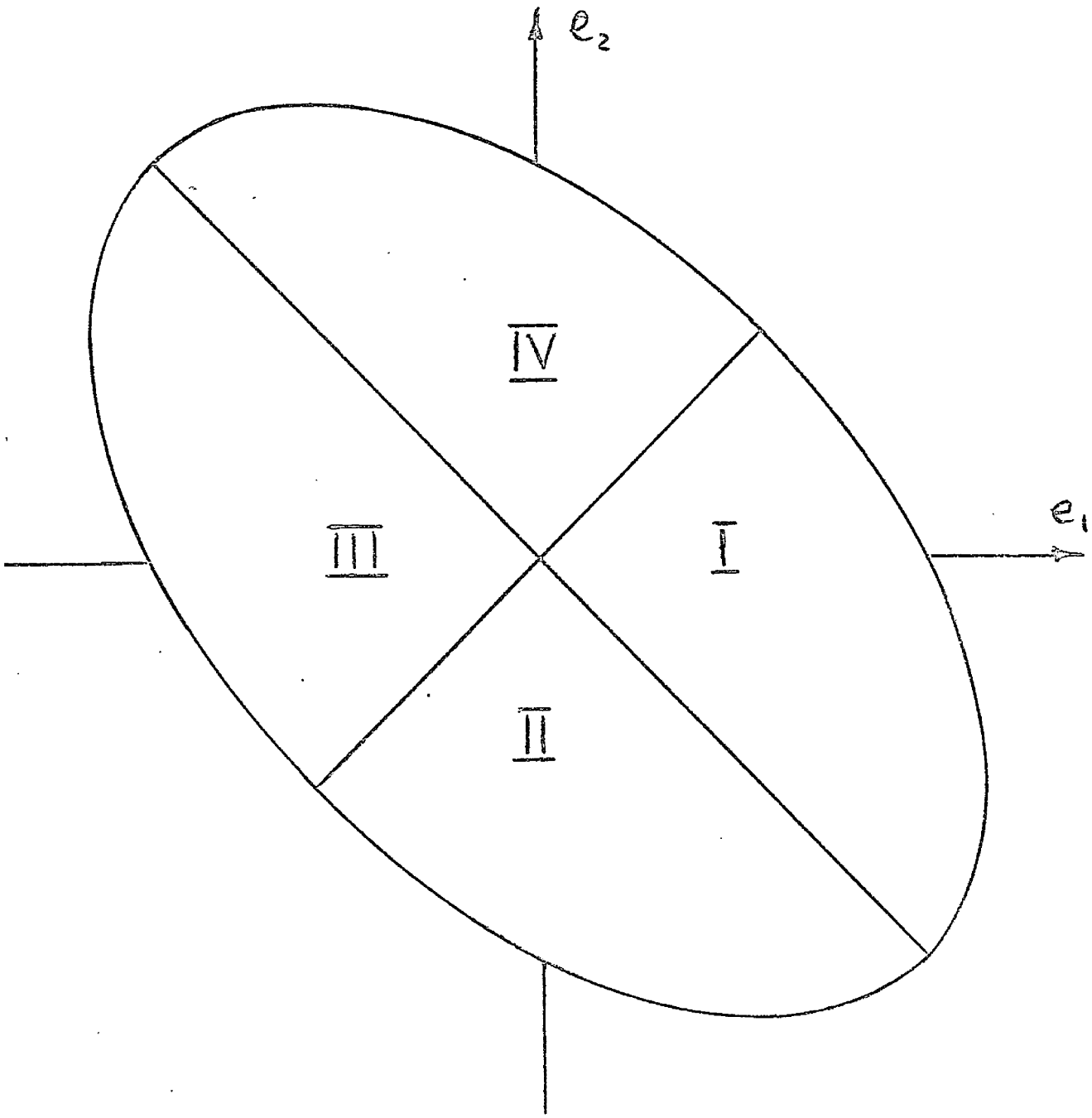

FIG 4.3 QUADRANTS OF THE W-SURFACES

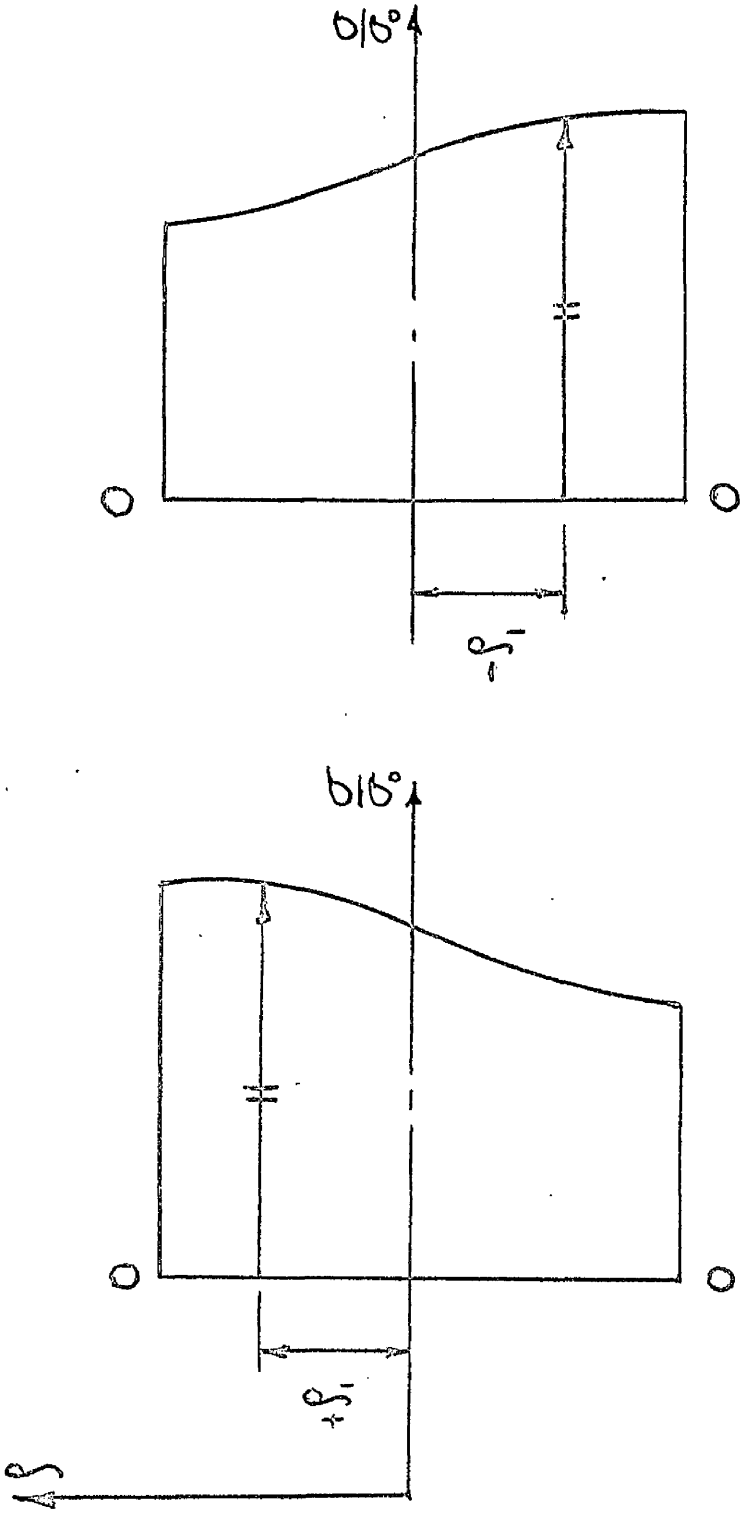

DISTRIBUTION OF (σ/σ_0) AND (σ_z/σ_0) FOR $\pm k_1$

Fig. 4.4

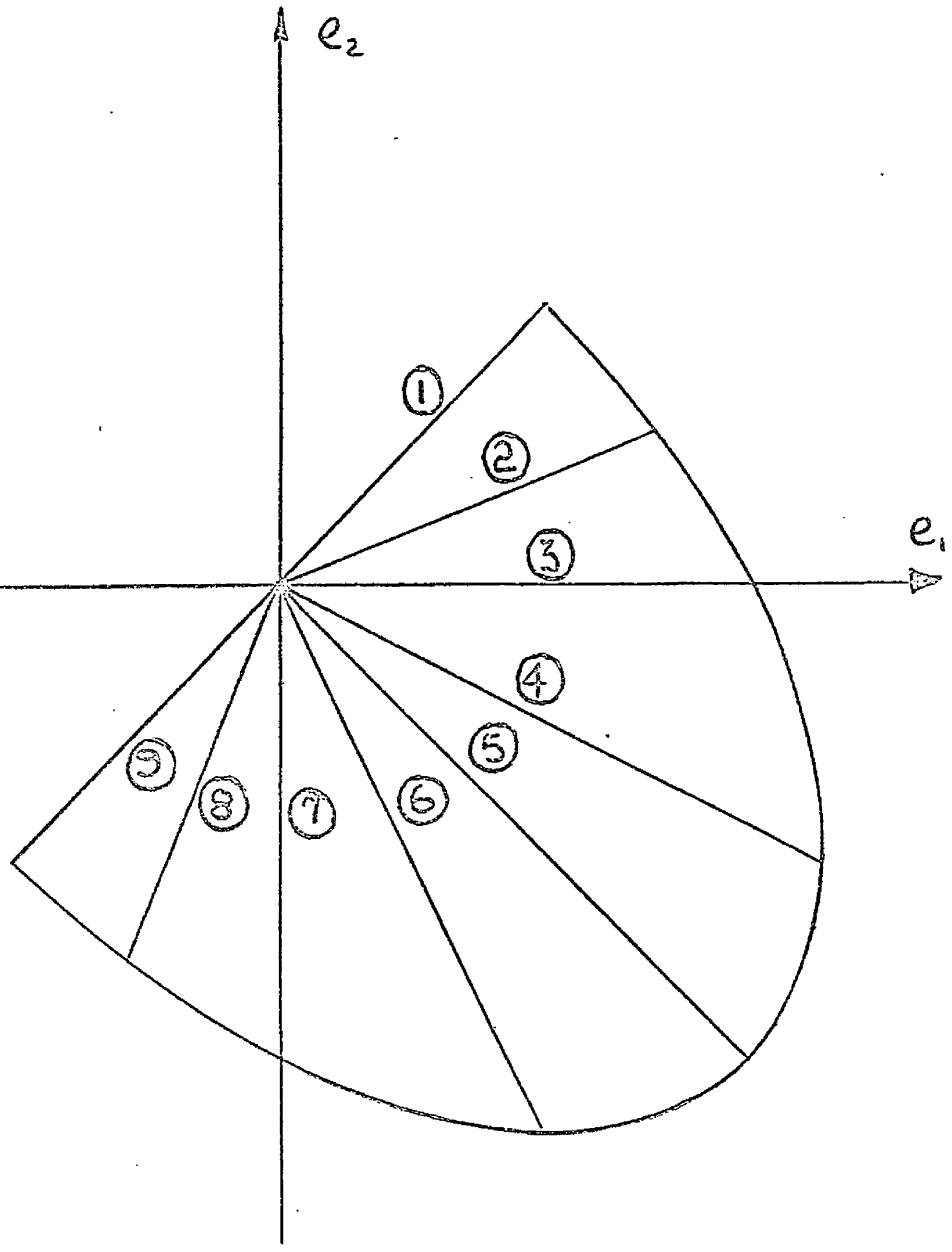

SECTION

①	$e_2 = e_1$
②	$e_2 = 0.4e_1$
③	$e_2 = 0$
④	$e_2 = -0.5e_1$
⑤	$e_2 = -e_1$
⑥	$e_1 = -0.5e_2$
⑦	$e_1 = 0$
⑧	$e_1 = 0.4e_2$
⑨	$e_1 = e_2$

FIG. 4.5

SECTIONS OF THE Ψ-SURFACES

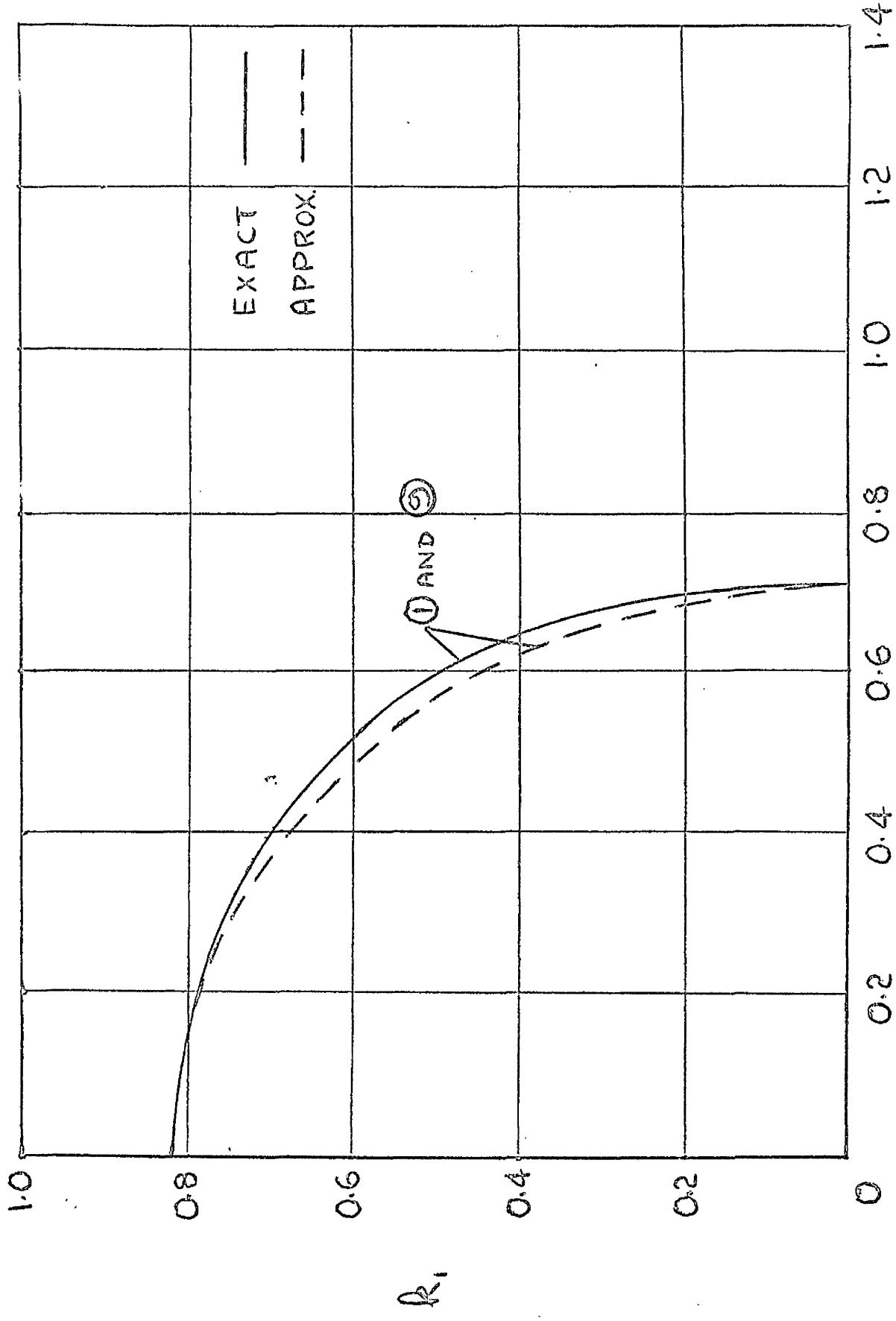

FIG. 4.6 SECTIONS ① AND ⑤ ; n = 3

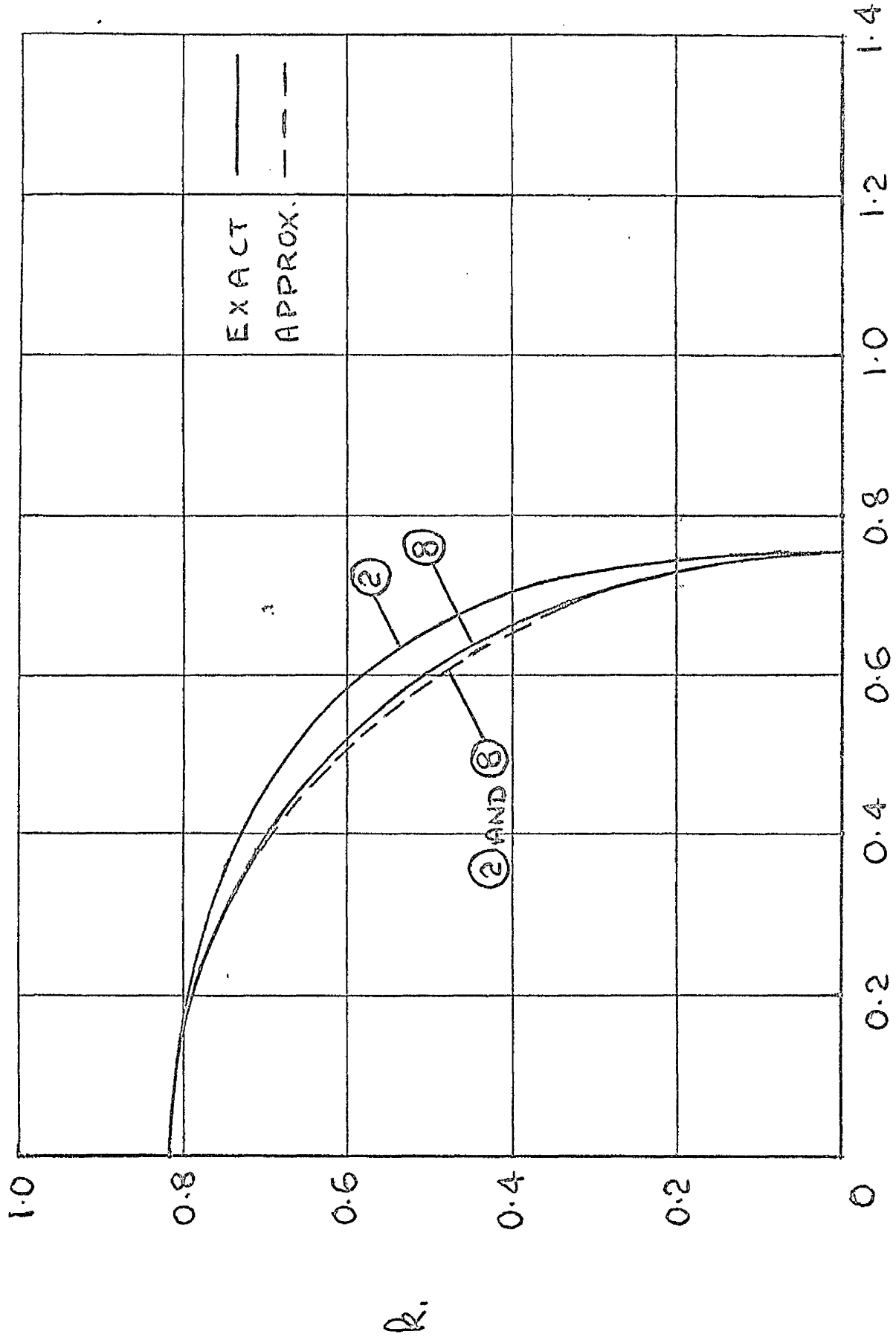

FIG. 4.7 SECTIONS ② AND ⑧ ; $n=3$

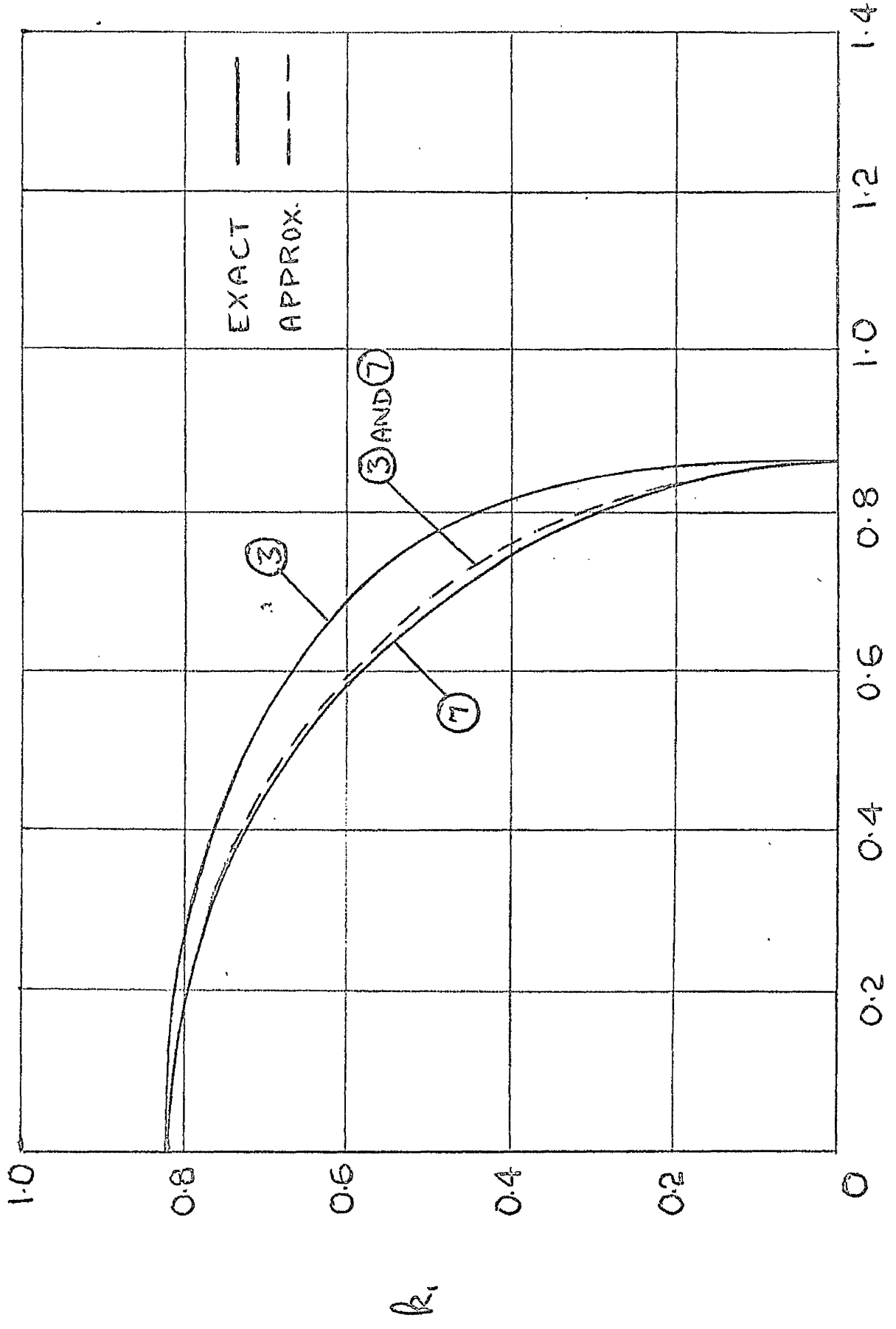

FIG. 4.8 SECTIONS ③ AND ⑦ ; $n=3$

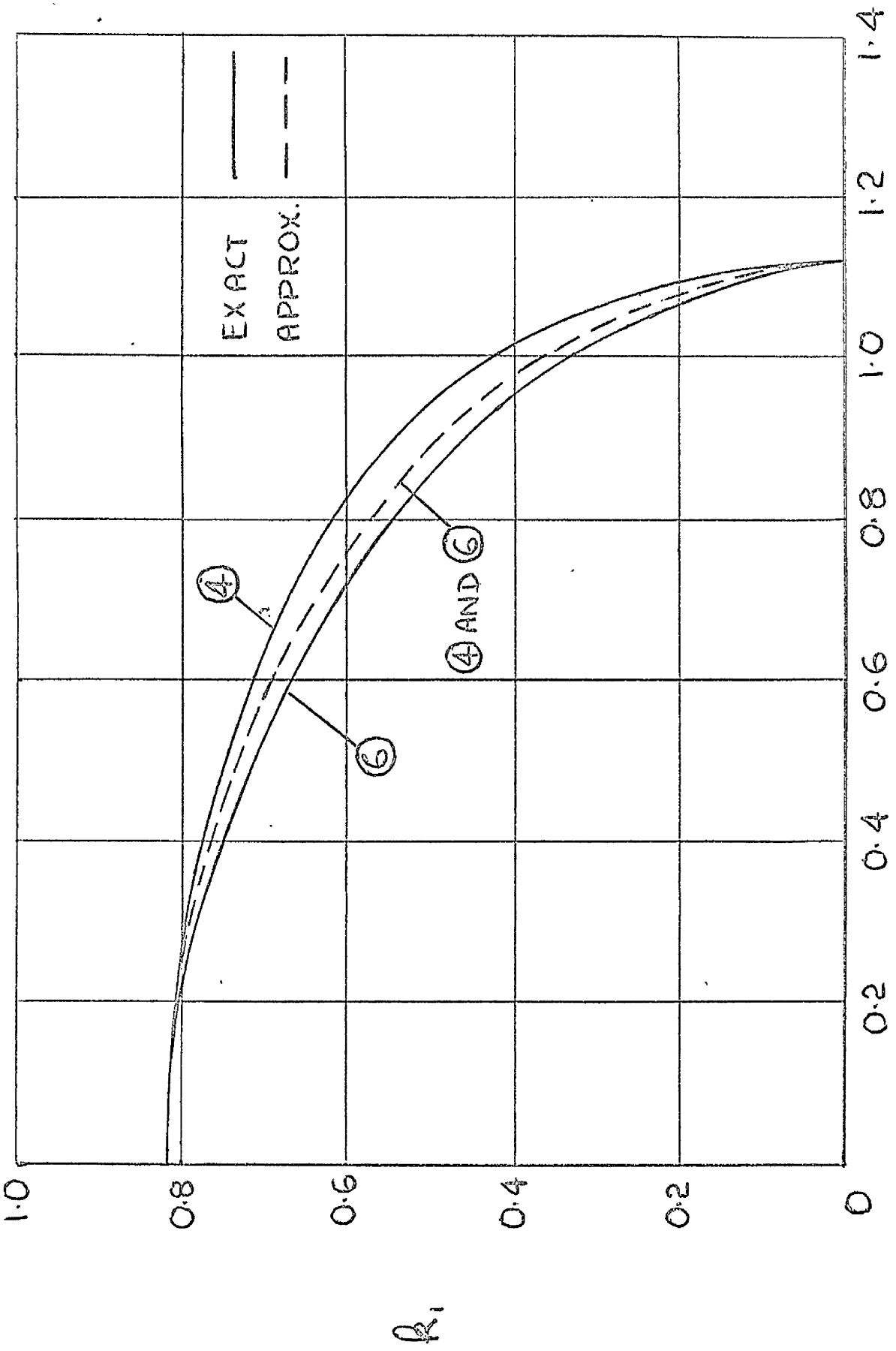

FIG. 4.9 SECTIONS ④ AND ⑥ ; n=3

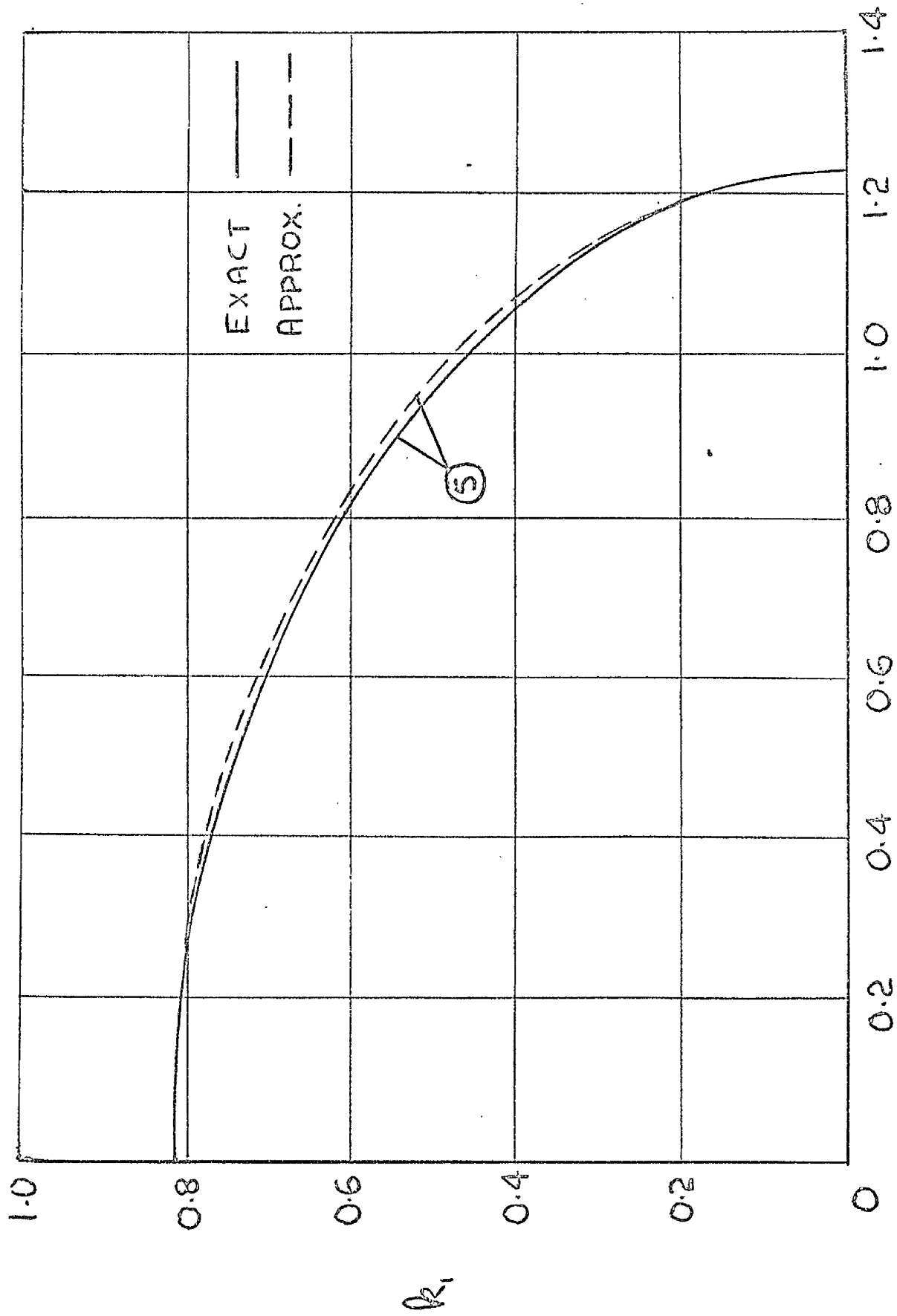

SECTION ⑤ ; n = 3

FIG. 4.10

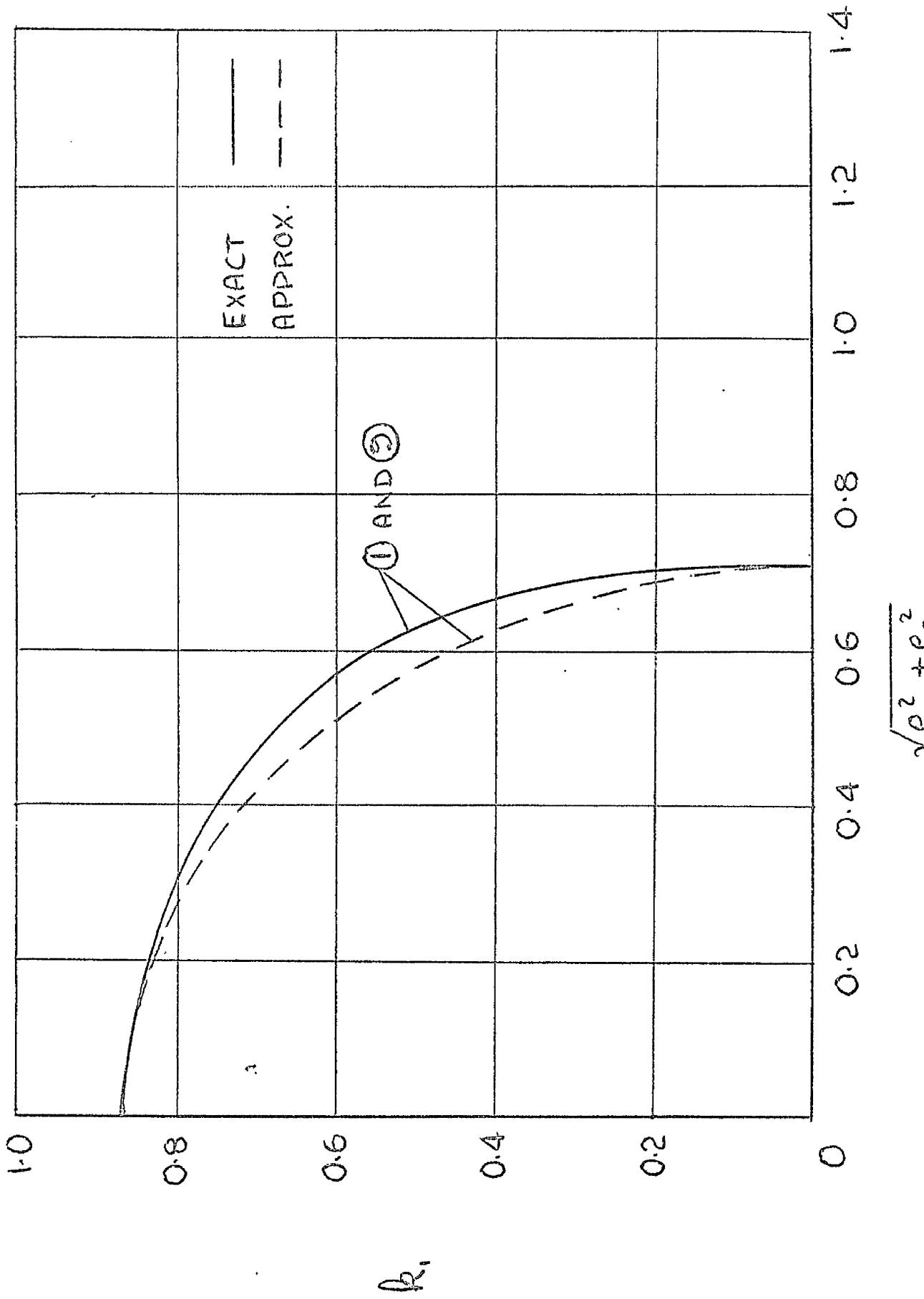

FIG. 4.11 SECTIONS ① AND ② ; $n \to \infty$

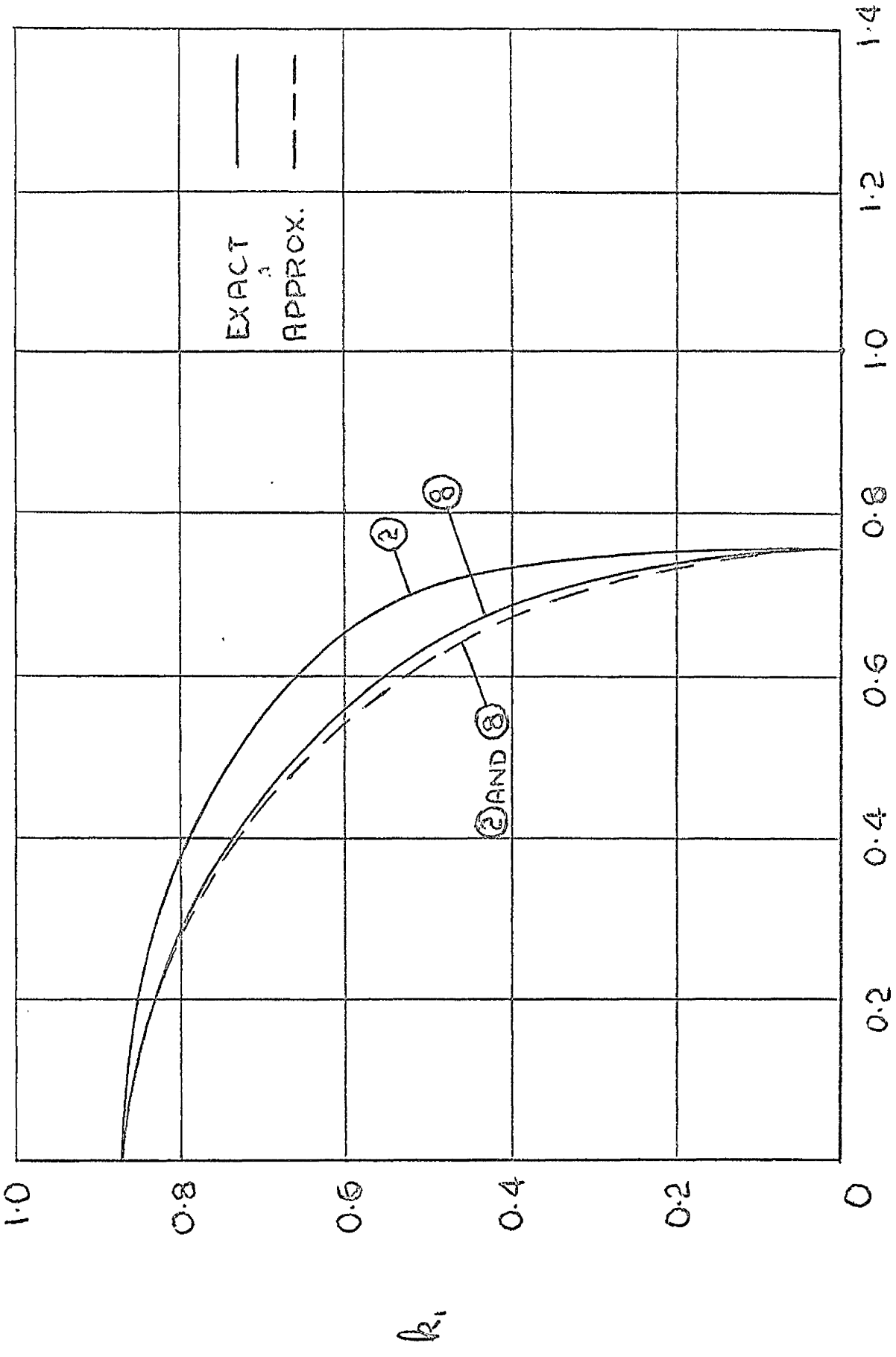

FIG. 4.12 SECTIONS ② AND ⑧ ; $n \to \infty$

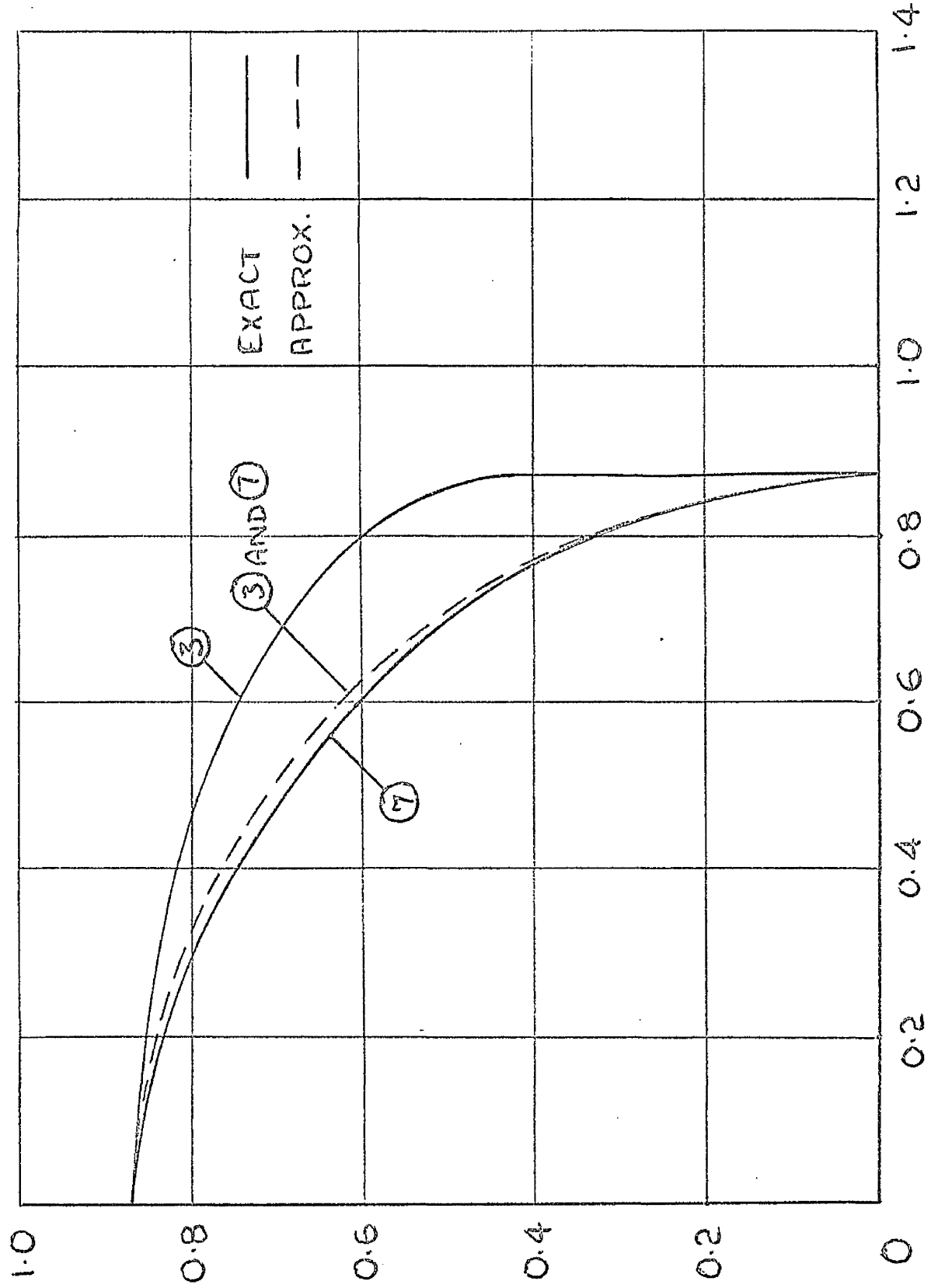

FIG. 4.13 SECTIONS ③ AND ⑦ ; $n \to \infty$

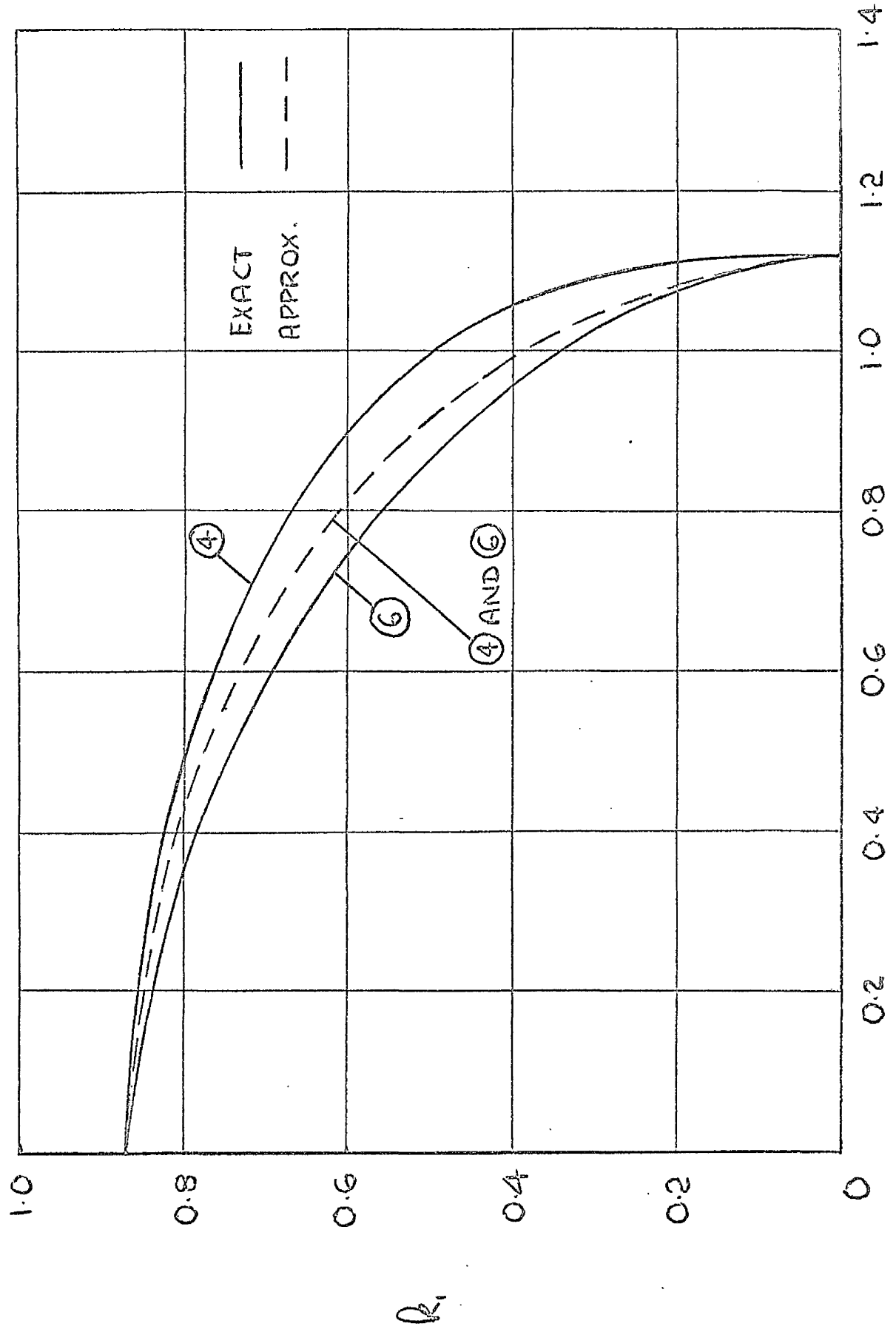

FIG. 4.14 SECTIONS ④ AND ⑥ ; $n \to \infty$

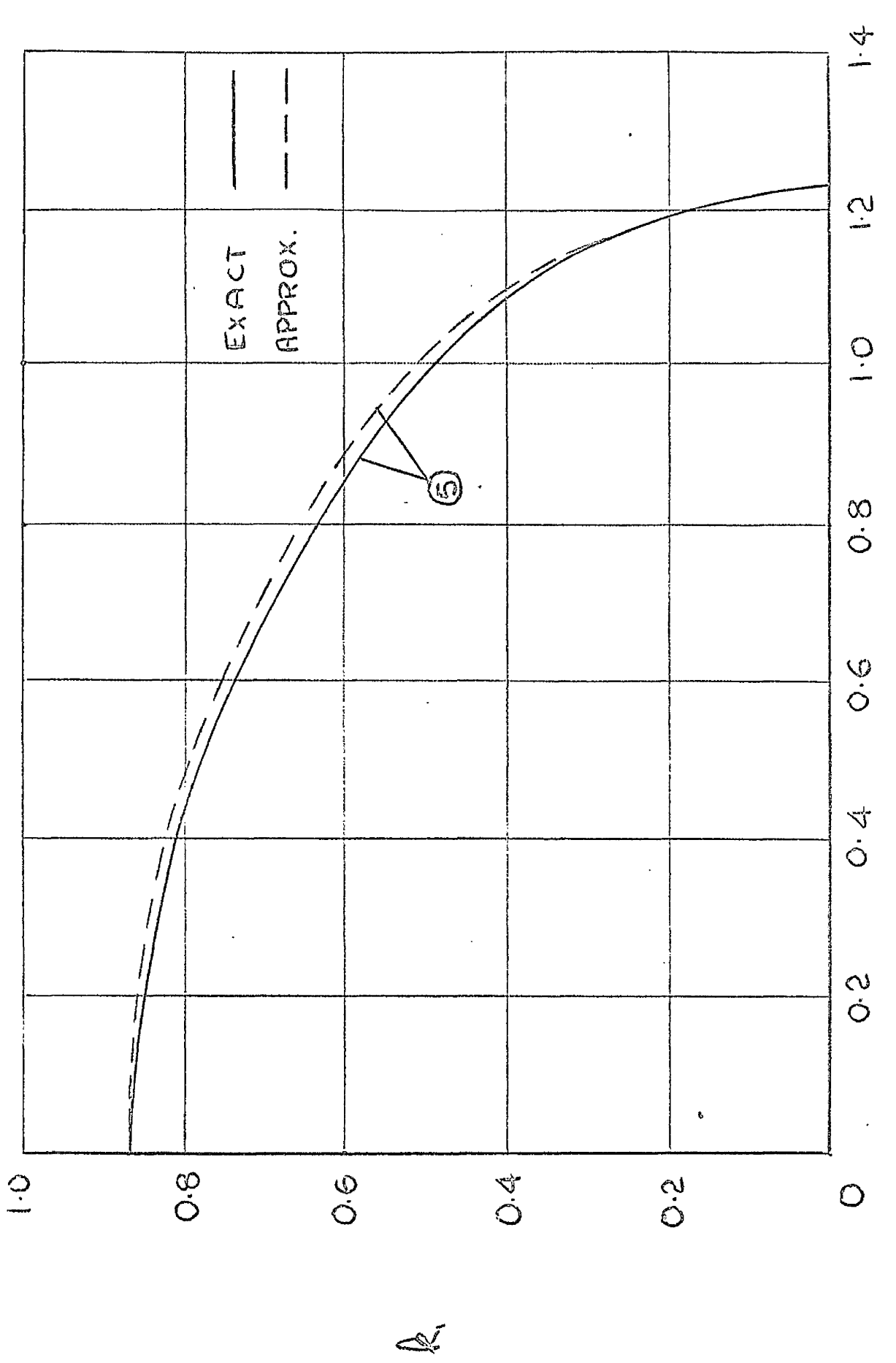

SECTION ⑤ ; $n \to \infty$

FIG. 4.15

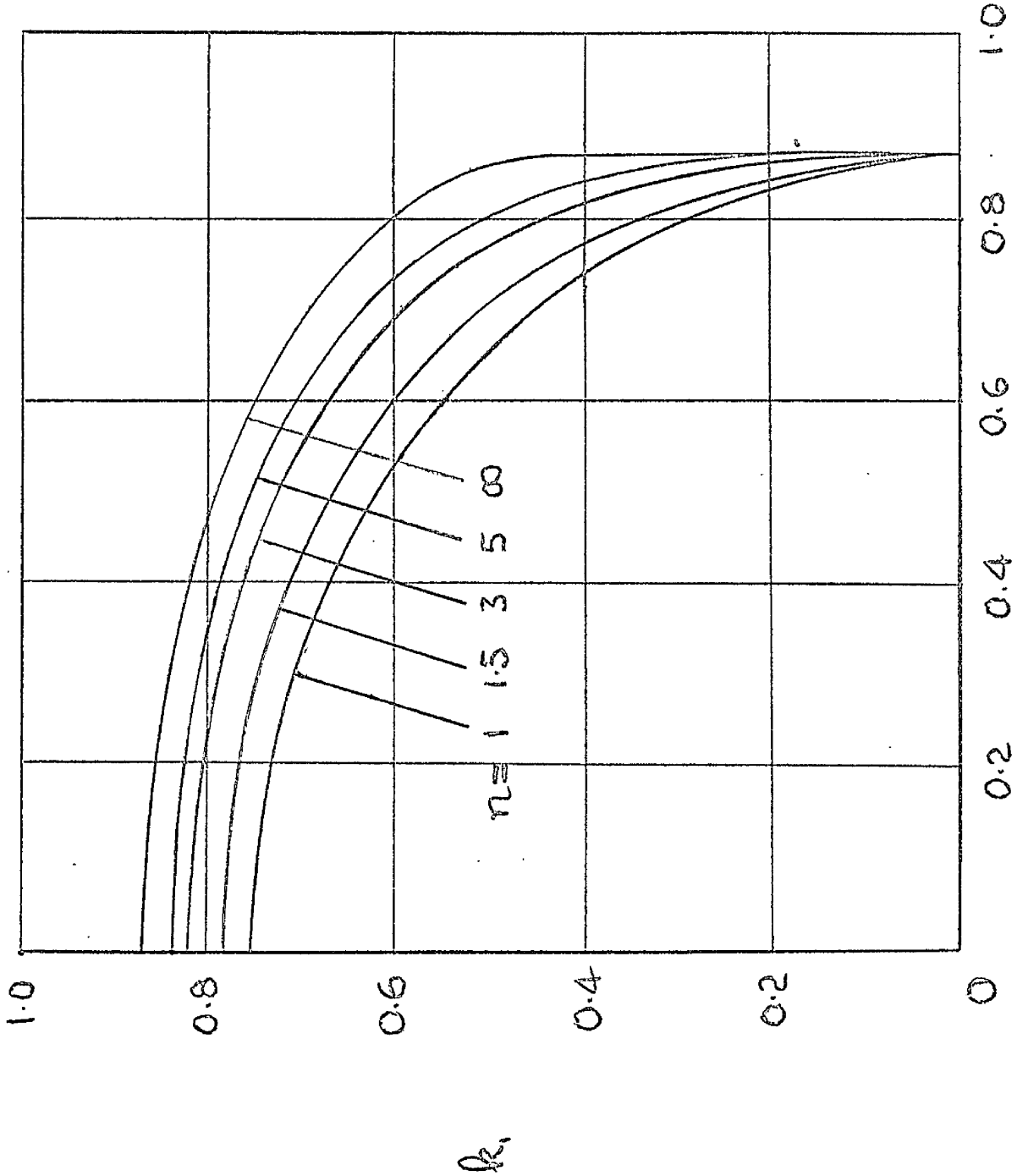

SECTION ③ ; EXACT

FIG. 4.16

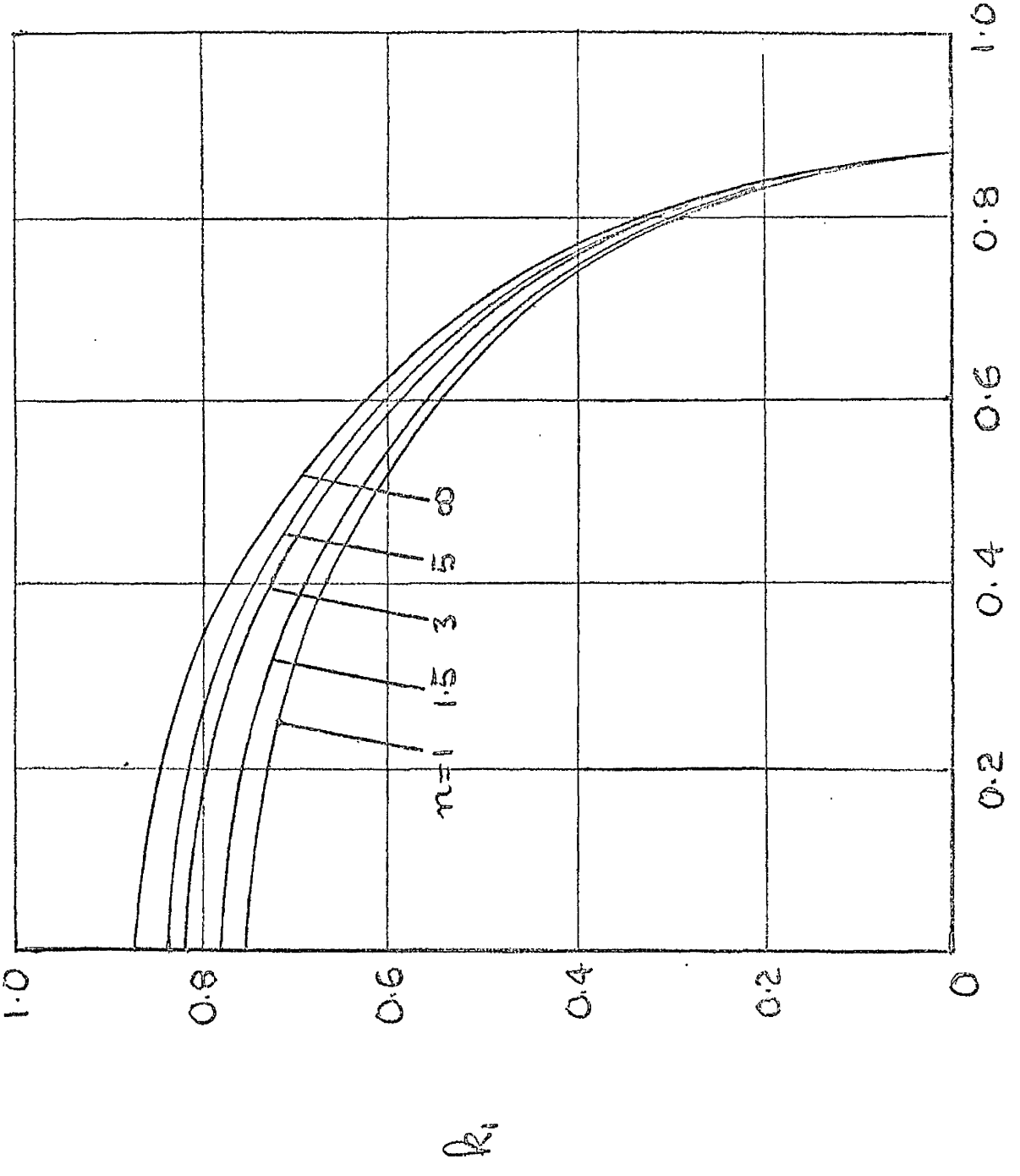

FIG. 4.17 SECTION ③ ; APPROX.

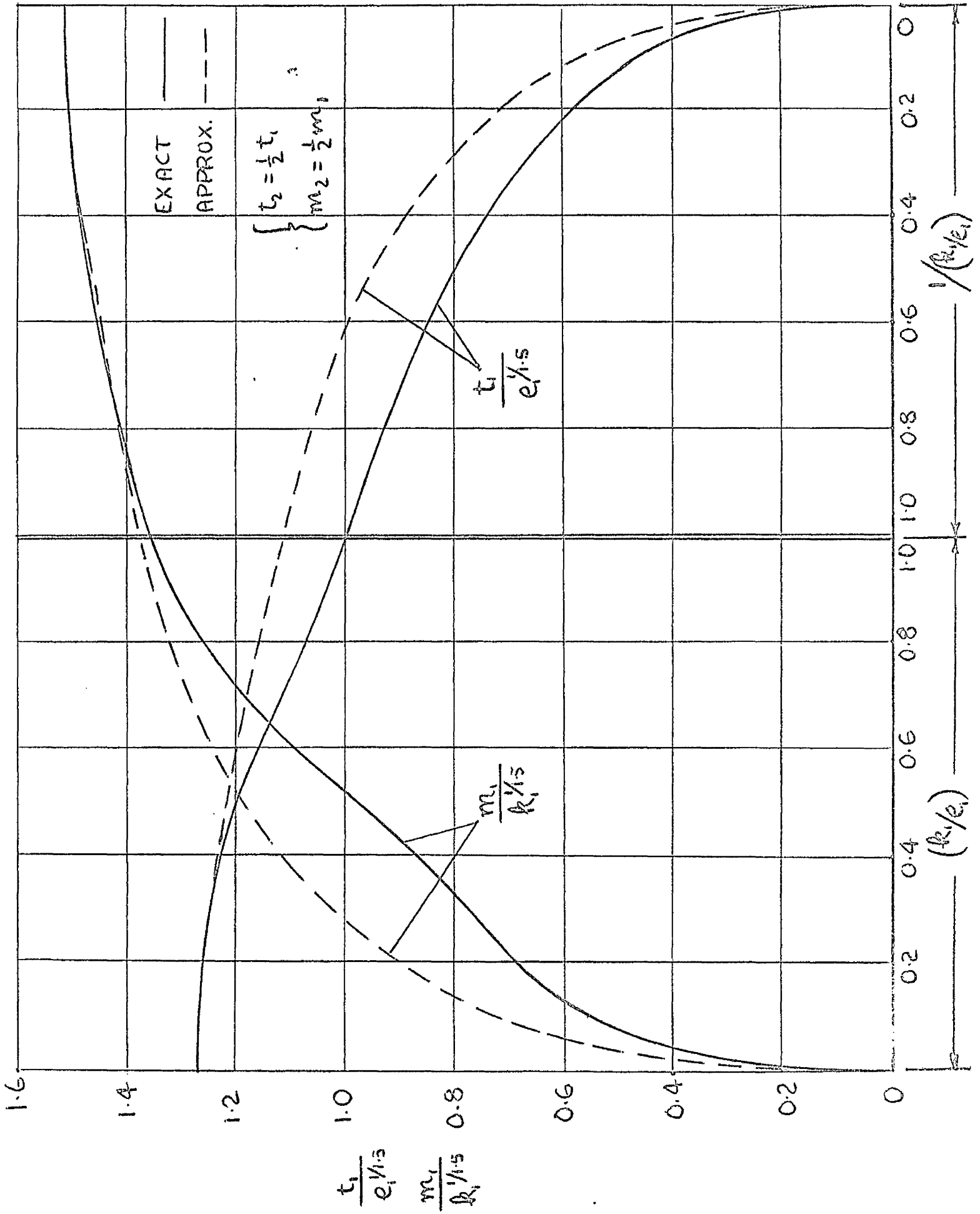
EXACT
APPROX.
$t_2 = \frac{1}{2} t_1$
$m_2 = \frac{1}{2} m_1$
$\frac{t_1}{e_1^{1/1.5}}$
$\frac{m_1}{R_1^{1/1.5}}$
$\frac{t_1}{e_1^{1/1.5}}$ $\frac{m_1}{R_1^{1/1.5}}$
(R_1/e_1)
$1/(R_1/e_1)$
0 0.2 0.4 0.6 0.8 1.0 1.2 1.4 1.6
0 0.2 0.4 0.6 0.8 1.0 1.0 0.8 0.6 0.4 0.2 0

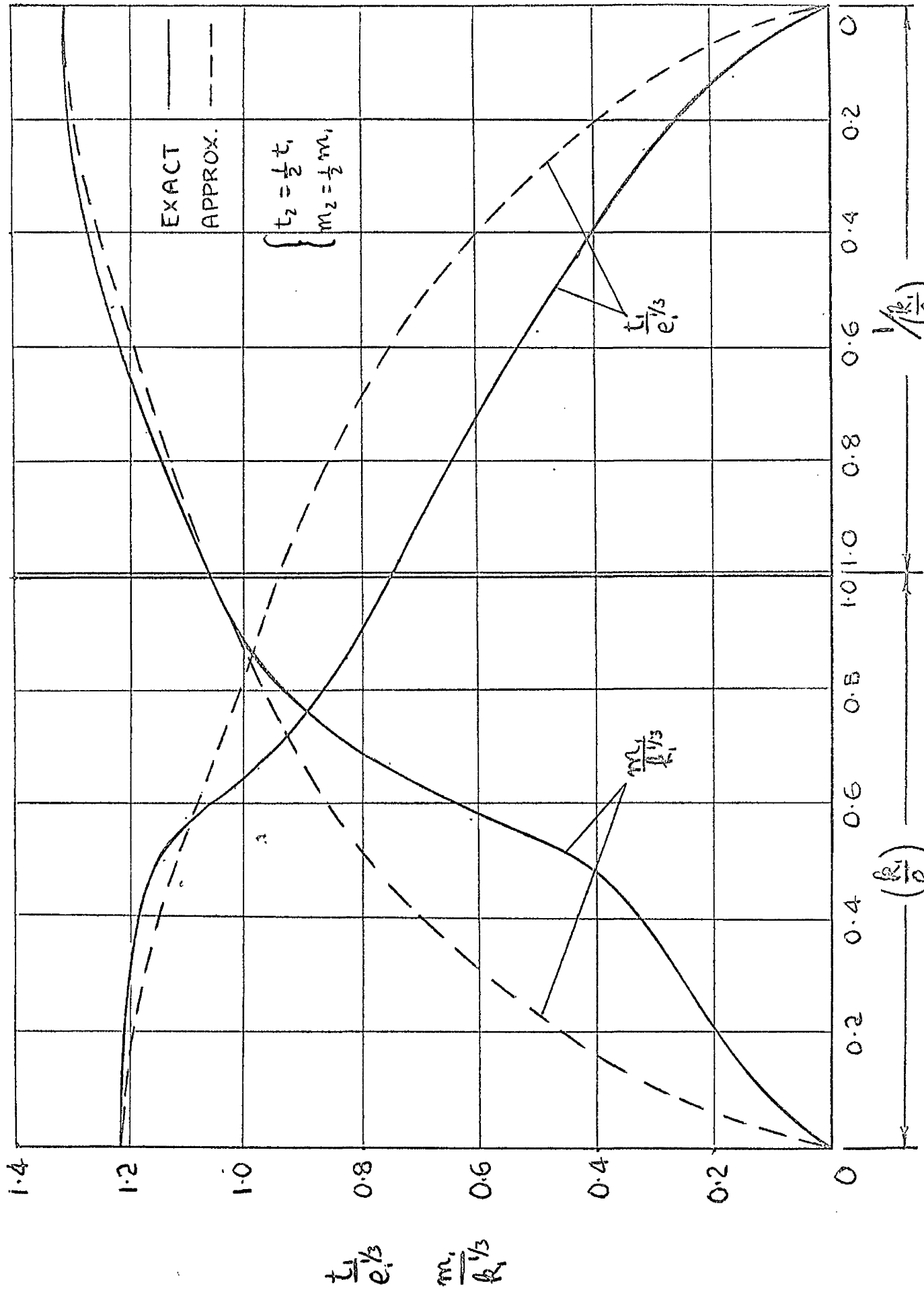

FIG. 4.19 SECTION ③ ; n = 3

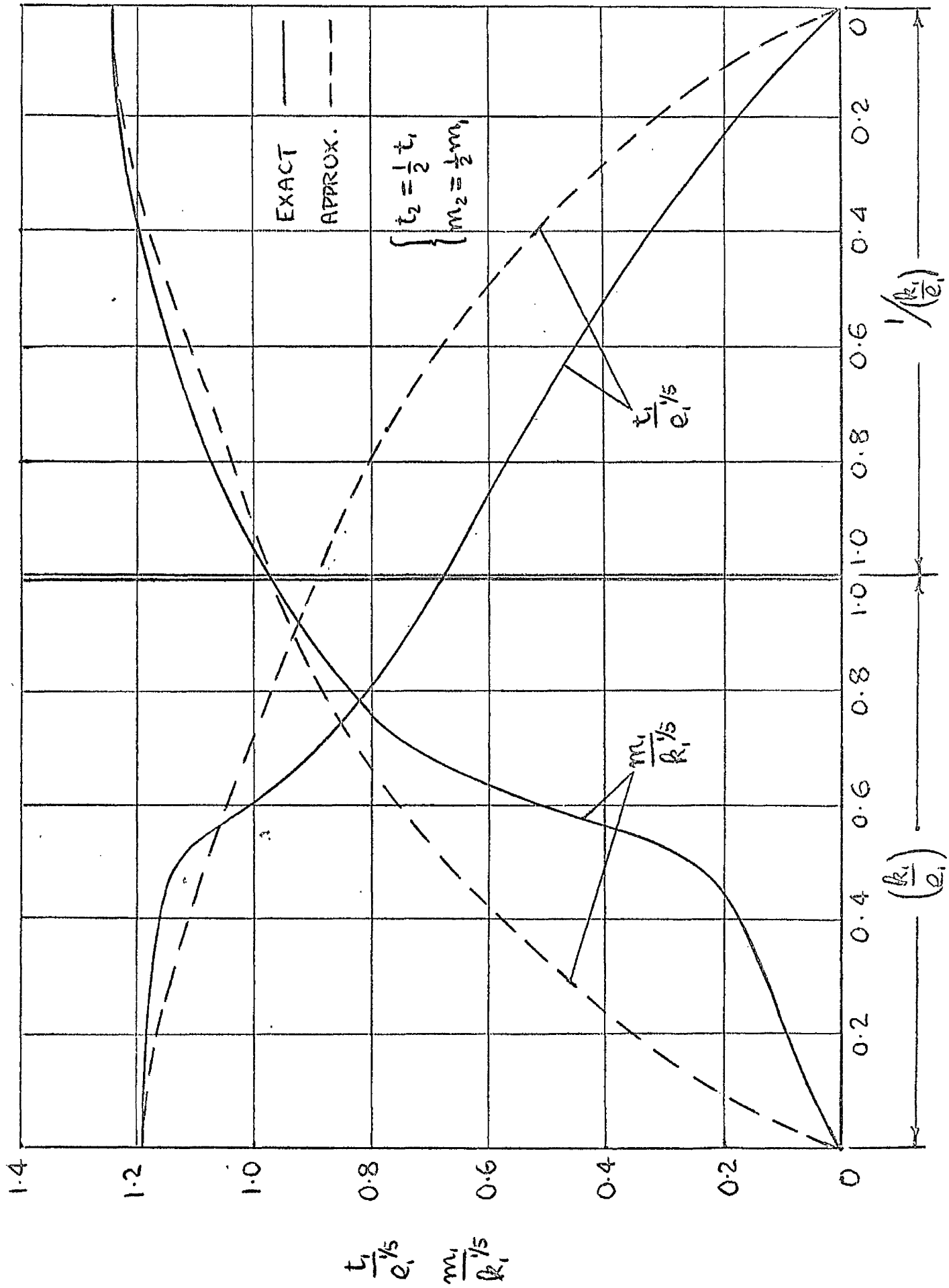

SECTION ③ ; n = 5

FIG. 4.20

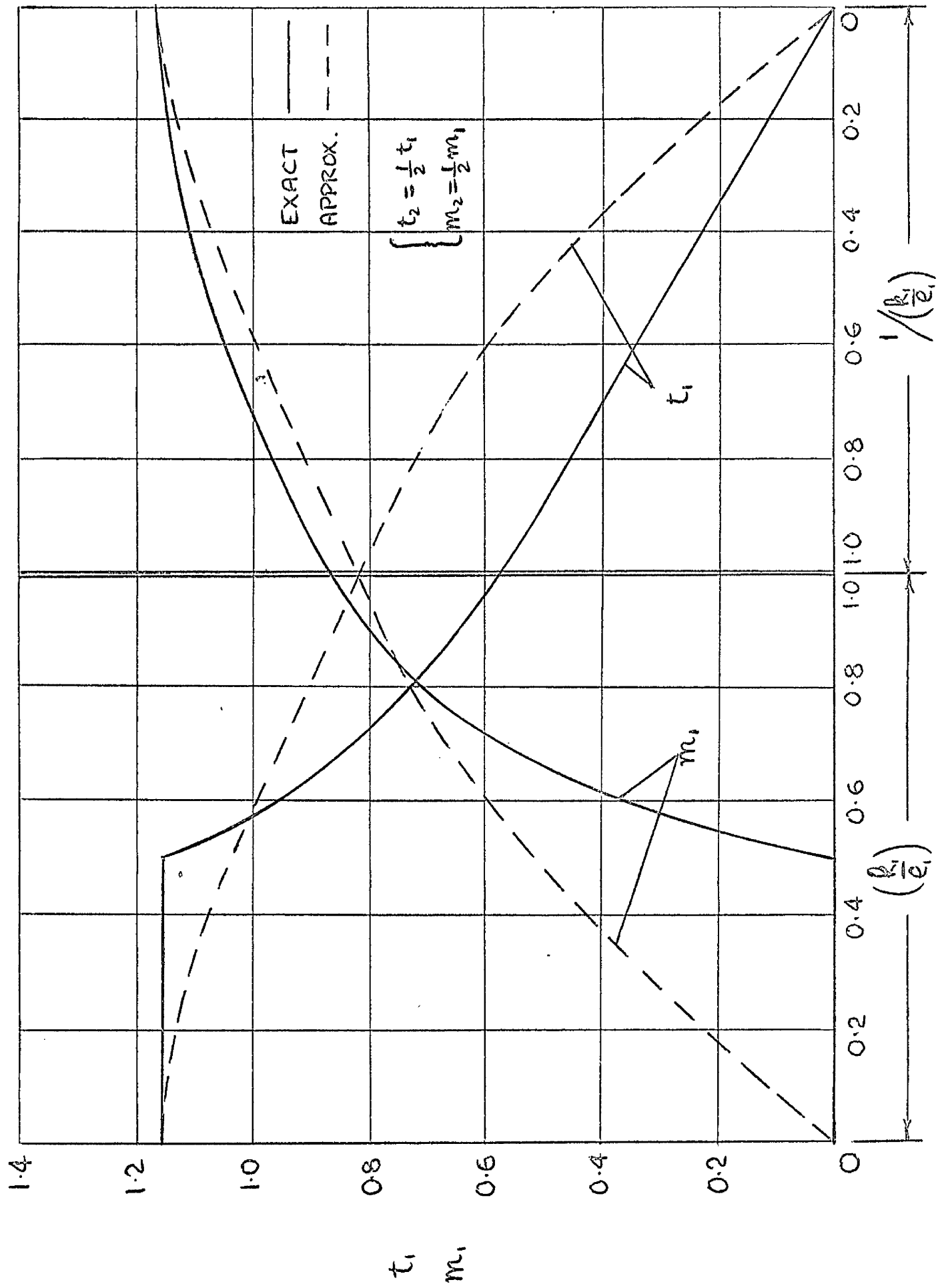

FIG. 4.21 SECTION ③ : $n \to \infty$

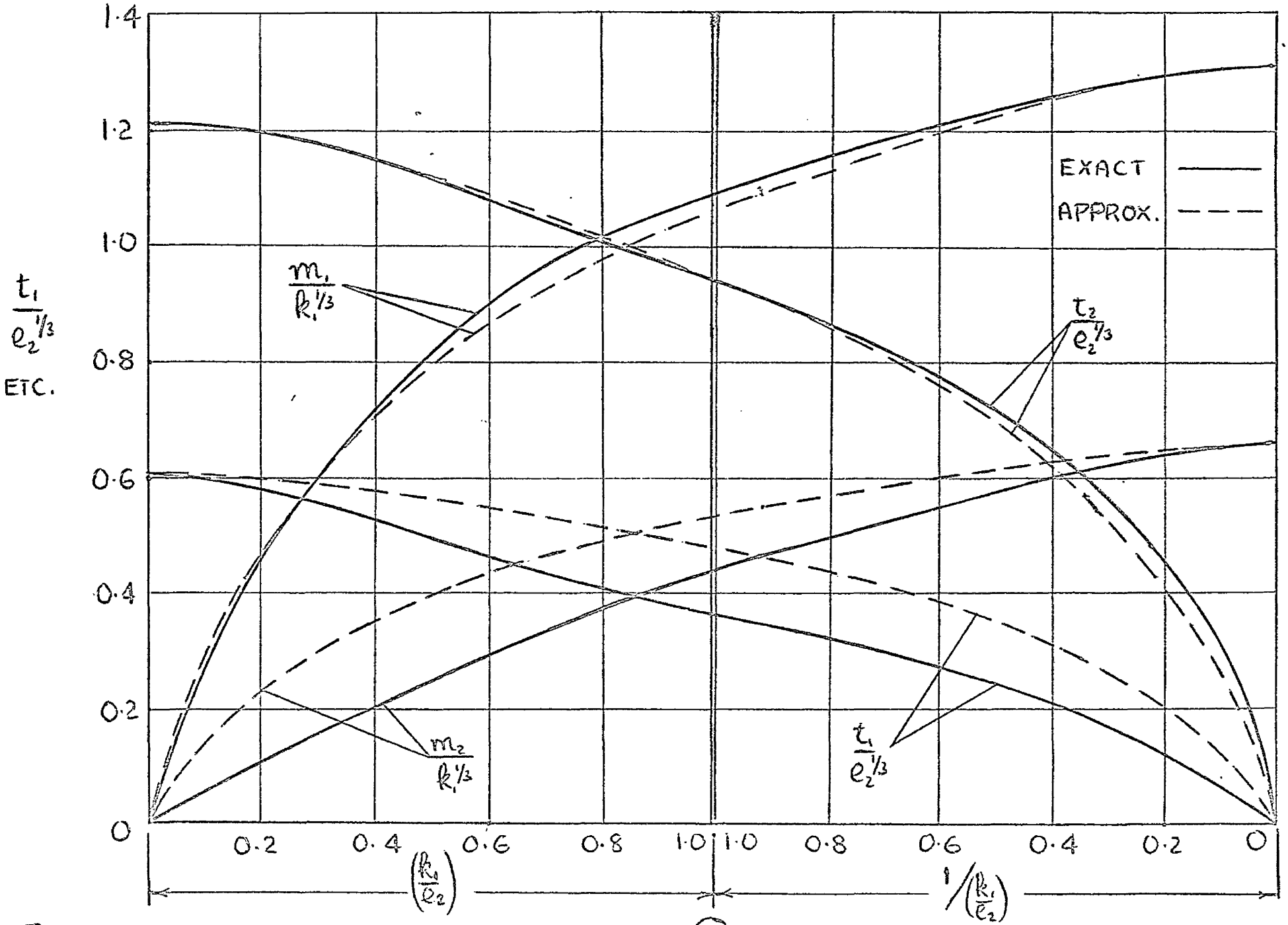

FIG 4.22 SECTION (7) : $n = 3$

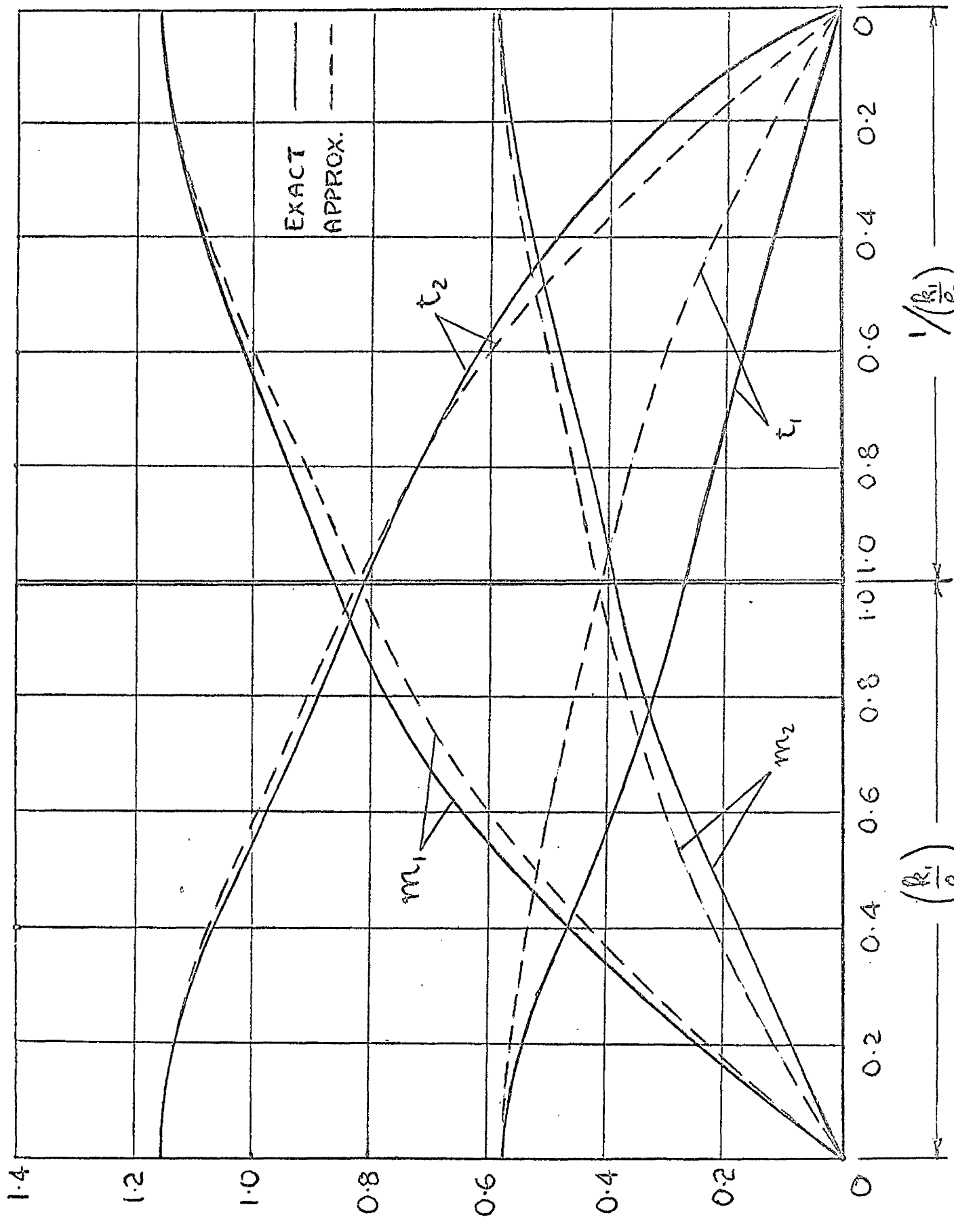

SECTION ⑦ ; $n \to \infty$

FIG. 4.23

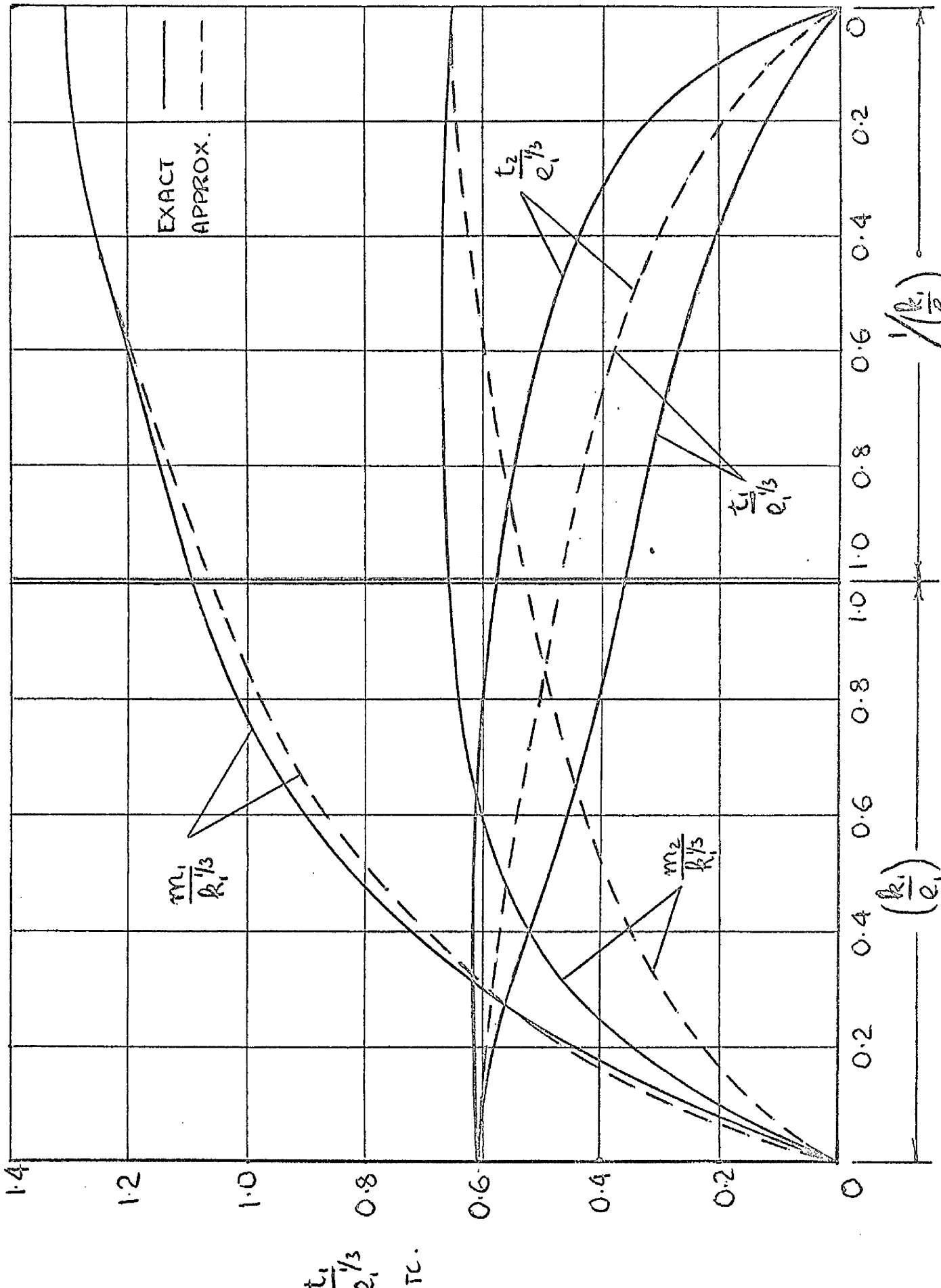

FIG. 4.24 SECTION (5) : n = 3

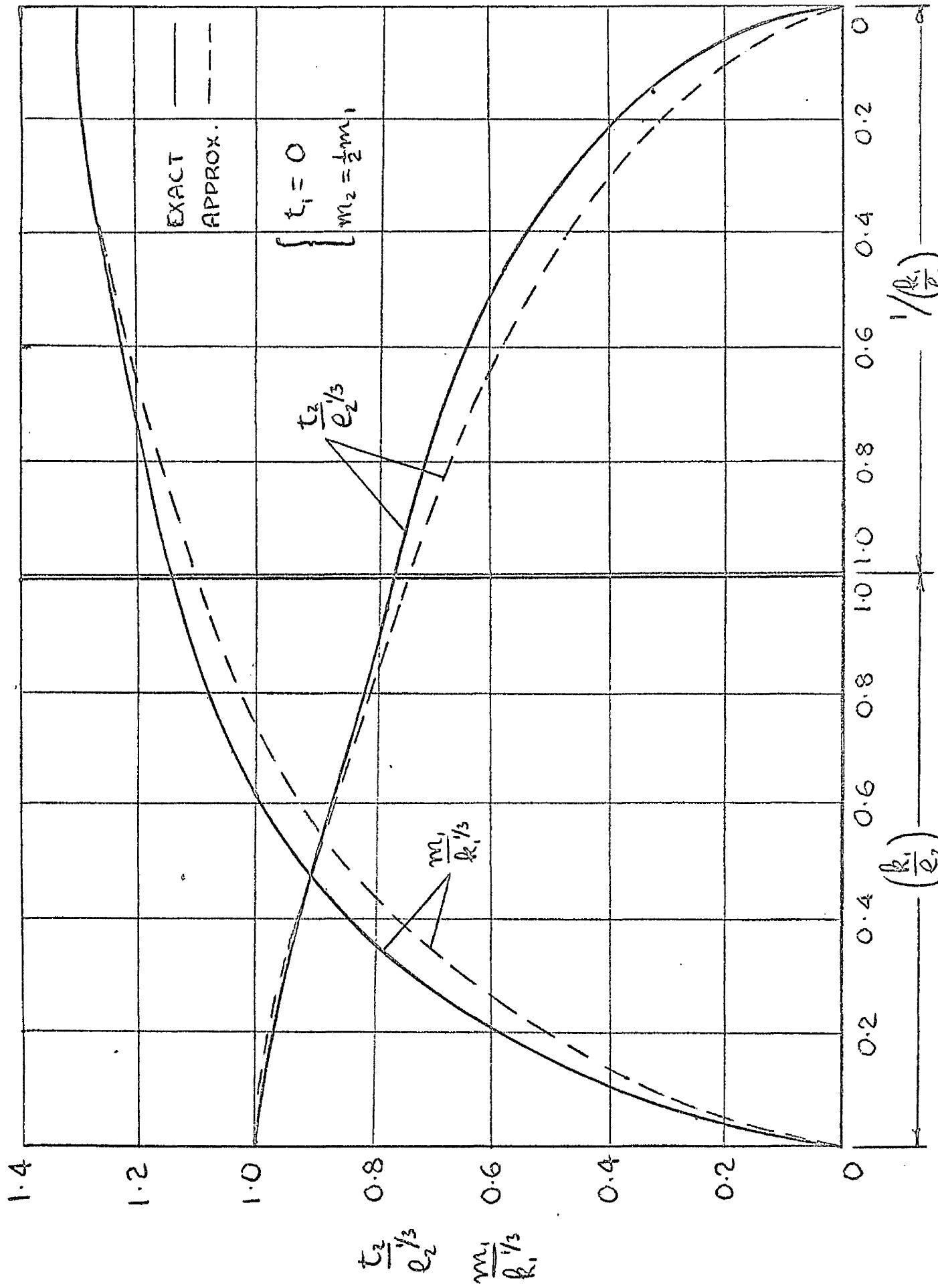

FIG 4.25 SECTION ⑥ : $n = 3$

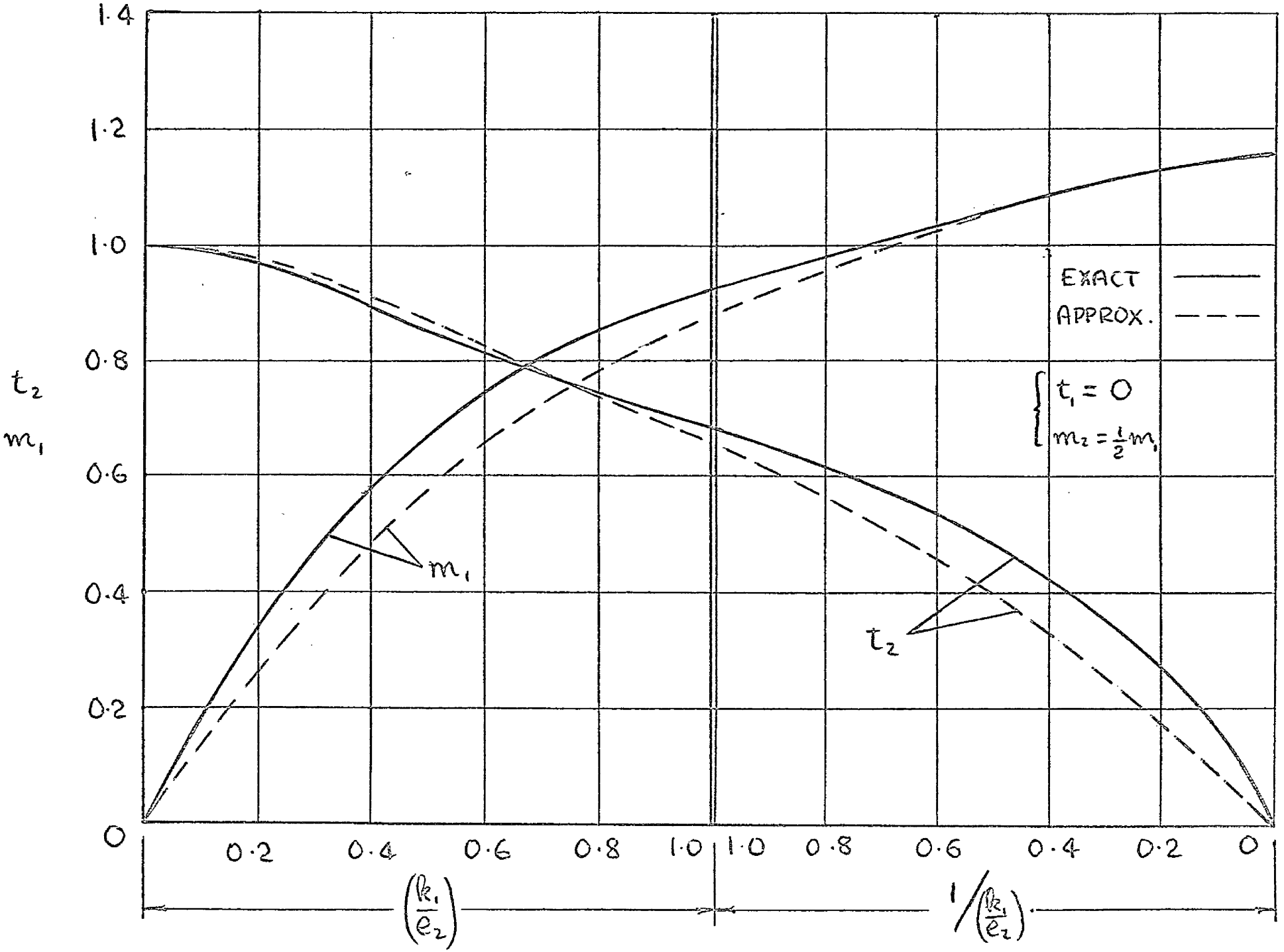

FIG. 4.26

SECTION ⑥ : $n \to \infty$

CHAPTER 5

FORMULATION OF BOUNDARY VALUE PROBLEMS IN CIRCULAR CYLINDRICAL SHELLS

5.1 Basic equations

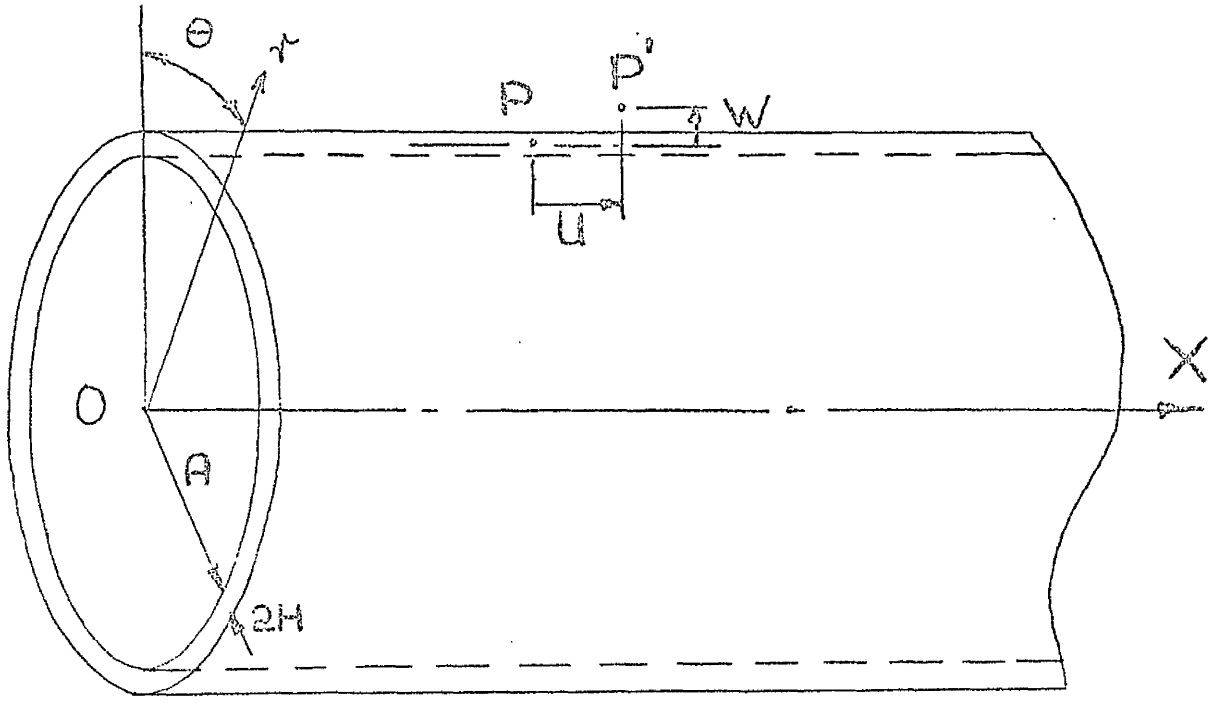

Fig. 5.1

Fig 5.1 shows a length of thin cylindrical shell and defines the co-ordinate system. The shell has an inner radius A and wall thickness 2H. Movement of a point on the mid-surface from P in the undeformed shell to P' after deformation defines the positive axial and radial displacements U and W, respectively.

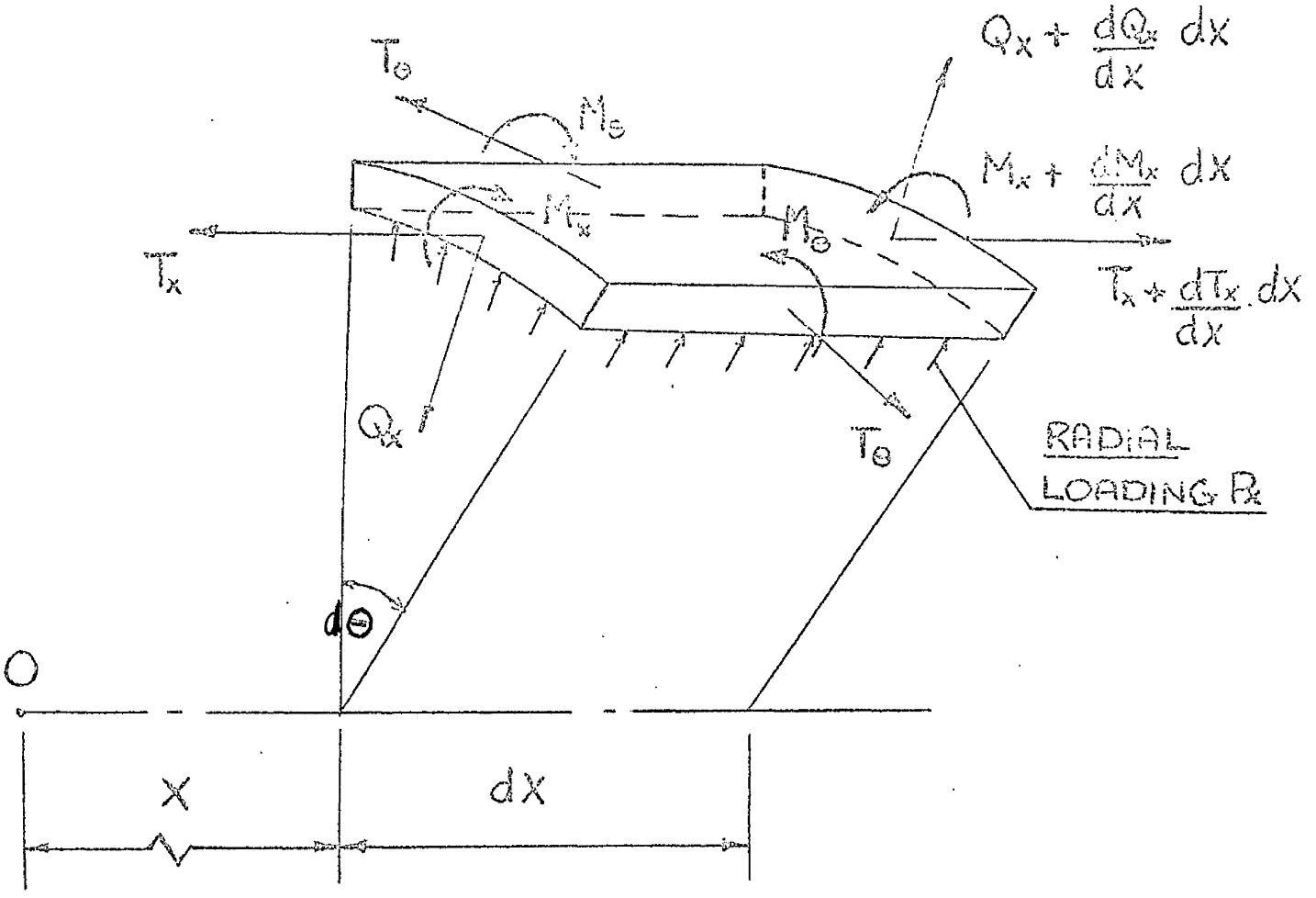

Fig 5.2

Fig 5.2 shows an element of the shell at X and defines the positive forces and moments acting on the element.

Forces T_x, T_θ , Q_x and moments M_x, M_θ are per unit length of mid-surface.

Radial loading P_x is per unit area of mid-surface.

Equilibrium Equations

The conditions for equilibrium of the element of Fig 5.2 are:

$$\frac{dT_x}{dX} = 0 \qquad (5.1)$$

$$\frac{dQ_x}{dX} - \frac{1}{A} T_\Theta + P_x = 0 \qquad (5.2)$$

$$Q_x + \frac{dM_x}{dX} = 0 \qquad (5.3)$$

Strain/displacement relations

For small displacements, the mid-surface strains ϵ_{mx}, $\epsilon_{m\Theta}$ and curvature changes K_x, K_Θ, expressed in terms of displacements are approximately:

$$\epsilon_{mx} = \frac{dU}{dx}$$

$$\epsilon_{m\Theta} = \frac{W}{A} \qquad (5.4)$$

$$K_x = \frac{d^2W}{dX^2}$$

$$K_\Theta = 0$$

Non-dimensional form of equilibrium and strain/displacement equations

It has been found in the linear elastic analysis of thin shells that the decay of edge effects can be conveniently described in terms of a "characteristic length" $\sqrt{AH}$. A similar behaviour is anticipated in

shells obeying non-linear stress/strain relations, and a non-dimensional parameter.

$$x = \frac{X}{\sqrt{AH}}$$

is used to define distances along the shell.

The non-dimensional forces, moments, and strains defined in paragraph 4.2 are also used, i.e.

$$t_x = \frac{T_x}{2H\sigma_o} \quad ; \quad t_\theta = \frac{T_\theta}{2H\sigma_o} \quad ; \quad m_x = \frac{M_x}{H^2\sigma_o}$$

$$e_x = \frac{\epsilon_{mx}}{\epsilon_o} \quad ; \quad e_\theta = \frac{\epsilon_{m\theta}}{\epsilon_o}$$

$$k_x = \frac{H K_x}{2\epsilon_o} \quad ; \quad k_\theta = \frac{H K_\theta}{2\epsilon_o}$$

These in equations 5.1 to 5.4 lead to the definition of the further non-dimensional parameters

$$p_x = \frac{P_x A}{\sigma_o H} \quad ; \quad q_x = \frac{Q_x \sqrt{AH}}{\sigma_o H^2}$$

$$w = \frac{W}{2A\epsilon_o} \quad ; \quad u = \frac{U}{\epsilon_o \sqrt{AH}}$$

Equations 5.1 to 5.4 become finally

$$\frac{dt_x}{dx} = 0 \qquad (5.5)$$

$$\frac{dq_x}{dx} - 2t_\theta + p_x = 0 \qquad (5.6)$$

$$q_x + \frac{dm_x}{dx} = 0 \tag{5.7}$$

$$\left.\begin{aligned} e_x &= \frac{du}{dx} \\ e_\theta &= 2w \\ k_x &= \frac{d^2w}{dx^2} \\ k_\theta &= 0 \end{aligned}\right\} \tag{5.8}$$

Force/deformation and moment/curvature relations

In Chapter 4, approximate relations between edge forces and moments and mid-surface deformations were obtained for an element of a thin shell subject only to in-plane edge forces and edge bending moments. It is assumed that they can be applied without serious error in the presence of transverse edge shear forces associated with changing bending moments in the shell.

One effect of transverse shear forces is distortion of normals to the undeformed mid-surface. Solutions obtained for linear elastic thin shells have shown satisfactory agreement with experiment and suggest that the strain field - equations 4.1 — obtained by assuming that normals to the undeformed mid-surface remain normals to the deformed mid-surface, is sufficiently accurate for most purposes. In the

non-linear analysis, further errors will arise from the presence of transverse shear forces because of the coupling between normal and shear stresses and strains in the stress/strain relations. However, to introduce these effects would make the problem much more complicated and is not justified at this stage.

Written in terms of the co-ordinates α, θ the approximate relations are :

$$
\begin{aligned}
t_x &= \left(\frac{4}{3}\right)^{\frac{n+1}{2n}} F_3^{\frac{1-n}{2n}} \left(e_x + \tfrac{1}{2} e_\theta\right) \\
t_\theta &= \left(\frac{4}{3}\right)^{\frac{n+1}{2n}} F_3^{\frac{1-n}{2n}} \left(e_\theta + \tfrac{1}{2} e_x\right) \\
m_x &= \left(\frac{4}{3}\right)^{\frac{n+1}{2n}} F_3^{\frac{1-n}{2n}} 4\left(\frac{n}{2n+1}\right)^{\frac{2n}{n+1}} \left(k_x + \tfrac{1}{2} k_\theta\right) \\
m_\theta &= \left(\frac{4}{3}\right)^{\frac{n+1}{2n}} F_3^{\frac{1-n}{2n}} 4\left(\frac{n}{2n+1}\right)^{\frac{2n}{n+1}} \left(k_\theta + \tfrac{1}{2} k_x\right)
\end{aligned}
\qquad (5.9)
$$

where

$$
F_3 = \left(e_x^2 + e_x e_\theta + e_\theta^2\right) + \left(\frac{n}{2n+1}\right)^{\frac{2n}{n+1}} \left(k_x^2 + k_x k_\theta + k_\theta^2\right)
$$

5.2 Reduction to form suitable for analogue computation

For solutions to boundary value problems in cylindrical shells, equations 5.5 to 5.9 must be

satisfied simultaneously, together with the boundary conditions. There are several ways in which the equations may be reduced to a fourth order system of non-linear differential equations. The following formulation has proved suitable for analogue computation.

Substitution of equations 5.8 into equations 5.9 expresses the forces and moments in terms of displacements, i.e.

$$t_x = f_1 F_4^{\frac{1-n}{2n}} \left(\frac{du}{dx} + w \right) \tag{5.10}$$

$$t_\Theta = f_1 F_4^{\frac{1-n}{2n}} \left(2w + \tfrac{1}{2} \frac{du}{dx} \right) \tag{5.11}$$

$$m_x = f_1 f_2 F_4^{\frac{1-n}{2n}} \frac{d^2 w}{dx^2} \tag{5.12}$$

$$m_\Theta = f_1 f_2 F_4^{\frac{1-n}{2n}} \tfrac{1}{2} \frac{d^2 w}{dx^2} \tag{5.13}$$

where

$$F_4 = \left(\frac{du}{dx} \right)^2 + 2w \frac{du}{dx} + 4w^2 + f_2 \left(\frac{d^2 w}{dx^2} \right)^2$$

$$f_1 = \left(\frac{4}{3} \right)^{\frac{n+1}{2n}}$$

$$f_2 = 4 \left(\frac{n}{2n+1} \right)^{\frac{2n}{n+1}}$$

Integration of equation 5.5 gives

$$t_x = \text{constant} = T, \text{ say}$$

and, thus, from equation 5.10

$$T = f_1\left[\left(\frac{du}{dx}\right)^2 + 2w\frac{du}{dx} + 4w^2 + f_2\left(\frac{d^2w}{dx^2}\right)^2\right]^{\frac{1-n}{2n}} \times \left(\frac{du}{dx} + w\right) \qquad (5.14)$$

From equation 5.6

$$q_x = \int (2t_\Theta - p_x)dx$$

and from equation 5.7

$$q_x = -\frac{dm_x}{dx}$$

$$\therefore \quad m_x = -\iint (2t_\Theta - p_x)dx\,dx \qquad (5.15)$$

Finally, substituting for t_Θ and m_x from equations 5.11 and 5.12 in equation 5.15 gives

$$f_1 f_2\left[\left(\frac{du}{dx}\right)^2 + 2w\frac{du}{dx} + 4w^2 + f_2\left(\frac{d^2w}{dx^2}\right)^2\right]^{\frac{1-n}{2n}}\frac{d^2w}{dx^2}$$

$$= -\iint\left\{f_1\left[\left(\frac{du}{dx}\right)^2 + 2w\frac{du}{dx} + 4w^2 + f_2\left(\frac{d^2w}{dx^2}\right)^2\right]^{\frac{1-n}{2n}}\left(4w + \frac{du}{dx}\right) - p_x\right\} dx\,dx \qquad (5.16)$$

The problem is thus reduced to the solution of the simultaneous equations 5.14 and 5.16 in $\frac{du}{dx}$ and w with the appropriate boundary conditions.

5.3 Simplification for zero axial load

With T = 0, equation 5.14 gives

$$\frac{du}{dx} = - w$$

Substitution for $\frac{du}{dx}$ in equation 5.16 leads to

$$f_i f_2 \left[3 w^2 + f_2 \left(\frac{d^2w}{dx^2} \right)^2 \right]^{\frac{1-n}{2n}} \frac{d^2w}{dx^2}$$

$$= - \iint \left\{ f_1 \left[3w^2 + f_2 \left(\frac{d^2w}{dx^2} \right)^2 \right]^{\frac{1-n}{2n}} \cdot 3w - p_x \right\} dx\, dx \qquad (5.17)$$

In the problems to be considered, the radial loading p_x is assumed to be independent of x. Rearranging equation 5.17, and with

$p_x = p$ = uniform radial loading

$$\frac{d^2w}{dx^2} = - \frac{1}{f_1 f_2} \left[3 w^2 + f_2 \left(\frac{d^2w}{dx^2} \right)^2 \right]^{\frac{n-1}{2n}}$$

$$\times \iint \left\{ 3 f_1 w \left[3w^2 + f_2 \left(\frac{d^2w}{dx^2} \right)^2 \right]^{\frac{1-n}{2n}} - P \right\} dx\, dx \qquad (5.18)$$

5.4 Reduction to equations of linear elasticity

With n = 1

$$f_1 = \left(\frac{4}{3}\right)^{\frac{n+1}{2n}} = \frac{4}{3}$$

$$f_2 = 4\left(\frac{n}{2n+1}\right)^{\frac{2n}{n+1}} = \frac{4}{3}$$

and equations 5.14 and 5.16 become

$$\frac{4}{3}\left(\frac{du}{dx} + w\right) = T \qquad (5.19)$$

and

$$\frac{16}{9}\frac{d^2w}{dx^2} = -\iint\left[\frac{4}{3}\left(4w + \frac{du}{dx}\right) - p_x\right] dx\, dx$$

or

$$\frac{16}{9}\frac{d^4w}{dx^4} = -\left[\frac{4}{3}\left(4w + \frac{du}{dx}\right) - p_x\right] \qquad (5.20)$$

From 5.19

$$\frac{du}{dx} = \frac{3}{4}T - w$$

and substitution for $\frac{du}{dx}$ in equation 5.20 gives

$$\frac{d^4w}{dx^4} + \frac{9}{4}w = \frac{9}{16}(p_x - T) \qquad (5.21)$$

This is the governing equation for a cylindrical shell

of linear elastic material with the modulus of elasticity written as $\frac{\sigma_o}{\epsilon_o}$ and Poisson's ration $\frac{1}{2}$.

With $p_x = p$ = constant, the general solution to equation 5.21 is

$$w = e^{\alpha x}\left(C_1 \cos \alpha x + C_2 \sin \alpha x\right) + e^{-\alpha x}\left(C_3 \cos \alpha x + C_4 \sin \alpha x\right) + \frac{1}{4}(p-T) \qquad (5.22)$$

where $\alpha = \sqrt[4]{\frac{9}{16}}$.

C_1, C_2, C_3 and C_4 are constants.

CHAPTER 6

USE OF AN ANALOGUE COMPUTER TO SOLVE PROBLEMS IN CYLINDRICAL SHELLS

6.1 Explanation of method

It is convenient to describe the method of using an analogue computer to solve boundary value problems in semi-infinite cylindrical shells by referring to the linear problem. For this, the governing differential equation is

$$\frac{d^4 w}{dx^4} = -\frac{9}{4} w + \frac{9}{16} (p - T) \qquad (6.1)$$

and it must be solved with four boundary conditions. In a semi-infinite cylinder two of these are prescribed at x = 0 and the other two are implied by the condition that w assumes a constant value at large values of x.

The simple analogue computer circuit shown in Fig 6.1 may be used to solve equation 6.1. The distance variable x is represented by time, and voltages represent the displacement w, its derivatives and the applied loading p. The values of w and its derivatives at x = 0 must be set by applying initial voltages at the outputs of the integrators.

Consider the problem of a semi-infinite cylinder in which the following boundary conditions have to be satisfied:

At $x = 0$

$$W = W_o$$

$$\frac{dw}{dx} = \left.\frac{dw}{dx}\right]_o$$

At $x \to \infty$

$w \to w_\infty$, calculated for given applied loading p and T.

(In what follows, subscripts 0 and ∞ will always refer to values of variables at $x = 0$ and $x \to \infty$, respectively)

$\left.\frac{dw}{dx}\right]_o$ and w_o are set as initial conditions on the integrators I_3 and I_4. It is then necessary to find the values of $\left.\frac{d^2w}{dx^2}\right]_o$ and $\left.\frac{d^3w}{dx^3}\right]_o$ which will make $w \to w_\infty$ as $x \to \infty$. Since $\frac{d^2w}{dx^2}$ and $\frac{d^3w}{dx^3}$ are proportional to the bending moment m_x and shear force q_x respectively, this is equivalent to finding the correct values of m_o and q_o. Estimated values of

$\left.\frac{d^2w}{dx^2}\right]_o$ and $\left.\frac{d^3w}{dx^3}\right]_o$ are applied as initial conditions to integrators I_2 and I_1 and the displacement w is monitored as the circuit operates. The procedure is repeated with adjustments to $\left.\frac{d^2w}{dx^2}\right]_o$ and $\left.\frac{d^3w}{dx^3}\right]_o$ until $w \longrightarrow w_\infty$ at large values of x.

Four typical runs are shown diagrammatically in Fig 6.2 for the boundary conditions

$$w_o = \left.\frac{dw}{dx}\right]_o = 0$$

$$w_\infty = 0.5 \quad (p = 2,\ T = 0)$$

The analytical solution is shown for comparison. The two very different curves (a) and (b) are obtained for values of $\left.\frac{d^2w}{dx^2}\right]_o$ and $\left.\frac{d^3w}{dx^3}\right]_o$ which differ by only approximately $\pm$ 0.5 % from the theoretical values and a difference of only $\pm$ 0.1% can give curves (c) and (d).

Although there are thus well-defined values of $\left.\frac{d^2w}{dx^2}\right]_o$ and $\left.\frac{d^3w}{dx^3}\right]_o$ which make $w \longrightarrow w_\infty$ for a short range of x, the solutions become unstable at large values of x. The reason for the instability can be understood

from the general solution of equation 6.1, i.e.

$$w = e^{\alpha x}\left[C_1 \cos \alpha x + C_2 \sin \alpha x\right] + e^{-\alpha x}\left[C_3 \cos \alpha x + C_4 \sin \alpha x\right] + \tfrac{1}{4}(p - T)$$

For the semi-infinite cylinder, the growth exponential terms are removed by putting the constants C_1 and C_2 to zero. This is effectively what is done in an analogue computer solution by adjusting the initial values of w and its derivatives. If the growth exponential is not completely suppressed, the result is the behaviour shown in curves (c) and (d) of Fig 6.2; the two curves are associated with small growth exponential terms of opposite sign.

The solutions represented by curves (c) and (d) compare very favourably with the analytical solution for values of $0 \leq x \leq 2.5$ approximately. The most important features occur within this range and it is concluded that the solutions are acceptable despite the behaviour at large values of x. The same effects occur in solutions to the non-linear problems.

The early tests were performed on a 40 - amplifier computer designed and constructed in the Engineering Department, and difficulties in obtaining solutions were aggravated by drift in the circuit components and by coarse potentiometer adjustment.

Later tests, leading to all the solutions given in Chapter 7, were conducted on an Electronic Associates Ltd. Pace 231 R computer.

6.2 Time and Magnitude scaling

Records were required of the distribution of m_x and q_x along the shell and rapid changes in these variables occurred near $x = 0$. The only available recorder which gave a record of reasonable size was a Bryant x - y plotter which has a slow response. It was necessary thus to slow down the problem by scaling the relationship between time τ and x. Running the problem for long times, however, leads to a build-up in errors from drift in circuit components and the final time scaling was a compromise between the conflicting requirements., The chosen scaling between the time τ in seconds and x was

$$\tau = 4x$$

and the relationships between derivatives are then

$$\frac{d}{dx} = 4\frac{d}{d\tau} \quad ; \quad \frac{d^2}{dx^2} = 16\frac{d^2}{d\tau^2} \quad ;$$

$$\frac{d^3}{dx^3} = 64\frac{d^3}{d\tau^3} \quad ; \quad \frac{d^4}{dx^4} = 256\frac{d^4}{d\tau^4} \quad .$$

For the linear problem the differential equation becomes in terms of τ

$$256 \frac{d^4 w}{d\tau^4} = -\frac{9}{4} w + \frac{9}{16} (p - T) \qquad (6.2)$$

(b) Magnitude scaling

Direct use of the circuit in Fig 6.1 will lead to very different values for the maximum outputs of the amplifiers and may lead to overloading in some of them. This is because of the differences in numerical values of w and its derivatives. The purpose of magnitude scaling is to ensure that the output of each computing element covers as nearly as possible the working range of $\pm$ 100 volts. This gives greatest accuracy and avoids overloading.

The method adopted was to estimate the maximum values of all the variables and then to work with the normalised variables

$$w \Big/ \left| w_{max} \right| \quad , \quad \frac{dw}{d\tau} \Big/ \left| \left[\frac{dw}{d\tau} \right]_{max} \right| \quad , \quad \text{etc.}$$

The circuit is designed so that these normalised variables appear as the outputs of all computing elements. If unity is represented by 100 volts in the computer, all outputs will fall in the range $\pm$ 100 volts.

The estimates of maximum values depend on the particular boundary conditions, and a problem may have to be rescaled when boundary conditions are changed.

The procedure for magnitude scaling is illustrated for the linear problem with the boundary conditions

$$\underline{x = 0} \qquad w_o = \left.\frac{dw}{dx}\right]_o = 0$$

$$\underline{x \to \infty} \qquad w_\infty = 0.5 \quad (p = 2,\ T = 0) .$$

In this case an analytical solution can be obtained, and gives the following maximum values:

$$\left|w_{max}\right| = 0.521$$

$$\left|\left.\frac{dw}{dx}\right]_{max}\right| = 0.278 \quad ; \quad \left|\left.\frac{dw}{d\tau}\right]_{max}\right| = 0.0695$$

$$\left|\left.\frac{d^2w}{dx^2}\right]_{max}\right| = 0.750 \quad ; \quad \left|\left.\frac{d^2w}{d\tau^2}\right]_{max}\right| = 0.0469$$

$$\left|\left.\frac{d^3w}{dx^3}\right]_{max}\right| = 1.298 \quad ; \quad \left|\left.\frac{d^3w}{d\tau^3}\right]_{max}\right| = 0.0203$$

$$\left|\left.\frac{d^4w}{dx^4}\right]_{max}\right| = 1.122 \quad ; \quad \left|\left.\frac{d^4w}{d\tau^4}\right]_{max}\right| = 0.00439$$

Rounding out these maximum values leads to the use of the normalised variables:

$$\frac{w}{0.6} \quad ; \quad \frac{\frac{dw}{d\tau}}{0.08} \quad ; \quad \frac{\frac{d^2w}{d\tau^2}}{0.05} \quad ; \quad \frac{\frac{d^3w}{d\tau^3}}{0.03} \quad ; \quad \frac{\frac{d^4w}{d\tau^4}}{0.005} \quad .$$

The differential equation 6.2 then becomes

$$256 \times 0.005 \left(\frac{\frac{d^4 w}{d\tau^4}}{0.005} \right) = - \frac{9}{4} \times 0.6 \left(\frac{w}{0.6} \right) + \frac{9}{16} (2 - 0)$$

or

$$1.28 \left(\frac{\frac{d^4 w}{d\tau^4}}{0.005} \right) = - 1.35 \left(\frac{w}{0.6} \right) + \frac{9}{8}$$

Dividing through by 1.35, the highest coefficient, gives finally

$$0.948 \left(\frac{\frac{d^4 w}{d\tau^4}}{0.005} \right) = - \left(\frac{w}{0.6} \right) + 0.833$$

The computer diagram for solving this equation with the given boundary conditions is shown in Fig 6.3.

6.3 Problems without axial load

The governing equation obtained in paragraph 5.3 for the non-linear problem without axial load may be written

$$\frac{d^2 w}{dx^2} = - \frac{1}{f_1 f_2} G_1^{\frac{n-1}{2n}} \iint \left[3 f_1 w G_1^{\frac{1-n}{2n}} - p \right] dx \, dx \qquad (6.3)$$

where

$$G_1 = 3w^2 + f_2 \left(\frac{d^2 w}{dx^2} \right)^2$$

To solve this equation the function $G_1^{\frac{n-1}{2n}}$ must be generated and a number of multiplying and dividing

operations must be performed. A block diagram of a suitable circuit is shown in Fig 6.4.

The function $G_1^{\frac{n-1}{2n}}$ was generated as a series of straight line segments on a 20-segment diode function generator. The following table gives the index $\frac{n-1}{2n}$ for a number of values of n.

n	1.5	3	5	7
$\frac{n-1}{2n}$	1/6	1/3	2/5	3/7

G_1 is always positive, and, as a normalised variable in the scaled problem, varies in the range 0 to + 1. $G_1^{\frac{n-1}{2n}}$ is plotted for this range, and for n = 3, in Fig 6.5. The function is also plotted on an extended scale for values of G_1 from 0 to 0.1.

Use of the diode function generator (D.F.G.) to represent the function presents two main difficulties:

(a) The maximum number of segments is available, and hence the best fit to the curve is possible, when the input to the function generator varies from - 100 to + 100 volts;

(b) There is a restriction on the maximum gradient obtainable for any segment and the infinite gradient at G_1 = 0 cannot be accommodated.

The first of these difficulties was overcome by scaling the input to the D.F.G. in the following simple circuit

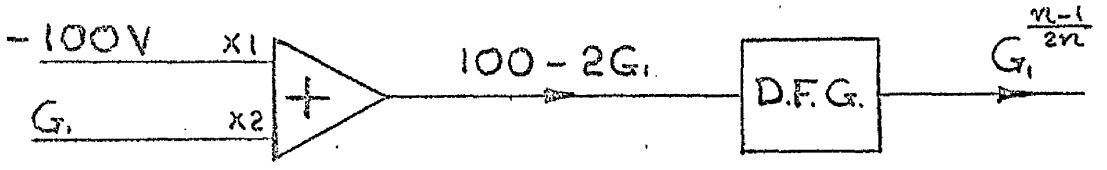

Clearly, as G_1 varies from 0 to + 100 volts, the input to the D.F.G. varies from - 100 to + 100 volts. For a given number and positioning of segments, scaling the input in this way reduces the gradients by $\frac{1}{2}$ and thus partly relieves the second difficulty.

The segment break points finally selected for n = 3 are shown on the curves of Fig 6.5. With these segments, the D.F.G. output was within approximately 2% of $G_1^{\frac{1}{3}}$ for values of G_1 from 0.005 to 0.100 and the difference was smaller for higher values of G_1, being less than 1% as G_1 approached unity. For values of G_1 less that 0.005 it was not possible to represent the function. Approximate calculations based on solutions to the linear problem showed, however, that G_1 was not likely to have a value below 0.005 for the boundary value problems considered. This was verified when the problems were run, the lowest value of G_1 recorded being about 0.01. The function was generated

with similar accuracy for n = 5 and n = 7.

The problem was time scaled in the manner described for the linear problem in paragraph 6.1, i.e. with

$$\tau = 4\,x$$

Estimates of the maximum values of w, $\frac{dw}{dx}$ and $\frac{d^2w}{dx^2}$ for magnitude scaling were based on the linear solution. It was also necessary to make estimates of the maximum values of

$$G_1 \,,\; G_1^{\frac{n-1}{2n}} \,,\; G_1^{\frac{1-n}{2n}} \,,$$

$$\int \left[3\, f_1\, w\, G_1^{\frac{1-n}{2n}} - p\right] dx,$$

and $$\iint \left[3\, f_1\, w\, G_1^{\frac{1-n}{2n}} - p\right] dx\, dx$$

Here it is important to note that $\int [\quad]\, dx$ and $\iint [\quad]\, dx\, dx$ are proportional to the shear force q_x and bending moment m_x, respectively. Details are given in Appendix 5.1 of the estimates of maximum values for the particular problem of the semi-infinite cylinder with zero edge slope and displacement (termed

in what follows the fixed end cylinder).

The computer circuit used for the scaled problem of the fixed end cylinder without axial load is shown in Fig 6.6 for n = 3 and p = 2. The corresponding diagrams for n = 5 and n = 7 are given in Appendix 5.1.

The technique of obtaining solutions was that described in paragraph 6.1 for the linear problem. The displacement w_∞ away from the end was calculated for the particular loading p and value of n. The initial conditions for w and $\frac{dw}{dx}$ were set and the values of q_o and m_o estimated (initial estimates of q_o and m_o were obtained from the linear solution). The problem was run and q_o and m_o systematically adjusted until w attained the calculated value of w_∞ over a range of x. As in the linear problem, the values of q_o and m_o to give this behaviour were sharply defined.

6.4 Problems with axial load

For problems with axial load, the two equations 5.14 and 5.16 in the displacements u and w must be solved simultaneously. The equations may be written

$$\frac{d^2w}{dx^2} = -\frac{1}{f_1 f_2} G_2^{\frac{n-1}{2n}} \iint \left[f_1 G_2^{\frac{1-n}{2n}} \left(4w+\frac{du}{dx}\right) - p \right] dx\, dx \qquad (6.4)$$

$$\frac{du}{dx} = \frac{T}{f_1} G_2^{\frac{n-1}{2n}} - w$$

where

$$G_2 = \left(\frac{du}{dx}\right)^2 + 2\,w\,\frac{du}{dx} + 4\,w^2 + f_2\left(\frac{d^2w}{dx^2}\right)^2$$

Fig 6.7 shows the block diagram of a circuit to solve these equations. The upper loop is basically the same as the circuit for zero axial load and the lower loop is concerned with the generation of $\frac{du}{dx}$. The potentiometer marked with an asterisk in the lower loop is used to vary the axial load. Setting this potentiometer to zero gives

$$\frac{du}{dx} = -\,w$$

and the solution can be compared with that obtained from the simpler circuit for zero axial load.

The same time scaling was used as previously, and the solutions to problems without axial load were used as a basis for magnitude scaling. Details are given in Appendix 5.2, and the time scaled computer diagram with normalised variables is shown in Fig 6.8.

Apart from the increased number of components in the circuit, this problem presented little more difficulty than that without axial load; the technique of solution was the same.

6.5 Comments on accuracy and discussion

The accuracy of solutions depends on the accuracy with which the individual operations are performed in the computer circuit. The makers of the Pace 231R claim an accuracy of better than $\pm$ 0.1% of full scale ($\pm$ 100 volts) on the outputs of operational amplifiers and multipliers; decade coefficient potentiometers can be set to $\pm$ 0.0001 and voltages can be read to $\pm$ 0.01 volt with the electronic digital voltmeter.

In the course of solving the problem of a fixed end cylinder, the output of each summing amplifier and non-linear element in the circuit of Fig 6.6 was recorded at x = 0 and x = 0.5 and 1.0 approximately. (The problem can be stopped at any stage and voltages read throughout the circuit.) The input to each component was obtained from the outputs of preceding components, and the output which should have been obtained from this input was calculated. The results are given in Appendix 5.3. In many of the operations no difference between measured and calculated outputs could be detected and, with few exceptions, the differences were within the makers' specified limits. A multiplier output as low as 0.15 volts differed by only approximately 5% from the calculated output. Although it was not possible to calculate the outputs

of the integrators, separate checks on these with known inputs showed the errors to be generally within the specified limits.

It would be very difficult, if possible at all, to make a formal estimate of the combined effect of these errors on the solution to a boundary value problem. The effect is for a slightly different equation to be solved at each value of x. For example, if all the operations were performed without error except the integration of $\frac{dw}{dx}$ to give w, and a constant error of $+\alpha$ was incurred in this operation, the equation solved would be

$$\frac{d^2w}{dx^2} = -\frac{1}{f_1 f_2}\left[3(w+\alpha)^2 + f_2\left(\frac{d^2w}{dx^2}\right)^2\right]^{\frac{n-1}{2n}}$$

$$X \iint \left\{3f_1(w+\alpha)\left[3(w+\alpha)^2+f_2\left(\frac{d^2w}{dx^2}\right)^2\right]^{\frac{1-n}{2n}} - p\right\} dx\, dx$$

and not equation 6.3

Two useful checks on the combined accuracy of a number of circuit components, and on errors in setting up the diode function generator can be made under the following conditions.

(a) Check on w_{oo}

With

$$\left.\frac{dw}{dx}\right]_o = m_o = q_o = 0$$

the problem is one of a cylinder under uniform radial loading without end restraint. The displacement w should remain at a constant value for all values of x. This value for w can be obtained from equation 6.3 as follows:

with w = constant, equation 6.3 becomes

$$0 = -\frac{1}{f_1 f_2}\,(3\,w^2)^{\frac{n-1}{2n}} \iint \left[3f_1 w(3\,w^2)^{\frac{1-n}{2n}} - p\right] dx\,dx$$

$$= -\frac{1}{f_1 f_2}\,(3\,w^2)^{\frac{n-1}{2n}} \left[3f_1 w(3w^2)^{\frac{1-n}{2n}} - p\right] \iint dx\,dx$$

This requires

$$3\,f_1\,w\,(3\,w^2)^{\frac{1-n}{2n}} - p = 0 \qquad (6.5)$$

and with

$$f_1 = \left(\frac{4}{3}\right)^{\frac{n+1}{2n}}$$

gives

$$w = \frac{p}{2}^{\frac{n}{n+1}} \qquad (6.6)$$

With the initial conditions set as

$$\left.\frac{dw}{dx}\right]_o = m_o = q_o = 0$$

successive runs were made until a value for w was found which was constant over a range of x of at least 0 to 5. The value for w was compared with that calculated from equation 6.6 for the particular values of p and n.

This test checks the accuracy of a substantial part of the circuit. It also gives a sensitive indication of errors in the diode function generator, as can be deduced from equation 6.5. If a fractional error $\pm \beta$ occurs in generating the function $G_{\frac{n-1}{2n}}$, then equation 6.5 gives

$$3 f_1 \frac{w}{(3w^2)^{\frac{n-1}{2n}} (1 \pm \beta)} - p = 0$$

or

$$w = \frac{p^n}{2^{n+1}} (1 \pm \beta)^n$$

$$\pm n \frac{p^n}{2^{n+1}} (1 \pm n\beta) \qquad (6.7)$$

This dependence of the error in w on n was observed,

but with G_1 approaching unity, where the error in generating $G_1^{\frac{n-1}{2n}}$ is less than 1%, the error in w was below 5% even for n = 7. For n = 3, the error was less than 2%.

(b) Check on $\left.\frac{d^2w}{dx^2}\right]_o$

With $w_o = 0$, equation 6.3 may be written at x = 0

$$\left.\frac{d^2w}{dx^2}\right]_o = - \frac{1}{f_1 f_2} \left\{ f_2 \left(\left.\frac{d^2w}{dx^2}\right]_o \right)^2 \right\}^{\frac{n-1}{2n}} \lambda_o$$

where λ_o is proportional to the value of the edge bending moment m_o, and thus

$$\left.\frac{d^2w}{dx^2}\right]_o = - \frac{1}{f_1^{\,n} f_2^{\frac{n+1}{2}}} \lambda_o^{\,n} \qquad (6.8)$$

Values of $\left.\frac{d^2w}{dx^2}\right]_o$ were read from the computer for a number of values of λ_o and checked with those calculated from equation 6.8. This test was a check on the combined accuracy of a further combination of circuit elements, and was again sensitive to errors in the D.F.G. A similar argument to that used in

establishing equation 6.7 gives

$$\left.\frac{d^2w}{dx^2}\right]_o \simeq \left(\frac{1}{f_1^{\,n}\; f_2^{\,\frac{n+1}{2}}}\right) \lambda_o^{\,n} (1 \pm n\beta) \qquad (6.9)$$

where β is the fractional error in generation of $G_1^{\frac{n-1}{2n}}$.

With values of λ_o giving solutions to the fixed end problem, differences between observed values of $\left.\frac{d^2w}{dx^2}\right]_o$ and those calculated from equation 6.8 were as high as 10% for n = 7. However, upsetting the D.F.G. locally to produce errors in $\left.\frac{d^2w}{dx^2}\right]_o$ in the range 0 to $\pm$ 10% showed that corresponding differences in the values of m_o and q_o to give solutions were less than 2%.

Both the checks (a) and (b) were carried out as part of the procedure of setting up the circuit for each boundary value problem.

Perhaps the best indication of likely errors in the maximum, and for practical purposes the most important, values of the variables was obtained from checks on reproducibility. It was found that for a number of runs performed over a period of a few hours with the same circuit and setting of the D.F.G., the

values of m_o and q_o obtained for the fixed end problem differed by less than $\frac{1}{2}\%$. When the solutions were repeated after a period of months with different circuit components, and after the D.F.G. had been reset, the values of m_o and q_o were within $\pm$ 2% of the values obtained originally. This was true for n values up to 7,, but reproducibility was generally better for the lower n values. Reproducibility of $\left.\frac{d^2w}{dx^2}\right]_o$ was more sensitive to n, and differences of the order of $\pm$ 10% were obtained with n = 7. This is consistent with the findings of circuit check (b), discussed above, the main factor governing reproducibility being the D.F.G. setting.

From observations on the accuracy of individual components and checks on reproducibility, it is reasonable to conclude that errors in the values obtained for m_o and q_o are probably less than $\pm$ 2%, and unlikely to be greater than $\pm$ 5%. Errors in $\left.\frac{d^2w}{dx^2}\right]_o$, however, might be as high as 2 n %, but are unlikely to be greater than $\pm$ 5 n%.

The analogue computer has proved to be a useful tool for solving boundary value problems in semi-infinite cylindrical shells, with an accuracy acceptable for most engineering purposes. A big advantage is the ease with which changes in boundary conditions can be studied.

Although manual adjustment of two initial conditions to achieve the required displacement away from the restrained end might appear to be a tedious procedure, a trend of adjustment is soon established, and solutions can be obtained fairly quickly. It is likely that a method of automatic adjustment of these initial conditions could be devised, although no attempt was made to do this.

It should also be possible to solve problems of cylinders of finite length. Consider, for example, a cylinder of length 1 under internal pressure, having the prescribed boundary conditions

$$x = 0 \quad ; \quad w = w_o$$

$$\frac{dw}{dx} = \frac{dw}{dx}\Big]_o$$

$$x = 1 \quad ; \quad w = w_1$$

$$\frac{dw}{dx} = \frac{dw}{dx}\Big]_1$$

The values of w_o and $\frac{dw}{dx}\Big]_o$ can be set at $x = 0$, and the

values of m_o and q_o adjusted to give the required values w_1 and $\frac{dw}{dx}\Big]_1$ at $x = 1$. Both w and $\frac{dw}{dx}$ would have to be monitored, and adjustment of m_o and q_o to satisfy the two conditions at $x = 1$ would be considerably more tedious than in the semi-infinite problem.

A preliminary investigation has also shown that, in principle, the analogue computer may be used to solve problems in shells of revolution of other shapes. The governing equations are considerably more complex than those for the cylindrical shell, and a greater number of computing elements are required. There are not enough elements in the computer at present available in the Department for such solutions to be attempted.

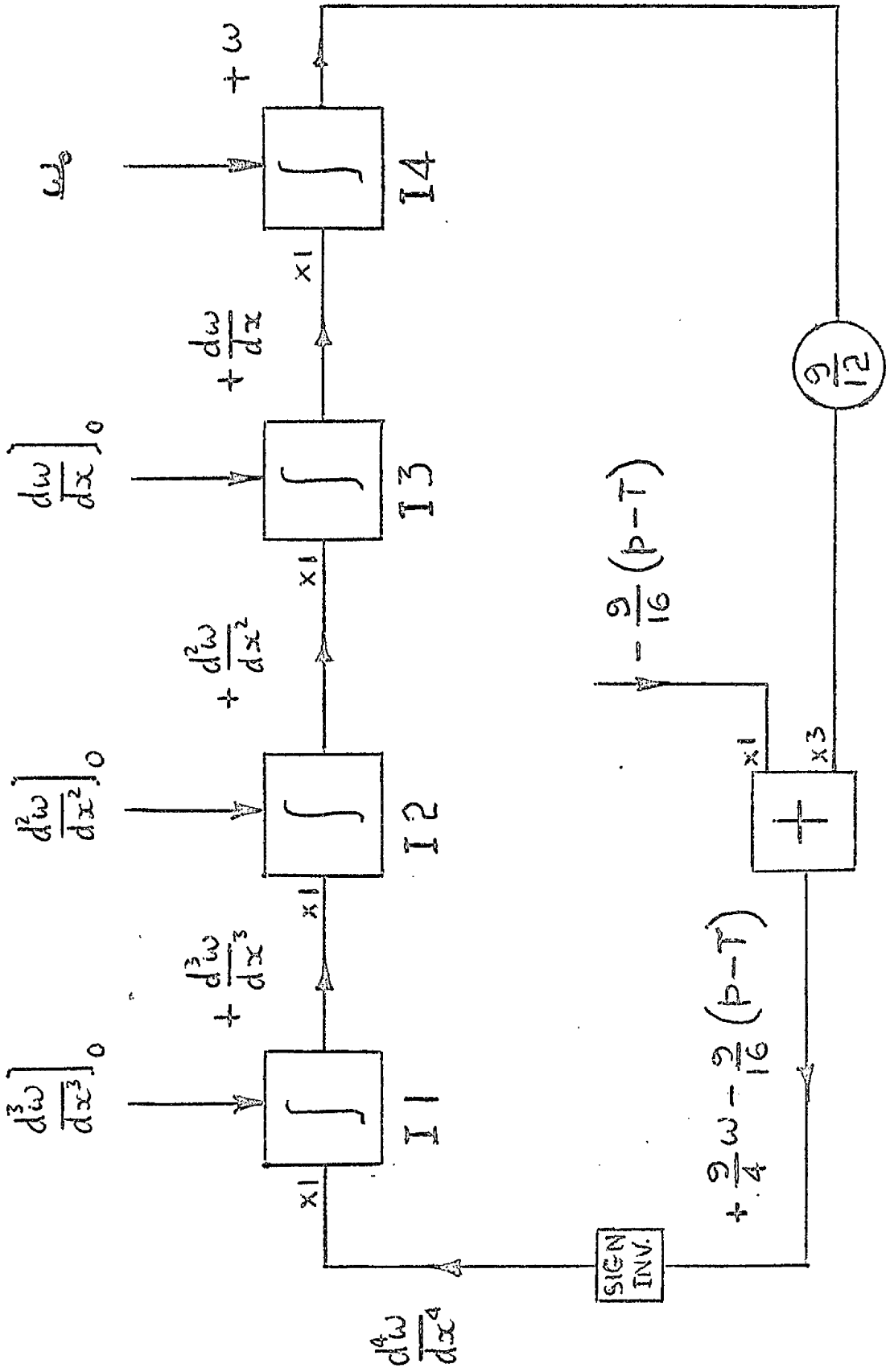

COMPUTER CIRCUIT FOR n=1

FIG. 6.1

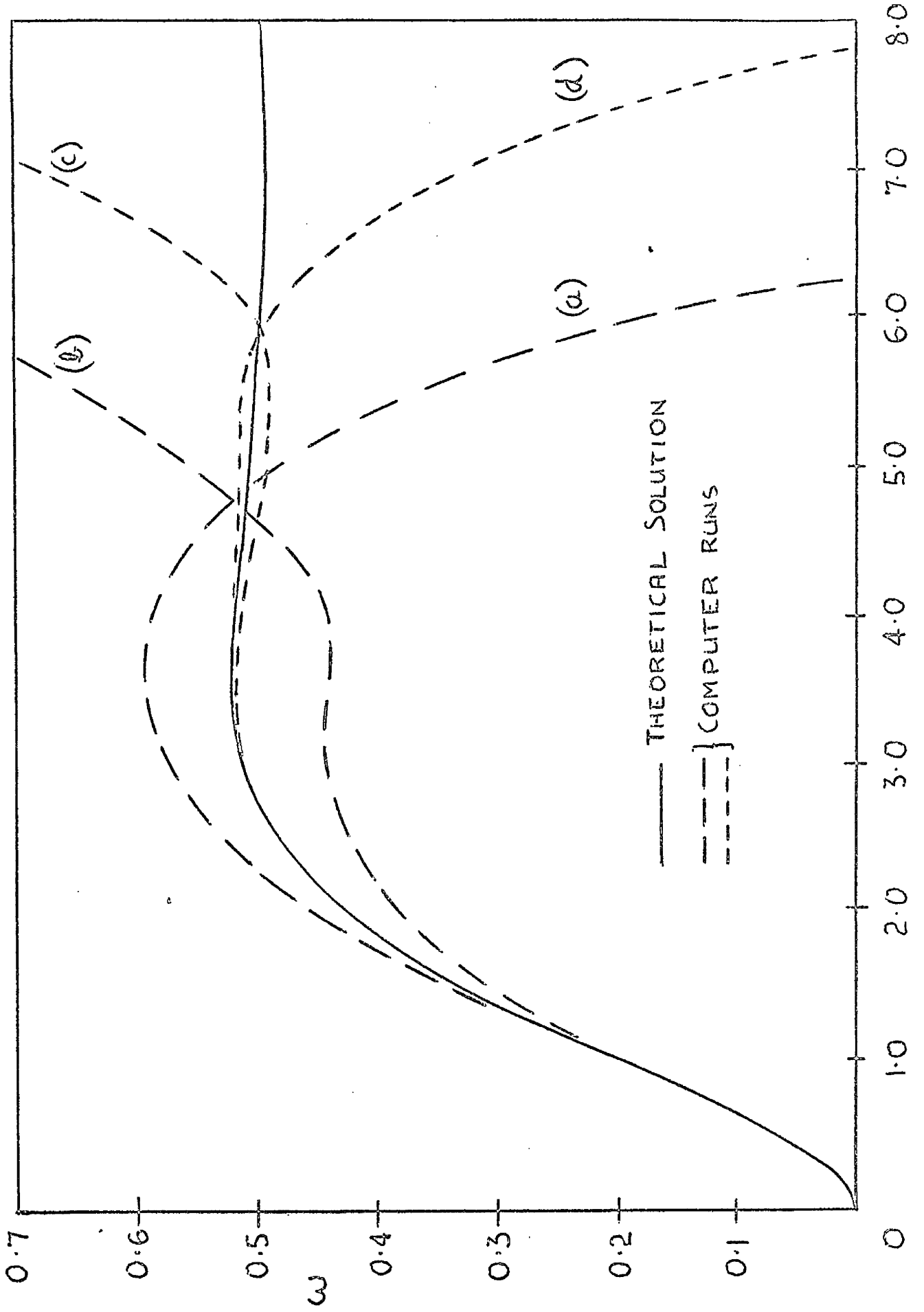

FIG. 6.2 EXAMPLES OF COMPUTER RUNS

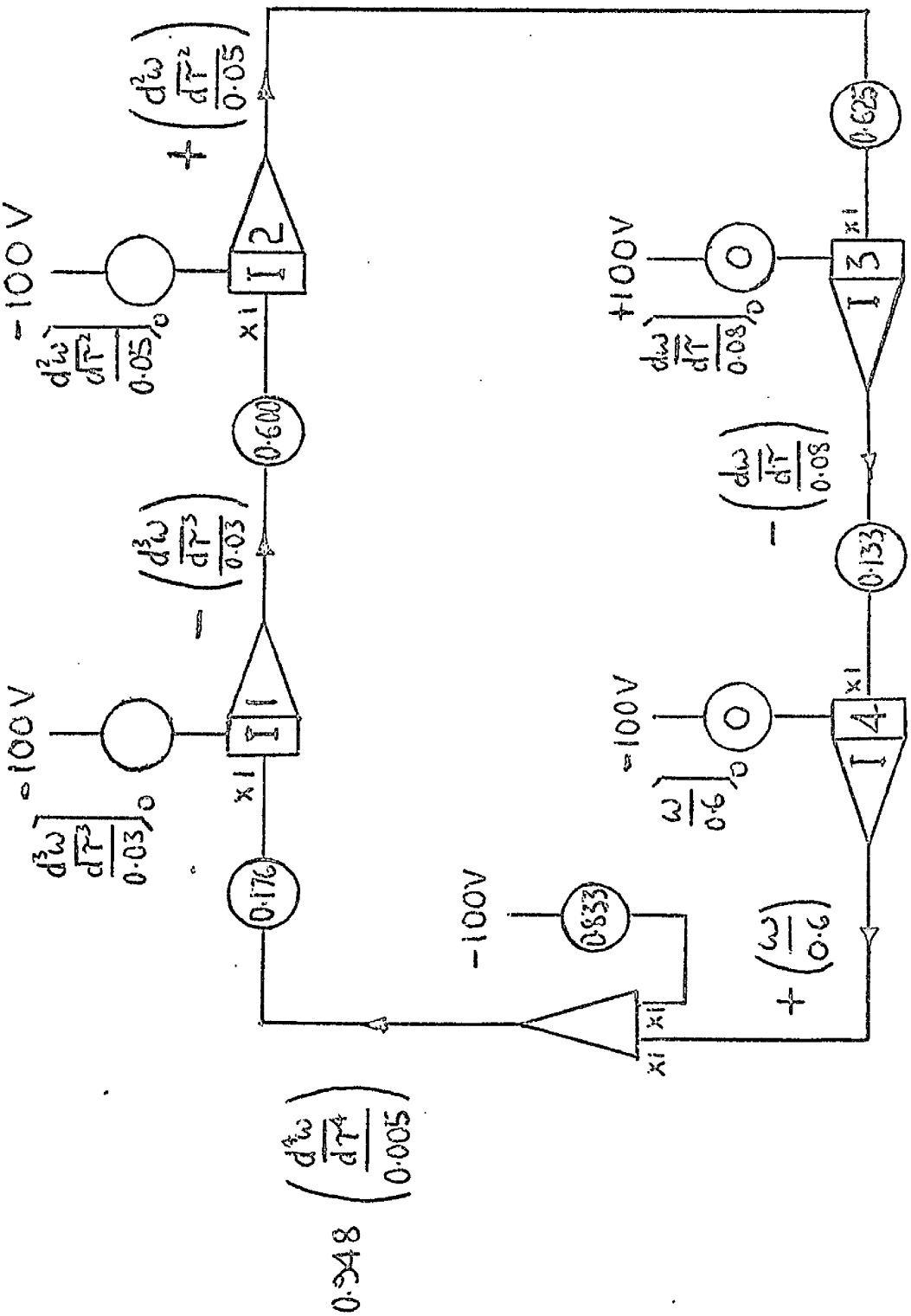

SCALED COMPUTER CIRCUIT FOR $n=1$

$\left(p=2\ ;\ T=0\right)$

FIG. 6.3

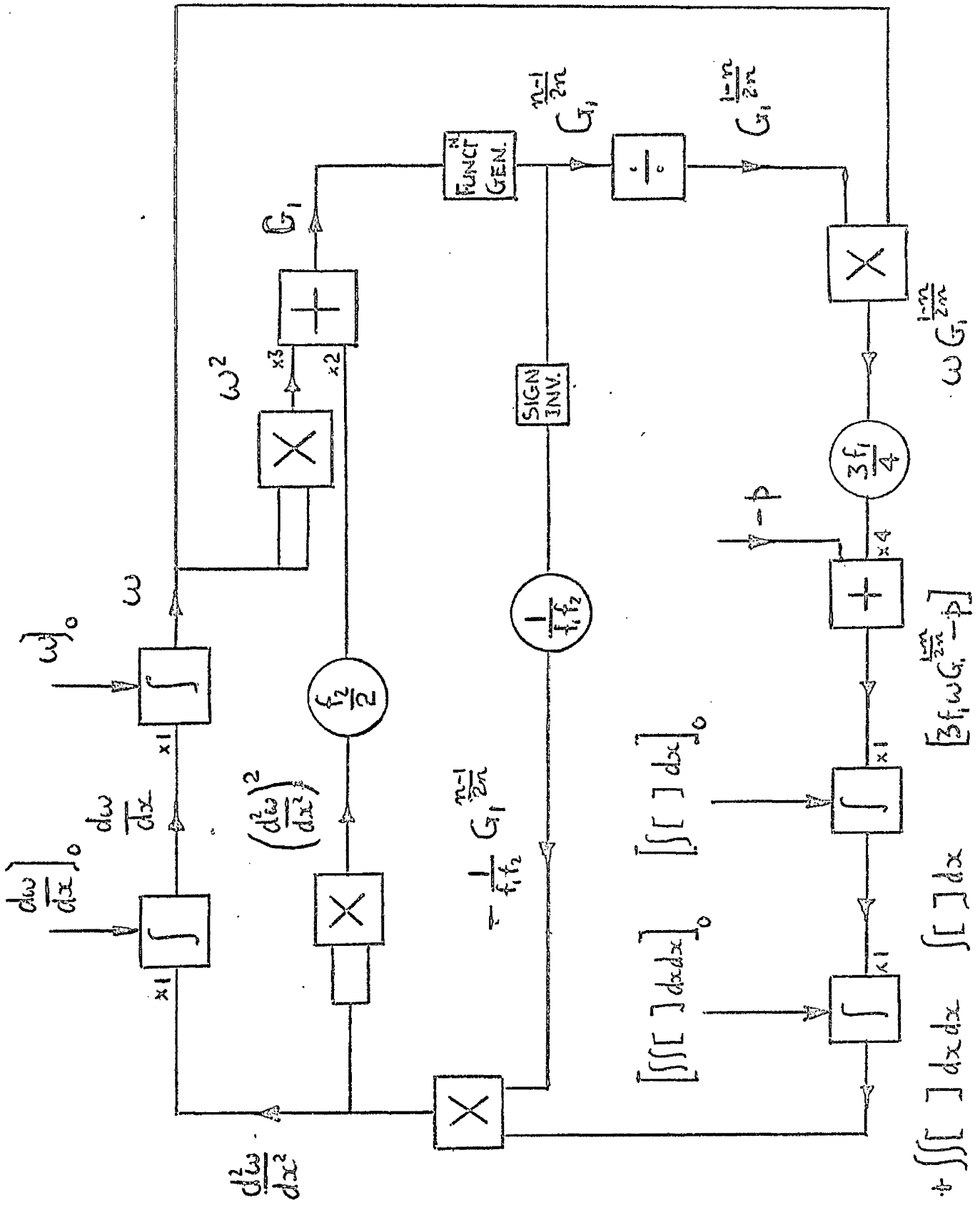

COMPUTER CIRCUIT FOR $n>1$
(ZERO AXIAL LOAD)

FIG. 6.4

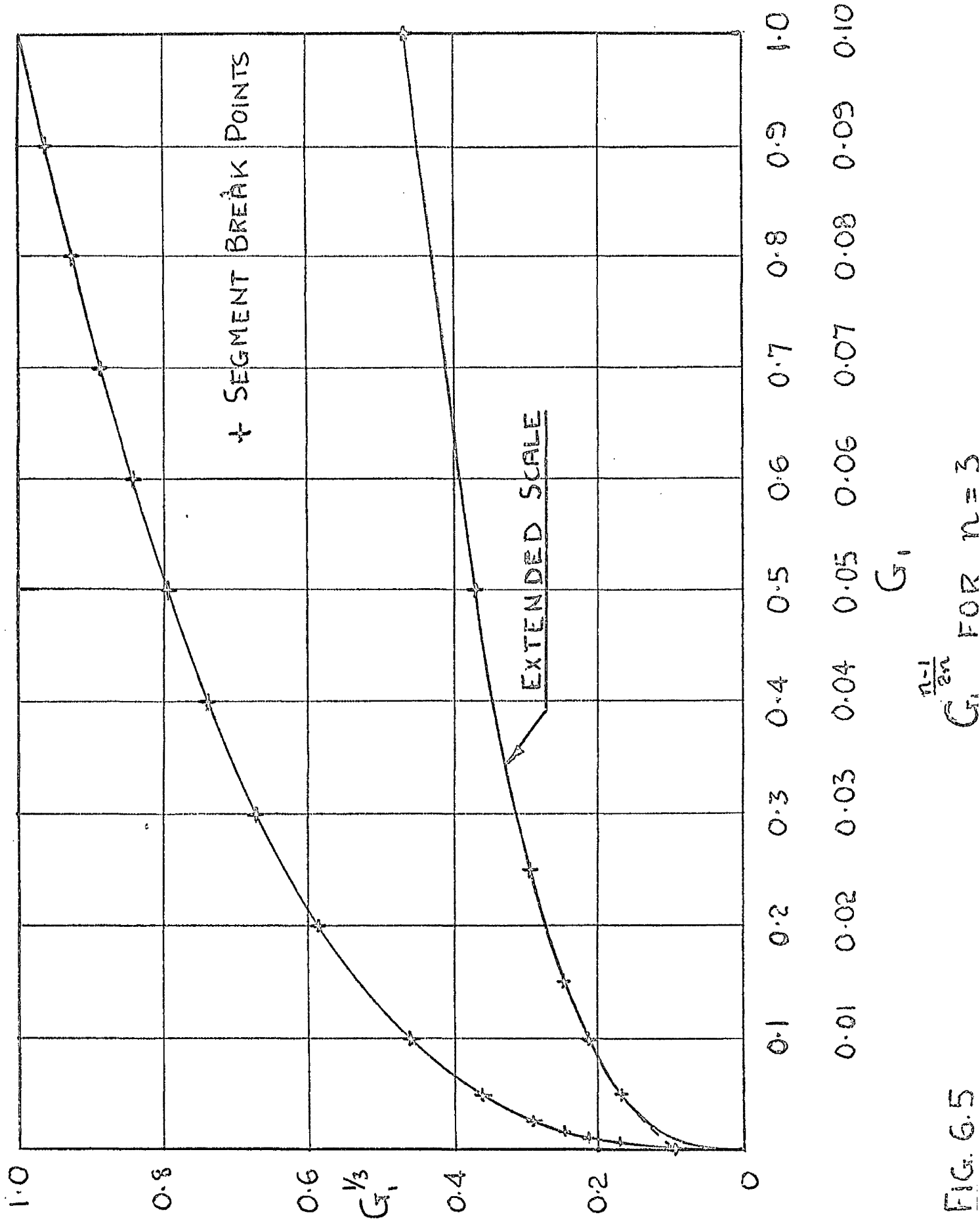

FIG. 6.5 $G_1^{\frac{n-1}{2n}}$ FOR $n=3$

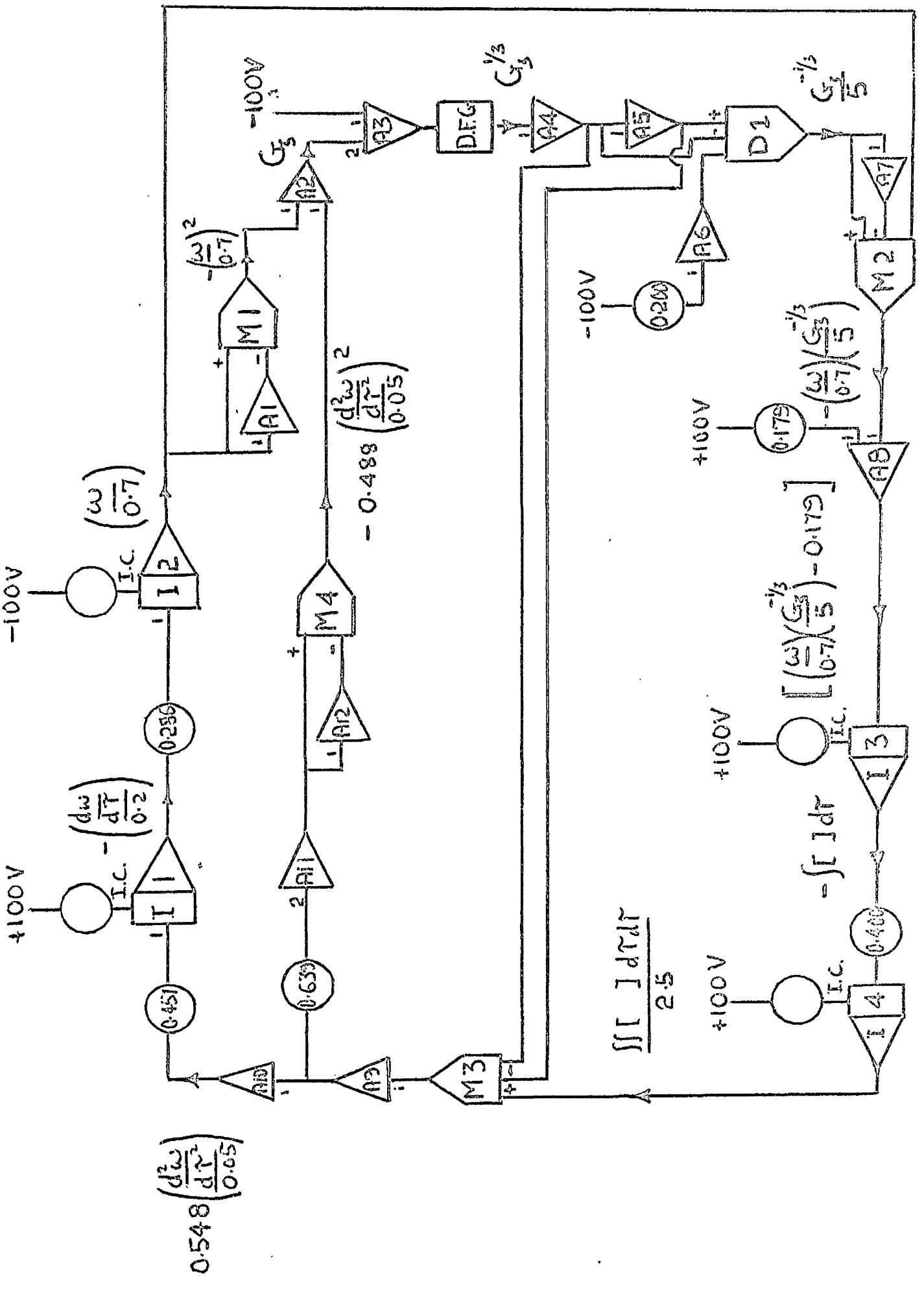
SCALED COMPUTER CIRCUIT FOR n=3; p=2
(ZERO AXIAL LOAD)
+100V
-100V
I.C.
I 1
I 2
I 3
I 4
M 1
M 2
M 3
M 4
D 1
D.F.G
A 1
A 2
A 3
A 4
A 5
A 6
A 7
A 8
A 9
A 10
A 11
A 12
A i1
A i2
0.451
0.256
0.633
0.488
0.200
0.179
0.400
0.548
$\left(\frac{d\omega}{d\tau}\frac{1}{0.2}\right)$
$\left(\frac{\omega}{0.7}\right)$
$\left(\frac{\omega}{0.7}\right)^2$
$\left(\frac{d^2\omega}{d\tau^2}\frac{1}{0.05}\right)^2$
$-0.488\left(\frac{d^2\omega}{d\tau^2}\frac{1}{0.05}\right)$
$\left(\frac{d^3\omega}{d\tau^2}\frac{1}{0.05}\right)$
$\frac{\iiint I\,d\tau\,d\tau}{2.5}$
$-\int\int I\,d\tau$
$\left[\left(\frac{\omega}{0.7}\right)\left(\frac{G_3}{5}\right)^{-1/3}-0.179\right]$
$-\left(\frac{\omega}{0.7}\right)\left(\frac{G_3}{5}\right)^{-1/3}$
G_3
$G_3^{1/3}$
$\frac{G_3^{-1/3}}{5}$

FIG. 6.6

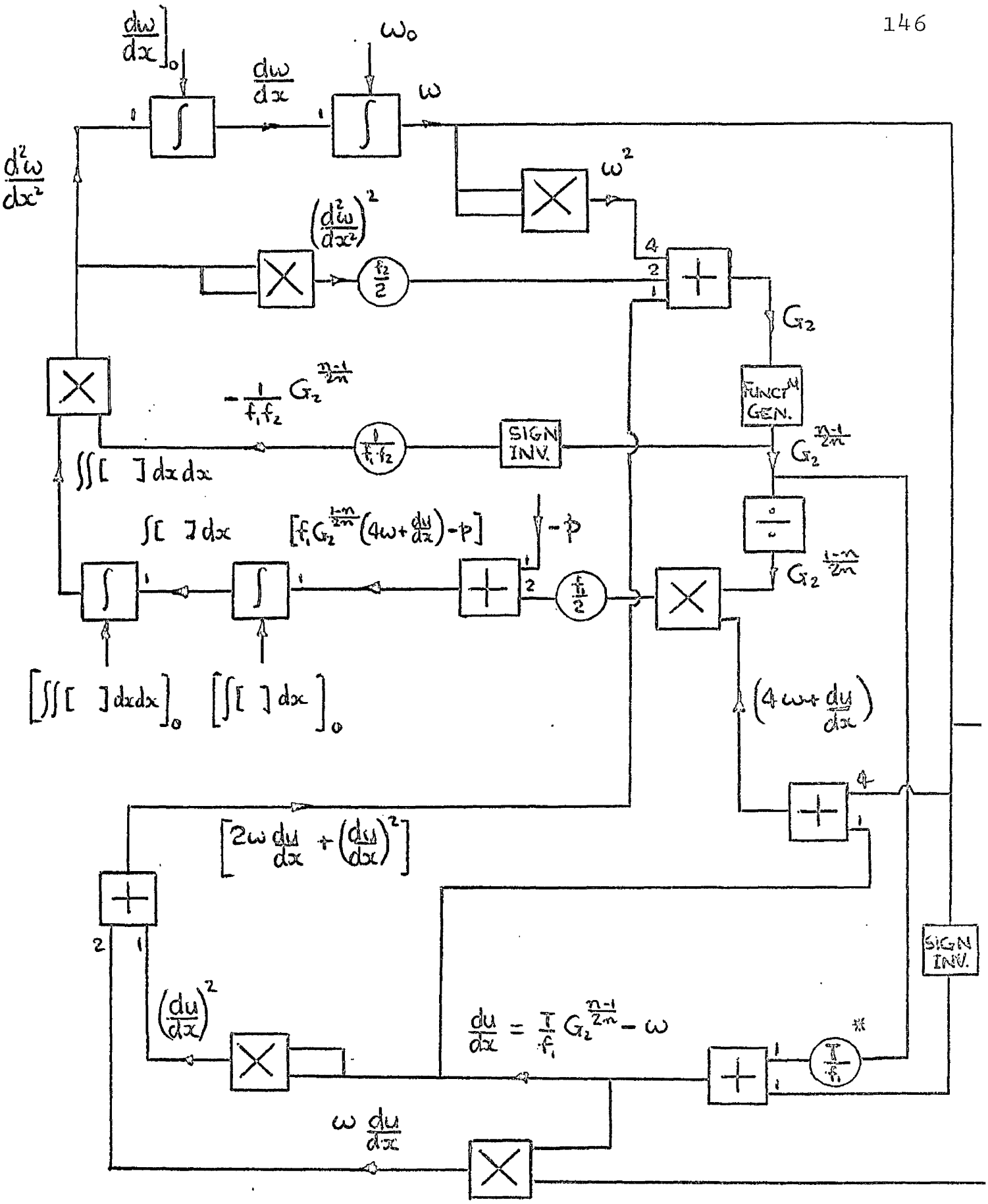

COMPUTER CIRCUIT FOR $n > 1$

CYLINDER WITH AXIAL LOAD

FIG. 6.

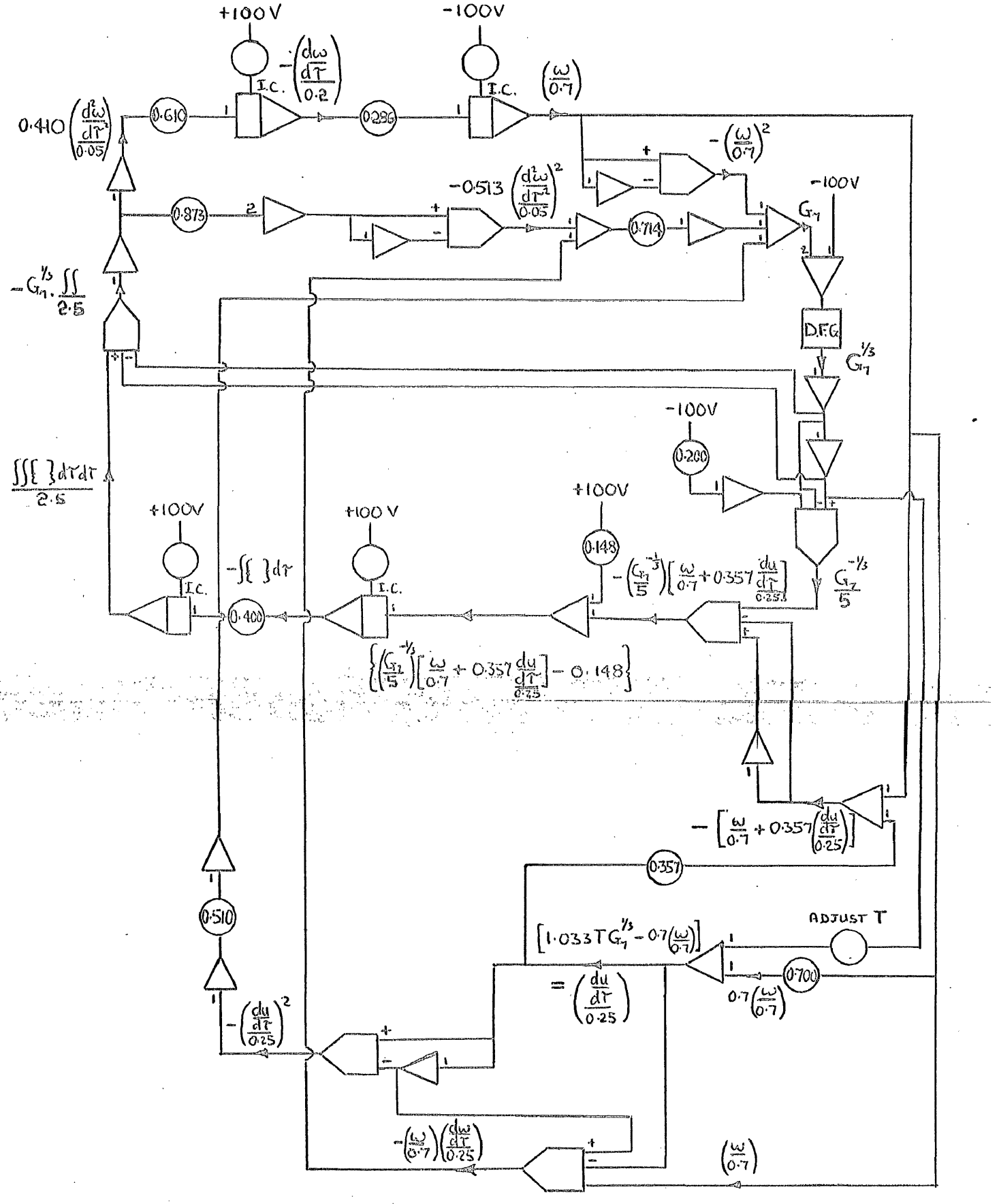

SCALED COMPUTER CIRCUIT FOR $n=3$; $p=2$

FIG. 6.8 CYLINDER WITH AXIAL LOAD

CHAPTER 7

RESULTS FOR A SEMI-INFINITE CYLINDER WITH FIXED END

7.1 Cylinder without axial load

The boundary conditions for the semi-infinite cylinder with fixed end are:

at $x = 0$ $\quad w = 0$

$$\frac{dw}{dx} = 0$$

at $x \longrightarrow \infty$ $\quad w \longrightarrow w_\infty$

If solutions are obtained for an arbitrary value of the loading parameter p, w_∞ is different for each value of n. However, p can be chosen such that w_∞ is the same for all values of n, and this gives a better basis for comparison of solutions.

p has been defined as

$$p = \frac{PA}{\sigma_0 H}$$

If σ_0 is taken as the circumferential stress in the cylinder at $x \longrightarrow \infty$, the circumferential strain, and hence the radial displacement w_∞, will be the same for all values of n.

The circumferential stress at $x \longrightarrow \infty$ is $\frac{PA}{2H}$ and if σ_0 is given this value

$$p = \frac{P\ A}{\left(\frac{PA}{2H}\right) H} = 2$$

This result also follows from equation 6.6.

The corresponding value of w_∞ is obtained from

$$\frac{W_\infty}{A} = \epsilon_o$$

and $$w_\infty = \frac{W_\infty}{2A\,\epsilon_o} = \frac{1}{2}$$

The distributions of w, $\frac{d^2w}{dx^2}$ m_x, q_x and t_θ are plotted in Figs 7.1 to 7.5 for p = 2 and n = 3, 5 and 7. The curves for n = 1 are shown for comparison. For $x > 3.0$ the curves for n = 3, 5 and 7 are shown with broken lines; the analogue computer solutions cannot be relied on for detailed trends in this region.

7.2 The effect of axial load

The effect of changes in axial load T was investigated with p = 2 and n = 3. Solutions were obtained for $0 \leq T \leq 0.6$. The value of w_∞ is different for each value of T and can be deduced as follows:

For p = 2, $$\sigma_\theta]_\infty = \sigma_o$$

and $$t_\theta]_\infty = \frac{\sigma_\theta]_\infty\ 2H}{2H\ \sigma_o} = 1$$

From equations 4.24 with, $m_x = 0$,

$$e_\theta = (t_\theta^2 - t_\theta t_x + t_x^2)^{\frac{n-1}{2}} (t\theta - \tfrac{1}{2} t_x)$$

$\therefore$ with $t_\theta\big]_\infty = 1$ and $t_x = T$

$$e_\theta\big]_\infty = (1 - T + T^2)^{\frac{n-1}{2}} (1 - \frac{T}{2})$$

But $e_\theta\big]_\infty = 2 w_\infty$ from equations 5.8

$$\therefore \quad w_\infty = \tfrac{1}{2} (1 - T + T^2)^{\frac{n-1}{2}} (1 - \frac{T}{2})$$

and, for n = 3,

$$w_\infty = \tfrac{1}{2} (1 - T + T^2)(1 - \frac{T}{2}) \qquad (7.1)$$

Values of w_∞ computed from equation 7.1 are plotted against T in Fig 7.6 together with values obtained from computer solutions for the curvature and axial strain at the fixed end, $\frac{d^2w}{dx^2}\big]_o$ and $\frac{du}{dx}\big]_o$, respectively. The bending moment m_o and shear force q_o at the fixed end are plotted against T in Fig 7.7. The curves for n = 1 are shown in each case.

The value T = 0.5 is the axial load in a cylinder with closed ends under uniform internal pressure p = 2.

This follows from

$$T = \frac{T_x}{2H\sigma_o} = \frac{\pi A^2}{2\pi A}\frac{P}{2H\sigma_o}$$

with $P = p\frac{\sigma_o H}{A}$

$$T = \frac{p}{4}$$

and for $p = 2$, $T = \frac{1}{2}$.

7.3 Cylinder under internal pressure

Because of its practical importance, the long cylinder with fixed ends under internal pressure was investigated further for $n = 3$. With the result obtained in paragraph 3.2 (c), it is again possible to choose a value of p which will give the same w_∞ for all values of n. From equation 3.9, the condition for this is

$$\sigma_o = 0.433\,\frac{PA}{H}$$

and $$\phi = \frac{PA}{\sigma_o H} = \left(\frac{H}{0.433PA}\right)\cdot\frac{PA}{H} = 2.31$$

It can be shown, as in paragraph 7.2, that with this value of ϕ

$$w_\infty = 0.433$$

Graphs of w, $\frac{d^2w}{dx^2}$, $\frac{du}{dx}$ and q_x, m_x plotted against x are given in Figs 7.8 to 7.10 for n = 3 and n = 1.

It was considered to be of interest to compare the solution for the cylinder under internal pressure with that for a cylinder under uniform radial loading p = 2 and zero axial load, when w_∞ was the same in the two cases. It is easily shown that this condition is achieved if p = 2.42 for internal pressure. The solutions for the two conditions are plotted together in Figs 7.11 to 7.13.

7.4 Discussion

The rate at which the radial displacement w builds up from the fixed end in the cylinder without axial load, depends on the value of n, and is greatest when n = 1. The curvature $\frac{d^2w}{dx^2}$ reduces rapidly from a maximum value at the fixed end; the higher the value of n, the greater is the rate of decay.

For n = 1, the bending moment m_x is directly proportional to $\frac{d^2w}{dx^2}$, and the curves of m_x and $\frac{d^2w}{dx^2}$ plotted against x have the same shape. With $n > 1$, m_x is a non-linear function of both $\frac{d^2w}{dx^2}$ and w, and the

curves of $\frac{d^2w}{dx^2}$ and m_x have markedly different shapes; although raising the value of n increases the rate at which $\frac{d^2w}{dx^2}$ decays, it reduces the rate of decay of m_x. The curves of w and t_θ for different values of n show a similar effect, t_θ being directly proportional to w for n = 1.

The analogue computer results are not accurate enough at large values of x to give precise information on the decay of end effects. The indications are, however, that even for n = 7, a cylinder having a length x = 8, approximately, may be regarded as semi-infinite. For a thickness to radius ratio of $\frac{1}{100}$, for example, x = 8 is 0.565x radius, and for a ratio of $\frac{1}{10}$ it is 1.79x radius.

Two important factors in the design of cylindrical shells with fixed ends are the maximum values of bending moment and curvature change, m_o and $\left.\frac{d^2w}{dx^2}\right]_o$, respectively; the former in calculations for the maximum stress, the latter in calculations for the maximum strain. The results for the cylinder without axial load show small variations in these maximum values with n. m_o decreases with n, being about 8% lower for

n = 3 than for n = 1, and about 12% lower for n = 7. The values of $\left.\frac{d^2w}{dx^2}\right]_o$ for n = 3, 5 and 7 fall within 10% of the value for n = 1. Observations made on errors in paragraph 6.5 suggest that $\left.\frac{d^2w}{dx^2}\right]_o$ might be in error by $\pm$ 2 n%. Even with allowance for such error, the value for n = 7 is unlikely to be more than 20 - 30% greater than that for n = 1.

These results suggest that the linear solution may be used to make reasonable estimates of important quantities in shells behaving in the assumed non-linear manner. For given radial loading P and dimensions of shell A, H, the loading parameter p = 2 defines the reference stress σ_o, i.e.

$$\sigma_o = \frac{PA}{2H}$$

The reference strain is obtained from equation 1.1, or directly from the stress/strain diagram, and the ratio $\frac{\sigma_o}{\epsilon_o}$ is used for the modulus of elasticity in the linear analysis, Poisson's ratio being taken as $\frac{1}{2}$. The solution so obtained gives the correct value for the radial displacement away from the fixed end and reasonable estimates of m_o and $\left.\frac{d^2w}{dx^2}\right]_o$ for $1 \leq n \leq 7$.

This method for estimating important quantities in the fixed end cylinder is analogous to that applied to simple structures in Chapter 3. It may be expected to give reasonable estimates with non-linear laws besides the n-power law.

It is likely, furthermore, that the method may be useful for other boundary value problems, In a preliminary investigation, a series of solutions was obtained in which the edge slope $\left.\frac{dw}{dx}\right]_o$ was zero, but the edge displacement w_o was given different values. The displacement w_∞ was again made the same for all values of n by choosing p = 2. In Figs 7.14 to 7.16 m_o, $\left.\frac{d^2w}{dx^2}\right]_o$ and q_o are plotted for w_o varying from 0 to w_∞ for n = 1, 3 and 7. For this range of w_o, the n = 1 solution will always lead to overestimation of m_o and q_o. Except with small values of w_o, it should also give conservative estimates for $\left.\frac{d^2w}{dx^2}\right]_o$.

For a given uniform radial loading, the effect of increasing the axial load in a fixed end cylinder is to reduce w_∞, $\left.\frac{d^2w}{dx^2}\right]_o$, m_o and q_o and to increase the

maximum mid-surface axial strain $\left.\frac{du}{dx}\right]_o$ —Figs 7.6 and 7.7. For n = 3, w_∞ , $\left.\frac{d^2w}{dx^2}\right]_o$ and $\left.\frac{du}{dx}\right]_o$ are non-linear functions of the axial load T but q_o and m_o depend linearly on T . It may be shown[27],[28] that for the assumed homogeneous stress/strain relations, the stresses in the shell vary linearly with the applied load for all values of n. The results of Fig 7.7 are thus a further indication of the accuracy of solutions obtainable on the analogue computer. Solutions were obtained at 0.1 intervals of T and the maximum deviation of q_o and m_o from the straight lines drawn was less than 1%.

The solution for the fixed end cylinder under internal pressure with n = 3 - Figs 7.8 to 7.10 - again suggests that the linear solution may be used to make reasonable estimates of important quantities if p is chosen to make w_∞ the same for all n-values. The values for $\left.\frac{d^2w}{dx^2}\right]_o$, mo and q_o for the cylinder under internal pressure are close to those for the cylinder under radial loading with zero axial load when w_∞ is made the same, and there is little difference in the deflected shapes - Figs 7.11 to 7.13. The

distribution of mid-surface axial strain $\frac{du}{dx}$, however, is entirely different in the two cases - Fig 7.13.

In paragraph 4.5, it was suggested that when solutions to boundary value problems had been obtained with the approximate relations, a check should be made on the domain of the Ψ-surface in which the solutions lie. This has been done for the fixed end cylinder under internal pressure with n = 3. In Table 7.1, the ratios $\frac{e_\theta}{e_x}$, and $\frac{k_x}{e_x}$ are given for $0 \leq x \leq 3$.

x	$\frac{e_\theta}{e_x}$	$\frac{1}{\frac{e_\theta}{e_x}}$	$\frac{k_x}{e_x}$	$\frac{1}{\frac{k_x}{e_x}}$
0	0.000			0.614
0.1	0.012			0.709
0.2	0.089			0.822
0.4	0.447		0.987	
0.6		0.910	0.791	
0.8		0.518	0.567	
1.0		0.338	0.267	
1.5		0.149	-0.594	
2.0		0.073		-0.705
3.0		0.005		-0.125

Table 7.1

Referring to Fig 4.5, and identifying e_x with e_1 and e_θ with e_2 ($k_\theta = k_2 = 0$) shows that the solution lies between $e_2 = 0$ and $e_1 = 0$ and includes sections ③ , ② , ① , ⑧ and ⑦. It was in the region of section ③ that agreement between the exact and approximate relations was poorest. Experiments on the fixed and cylinder under internal pressure might provide a critical test of analyses based on the approximate relations.

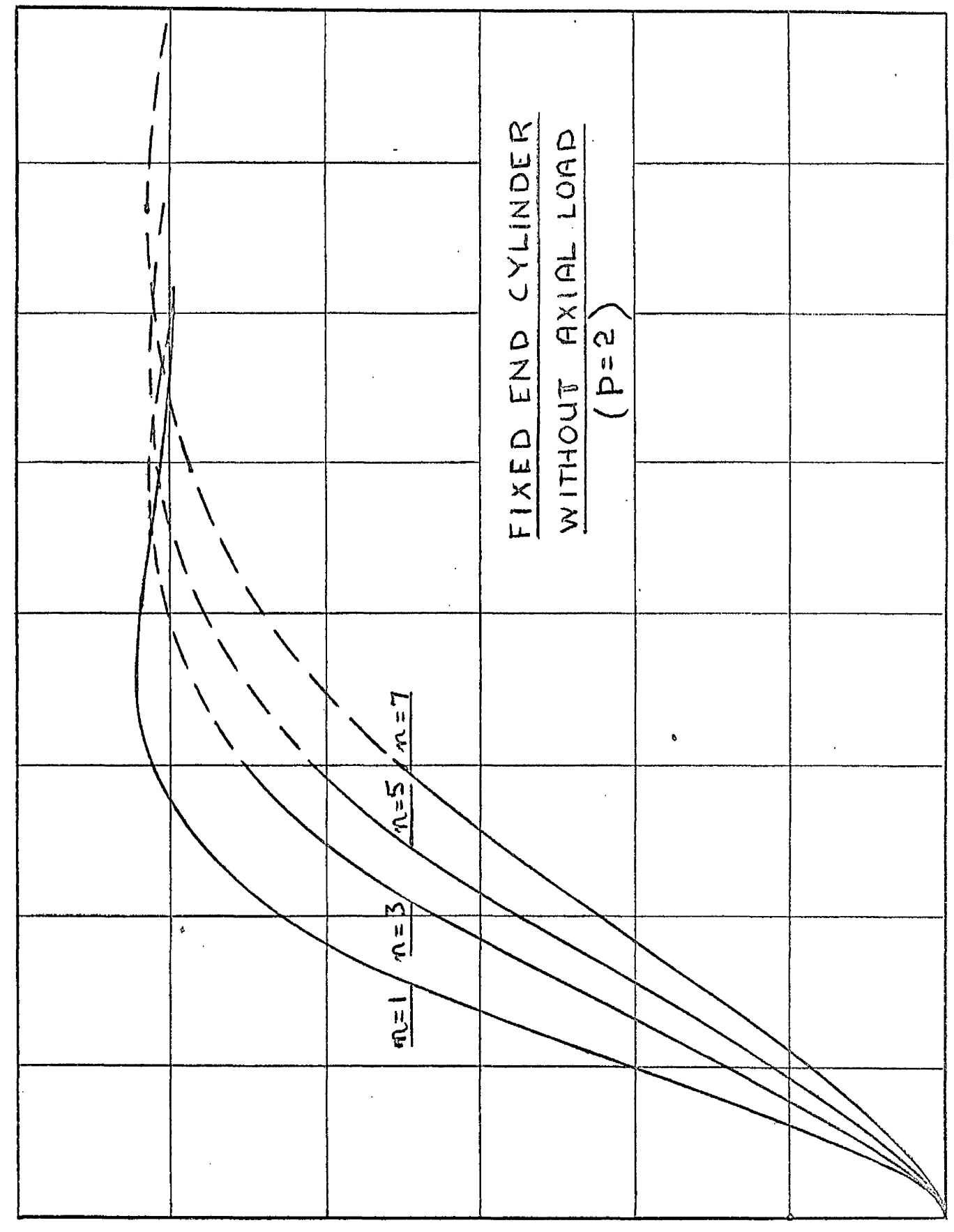
FIXED END CYLINDER
WITHOUT AXIAL LOAD
(P=2)
n=1
n=3
n=5
n=7
ω
χ
0·6
0·5
0·4
0·3
0·2
0·1
0
1
2
3
4
5
6
7
8

FIG. 7.1

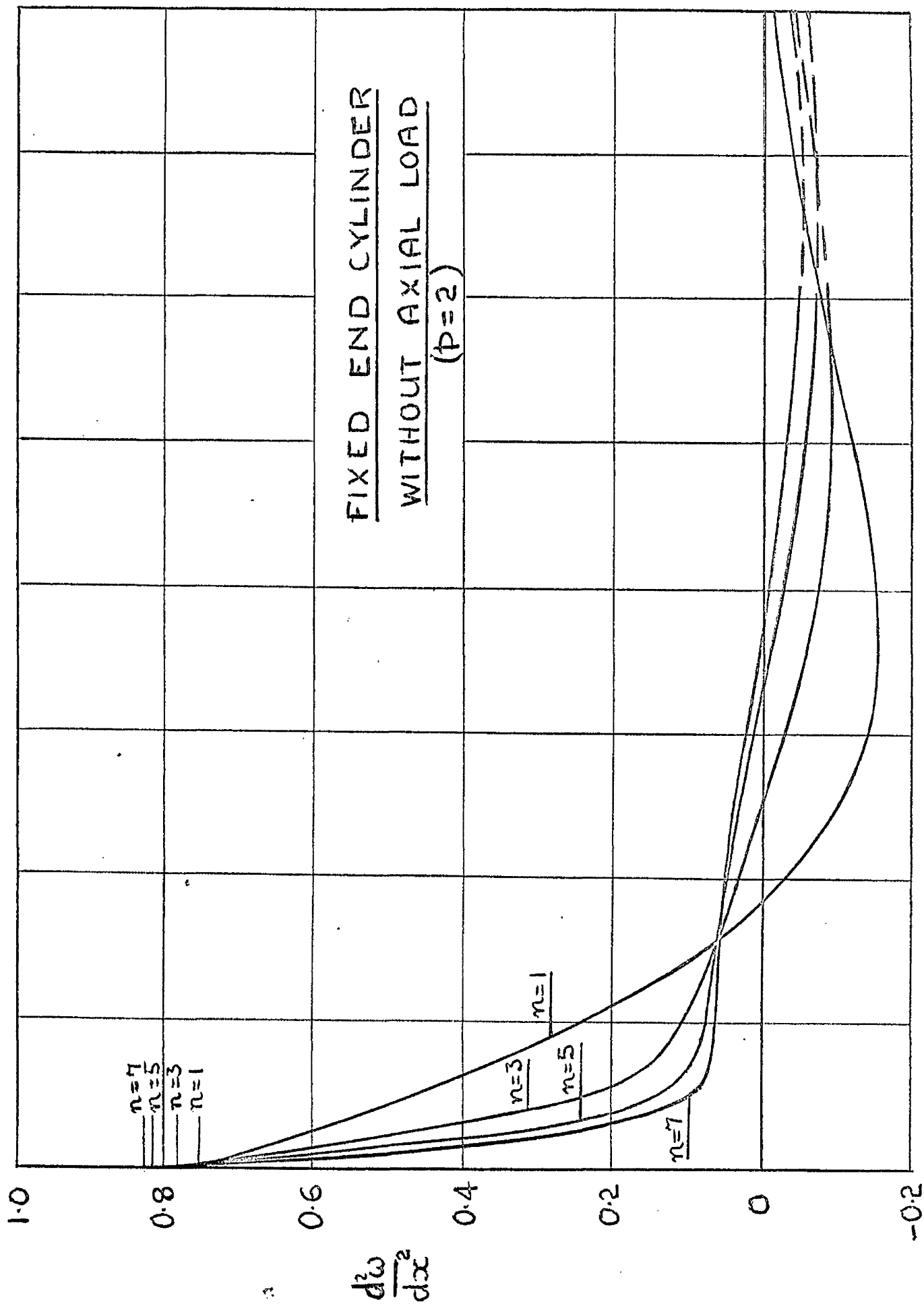
FIXED END CYLINDER
WITHOUT AXIAL LOAD
(p=2)
n=7
n=5
n=3
n=1
1·0
0·8
0·6
0·4
0·2
0
-0·2
0
1
2
3
4
x
$\frac{d^2\omega}{dx^2}$

FIG. 7.2

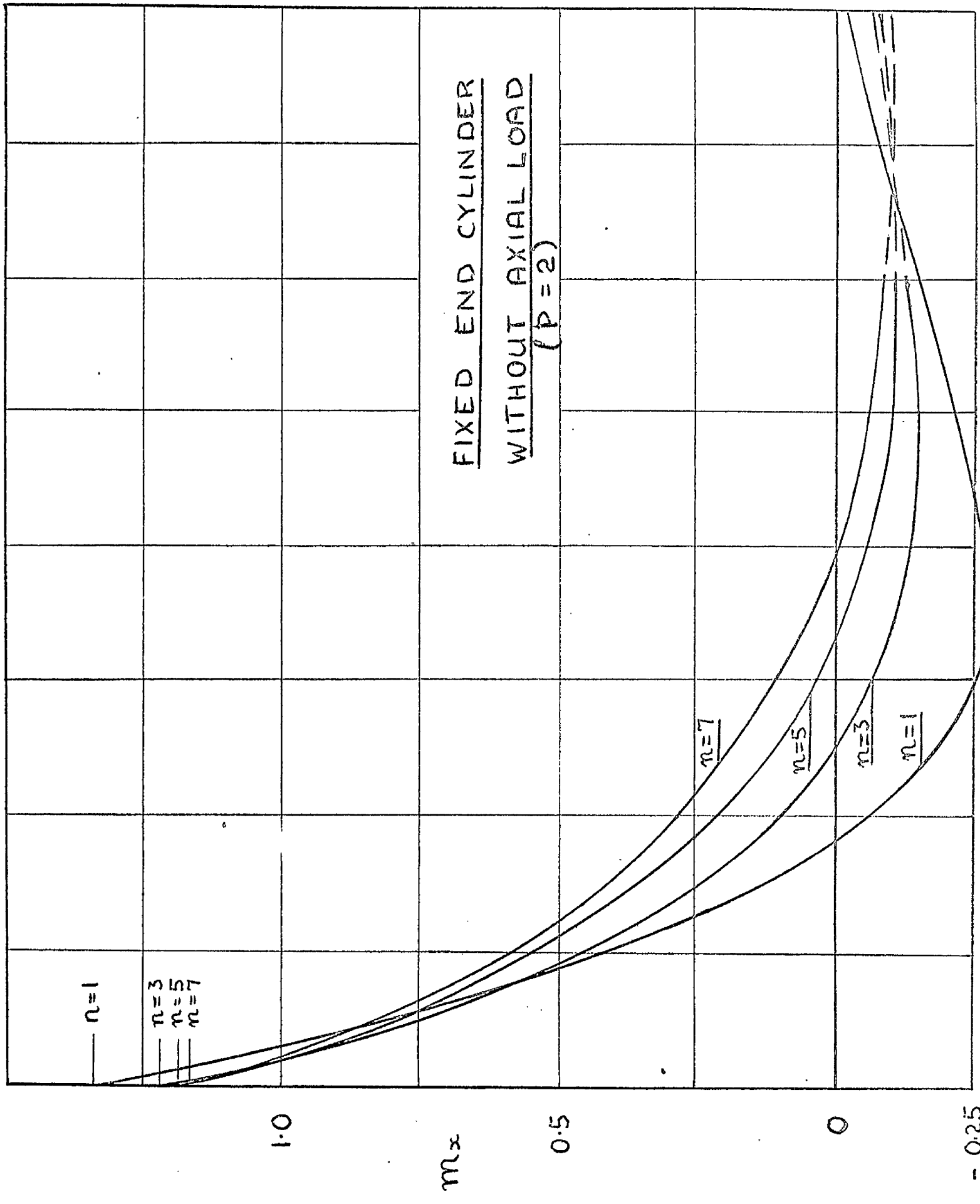
FIXED END CYLINDER
WITHOUT AXIAL LOAD
(P=2)
n=1
n=3
n=5
n=7
n=1
n=3
n=5
n=7
1.0
0.5
0
- 0.25
m_x
0
1
2
3
4

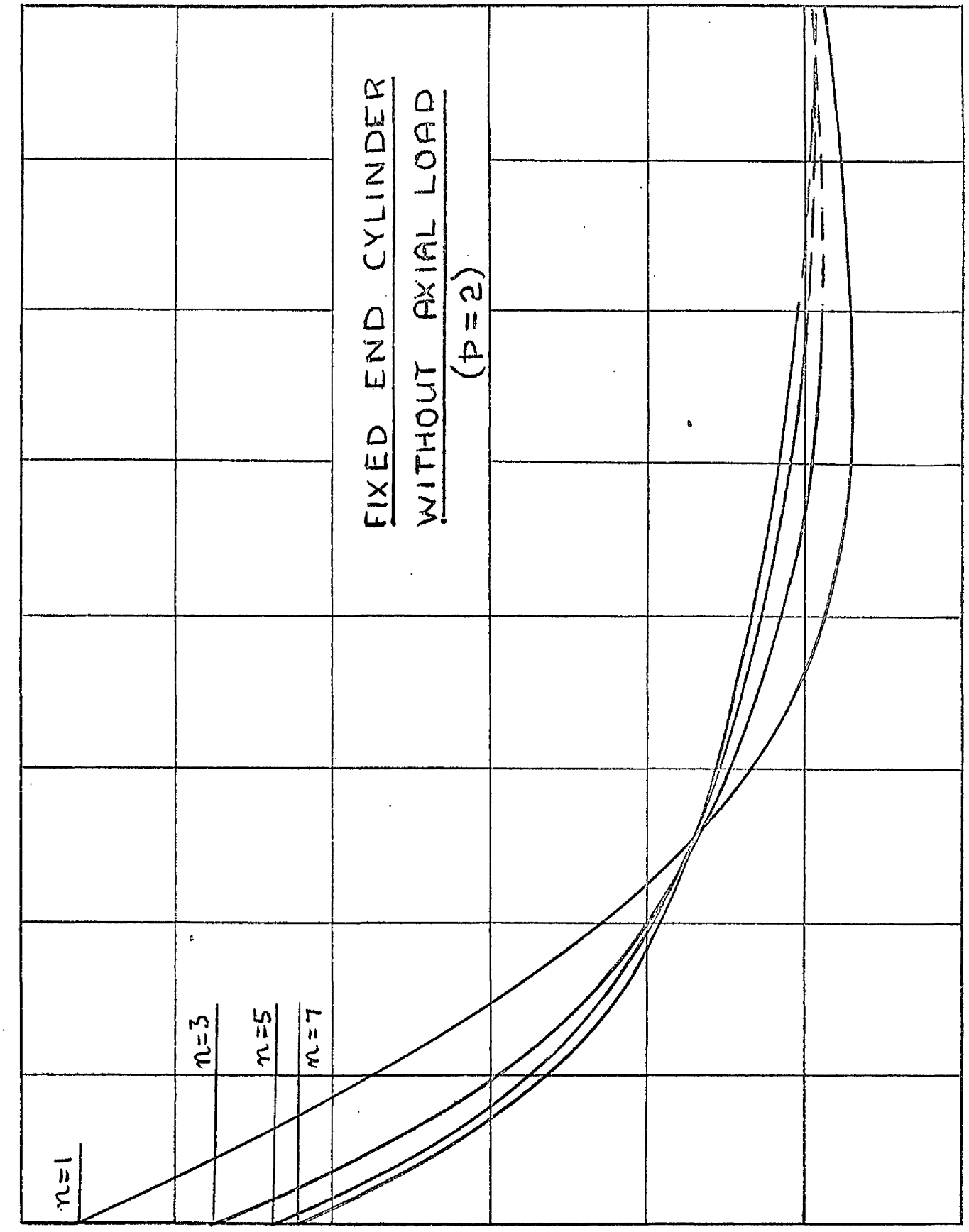
FIXED END CYLINDER
WITHOUT AXIAL LOAD
(p=2)
n=1
n=3
n=5
n=7
2.5
2.0
1.5
1.0
0.5
0
-0.5
0
1
2
3
4
x
q_x

Fig. 7.4

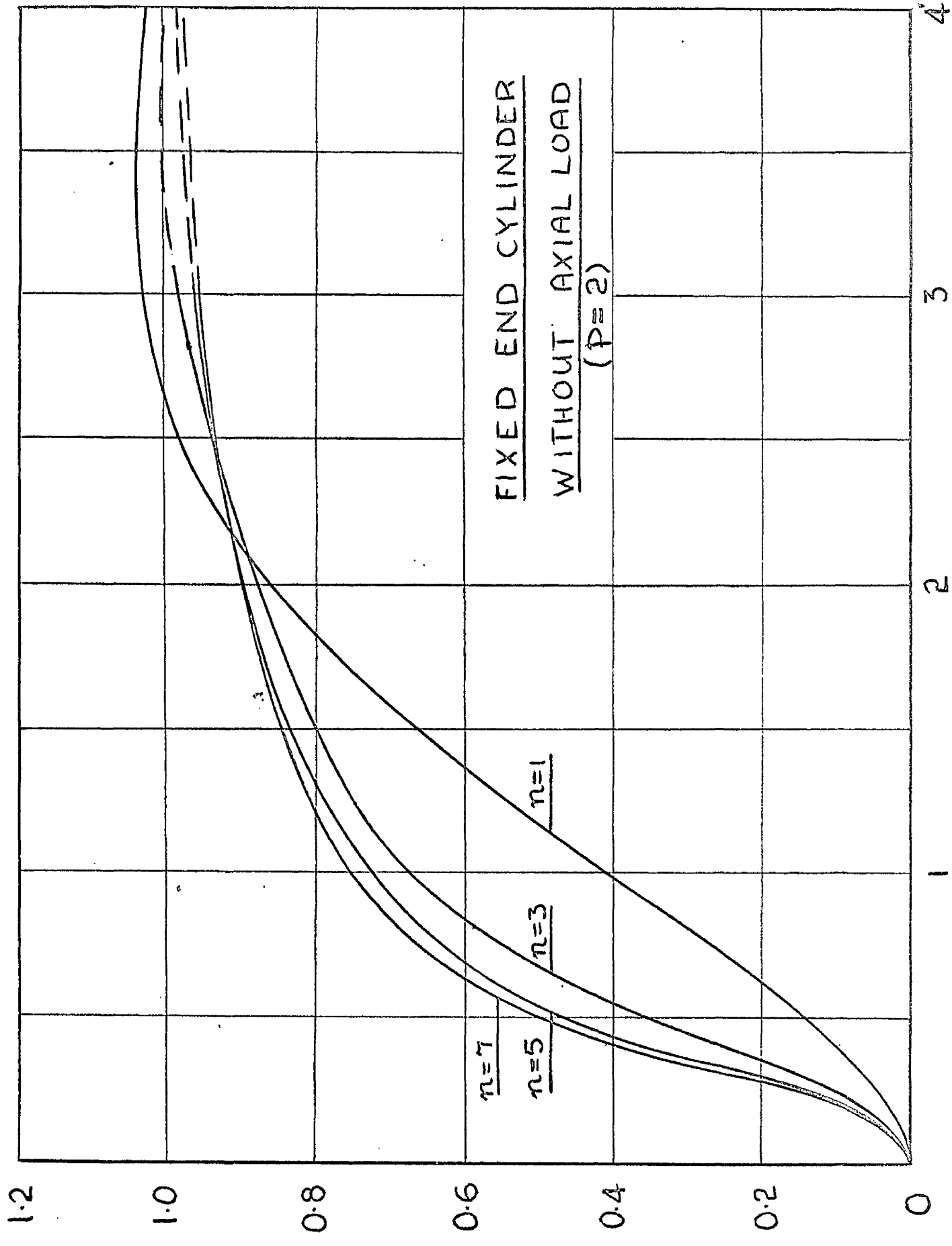
FIXED END CYLINDER
WITHOUT AXIAL LOAD
(P=2)
n=1
n=3
n=5
n=7
t_e
1·2
1·0
0·8
0·6
0·4
0·2
0
1
2
3
4
α

FIG. 7.5

EFFECT OF AXIAL LOAD IN FIXED END CYLINDER

(p=2)

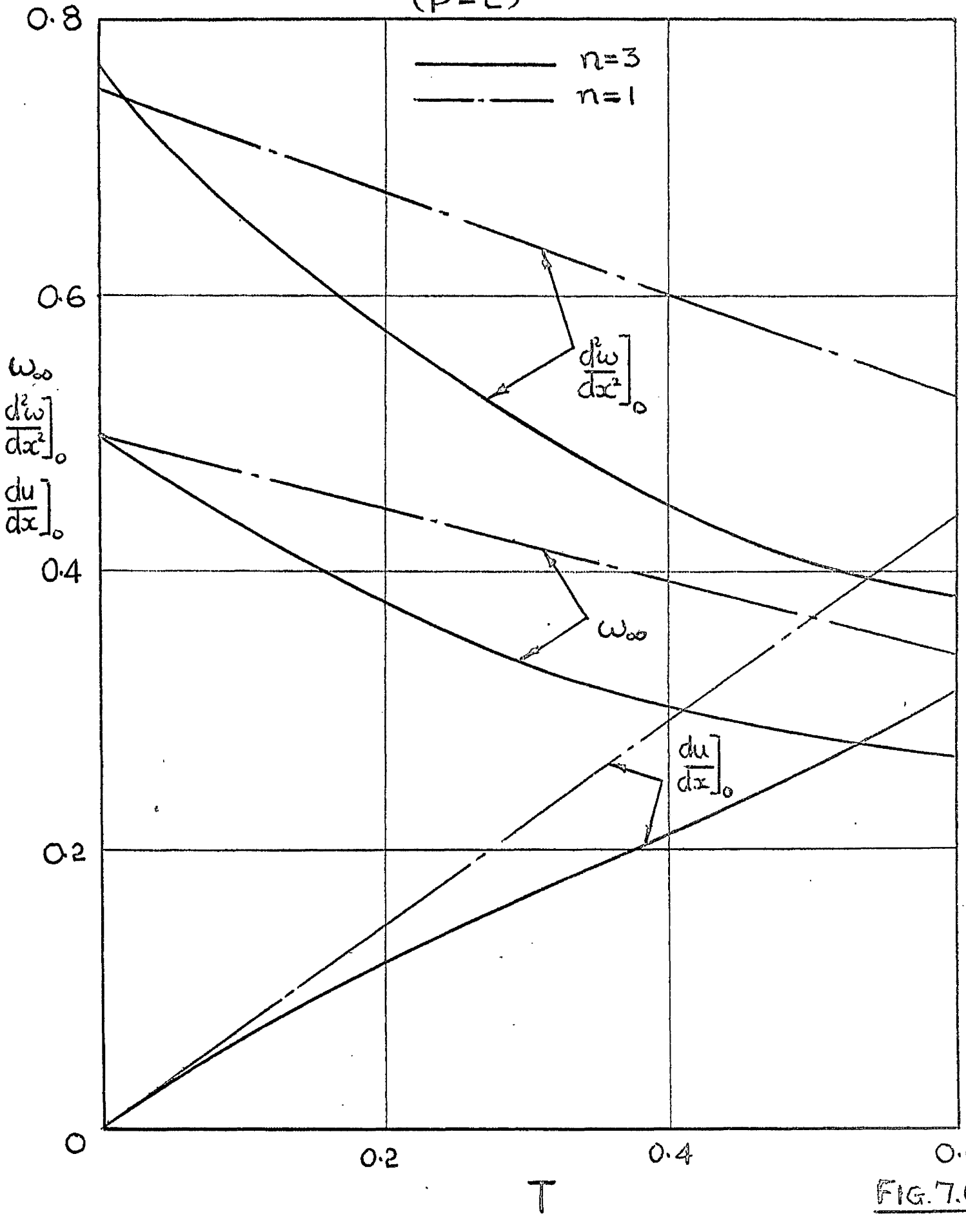

FIG. 7.6

EFFECT OF AXIAL LOAD IN FIXED END CYLINDER

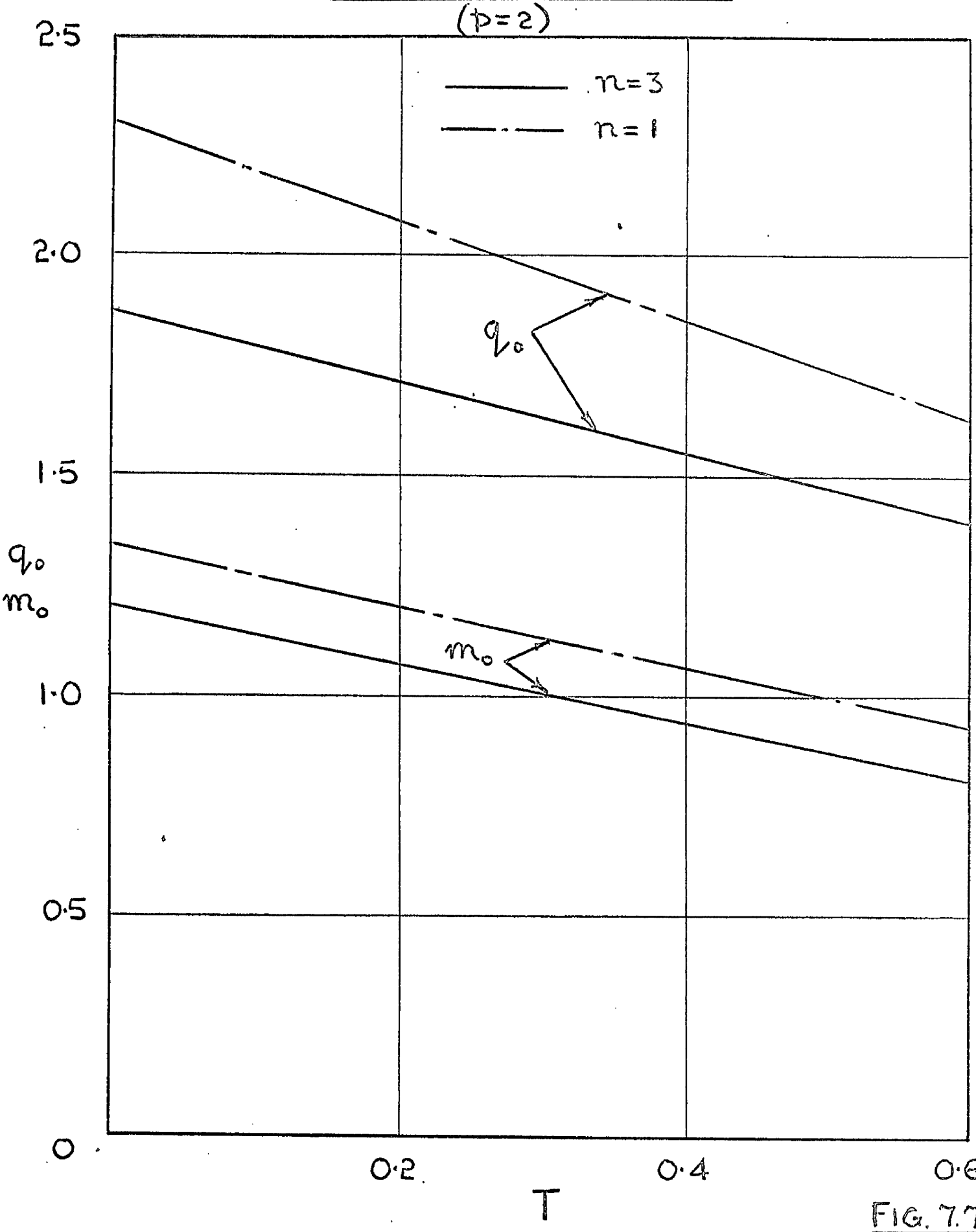

FIG. 7.7

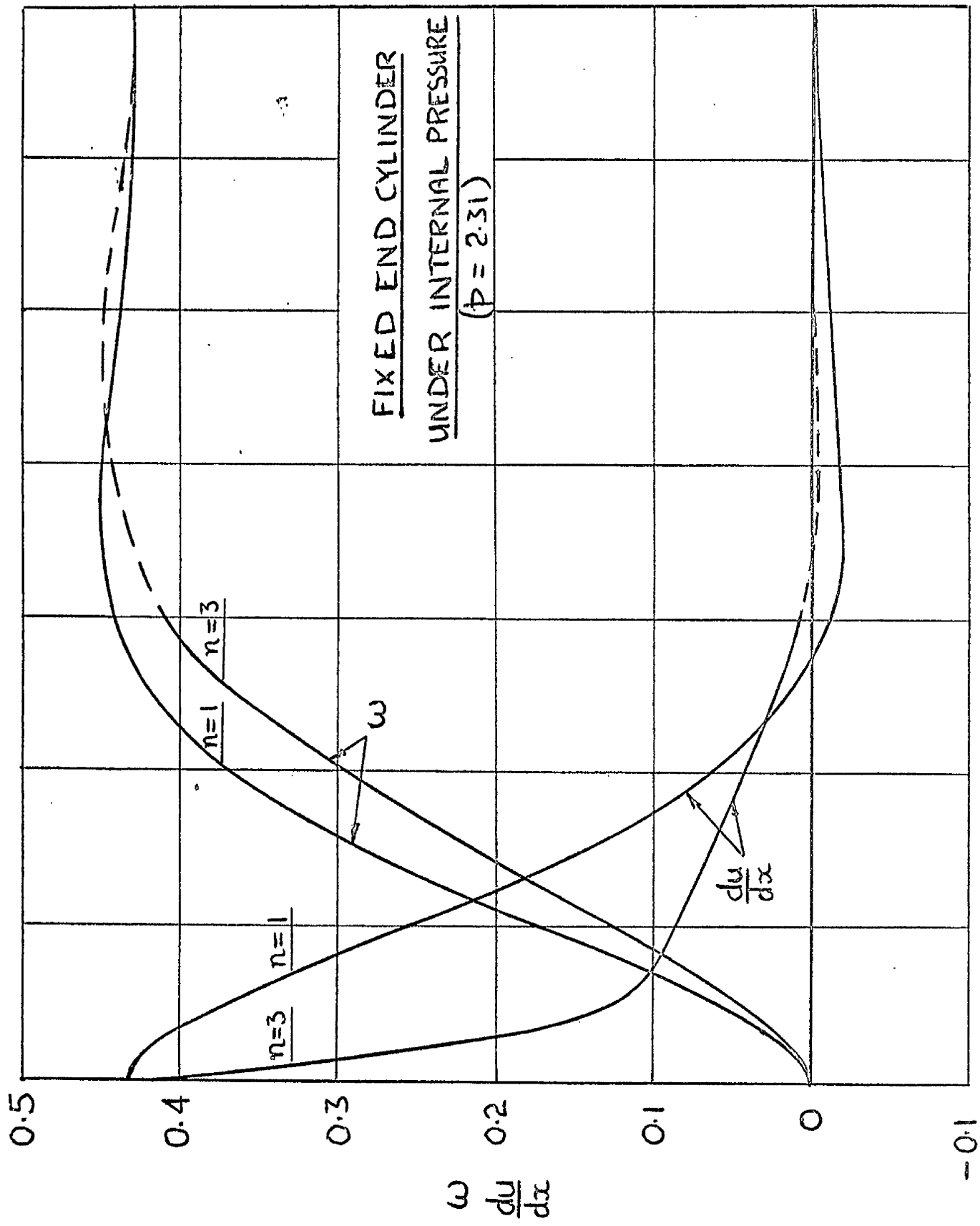
FIXED END CYLINDER
UNDER INTERNAL PRESSURE
(p = 2.31)
n=3
n=1
n=1
n=3
ω
dy/dx
ω dy/dx
x
0.5
0.4
0.3
0.2
0.1
0
-0.1
0
1
2
3
4
5
6
7

FIG. 7.8

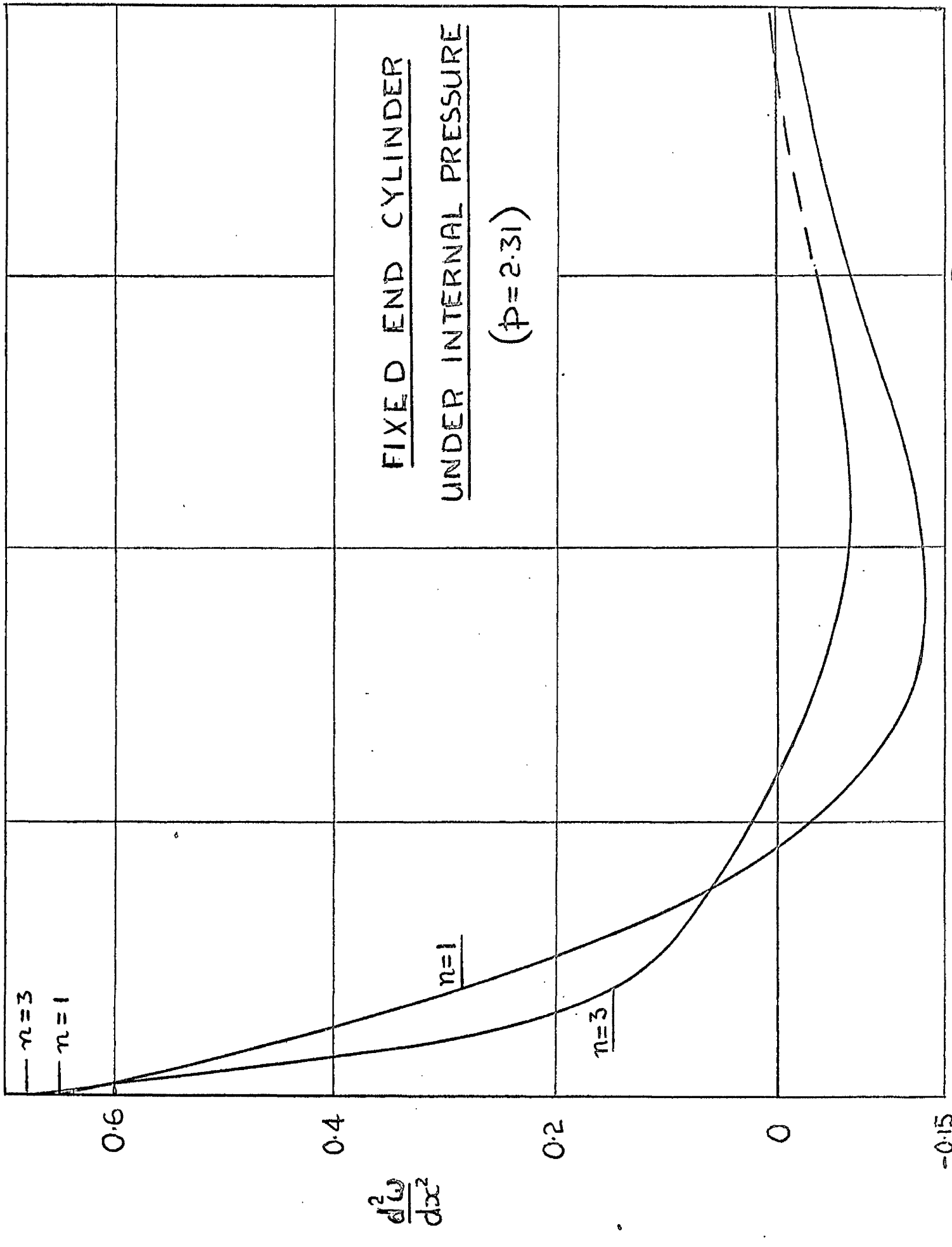
FIXED END CYLINDER
UNDER INTERNAL PRESSURE
(p=2.31)
n=3
n=1
n=1
n=3
0·6
0·4
0·2
0
-0·15
0
1
2
3
4
$\frac{d^2w}{dx^2}$

FIXED END CYLINDER UNDER INTERNAL PRESSURE

($\beta = 2.31$)

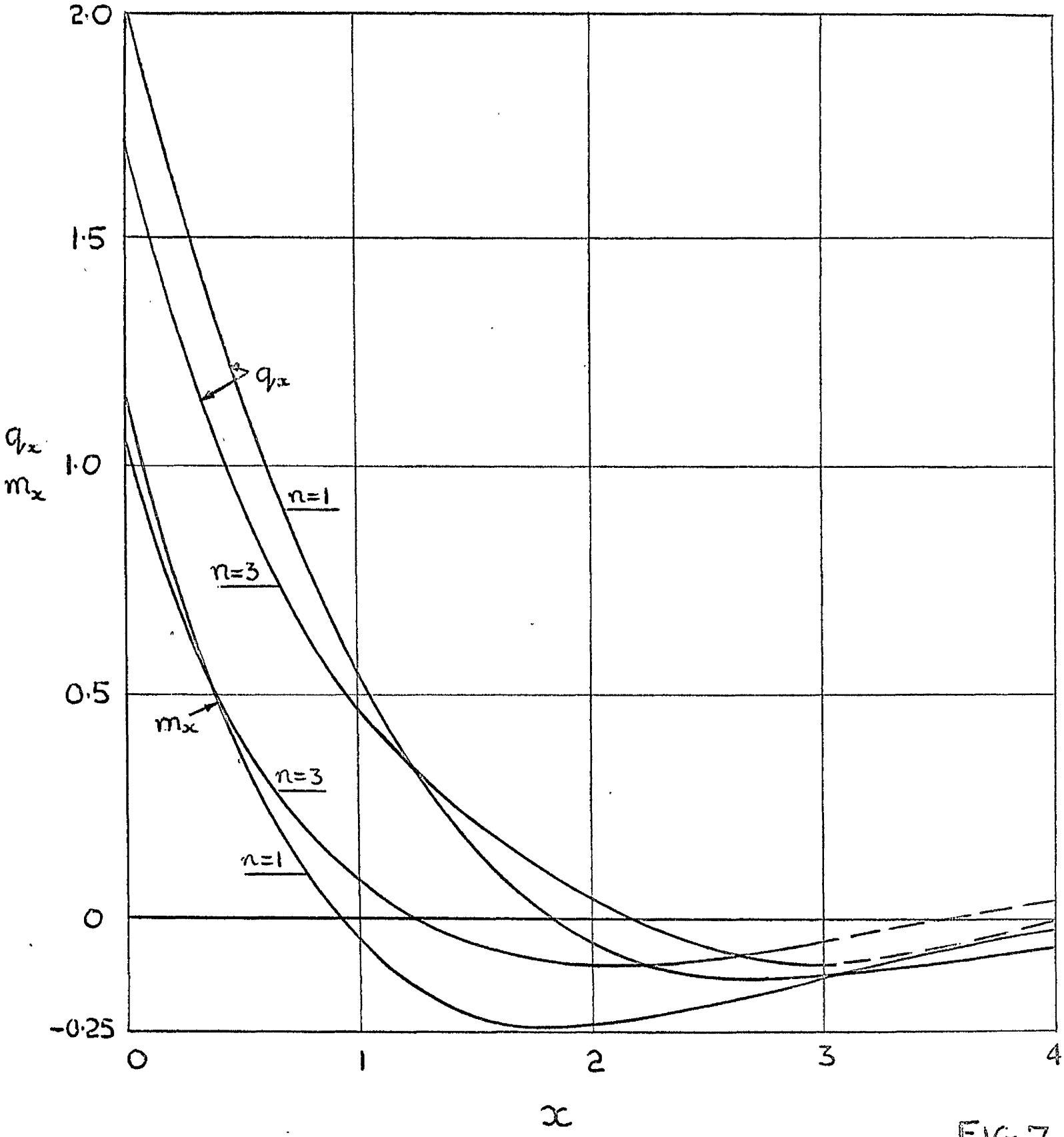

FIG. 7.1(

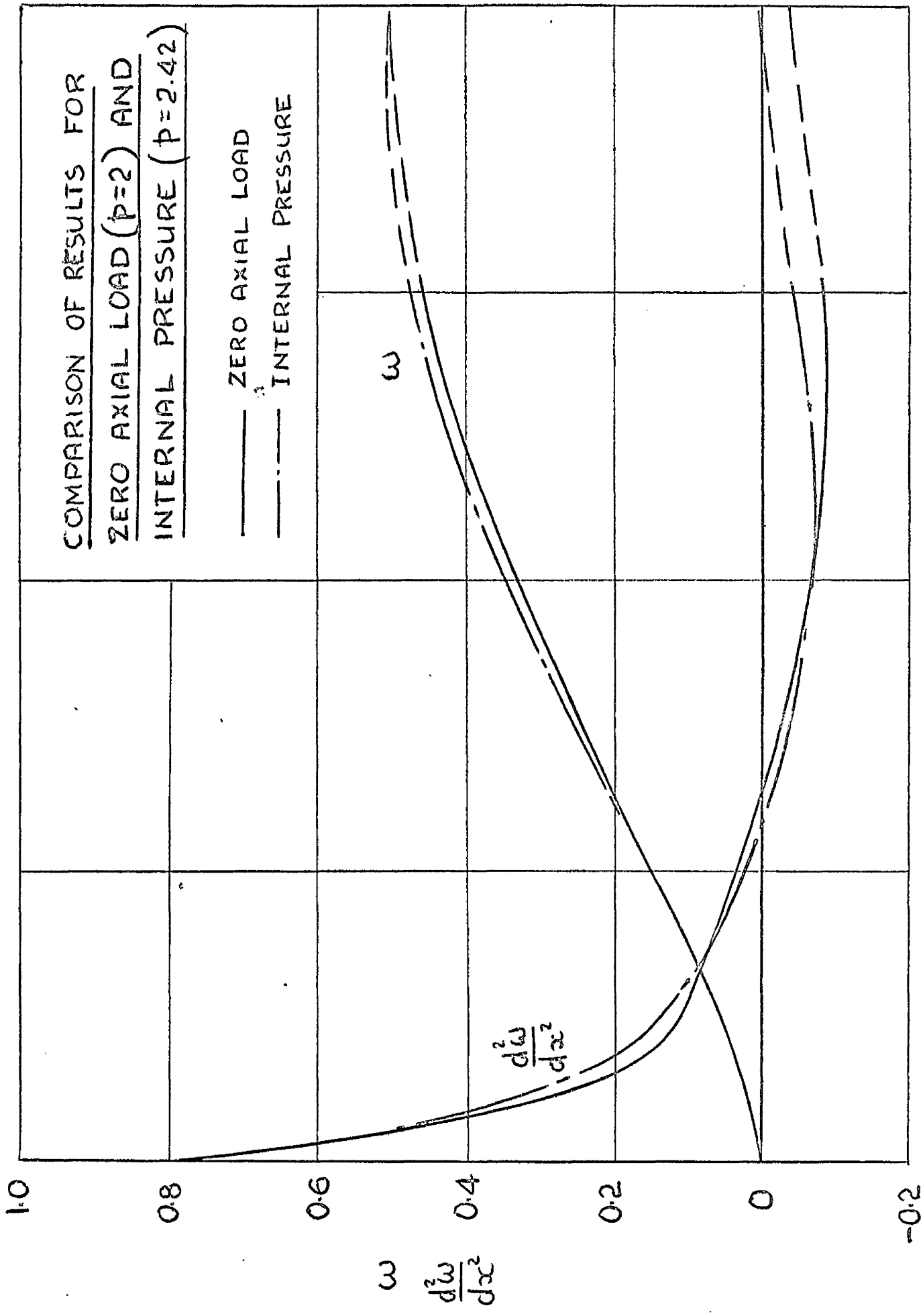
COMPARISON OF RESULTS FOR
ZERO AXIAL LOAD (p=2) AND
INTERNAL PRESSURE (p=2.42)
ZERO AXIAL LOAD
INTERNAL PRESSURE
ω
$\frac{d^2\omega}{dx^2}$
$3\frac{d^3\omega}{dx^2}$
x
1.0
0.8
0.6
0.4
0.2
0
-0.2
0
1
2
3
4

FIG. 7.11

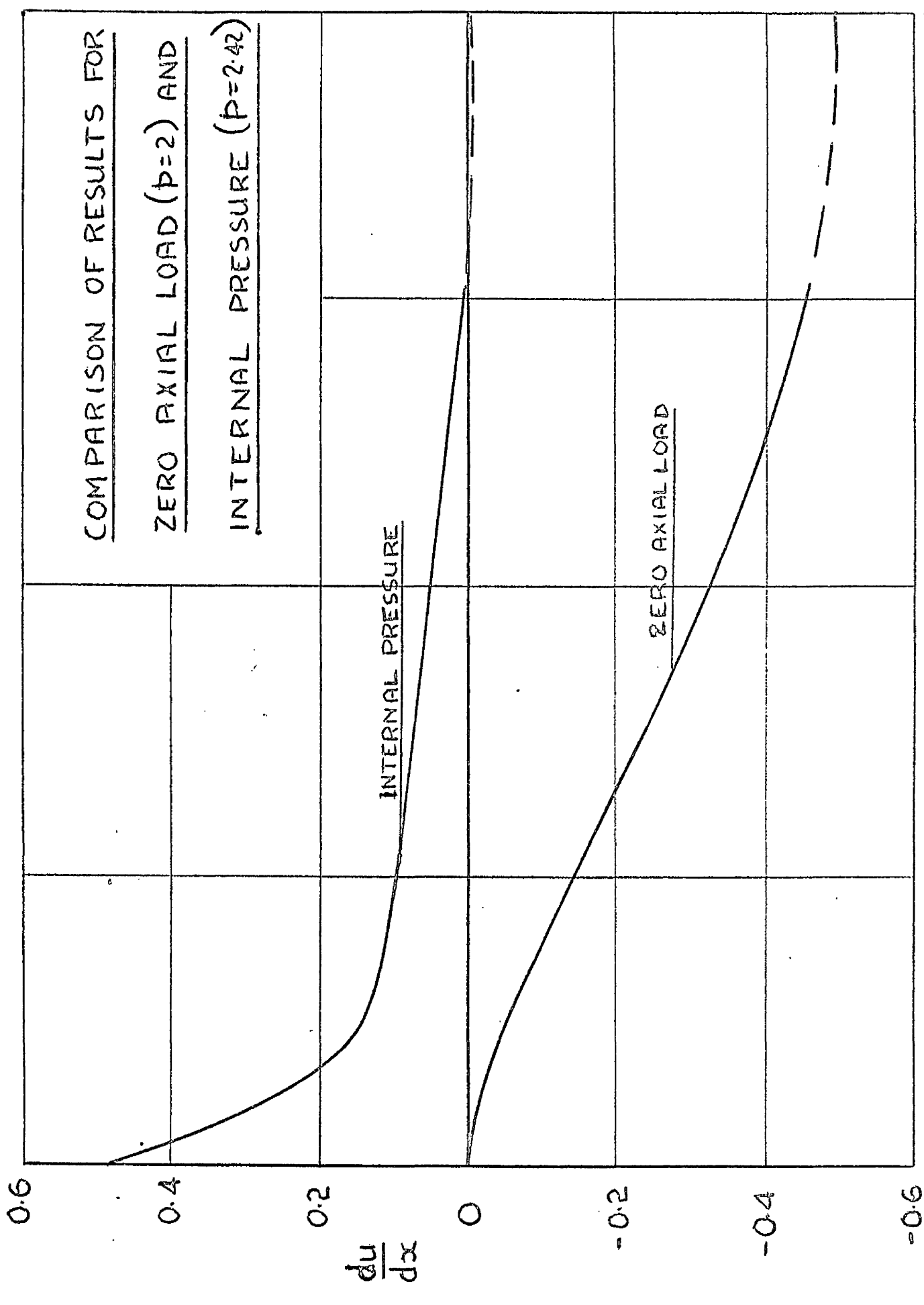
COMPARISON OF RESULTS FOR
ZERO AXIAL LOAD (p=2) AND
INTERNAL PRESSURE (p=2·42)
INTERNAL PRESSURE
ZERO AXIAL LOAD
0·6
0·4
0·2
0
-0·2
-0·4
-0·6
du/dx
0
1
2
3
4

FIG 7.2

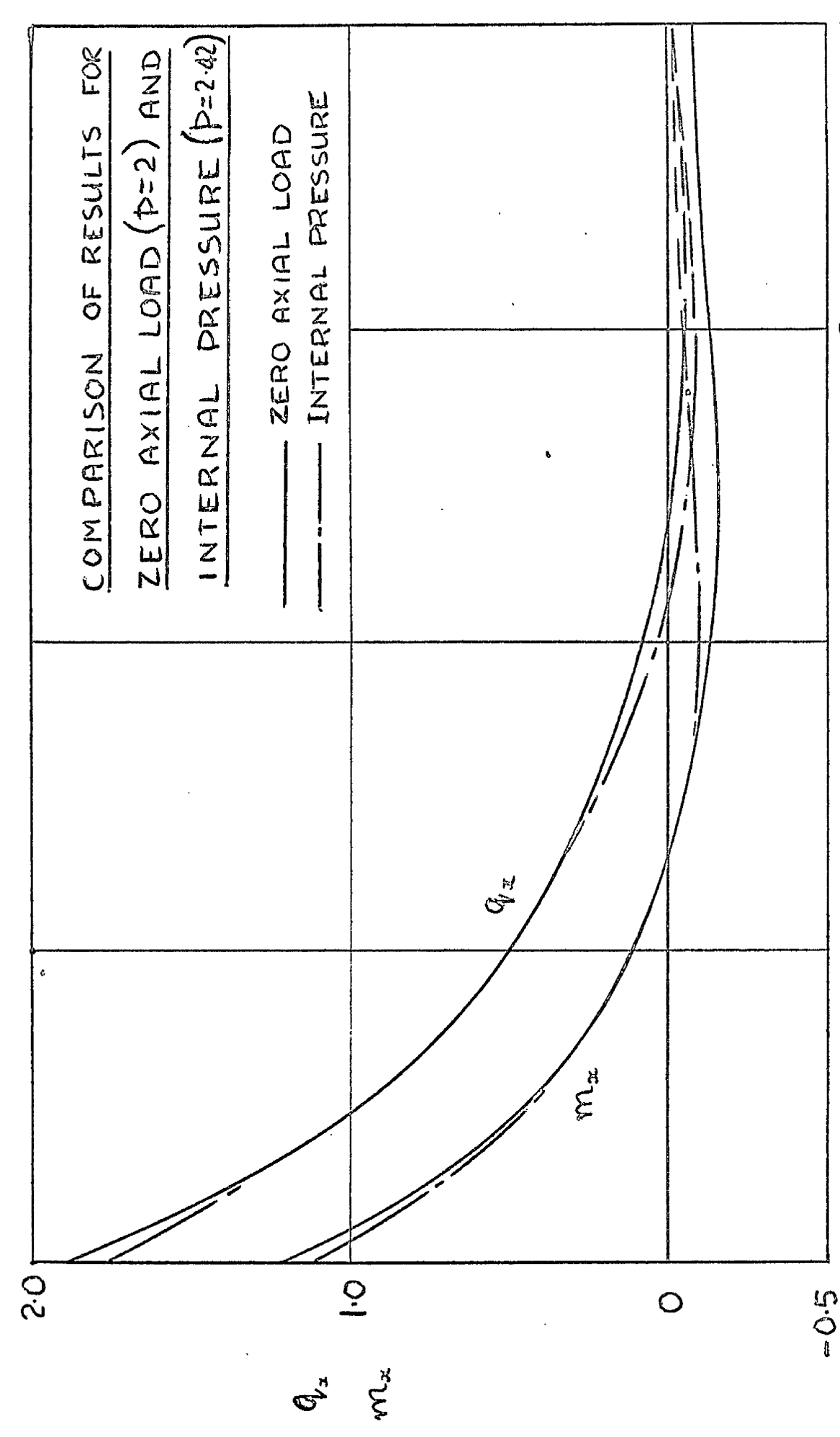
COMPARISON OF RESULTS FOR
ZERO AXIAL LOAD (P=2) AND
INTERNAL PRESSURE (P=2·42)
ZERO AXIAL LOAD
INTERNAL PRESSURE
q_x
m_x
2·0
1·0
0
-0·5
0
1
2
3
4
x

FIG. 7.13

END DISPLACEMENT WITH ZERO END SLOPE

(T=0 ; P=2)

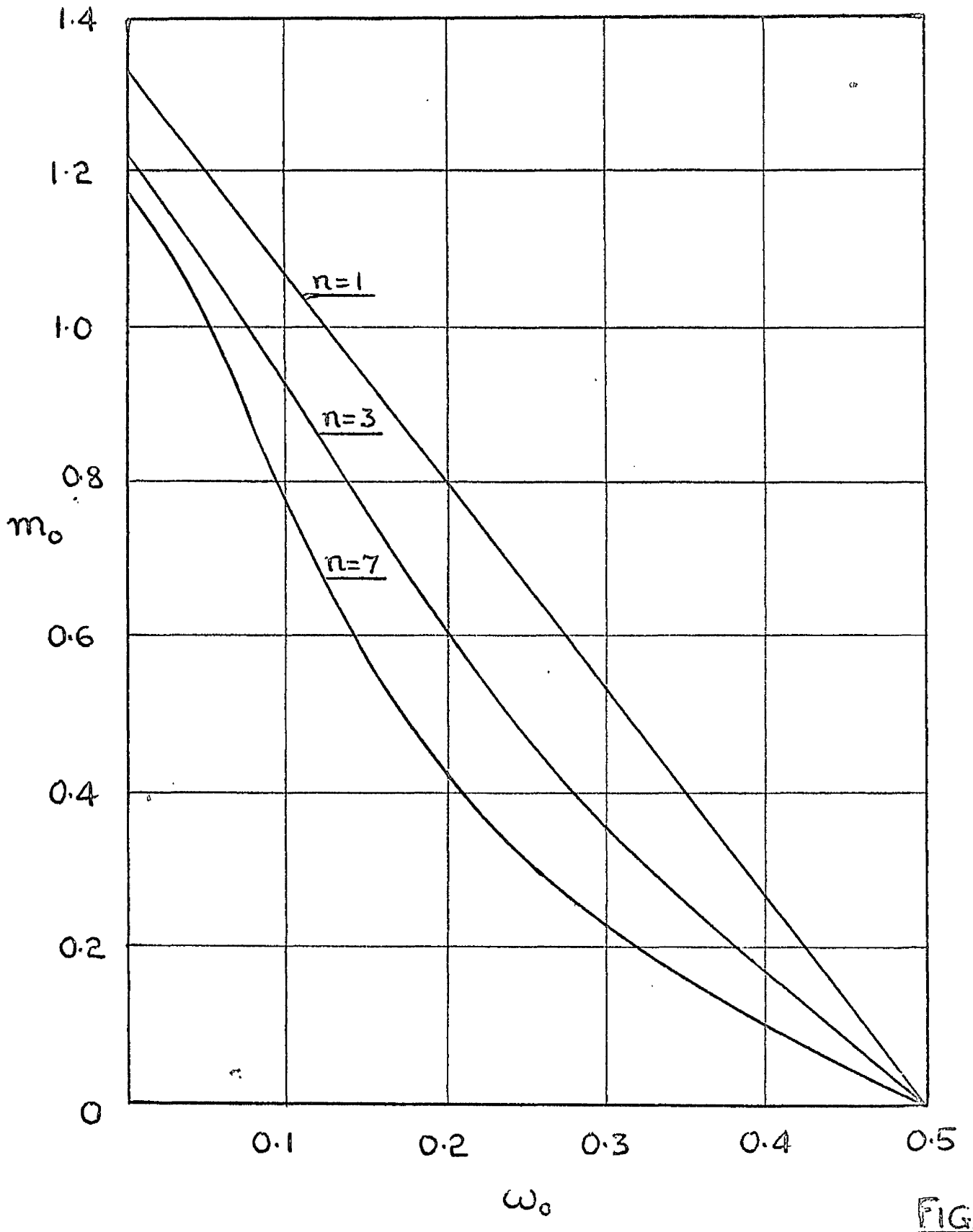

FIG. 7.14

END DISPLACEMENT WITH ZERO END SLOPE

(T = 0 ; p = 2)

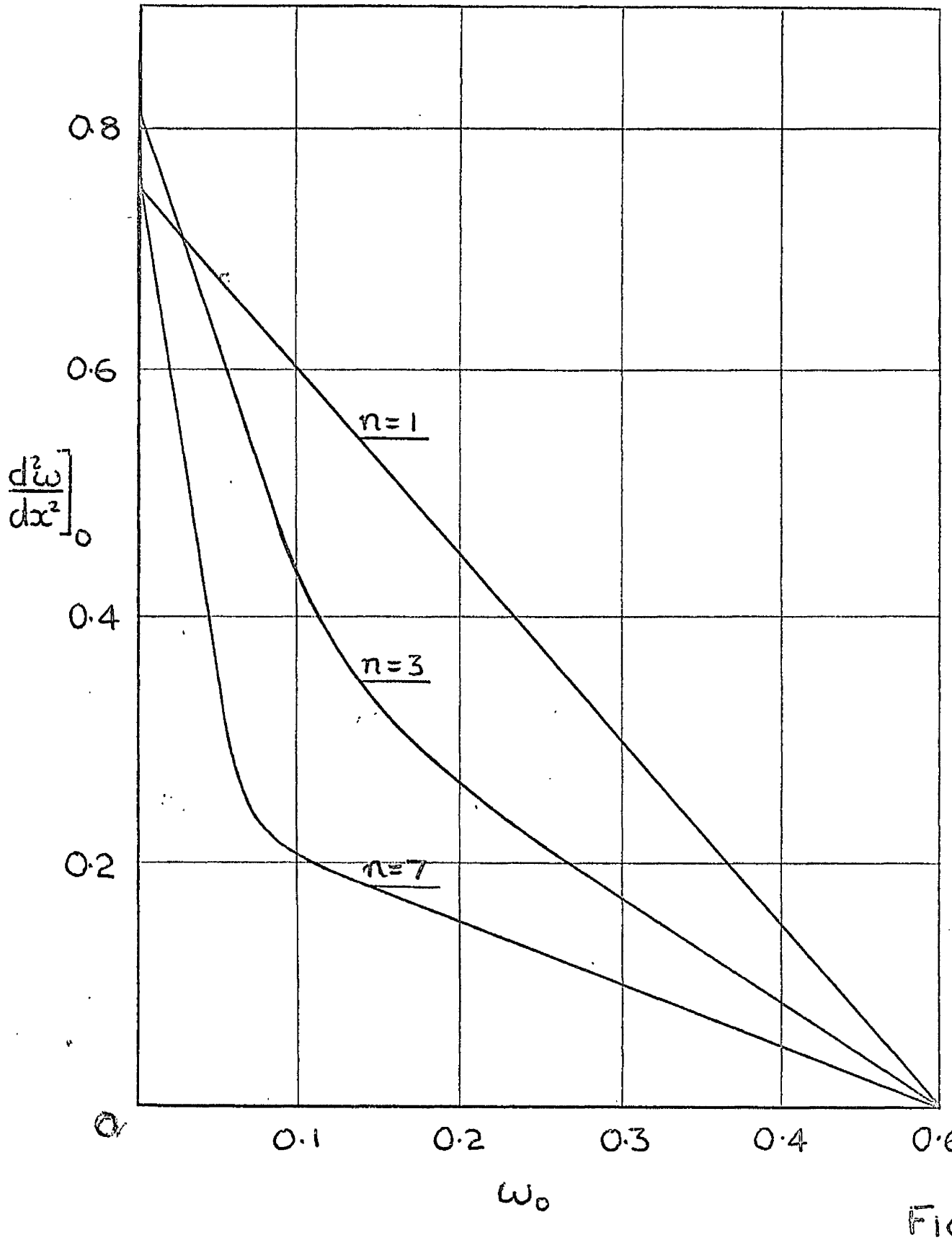

FIG. 7.15

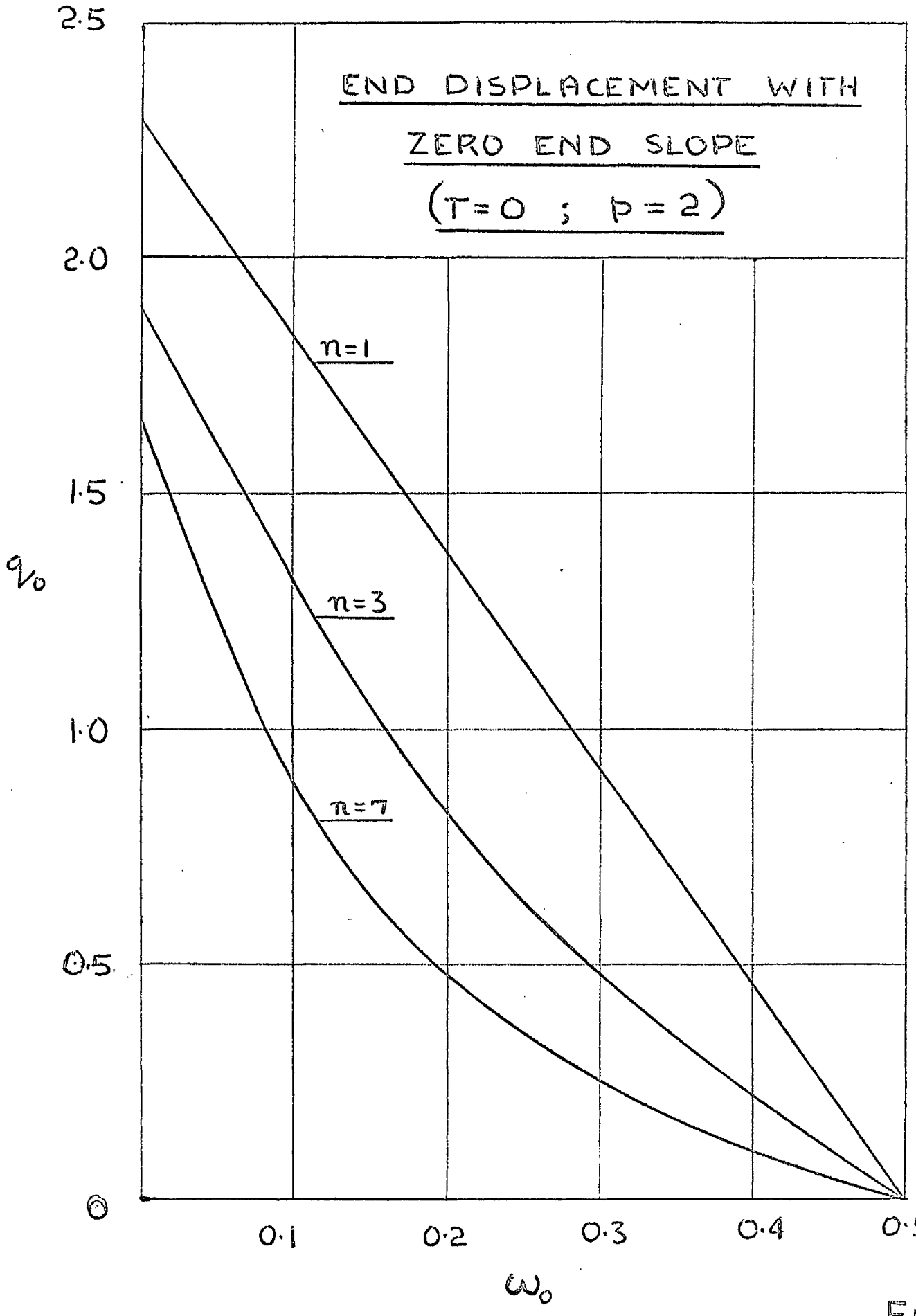
END DISPLACEMENT WITH
ZERO END SLOPE
(T=0 ; P=2)
2·5
2·0
1·5
1·0
0·5
0
q_0
n=1
n=3
n=7
0·1
0·2
0·3
0·4
0·5
ω_0

FIG. 7.16

CHAPTER 8

CONCLUSIONS.

1. Deformations in a number of structures obeying an n-power stress/strain law can be predicted by a simple method based on the linear elastic solution; it makes direct use of the stress/strain curve without need to determine material constants. The basis for the method suggests that it may give reasonable estimates of deformations with other non-linear laws. The limited experimental evidence available supports this claim.

2. The relations between forces and moments and mid-surface deformations for a thin shell obeying an n-power law can be derived from an energy function. This function gives a basis for postulating approximate relations and for comparing them with exact relations computed numerically. Approximate relations have been suggested for shells which are rotationally symmetric both in geometry and loading. In the form in which they are used for the analysis of circular cylindrical shells, they compare favourably with the exact relations.

3. For the cylindrical shell, the approximate relations lead to non-linear differential equations

which can be solved, with particular boundary conditions, on an analogue computer.

4. Solutions obtained for a cylinder with fixed ends under uniform radial loading, and under uniform internal pressure, suggest that the linear elastic solution may be used to give reasonable estimates of quantities important in the design of such shells.

5. The solution for the fixed end cylinder under internal pressure includes the region of the strain field in which the agreement between approximate and exact relations was poorest. Experiments on the fixed and cylinder may provide a critical test of analyses based on the approximate relations.

Further Work

Analytical

The comparison of exact and approximate relations between forces and moments and mid-surface deformations has been made with one curvature change zero ($k_2 = 0$), the condition which applies in the analysis of circular cylindrical shells. Drucker and Shield[29] have suggested that, for $n \to \infty$, relations for the cylindrical shell may be used with sufficient accuracy for the analysis of more general shells of revolution, and have

suggested a formulation of the more general problem in which m_2 and k_2 are assumed to be zero. The writer hopes to examine these suggestions for other values of n. An indication of whether or not they are likely to be generally useful may be had from examination of available linear solutions to particular shell problems. If it is desirable to use the approximate relations with $k_2 \neq 0$, it may be worthwhile to compare them with the exact relations for a number of values of k_2 in a manner similar to that described for $k_2 = 0$ in Chapter 4.

As a check on the analogue computer solutions given in Chapter 7, and to include the effect of a change in wall thickness, a numerical method has recently been developed[30] for the analysis of cylindrical shells with the approximate relations. Where solutions have been obtained both with the analogue computer and by the numerical method, there is better than $\pm$ 5% agreement in all important values.

Experimental

A start has been made on an experimental programme in which thin fixed end cylinders of annealed copper and other soft metals are to be tested under short term loading conditions of both uniform radial

load and internal pressure. Measurements are to be made of radial displacements and surface strains, and the results compared with the findings of Chapter 7.

In a further experimental programme,[30] the creep behaviour of long, fixed end thin cylinders with a change in wall thickness is to be examined. Cylinders of polymeric materials and soft metals are to be tested at relatively low temperatures (ambient to 150°C), and with the collaboration of the Research Department of Babcock and Wilcox Ltd, similar tests are being performed on steel cylinders at temperatures encountered in the operation of steam raising plant.

The writer also hopes to initiate further experimental work on the simple structures discussed in Chapter 3 and to test further the approximate method suggested for estimating deformations.

APPENDIX 1

R E F E R E N C E S

1. Hoff,N.J., "Approximate analysis of structures in the presence of moderately large creep deformations", Q. Appl. Math. 12, 1954, 49-55.

2. Williams, J.G. and Ford, H., "Stress/strain relations for some unreinforced plastics": J. Mech. Eng. Sci., vol 6., no. 4, 1964, 405-417.

3. Finnie, I. and Heller, W.R., "Creep of engineering materials", McGraw-Hill, 1959.

4. Odqvist, F.K.G. and Hult, J., "Kriechfestigkeit metallischer Werkstoffe", Springer-Verlag, 1962.

5. Calladine, C.R. and Drucker, D.C., "A bound method for creep analysis of structures : direct use of solutions in elasticity and plasticity," J. Mech. Eng. Sci., vol. 4, No.1, 1962.

6. Calladine, C.R. and Drucker,D.C., ""Nesting surfaces of constant rate of energy dissipation in creep," Q. Appl. Maths., vol XX, no.1, 1962.

7. Calladine, C.R., "A note on the bending of beams made of non-linear materials," J. Royal Aero. Soc., 67, 124, 1963.

8. Calladine, C.R., "Steady creep in a cylindrical shell: close upper and lower bound solutions for all values of the creep index," Proc. World Conf. on Shell Structures, p. 603 (U.S. Nat. Acad. Sci, 1964).

9. Calladine, C.R., "A rapid method for estimating the greatest stress in a structure subject to creep," Proc. Conf. on Thermal Loading and Creep - Structures - Inst. Mech. Engrs., 1964.

10. Onat, E.T. and Yuksel, H., "On the steady creep of shells," Proc. 3rd U.S. Nat. Congr. Appl. Mech., 1958, 625-630.

11. Bieniek, M.P. and Freudenthal, A.M., "Creep deformation and stresses in pressurised, long cylindrical shells," J. Aerospace Sci. 27, 10, 1960, 763-766.

12. Calladine, C.R., "The steady creep of shells: a method of analysis," Proc. Symp. on Nuclear Reactor Containment Buildings and Pressure Vessels": Glasgow, May 1960 (Butterworths).

13.. Rozenbluim, V.I., "Priblizhennye uravneniia polzuchesti tonkostennykh obolochek" (Approximate equations of creep of thin shells), P.M.M. 1963, 27 (no. 1).

14. Ilyushin, A.A., "Plastichnost" (Plasticity), Gostekhizdat, 1948.

15. Novozhilov, V.V., "Foundations of the non-linear theory of elasticity," Graylock Press, Rochester, N.Y., 1953.

16. Gill, S.S., "The behaviour of beams in bending," Aircraft Engineering, vol. 24, 1952, 336-343.

17. Bailey, R.W., "The utilisation of creep test data in engineering design," Proc. Inst. Mech. Engrs., 131, 131, 1935.

18. Malinin, N.N., "Continuous creep of round symmetrically loaded plates," (in Russian), Moskov. vysshe teknicheskoe uchilishche Trudy, 26, 221, 1953.

19. Professor G.D.S. MacLellan, private communication,

20. Preston, J.H., "The three-quarter radius pitot tube flow meter," The Engineer, 190, 1950, 400-402.

21. Campbell, A.A., "Plastic bending of beams," Report on project for degree of B.Sc., Dept. of Mech. Eng., Univ. of Glasgow, 1965.

22. Anderson, R.G., Gardner, L.R.T. and Hodgkins, W.R., "Deformation of uniformly loaded beams obeying complex creep laws," J. Mech. Eng. Sci., vol. 5, no.3, 1965, 238-244.

23. Marriot, D.L. and Leckie, F.A., "Some observations on the deflections of structures during creep," Proc. Conf. on Thermal Loading and Creep - Structures - Inst. Mech. Engrs., 1964.

24. King, R.H., "Creep of thick-walled cylinders under internal pressure," Ph.D. thesis, University of Glasgow, 1964.

25. Patel, S.A., Venkatraman, B. and Hodge, P.G., Jr., "Torsion of cylindrical and prismatic bars in the presence of steady creep," J. Appl. Mech., 25, 1958, 214-218.

26. Drucker, D.C., "A definition of a stable inelastic material," J. Appl. Mech. 26, 1959, 101-106.

27. Prager, W., "Total creep under varying loads," J. Aero, Sci. 24, 1957, 153-155.

28. Ilyuskin, A.A., "The theory of small elastic-plastic deformations," (Russian with English Summary), Prikladnaia Matematika i mekhanika, vol. 9, 1945, 207-218.

29. Drucker, D.C. and Shield, R.T., "Limit Analysis of symmetrically loaded thin shells of revolution," J. Appl. Mech., 25, 1958.

30. Byrne, T.P., Ph.D. project, Dept. of Mech. Eng., University of Glasgow.

31. Crandall, S.H. and Dahl, N.C., "An introduction to the mechanics of solids," McGraw-Hill, 1959.

32. Burington, R.S., "Handbook of Mathematical Tables and Formulas," Handbook Publishers, Inc., Sandusky, Ohio.

APPENDIX 2

2.1 Derivation of equations 2.7

From equation 2.3

$$\epsilon_1 - \epsilon_2 = \frac{3}{2} \frac{\bar{\epsilon}}{\bar{\sigma}} (\sigma_1 - \sigma_2)$$

$$\epsilon_2 - \epsilon_3 = \frac{3}{2} \frac{\bar{\epsilon}}{\bar{\sigma}} (\sigma_2 - \sigma_3)$$

Substracting,

$$\epsilon_1 - 2\epsilon_2 + \epsilon_3 = \frac{3}{2} \frac{\bar{\epsilon}}{\bar{\sigma}} (\sigma_1 - 2\sigma_2 + \sigma_3)$$

$$\therefore -3\epsilon_2 + (\epsilon_1 + \epsilon_2 + \epsilon_3) = \frac{3}{2} \frac{\bar{\epsilon}}{\bar{\sigma}} \left[-2\sigma_2 + (\sigma_1 + \sigma_3) \right]$$

But $\epsilon_1 + \epsilon_2 + \epsilon_3 = 0$ for constant volume

$$\therefore \epsilon_2 = \frac{\bar{\epsilon}}{\bar{\sigma}} \left[\sigma_2 - \tfrac{1}{2} (\sigma_1 + \sigma_3) \right]$$

With equation 2.5, i.e. $\bar{\epsilon} = B \bar{\sigma}^n$,

$$\epsilon_2 = B \bar{\sigma}^{n-1} \left[\sigma_2 - \tfrac{1}{2} (\sigma_1 + \sigma_3) \right]$$

ϵ_1 and ϵ_3 follow by symmetry.

APPENDIX 3

3.1 Beam in uniform bending

(a) Rectangular cross-section

Arguments of symmetry can be used[31] to show that plane sections remain plane and the strain at y from the neutral axis of the beam when bent to curvature K is

$$\epsilon = Ky$$

With equation 2.1 written in the form of equation 2.2b, the bending stress σ is given by

$$\sigma = (\text{sign } y)\ \sigma_o \left(\frac{K|y|}{\epsilon_o}\right)^{1/n}$$

$$\therefore M = \sigma_o \left(\frac{K}{\epsilon_o}\right)^{1/n} b \int_{-d/2}^{+d/2} (\text{sign } y)\ (|y|)^{\frac{n+1}{n}}\, dy$$

$$= \sigma_o \left(\frac{K}{\epsilon_o}\right)^{1/n} b \left(\frac{n}{2n+1}\right) \left[(\text{sign } y)(|y|)^{\frac{2n+1}{n}}\right]_{-d/2}^{+d/2}$$

$$= \sigma_o \left(\frac{K}{\epsilon_o}\right)^{1/n} b \left(\frac{n}{2n+1}\right) 2 \left(\frac{d}{2}\right)^{\frac{2n+1}{n}}$$

$$\text{or } K = \left(\frac{2n+1}{n}\right)^n 2^{n+1} \left(\frac{\epsilon_o}{\sigma_o^n b^n d^{2n+1}}\right) M^n$$

Note In this special case of a cross-section symmetrical about the neutral axis, the stress/strain law can be used in the form of equation 2.1 and integrated over half the cross-section, i.e.

$$M = 2 \int_0^{d/2} \sigma b_{y.} \, dy$$

(b) I - section

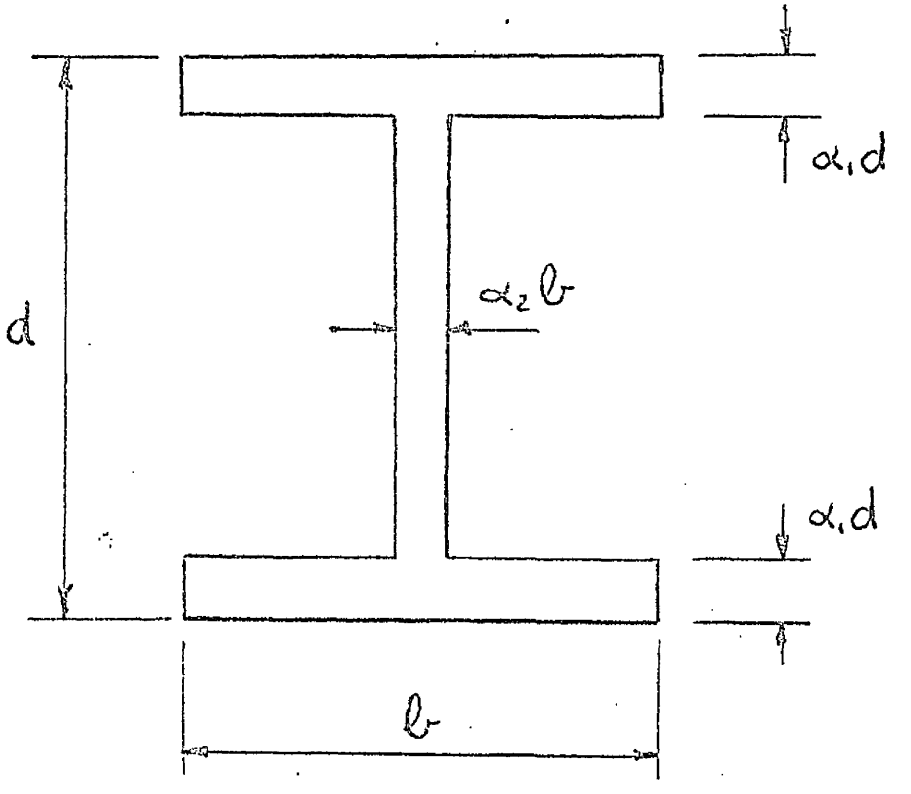

Integrating over half the cross-section

$$M = 2\sigma_o \left(\frac{K}{\epsilon_o}\right)^{1/n} \left\{ \int_0^{\left(\frac{d}{2} - \alpha_1 d\right)} \alpha_2 b y^{\frac{n+1}{n}} dy + \int_{\left(\frac{d}{2} - \alpha_1 d\right)}^{\frac{d}{2}} b y^{\frac{n+1}{n}} dy \right\}$$

$$= 2\sigma_o \left(\frac{K}{\epsilon_o}\right)^{1/n} b \left(\frac{n}{2n+1}\right) \times \left\{ \alpha_2 \left[\frac{d}{2}(1-2\alpha_1)\right]^{\frac{2n+1}{n}} + \left[\frac{d}{2}\right]^{\frac{2n+1}{n}} - \left[\frac{d}{2}(1-2\alpha_1)\right]^{\frac{2n+1}{n}} \right\}$$

$$= 2\sigma_o \left(\frac{K}{\epsilon_o}\right)^{1/n} b \left(\frac{n}{2n+1}\right) \left(\frac{d}{2}\right)^{\frac{2n+1}{n}} \left[1 - (1-\alpha_2)(1-2\alpha_1)^{\frac{2n+1}{n}}\right]$$

$$\therefore K = \left(\frac{2n+1}{n}\right)^n 2^{n+1} \frac{\epsilon_o}{\sigma_o^n b^n d^{2n+1}} \frac{M^n}{\left[1-(1-\alpha_2)(1-2\alpha_1)^{\frac{2n+1}{n}}\right]^n}$$

(when $\alpha_2 = 1$, or $\alpha_1 = \frac{1}{2}$, this reduces to the expression for a rectangular cross-section)

For n = 1

$$K_1 = \frac{12\,\epsilon_o}{\sigma_o b d^3} \frac{M}{\left[1-(1-\alpha_2)(1-2\alpha_1)^3\right]}$$

and the expression for K may be written

$$K = K_1 \left(\frac{M}{\sigma_0 b d^2}\right)^{n-1} \quad \frac{2}{3}^{n-1} \quad \left(\frac{2n+1}{n}\right)^n$$

$$X \quad \frac{\left[1-(1-\alpha_2)(1-2\alpha_1)^3\right]}{\left[1-(1-\alpha_2)(1-2\alpha_1)^{\frac{2n+1}{n}}\right]^n}$$

For $K = K_1$

$$\frac{M}{\sigma_0 b d^2} = \left\{ \frac{\left[1-(1-\alpha_2)(1-2\alpha_1)^{\frac{2n+1}{n}}\right]^n}{\left[1-(1-\alpha_2)(1-2\alpha_1)^3\right]} \right\}^{\frac{1}{n-1}} \quad \frac{3}{2}^{\frac{1}{n-1}} \left(\frac{n}{2n+1}\right)^{\frac{n}{n-1}}$$

$$= \gamma_5 (n)$$

The variation of $\gamma_5 (n)$ with n is shown below for

$\alpha_1 = \alpha_2 = 0.1$

n	$\gamma_5(n)$
2	0.1045
3	0.1047
5	0.1058
7	0.1060

For the beam tested by Gill - Fig 3.5

$$\alpha_1 = \frac{0.25}{1.75} = 0.143$$

$$\alpha_2 = \frac{0.375}{1.5} = 0.250$$

Taking $\frac{M}{\sigma_o b d^2}$ as the value of $\gamma_5(n)$ for $n = 5$ gives

$$\frac{M}{\sigma_o b d^2} = 0.153$$

or $\sigma_o = 1.425\ M.$

3.2 Lt $\gamma_1(n)$ as $n \to 1$*

$$\gamma_1 = \frac{3}{2}^{\frac{1}{n-1}} \left(\frac{n}{2n+1}\right)^{\frac{n}{n-1}}$$

$$= \frac{1}{6} \left(\frac{3n}{2n+1}\right)^{\frac{n}{n-1}}$$

Taking logarithms of both sides

$$\log_e \gamma_1 = \log_e \frac{1}{6} + \left(\frac{n}{n-1}\right) \log_e \left(\frac{3n}{2n+1}\right)$$

$$\operatorname*{Lt}_{n \to 1} \log_e \gamma_1 = \operatorname*{Lt}_{n \to 1} \left[\log_e \frac{1}{6} + \frac{n \log_e \left(\frac{3n}{2n+1}\right)}{n - 1} \right]$$

Applying L'Hôpital's rule to the second term and differentiating,

* The writer is grateful to Professor MacLellan for suggesting this method of investigating Lt $\gamma_1(n)$ as $n \to 1$.

$$\lim_{n \to 1} \left[\frac{n \log_e \left(\frac{3n}{2n+1} \right)}{n-1} \right]$$

$$= \lim_{n \to 1} \left[\frac{\log_e \left(\frac{3n}{2n+1} \right) + n \left(\frac{2n+1}{3n} \right) \cdot \frac{(2n+1).3 - 3n.2}{(2n+1)^2}}{1} \right]$$

$$= 0 + \lim_{n \to 1} \frac{1}{2n+1}$$

$$= \frac{1}{3}$$

$$\therefore \lim_{n \to 1} \log_e \gamma_1 = \log_e \frac{1}{6} + \frac{1}{3}$$

$$\text{or} \lim_{n \to 1} \gamma_1 = \frac{1}{6} e^{1/3}$$

This limit can also be obtained by writing $n = 1 + \delta$ and investigating the behaviour of $\gamma_1(\delta)$ as $\delta \to 0$.

3.3 Simply supported beam with central point load - equation 3.7

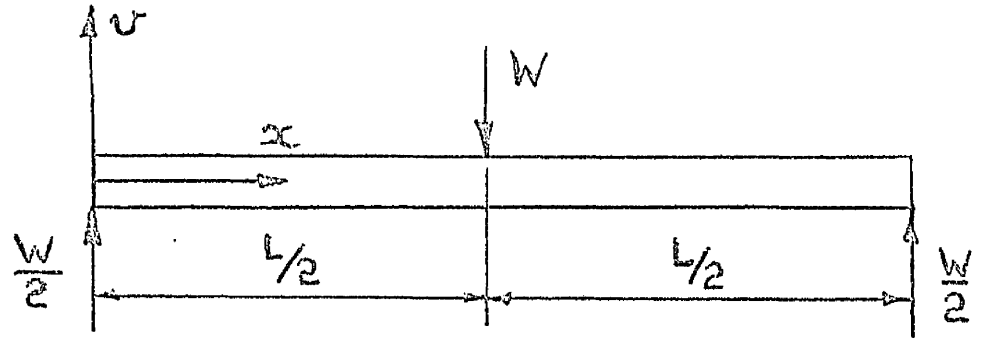

It is assumed that the moment/curvature relation developed for the beam in uniform bending can be applied without serious error in the presence of shear stresses associated with the shear forces in the beam.

Thus, with

$$K \simeq \frac{d^2v}{dx^2} \quad \text{for small deflections}$$

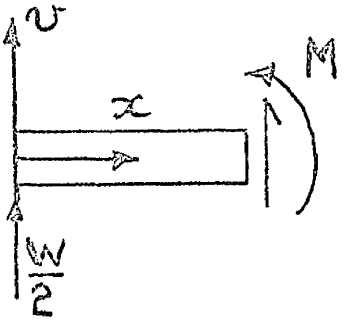

and $M = \frac{w}{2} x$,

equation 3.1 gives

$$\frac{d^2v}{dx^2} = \Omega \left(\frac{w}{2} x\right)^n$$

where

$$\Omega = \left(\frac{2n+1}{n}\right)^n \; 2^{n+1} \; \frac{\epsilon_o}{\sigma_o^n b^n d^{2n+1}}$$

This, with the boundary conditions, gives

$$v = \left(\frac{1}{n+1}\right) \Omega \left(\frac{w}{2}\right)^n \left[\frac{x}{n+2}^{n+2} - \left(\frac{L}{2}\right)^{n+1} x\right]$$

At $x = L/2$, and substituting for Ω,

$$v\Big]_{L/2} = \delta = -\frac{w^n}{b^n} \frac{L^{n+2}}{d^{2n+1}} \frac{\epsilon_o}{\sigma_o^n} \left(\frac{2n+1}{n}\right)^n \frac{1}{n+2} \frac{1}{2^{n+1}}$$

3.4 Other examples of non-uniform bending

(i)

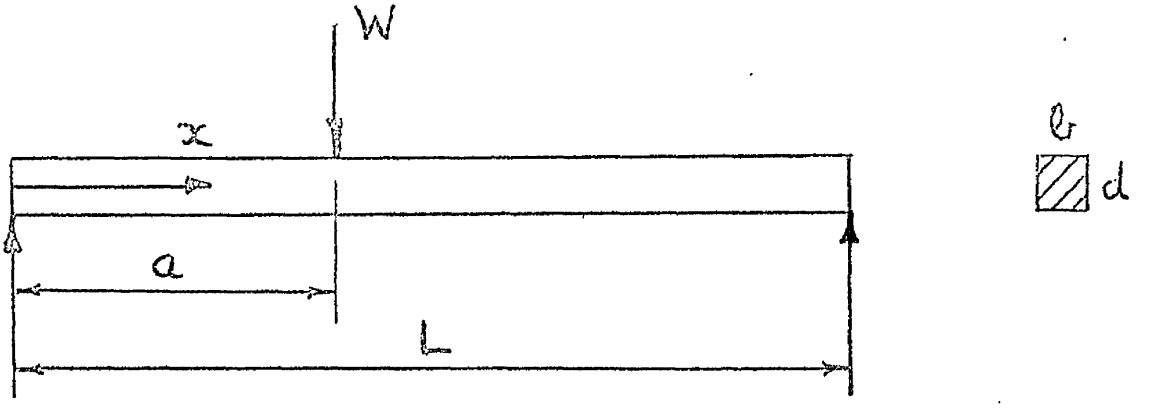

An alternative, and often simpler, method of determining the deflection under a single point load is to use the principle of virtual work. In this simple case, considering only the uniaxial bending stress, the principle may be written as

$$\int_V \sigma_x \epsilon_x \, dV - W\delta = 0 \qquad \text{A3.1}$$

where

σ_x, ϵ_x are stress and strain in the x-direction,

W is the applied point load

δ is the deflection under W.

Also

$$\int_V \sigma_x \epsilon_x \, dV = \int_V \sigma_x \, Ky \, dV$$

$$= \int_L K \left[\int_A \sigma_x \, y \, d\, A \right] dx$$

But

$$\int_A \sigma_x \, y \, d\, A = M$$

$$\therefore \int_v \sigma_x \epsilon_x \, d\, V = \int_L M \, K \, dx$$

With $K = \Omega \, M^n$ (Ω as in Appendix 3.3),

equation A3.1 gives finally

$$W\delta = \Omega \int_L M^{n+1} \, dx$$

Thus, in the above example,

$$W\delta = \Omega \left\{ \int_0^a \left[W \left(1 - \frac{a}{L}\right) x \right]^{n+1} dx \right.$$

$$\left. + \int_a^L \left[Wa\left(1 - \frac{x}{L}\right) \right]^{n+1} dx \right.$$

which gives finally

$$\delta = \frac{W^{n} L^{n+2} \epsilon_o}{\sigma_o{}^{n} b^{n} d^{2n+1}} \left(1 - \frac{a}{L}\right)^{n+1} \left(\frac{a}{L}\right)^{n+1} \left(\frac{2n+1}{n}\right)^{n} \left(\frac{2}{n+2}\right)^{n+1}$$

with n = 1

$$\delta_1 = \frac{W L^3}{\frac{\sigma_o}{\epsilon_o} b d^3} \left(1 - \frac{a}{L}\right)^2 \left(\frac{a}{L}\right)^2 \cdot \frac{4}{}$$

and

$$\delta = \delta_1 \left[\frac{W L}{\sigma_o b d^2} \left(1 - \frac{a}{L}\right)\left(\frac{a}{L}\right)\right]^{n-1} \frac{1}{4} \left(\frac{2n+1}{n}\right)^{n} \left(\frac{2}{n+2}\right)^{n+1}$$

Thus,

$$\delta = \delta_1$$

if $$\frac{Wa}{\sigma_o b d^2} \left(1 - \frac{a}{L}\right) = 4^{\frac{1}{n-1}} \left(\frac{n}{2n+1}\right)^{\frac{n}{n-1}} \frac{(n+2)^{\frac{1}{n-1}}}{2^{\frac{n+1}{n-1}}}$$

$$= \gamma_6 (n)$$

$\gamma_6(n)$ varies from 0.325 for n = 1.1 to 0.298 for n = 7. A value of 0.300 for $\frac{Wa}{\sigma_o b d^2} \left(1 - \frac{a}{L}\right)$ gives $\delta = \delta_1 \pm 10\%$ for $1.1 \leq n \leq 7$.

(ii)

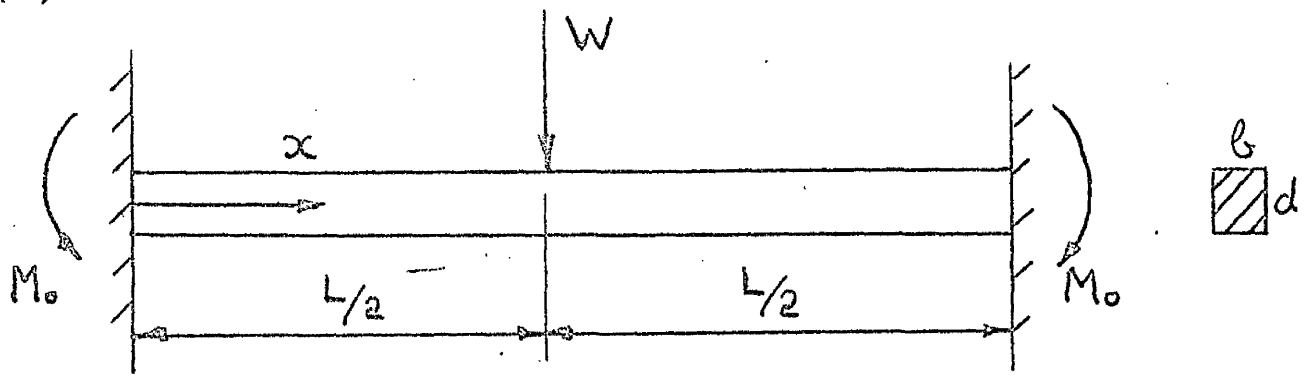

For this encastre beam, the edge fixing moment M_o for a linear elastic material (n = 1) is $\frac{WL}{8}$.

With a rigid - non - work - hardening plastic material ($n \to \infty$), plastic hinges develop under equal moments M_o at the ends and centre of the beam, and equilibrium requires that $M_o = \frac{WL}{8}$. A more general analysis shows that $M_o = \frac{WL}{8}$ for all values of n.

Again, using the principle of virtual work,

$$W\delta = 2\Omega \int_0^{\frac{L}{2}} \left(\frac{W}{2}x - M_o\right)^{n+1} dx$$

$$= 2\Omega\,(WL)^{n+1} L \int_0^{\frac{1}{2}} \left[\tfrac{1}{2}\left(\frac{x}{L}\right) - \tfrac{1}{8}\right]^{n+1} d\left(\frac{x}{L}\right)$$

which gives finally*

* A change in the sign of M occurs in the range 0 - $L/2$. To avoid difficulty when n is even, the moment/curvature relation can be used in a form analogous to equation 2.2a, i.e.

$$K = \Omega\,(\text{sign } M)(\,|M|\,)^n$$

$$\delta = \frac{\epsilon_o}{\sigma_o^n \ell_d^{n\ 2n+1}} \overline{W}^n L^{n+2} \left(\frac{2n+1}{n}\right)^n \left(\frac{1}{n+2}\right) \frac{1}{2^{2n+2}}$$

Proceeding as before

$$\delta = \delta_1$$

if $\frac{W L}{\sigma_o \ell d^2} = \left(\frac{n}{2n+1}\right)^{\frac{n}{n-1}} (n+2)^{\frac{1}{n-1}} \cdot 4 = \gamma_7(n)$.

$\gamma_7(n)$ varies from 2.60 fro n = 1.1 to 2.37 for n = 7

and $\frac{W L}{\sigma_o \ell d^2} = 2.4$ gives

$\delta = \delta_1 \pm 10\%$ for $1.1 \leq n \leq 7$.

(iii)

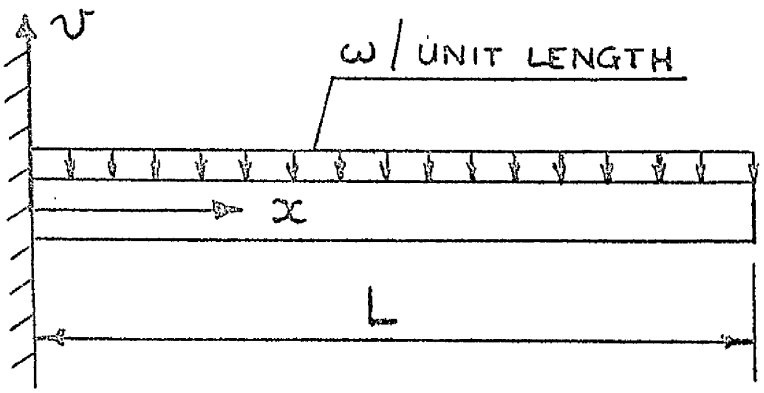

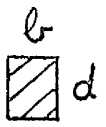

$$M = -\frac{w}{2}(L - x)^2$$

and

$$\frac{d^2v}{dx^2} = -\Omega\left(\frac{w}{2}\right)^n (L - x)^{2n}$$

is integrated to give the end deflection

$$\delta = \frac{\epsilon_o}{\sigma_o^n \ell^n d^{2n+1}} \left(\frac{2n+1}{n}\right)^n 2^{n+1} \left(\frac{w}{2}\right)^n \frac{L}{2n+2}^{2n+2}$$

Also

$$\delta = \delta_1$$

if $\frac{\omega L^2}{\sigma_o \ell d^2} = \left(\frac{n}{2n+1}\right)^{\frac{n}{n-1}} \left(\frac{3}{2}\right)^{\frac{1}{n-1}} (n+1)^{\frac{1}{n-1}} = \gamma_8(n)$

$\gamma_8(n)$ varies from 0.762 for n = 1.1 to 0.621 for

n = 7 and $\frac{\omega L^2}{\sigma_o \ell d^2} = 0.635$ gives

$\delta = \delta_1 \pm 15\%$ for $1.1 \leq n \leq 7$.

3.5 The intersection "point" in Figs 3.9 and 3.10

(i) Fig 3.9 - the thick wall cylinder, $\alpha = 2$

The value of $\frac{\bar{\sigma}}{P}$ at the intersection "point" for $1.1 \leq n \leq 7$ is approximately

$$\frac{\bar{\sigma}}{P} = 1.27$$

or $$\bar{\sigma} = 1.27\ P.$$

If σ_o is taken to be 1.27 P, then the equivalent strain $\bar{\epsilon}$ at the intersection "point" will be ϵ_o, and the same for all n in the range 1.1 to 7.

Bailey's solution was based on the assumption that the axial strain in the cylinder wall is zero. The strain ratios are thus constant and $\bar{\epsilon}$ is directly proportional to ϵ_θ. Thus if $\bar{\epsilon}$ at the intersection "point" is the same for a range of n, so is ϵ_θ. Furthermore, the distribution of ϵ_θ through the cylinder wall is independent of n (equation 3.11) and if ϵ_θ has a value at one point in the wall which is the same for a range of n, it has values at all points in the wall which are independent of n in this range.

The assumption that $\sigma_o = 1.27\ P$ gives $\frac{P}{\sigma_o} = 0.789$, This result compares with the value $\frac{P}{\sigma_o} = 0.79$ obtained for $\alpha = 2$ in paragraph 3.2(d)

(ii) Fig 3.10 Beam in 3-point bending

If $\frac{M\ K\ L}{W\delta}$ at one point in the beam has the same value for a range of $n \geq 1$, then, since the bending moment M is independent of n, the curvature K at the point would have to be the same for the range of n.

(W, δ and L are the same for all n). From paragraph 3.1, the condition for K to be approximately the same for $1.1 \leq n \leq 7$ is

$$\sigma_o = \frac{M}{0.245\, \ell_d^2}$$

From Fig. 3.10, $\frac{MKL}{W\delta}$ for n = 3, 5, 7 is closest to that for n = 1 at $\frac{2x}{L}$ = 0.82 approximately. At this point

$$M = \frac{W}{2} \times \left(\frac{0.82}{2}\right) L$$

Thus

$$\sigma_o = \frac{W}{2} \times \left(\frac{0.82}{2}\right) L \frac{1}{0.245\, \ell_d^2}$$

$$= 0.837 \frac{W L}{\ell_d^2} .$$

The value suggested in paragraph 3.2(a) was

$$\sigma_o = 0.833 \frac{W L}{\ell_d^2}$$

APPENDIX 4

4.1 To demonstrate that $t_1 = \left(\frac{n}{n+1}\right) \frac{\partial \Psi}{\partial e_1}$, etc.

Consider the shell element of Fig 4.1, having sides of unit length and subject to edge forces T_1, T_2 and edge moments M_1, M_2.

The strain field described by equations 4.1 will give rise to stress distributions in the element which, for the correct values of ϵ_{m1}, ϵ_{m2}, K_1, K_2 will be in equilibrium with T_1, T_2, M_1 and M_2. The potential $\tilde{\Pi}$ defined for zero body forces by

$$\tilde{\Pi} = \int_V U \, dV - \int_{F_T} T_i \, u_i \, dF \qquad (A4.1)$$

where $dU = (\sigma_1 \, d\epsilon_1 + \sigma_2 \, d\epsilon_2 + \sigma_3 \, d\epsilon_3)$,

dV is an element of volume,

dF is a surface element,

F_T is that part of the surface on which forces T_i are prescribed,

u_i are displacements associated with prescribed forces,

is thus to be regarded as a function of ϵ_{m1}, ϵ_{m2},

K_1, and K_2, and will be a minimum when ϵ_{m1}, ϵ_{m2}, K_1 and K_2 have their correct values.

For the shell element, since $\sigma_3 = 0$,

$$dU = \sigma_1 \, d\epsilon_1 + \sigma_2 \, d\epsilon_2$$

Substituting for σ_1 and σ_2 from equations 2.9

$$dU = \frac{1}{B^{1/n}} \left(\frac{4}{3}\right)^{\frac{n+1}{2n}} \left\{ \left(\epsilon_1^2 + \epsilon_1 \epsilon_2 + \epsilon_2^2\right)^{\frac{1-n}{2n}} \left(\epsilon_1 + \tfrac{1}{2}\epsilon_2\right) d\epsilon_1 + \left(\epsilon_1^2 + \epsilon_1 \epsilon_2 + \epsilon_2^2\right)^{\frac{1-n}{2n}} \left(\epsilon_2 + \tfrac{1}{2}\epsilon_1\right) d\epsilon_2 \right.$$

$$= \frac{1}{B^{1/n}} \left(\frac{4}{3}\right)^{\frac{n+1}{2n}} \left\{ \left(\frac{n}{n+1}\right) d\left[\left(\epsilon_1^2 + \epsilon_1 \epsilon_2 + \epsilon_2^2\right)^{\frac{n+1}{2n}}\right] \right\}$$

$$\therefore \quad U = \int_0^{\epsilon_1, \epsilon_2} dU$$

$$= \frac{1}{B^{1/n}} \left(\frac{4}{3}\right)^{\frac{n+1}{2n}} \left(\frac{n}{n+1}\right)\left(\epsilon_1^2 + \epsilon_1 \epsilon_2 + \epsilon_2^2\right)^{\frac{n+1}{2n}}$$

Thus, with equations 4.1,

$$U = \frac{1}{B^{1/n}} \left(\frac{4}{3}\right)^{\frac{n+1}{2n}} \left(\frac{n}{n+1}\right)\left\{\left(\epsilon_{m1} + \gamma K_1\right)^2 + \left(\epsilon_{m1} + \gamma K_1\right)\left(\epsilon_{m2} + \gamma K_2\right) + \left(\epsilon_{m2} + \gamma K_2\right)^2\right\}^{\frac{n+1}{2n}}$$

$$= \frac{1}{B^{1/n}} \left(\frac{4}{3}\right)^{\frac{n+1}{2n}} \left(\frac{n}{n+1}\right)\left\{\left(\epsilon_{m1}^2 + \epsilon_{m1}\epsilon_{m2} + \epsilon_{m2}^2\right) + \gamma\left[K_1(2\epsilon_{m1} + \epsilon_{m2}) + K_2(2\epsilon_{m2} + \epsilon_{m1})\right] + \gamma^2\left(K_1^2 + K_1K_2 + K_2^2\right)\right\}^{\frac{n+1}{2n}}$$

$$\text{or} \quad U = \frac{1}{B^{1/n}} \left(\frac{4}{3}\right)^{\frac{n+1}{2n}} \left(\frac{n}{n+1}\right) F_1^{\frac{n+1}{2n}}$$

For unit area of element

$$\int_V U \, dV = \int_{-H}^{+H} U \, d\gamma$$

$$= \frac{1}{B^{1/n}} \left(\frac{4}{3}\right)^{\frac{n+1}{2n}} \left(\frac{n}{n+1}\right) \int_{-H}^{+H} F_1^{\frac{n+1}{2n}} \, d\gamma$$

Also, for unit length of side,

$$\int_{F_T} T_i\, u_i\, dF = T_1\,(\epsilon_{m1} \times 1) + T_2\,(\epsilon_{m2} \times 1) + M_1\,(1 \times K_1) + M_2\,(1 \times K_2).$$

Thus, from equation A4.1

$$\tilde{\Pi} = \frac{1}{B^{1/n}} \left(\frac{4}{3}\right)^{\frac{n+1}{2n}} \left(\frac{n}{n+1}\right) \int_{-H}^{+H} F_1^{\frac{n+1}{2n}}\, d\xi - T_1 \epsilon_{m1} - T_2 \epsilon_{m2} - M_1 K_1 - M_2 K_2$$

Introduction of the non-dimensional parameters defined by equations 4.5 gives

$$\frac{\tilde{\Pi}}{2\sigma_o \epsilon_o H} = \left(\frac{n}{n+1}\right)\Psi - t_1 e_1 - t_2 e_2 - m_1 k_1 - m_2 k_2$$

where

$$\Psi = \frac{1}{2}\left(\frac{4}{3}\right)^{\frac{n+1}{2n}} \int_{-1}^{+1} \left\{ \left(e_1^2 + e_1 e_2 + e_2^2\right) + 4\zeta \left[k_1\left(e_1 + \tfrac{1}{2}e_2\right) + k_2\left(e_2 + \tfrac{1}{2}e_1\right)\right] + 4\zeta^2\left(k_1^2 + k_1 k_2 + k_2^2\right) \right\}^{\frac{n+1}{2n}} d\zeta$$

$$= \frac{1}{2}\left(\frac{4}{3}\right)^{\frac{n+1}{2n}} \int_{-1}^{+1} F_2^{\frac{n+1}{2n}}\, d\zeta$$

If Π is a minimum

$$\frac{\partial \Pi}{\partial e_1} = \frac{\partial \Pi}{\partial e_2} = \frac{\partial \Pi}{\partial k_1} = \frac{\partial \Pi}{\partial k_2} = 0$$

$$\therefore \quad t_1 = \left(\frac{n}{n+1}\right) \frac{\partial \psi}{\partial e_1} \quad ; \quad t_2 = \left(\frac{n}{n+1}\right) \frac{\partial \psi}{\partial e_2}$$

$$m_1 = \left(\frac{n}{n+1}\right) \frac{\partial \psi}{\partial k_1} \quad ; \quad m_2 = \left(\frac{n}{n+1}\right) \frac{\partial \psi}{\partial k_2}$$

These relations can be verified directly by obtaining

$\frac{\partial \psi}{\partial e_1}$, etc.

For example,

$$\frac{\partial \psi}{\partial e_1} = \tfrac{1}{2} \left(\frac{4}{3}\right)^{\frac{n+1}{2n}} \left(\frac{n+1}{2n}\right) \int_{-1}^{+1} F_2^{\frac{1-n}{2n}} \left[(2e_1+e_2) + 4\rho \, (k_1+\tfrac{1}{2}k_2) \right] d\rho$$

The right hand side of this equation is the expression obtained for t_1 by direct integration of stresses through the thickness - the first of equations 4.6.

4.2 Integration of ψ to obtain $\psi_{(d)}$ and $\psi_{(e)}$

(a) $\psi_{(d)}$

With $k_2 = e_2 = 0$

$$\psi_{(d)} = \tfrac{1}{2}\left(\frac{4}{3}\right)^{\frac{n+1}{2n}} \int_{-1}^{+1} \left(e_1^2 + 4\rho k_1 e_1 + 4\rho^2 k_1^2\right)^{\frac{n+1}{2n}} d\rho$$

$$= \tfrac{1}{2}\left(\frac{4}{3}\right)^{\frac{n+1}{2n}} \int_{-1}^{+1} \left(e_1 + 2\rho k_1\right)^{\frac{n+1}{n}} d\rho$$

$$= \tfrac{1}{2}\left(\frac{4}{3}\right)^{\frac{n+1}{2n}} \left(\frac{n}{2n+1}\right) \frac{1}{2k_1} \left[\left(e_1 + 2\rho k_1\right)^{\frac{2n+1}{n}}\right]_{-1}^{+1}$$

$$\text{or } \psi_{(d)} = \tfrac{1}{2}\left(\frac{4}{3}\right)^{\frac{n+1}{2n}} \left(\frac{n}{2n+1}\right) \frac{1}{2k_1} \left[\left(e_1 + 2k_1\right)^{\frac{2n+1}{n}} - \left(e_1 - 2k_1\right)^{\frac{2n+1}{n}}\right]$$

(b) $\psi_{(e)}$

$$\text{As } n \to \infty, \quad \frac{n+1}{2n} = \tfrac{1}{2} + \frac{1}{n} \to \tfrac{1}{2}$$

and

$$\psi_{(e)} = \tfrac{1}{2}\left(\frac{4}{3}\right)^{\frac{1}{2}} \int_{-1}^{+1} \left(a\rho^2 + b\rho + c\right)^{\frac{1}{2}} d\rho \qquad \text{(A4.2)}$$

where $a = 4\left(k_1^2 + k_1 k_2 + k_2^2\right)$

$$b = 4\left[k_1\left(e_1 + \tfrac{1}{2} e_2\right) + k_2\left(e_2 + \tfrac{1}{2} e_1\right)\right]$$

$$c = e_1^2 + e_1 e_2 + e_2^2$$

The integral in equation A4.2 can be evaluated,[32] i.e.

$$\int_{-1}^{+1} (a\rho^2 + b\rho + c)d\rho = \left[\left(\frac{2a\rho + b}{4a}\right)\sqrt{a\rho^2 + b\rho + c}\right]_{-1}^{+1} + \left(\frac{4ac - b^2}{8a}\right)\int_{-1}^{+1} \frac{d\rho}{\sqrt{a\rho^2 + b\rho + c}}$$

But for $a > 0$

$$\int_{-1}^{+1} \frac{d\rho}{\sqrt{a\rho^2 + b\rho + c}} = \frac{1}{\sqrt{a}}\left[\log_e(2a\rho + b + 2\sqrt{a}\sqrt{a\rho^2 + b\rho + c})\right]_{-1}^{+1}$$

Hence,

$$\psi_{(e)} = \frac{1}{\sqrt{3}}\left\{\left(\frac{2a+b}{4a}\right)\sqrt{a + b + c} - \left(\frac{-2a-b}{4a}\right)\sqrt{a - b + c} + \left(\frac{4ac - b^2}{8a^{3/2}}\right)\log_e\left(\frac{2a + b + 2\sqrt{a}\sqrt{a + b + c}}{-2a + b + 2\sqrt{a}\sqrt{a - b + c}}\right)\right\}$$

4.3 Symmetry of the $\psi = 1$ surfaces.

Adjacent quadrants.

For given e_1, e_2, k_1, the stress distributions through the thickness of the shell are given by equations 4.18, i.e.

$$\left(\frac{\sigma_1}{\sigma_o}\right) = \left(\frac{4}{3}\right)^{\frac{n+1}{2n}} \left[(e_1^2 + e_1e_2 + e_2^2) + 4\rho k_1(e_1 + \tfrac{1}{2}e_2) + 4\rho^2 k_1^2\right]^{\frac{1-n}{2n}} \times \left[(e_1 + \tfrac{1}{2}e_2) + 2\rho k_1\right]$$

$$\left(\frac{\sigma_2}{\sigma_o}\right) = \left(\frac{4}{3}\right)^{\frac{n+1}{2n}} \left[(e_1^2 + e_1e_2 + e_2^2) + 4\rho k_1(e_1 + \tfrac{1}{2}e_2) + 4\rho^2 k_1^2\right]^{\frac{1-n}{2n}} \times \left[(e_2 + \tfrac{1}{2}e_1) + \rho k_1\right]$$

These expressions are not symmetrical in e_1 and e_2, i.e. the deformation states ($e_1 = e$; $e_2 = \alpha e$; k_1) and ($e_1 = \alpha e$; $e_2 = e$; k_1) will give different stress distributions and are associated with different values of t_1, t_2, m_1, m_2. The ψ-surfaces are thus not the same in the adjacent quadrants of Fig 4.3.

Diagonal quadrants

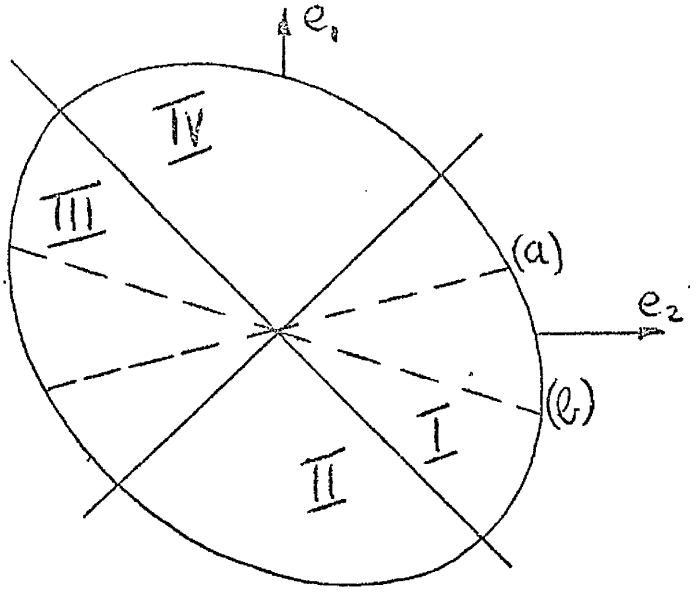

FIG. A4.1

Consider the deformation states (a) in the diagonal quadrants I and III of Fig A.4.1, i.e.

quadrant I $\quad (e_1 = e; \quad e_2 = \alpha e; \quad k_1)$

quadrant III $\quad (e_1 = -e; \quad e_2 = -\alpha e; \quad k_1)$

The distributions of σ_1 associated with these deformation states are:

$$\left(\frac{\sigma_1}{\sigma_o}\right)_I = \left(\frac{4}{3}\right)^{\frac{n+1}{2n}} \left[e^2(1+\alpha+\alpha^2) + 4\rho k_1 e(1+\tfrac{\alpha}{2}) + 4\rho^2 k_1^2\right]^{\frac{1-n}{2n}} \times \left[e(1+\tfrac{\alpha}{2}) + 2\rho k_1\right]$$

$$\left(\frac{\sigma_1}{\sigma_o}\right)_{III} = \left(\frac{4}{3}\right)^{\frac{n+1}{2n}} \left[e^2(1+\alpha+\alpha^2) - 4\rho k_1 e(1+\tfrac{\alpha}{2}) + 4\rho^2 k_1^2\right]^{\frac{1-n}{2n}} \times \left[(-e)(1+\tfrac{\alpha}{2}) + 2\rho k_1\right]$$

Clearly, for a given k_1,

$$\left(\frac{\sigma_1}{\sigma_o}\right)_I \text{ at } \rho = +\rho_1 = -\left(\frac{\sigma_1}{\sigma_o}\right)_{III} \text{ at } \rho = -\rho_1$$

This leads to the distributions of $\frac{\sigma_1}{\sigma_o}$ shown schematically in Fig A4.2 and the distributions of $\frac{\sigma_2}{\sigma_o}$ will be similar.

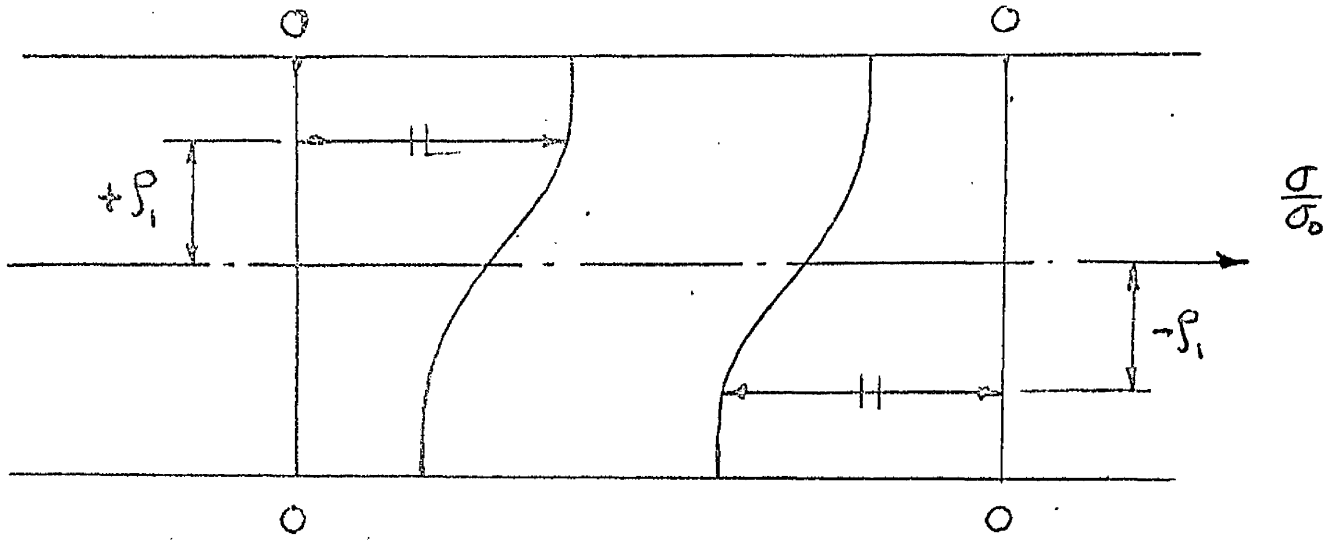

Fig A4.2.

The only difference in the applied forces t_1, t_2 and moments m_1, m_2 to produce the deformation states (a) in the diagonal quadrants I and III is in the sense of t_1 and t_2. Furthermore, replacing α by $-\beta$ to give the deformation states (b) in Fig A4.1 shows again that the only difference in t_1, t_2, m_1, m_2 to produce states (b) in the diagonal quadrants I and III is in the sense of t_1 and t_2. The $\psi = 1$ surface must thus be the same in the two quadrants.

The argument can be repeated to show that the $\psi = 1$ surfaces must also be the same in the diagonal quadrants II and IV.

Mathematical demonstration of symmetry

Properties of $\psi = 1$ surface for $n \to \infty$.

As shown in Appendix 4.2,

$$\psi_{n\to\infty} = \frac{1}{\sqrt{3}}\left\{\left(\frac{2a+b}{4a}\right)\sqrt{a+b+c} - \left(\frac{-2a+b}{4a}\right)\sqrt{a-b+c} + \left(\frac{4ac-b^2}{8a^{3/2}}\right)\log_e\left(\frac{2a+b+2\sqrt{a}\sqrt{a+b+c}}{-2a+b+2\sqrt{a}\sqrt{a-b+c}}\right)\right\}$$

where, for $k_2 = 0$

$$a = 4k_1^2$$

$$b = 4k_1\left(e_1 + \tfrac{1}{2}e_2\right)$$

$$c = e_1^2 + e_1e_2 + e_2^2$$

Symmetry about $k_1 = 0$

A change from $k_1 = +k$ to $k_1 = -k$ affects b, and not a or c.

Let $b = +b_1$ for $k_1 = +k$

$b = -b_1$ for $k_1 = -k$

In the expression for ψ, the first two terms taken together, i.e.

$$\left(\frac{2a+b}{4a}\right)\sqrt{a+b+c} - \left(\frac{-2a+b}{4a}\right)\sqrt{a-b+c}$$

has the same value for $b = + b_1$ and $b = - b_1$. Also,

$\left(\frac{4ac - b^2}{8a^{3/2}} \right)$ is the same for $b = \pm b_1$. Thus it is only necessary to prove that

$$\log_e \left(\frac{2a + b + 2\sqrt{a}\sqrt{a + b + c}}{-2a + b + 2\sqrt{a}\sqrt{a - b + c}} \right)$$

has the same value for $b = \pm b_1$.

For $b = + b_1$, the expression becomes

$$\frac{(2a + b_1) + 2\sqrt{a}\sqrt{a + b_1 + c}}{(-2a + b_1) + 2\sqrt{a}\sqrt{a - b_1 + c}}$$

If both the numerator and denominator are rationalised the expression may be written

$$\frac{(2a + b_1)^2 - 4a(a + b_1 + c)}{(-2a + b_1)^2 - 4a(a - b_1 + c)} \left[\frac{(-2a + b_1) - 2\sqrt{a}\sqrt{a - b_1 + c}}{(2a + b_1) - 2\sqrt{a}\sqrt{a + b_1 + c}} \right]$$

$$= 1 \times \left[\frac{2a - b_1 + 2\sqrt{a}\sqrt{a - b_1 + c}}{-2a - b_1 + 2\sqrt{a}\sqrt{a + b_1 + c}} \right]$$

This is the original expression with $b = - b_1$

$\therefore \quad \frac{2a + b + 2\sqrt{a}\sqrt{a + b + c}}{-2a + b + 2\sqrt{a}\sqrt{a - b + c}}$ has the same value for $b = \pm b_1$

The $\psi = 1$ surface for $n \to \infty$ is thus symmetrical about the plane $k_1 = 0$.

Symmetry in diagonal quadrants

The deformation states ($e_1 = e$; $e_2 = \alpha e$; k_1) and ($e_1 = -e$; $e_2 = -\alpha e$; k_1) in diagonal quadrants give the same magnitude and sign for a and c, and the same magnitude but opposite signs for b. So do the deformation states ($e_1 = e$; $e_2 = -\beta e$; k_1) and ($e_1 = -e$; $e_2 = \beta e$; k_1) Thus, by the argument used above to prove symmetry for $\pm k_1$, the surfaces $\psi = 1$ for $n \to \infty$ are the same in diagonal quadrants.

4.4 Computing the $\psi = 1$ surfaces for $k_2 = 0$

Although for given values of e_1, e_2, k_1, ψ could be obtained directly by numerical integration of equation 4.8 with $k_2 = 0$, it was convenient to have values for t_1, t_2, m_1, m_2 as well as values for ψ. The following procedure was thus adopted.

(a) For a particular value of n, and values of e_1, e_2, k_1, equations 4.18 were used to compute the non-dimensional stresses $\frac{\sigma_1}{\sigma_o}$ and $\frac{\sigma_2}{\sigma_o}$ at the mid-surface and at ten

equal intervals of ζ on both sides of the mid-surface. A standard numerical integration technique based on Simpson's rule was used to evaluate t_1, t_2, m_1 and m_2 from

$$t_1 = \tfrac{1}{2}\int_{-1}^{+1}\left(\frac{\sigma_1}{\sigma_o}\right)d\zeta \quad ; \quad t_2 = \tfrac{1}{2}\int_{-1}^{+1}\left(\frac{\sigma_2}{\sigma_o}\right)d\zeta \; ;$$

$$m_1 = \int_{-1}^{+1}\left(\frac{\sigma_1}{\sigma_o}\right)\zeta\, d\zeta \quad ; \quad m_2 = \int_{-1}^{+1}\left(\frac{\sigma_2}{\sigma_o}\right)\zeta\, d\zeta \; .$$

(b) ψ was obtained by applying the equation of virtual work to the unit shell element, i.e. (with $k_2 = 0$),

$$\psi - t_1 e_1 - t_2 e_2 - m_1 k_1 - m_2 k_2 = 0$$

Steps (a) and (b) were performed on an English Electric Deuce computer.

(c) To obtain a point on the $\psi = 1$ surface for given e_1, e_2, ψ was calculated for a number of values of k_1. A graph of ψ against k_1 gave the value of k_1 for which $\psi = 1$.

4.5 Integration of equations 4.19

(a) $\dfrac{t_1}{e_1^{1/n}}$

$$\frac{t_1}{e_1^{1/n}} = \tfrac{1}{2}\left(\frac{4}{3}\right)^{\frac{n+1}{2n}} \int_{-1}^{+1} \left[1+4\rho\left(\frac{k_1}{e_1}\right)+4\rho^2\left(\frac{k_1}{e_1}\right)^2\right]^{\frac{1-n}{2n}} \left[1+2\rho\left(\frac{k_1}{e_1}\right)\right] d\rho$$

$$= \tfrac{1}{2}\left(\frac{4}{3}\right)^{\frac{n+1}{2n}} \int_{-1}^{+1} \left(1+2\rho\,\frac{k_1}{e_1}\right)^{1/n} d\rho$$

$$= \left(\frac{4}{3}\right)^{\frac{n+1}{2n}} \left(\frac{n}{n+1}\right) \frac{1}{4\left(\frac{k_1}{e_1}\right)} \left[\left(1+2\,\frac{k_1}{e_1}\right)^{\frac{n+1}{n}} - \left(1-2\,\frac{k_1}{e_1}\right)^{\frac{n+1}{n}}\right]$$

(b) $\dfrac{m_1}{k_1^{1/n}}$

$$\frac{m_1}{k_1^{1/n}} = \left(\frac{4}{3}\right)^{\frac{n+1}{2n}} \left(\frac{e_1}{k_1}\right)^{1/n} \int_{-1}^{+1} \left[1+4\rho\left(\frac{k_1}{e_1}\right)+4\rho^2\left(\frac{k_1}{e_1}\right)^2\right]^{\frac{1-n}{2n}} \left[1+2\rho\left(\frac{k_1}{e_1}\right)\right]\rho\, d\rho$$

$$= \left(\frac{4}{3}\right)^{\frac{n+1}{2n}} \frac{1}{k_1^{1/n}} \int_{-1}^{+1} (e_1+2\rho k_1)^{1/n}\,\rho\, d\rho$$

$$= \left(\frac{4}{3}\right)^{\frac{n+1}{2n}} \cdot \frac{1}{k_1^{1/n}} \left\{\left[\rho\left(\frac{n}{n+1}\right)\frac{(e_1+2k_1)^{\frac{n+1}{n}}}{2k_1}\right]_{-1}^{+1} - \int_{-1}^{+1} \left(\frac{n}{n+1}\right)\frac{(e_1+2k_1)^{\frac{n+1}{n}}}{2k_1}\, d\rho\right\}$$

which gives finally

$$\frac{m_1}{k_1^{1/n}} = \tfrac{1}{2}\left(\frac{n}{n+1}\right)\left(\frac{4}{3}\right)^{\frac{n+1}{2n}} \frac{1}{\left(\frac{k_1}{e_1}\right)^{\frac{n+1}{n}}} \left\{\left(1+2\,\frac{k_1}{e_1}\right)^{\frac{n+1}{n}} + \left(1-2\frac{k_1}{e_1}\right)^{\frac{n+1}{n}}\right.$$

$$\left. -\left(\frac{n}{2n+1}\right)\frac{1}{2\left(\frac{k_1}{e_1}\right)}\left[\left(1+2\frac{k_1}{e_1}\right)^{\frac{2n+1}{n}} - \left(1-2\frac{k_1}{e_1}\right)^{\frac{2n+1}{n}}\right]\right\}$$

4.6 To show that $t_1 = 0$ when $e_1 = -\frac{1}{2}e_2$

From equations 4.6, with $k_2 = 0$,

$$t_1 = \tfrac{1}{2}\left(\frac{4}{3}\right)^{\frac{n+1}{2n}} \int_{-1}^{+1} F_2^{\frac{1-n}{2n}} \left[(e_1+\tfrac{1}{2}e_2) + 2\rho k_1\right] d\rho$$

where $F_2 = (e_1^2 + e_1e_2 + e_2^2) + 4\rho k_1(e_1 + \tfrac{1}{2}e_2) + 4\rho^2 k_1^2$

But $\dfrac{dF_2}{d\rho} = 4k_1\left[(e_1 + \tfrac{1}{2}e_2) + 2\rho k_1\right]$

$$\therefore\ t_1 = \tfrac{1}{2}\left(\frac{4}{3}\right)^{\frac{n+1}{2n}} \cdot \frac{1}{4k_1}\left(\frac{2n}{n+1}\right)\left[F_2^{\frac{n+1}{2n}}\right]_{-1}^{+1}$$

Thus, for $t_1 = 0$

$$\left[F_2^{\frac{n+1}{2n}} \right] \text{ for } \rho = +1 = \left[F_2^{\frac{n+1}{2n}} \right] \text{for } \rho = -1$$

This requires

$$e_1 + \tfrac{1}{2} e_2 = 0$$

$$\text{or } e_1 = -\tfrac{1}{2} e_2$$

The approximate relations - equations 4.15 — also give $t_1 = 0$ for $e_1 = -\frac{1}{2} e_2$.

4.7 Discontinuity at section (3) for $n \to \infty$

For the particular conditions $e_2 = k_2 = 0$ (and only for these conditions), the strain ϵ_2 is zero for all ζ.

For $\epsilon_2 = 0$, the first of equation 2.9 gives with

$$B = \frac{\epsilon_o}{\sigma_o^n}$$

$$\sigma_1 = \frac{\sigma_o}{\epsilon_o^{1/n}} \left(\frac{4}{3}\right)^{\frac{n+1}{2n}} \left(\epsilon_1^2\right)^{\frac{1-n}{2n}} \epsilon_1$$

As $n \to \infty$, $\sigma_1 \to \pm \frac{2}{\sqrt{3}} \sigma_o$, the sign depending on the sign of ϵ_1.

now $\epsilon_1 = \epsilon_{m1} + K_1 \zeta$

$$= \epsilon_{m1} \left(1 + \frac{K_1 H}{\epsilon_{m1}} \cdot \frac{\zeta}{H}\right)$$

Clearly, since ζ varies from - H to + H, the sign of ϵ_1 for given values of ϵ_{m1} and K_1 will depend on the ratio $\frac{K_1 H}{\epsilon_{m1}}$. For $\frac{K_1 H}{\epsilon_{m1}} \leq 1$, ϵ_1 will be positive throughout the thickness, and the stress σ_1 will be $+ \frac{2}{\sqrt{3}} \sigma_o$ throughout. Application of a curvature $K_1 \leq \frac{\epsilon_{m1}}{H}$ will not change the stress distribution, and hence will not require an applied moment M_1. The magnitude of the force T_1 to maintain ϵ_{m1} will remain unchanged.

For $\frac{K_1 H}{\epsilon_{m1}} > 1$, ϵ_1 will be negative over part of the thickness and the stress will be $- \frac{2}{\sqrt{3}} \sigma_o$, i.e. the stress distribution will be as shown below.

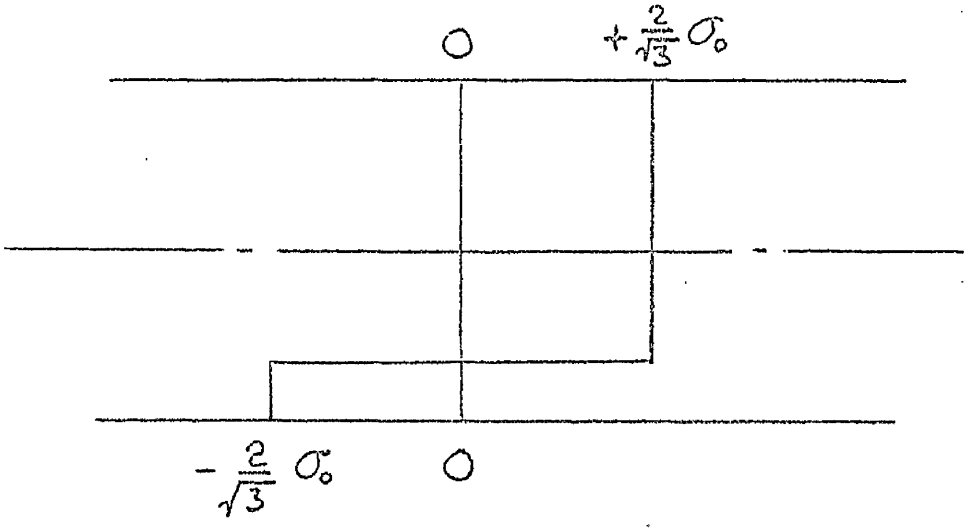

Application of a curvature $K_1 > \frac{\epsilon_{m1}}{H}$ will thus require an applied moment and the value of T_1 to maintain ϵ_{m1} is reduced.

In non-dimensional form, the ratio

$$\frac{K_1 H}{\epsilon_{m1}} = \frac{2 \epsilon_o k_1}{H} \quad \frac{H}{e_1 \epsilon_o} = 2 \frac{k_1}{e_1}$$

and $\frac{K_1 H}{\epsilon_{m1}} > 1$ gives $\frac{k_1}{e_1} > \frac{1}{2}$

This was the value of $\frac{k_1}{e_1}$ at which the discontinuity occurred at section (3)..

APPENDIX 5

5.1 Semi-infinite, fixed end cylinder without axial load - magnitude scaling for n = 3 and computer circuits for n = 5, 7.

(a) Magnitude scaling for n = 3

With time scaling $\tau = 4x$, equation 6.3 is

$$16\frac{d^2w}{d\tau^2} = -\frac{1}{f_1 f_2}\left[3w^2 + f_2 \times 256\left(\frac{d^2w}{d\tau^2}\right)^2\right]^{\frac{n-1}{2n}} \times \iint \left\{3f_1 w\left[3w^2 + 256f_2\left(\frac{d^2w}{d\tau^2}\right)^2\right]^{\frac{1-n}{2n}} - p\right\} \frac{d\tau}{4}\frac{d\tau}{4} \quad (A5.1)$$

For n = 3,

$$\frac{n-1}{2n} = \frac{1}{3}$$

$$f_1 = \left(\frac{4}{3}\right)^{\frac{n+1}{2n}} = 1.212$$

$$f_2 = 4\left(\frac{n}{2n+1}\right)^{\frac{2n}{n+1}} = 1.122$$

and equation A5.1 becomes with p = 2

$$256\frac{d^2w}{d\tau^2} = -0.735\left[3w^2 + 287\left(\frac{d^2w}{d\tau^2}\right)^2\right]^{\frac{1}{3}} \times \iint \left\{3.636w\left[3w^2+287\left(\frac{d^2w}{d\tau^2}\right)^2\right]^{-\frac{1}{3}} - 2\right\} d\tau\, d\tau \quad (A5.2)$$

Based on the maximum values obtained in the linear solution - paragraph 6.2(b) - the following normalised variables were selected for w and its derivatives:

$$\frac{w}{0.7} \quad , \quad \frac{\frac{dw}{d\tau}}{0.2} \quad , \quad \frac{\frac{d^2w}{d\tau^2}}{0.05} \quad .$$

with these, equation A5.2 becomes finally

$$\left(\frac{\frac{d^2w}{d\tau^2}}{0.05}\right) = -0.146 \; G_3^{\frac{1}{3}} \iint \left[\left(\frac{w}{0.7}\right) G_3^{-\frac{1}{3}} - 0.894 \right] d\tau \, d\tau \quad \text{(A5.3)}$$

where

$$G_3 = \left(\frac{w}{0.7}\right)^2 + 0.488 \left(\frac{\frac{d^2w}{d\tau^2}}{0.05}\right)^2$$

The linear solution shows that the decay of $\left(\frac{\frac{d^2w}{d\tau^2}}{0.05}\right)$ is more rapid than the growth of $\left(\frac{w}{0.7}\right)$ and it was assumed that G_3 would not have a value greater than 1. Furthermore, in setting up the D.F.G.. it was assumed that G_3 would not have a value less than 0.005. This gives a maximum value for $G_3^{\frac{1}{3}}$ of 0.171, and a reasonable estimate of the maximum value for $G_3^{-\frac{1}{3}}$ is 5.0. With $G_3^{-\frac{1}{3}}$ scaled by 5, equation A5.3 becomes

$$\left(\frac{\frac{d^2w}{d\tau^2}}{0.05}\right) = - 0.730\ G_3^{\frac{1}{3}} \iint \left[\left(\frac{w}{0.7}\right)\left(\frac{G_3^{-\frac{1}{3}}}{5}\right) - 0.179\right] d\tau\, d\tau \quad \text{(A5.4)}$$

It was necessary then to make estimates of the maximum values of $\int [\quad] d\tau$ and $\iint [\quad] d\tau d\tau$.

From equation 5.6

$$q_x = \int (2\ t_\theta - p)\ dx$$

and substituting for t_θ from equation 5.11 with $\frac{du}{dx} = - w$ gives

$$q_x = \int \left\{ 3f_1\ w \left[3w^2 + f_2 \left(\frac{d^2w}{dx^2}\right)^2 \right]^{\frac{1-n}{2n}} - p \right\} dx\ dx$$

With time scaling and normalised variables, this becomes for $n = 3$, $p = 2$

$$q_x = 2.8 \int \left[\left(\frac{w}{0.7}\right)\left(\frac{G_2^{-\frac{1}{3}}}{5}\right) - 0.179 \right] d\tau \quad \text{(A5.5)}$$

The maximum value for q_x in the linear solution is

$$q_o = \frac{16}{9} \left.\frac{d^3w}{dx^3}\right]_o$$

$$= \frac{16}{9} \times 1.298.$$

An estimate of the maximum value of $\int [\quad] d\tau$ is thus

$$\int [\ ]\, d\tau = \frac{16}{9} \times \frac{1.298}{2.8} = 0.824$$

It was assumed that $\left\{ \int [\ ]\, d\tau \right\}_{max} = 1.0.$

From equation 5.7,

$$m_x = - \int q_x dx$$

and substituting for q_x from equation A5.5

$$m_x = - \frac{2.8}{4} \iint \left[\left(\frac{w}{0.7} \right) \left(\frac{G_3^{-\frac{1}{3}}}{5} \right) - 0.179 \right] d\tau\ d\tau$$

With the maximum value of m_x from the linear solution, i.e.

$$m_o = \frac{16}{9} \times 0.75$$

$$\iint [\ ]\, d\tau\, d\tau = \frac{16}{9} \times 0.75 \times \frac{4}{2.8} = 1.9$$

It was assumed that

$$\left\{ \iint [\ ]\, d\tau\, d\tau \right\}_{max} = 2.5$$

These estimates of maximum values lead to the final equation

$$0.548 \left(\frac{\frac{d^2 w}{d\tau^2}}{0.05} \right) = - G_3^{\frac{1}{3}} \left\langle \frac{\iint \left[\left(\frac{w}{0.7} \right) \left(\frac{G_3^{-\frac{1}{3}}}{5} \right) - 0.179 \right] d\tau\, d\tau}{2.5} \right\rangle$$

and to the circuit diagram of Fig 6.6.

Similar reasoning leads to the following time and magnitude scaled equations for n = 5 and n = 7.

n = 5

$$0.653 \left(\frac{\frac{d^2w}{d\tau^2}}{0.05}\right) = -G_4^{2/5} \iint \left[\left(\frac{w}{0.7}\right)\left(\frac{G_4}{10}^{-2/5}\right) - 0.935\right] d\tau \, d\tau$$

where $G_4 = \left(\frac{w}{0.7}\right)^2 + 0.469 \left(\frac{\frac{d^2w}{d\tau^2}}{0.05}\right)^2$

n = 7

$$0.642 \left(\frac{\frac{d^2w}{d\tau^2}}{0.05}\right) = -G_5^{3/7} \iint \left[\left(\frac{w}{0.7}\right)\left(\frac{G_5}{10}^{-3/7}\right) - 0.0953\right] d\tau \, d\tau$$

where $G_5 = \left(\frac{w}{0.7}\right)^2 + 0.459 \left(\frac{\frac{d^2w}{d\tau^2}}{0.05}\right)^2$

The circuit diagrams for n = 5 and n = 7 are given in Figs A5.1 and A5.2.

5.2 Magnitude scaling for cylinder with axial load.

When time scaled with $\tau = 4x$, equations 6.4 become with n = 3 and p = 2

$$256\left(\frac{d^2w}{d\tau^2}\right) = -0.735\, G_6^{1/3} \iint \left[4.848\, G_6^{-1/3}\left(w + \frac{du}{d\tau}\right) - 2 \right] d\tau\, d\tau$$

A.5.6

$$4\,\frac{du}{d\tau} = \frac{T}{1.212}\, G_6^{1/3} - w$$

where

$$G_6 = 16\left(\frac{du}{d\tau}\right)^2 + 8w\left(\frac{du}{d\tau}\right) + 4w^2 + 287\left(\frac{d^2w}{d\tau^2}\right)^2$$

The estimates of maximum values made for the cylinder without axial load were assumed to apply here. The only additional estimate that had to be made was $\left.\frac{du}{d\tau}\right]_{max}$.

In the linear problem, equation 5.19 gives

$$\frac{du}{dx} = -w + \frac{3}{4}T$$

It was intended to vary T in the range 0 to 0.6, and thus the maximum value of $\frac{du}{dx}$ for the linear case would be $\left|w_{max}\right| = 0.521$. For the non-linear problem, a value

$$\left.\frac{du}{dx}\right]_{max} = 1.0 \quad \text{or} \quad \left.\frac{du}{d\tau}\right]_{max} = 0.25$$

was assumed.

The final forms for equations A5.6 with normalised variables are:

$$0.410 \left(\frac{\frac{d^2 w}{d\tau^2}}{0.05} \right)$$

$$= - G_7^{\frac{1}{3}} \left\langle \frac{\iint \left\{ \left(\frac{G_7}{5} \right)^{-\frac{1}{3}} \left[\left(\frac{w}{0.7} \right) + 0.357 \left(\frac{\frac{du}{d\tau}}{0.25} \right) \right] - 0.148 \right\} d\tau \, d\tau}{2.5} \right\rangle$$

$$\left(\frac{\frac{du}{d\tau}}{0.25} \right) = 1.033 \, T \, G_7^{\frac{1}{3}} - 0.7 \left(\frac{w}{0.7} \right)$$

where

$$G_7 = 0.510 \left(\frac{\frac{du}{d\tau}}{0.25} \right)^2 + 0.714 \left(\frac{w}{0.7} \right) \left(\frac{\frac{du}{d\tau}}{0.25} \right) + \left(\frac{w}{0.7} \right)^2 + 0.366 \left(\frac{\frac{d^2 w}{d\tau^2}}{0.05} \right)^2$$

5.3 Check on outputs of circuit components of Fig 6.6

Results are given in Tables A, B and C.

Table A - x = 0

Table B - x = 0.5 approx.

Table C - x = 1.0 approx.

notes

(i) A - amplifier

M - multiplier

D - multiplier used as divider.

(ii) Sign inversion occurs in all amplifiers and multipliers.

(iii) 1.0000 represents 100.00 volts.

TABLE A

Circuit Component	Input	Recorded Output	Calculated Output	Difference in Output Absolute	Difference in Output Percentage
A1	0.0000	0.0000	0.0000	0.0000	-
A2	+0.0001 -0.5420 } +	+0.5420	+0.5419	+0.0001	0.02
A3	-1.0000 +1.0840 } +	-0.0839	-0.0840	+0.0001	0.01
A4	+0.8169	-0.8169	-0.8169	0.0000	0.00
A5	-0.8169	+0.8169	+0.8169	0.0000	0.00
A6	-0.2000	+0.2000	-0.2000	0.0000	0.00
A7	+0.2450	-0.2450	-0.2450	0.0000	0.00
A8	-0.0001 +0.1790 } +	-0.1789	-0.1789	0.0000	0.00
A9	+0.5750	-0.5750	-0.5750	0.0000	0.00
A10	-0.5750	+0.5750	+0.5750	0.0000	0.00
A11	-0.7350	+0.7360	+0.7350	+0.0010	0.14
A12	+0.7360	-0.7361	-0.7360	-0.0001	0.01
M1	0.0000 0.0000 } x	+0.0001	0.0000	+0.0001	-
M2	+0.2450 0.0000 } x	-0.0001	0.0000	-0.0001	-
M3	+0.6975 +0.8169 } x	-0.5750	-0.5698	-0.0052	0.91
M4	+0.7360 +0.7360 } x	-0.5420	-0.5417	-0.000 3	0.06
D1	+0.2000 +0.8169 } ÷	+0.2450	+0.2448	+0.0002	0.08
D.F.G.	-0.0839	+0.8169	+0.8153	+0.0016	0.20

TABLE B

Circuit Component	Input	Recorded Output	Calculated Output	Difference in output Absolute	Difference in output Percentage
A1	+0.0752	-0.0751	-0.0752	+0.0001	0.01
A2	-0.0056 -0.0092 } +	+0.0148	+0.0148	0.0000	0.00
A3	-1.0000 +0.0296 } ÷	+0.9705	+0.9704	+0.0001	0.01
A4	+0.2509	-0.2510	-0.2509	-0.0001	0.04
A5	-0.2510	+0.2510	+0.2510	0.0000	0.00
A6	-0.2000	+0.2000	+0.2000	0.0000	0.00
A7	+0.7999	-0.7999	-0.7999	0.0000	0.00
A8	-0.0604 +0.1790 } ÷	-0.1186	-0.1186	0.0000	0.00
A9	+0.0745	-0.0746	-0.0745	-0.0001	0.13
A10	-0.0746	+0.0746	+0.0746	0.0000	0.00
A11	-0.0953	+0.0953	+0.0953	0.0000	0.00
A12	+0.0953	-0.0954	-0.0953	-0.0001	0.10
M1	+0.0752 +0.0752 } x	-0.0056	-0.0057	+0.0001	1.80
M2	+0.7999 +0.0752 } x	-0.0604	-0.0602	-0.0002	0.33
M3	-0.2943 +0.2509 } x	+0.0745	+0.0738	+0.0007	0.94
M4	-0.0953 -0.0953 } x	-0.0092	-0.0091	-0.0001	1.10
D1	+0.2000 +0.2510 } ÷	+0.7999	+0.7969	+0.0030	0.38
D.F.G.	+0.9705	+0.2509	+0.2455	+0.0054	2.15

TABLE C

Circuit Component	Input	Recorded Output	Calculated Output	Difference in Output Absolute	Difference in Output Percentage
A1	+0.1957	-0.1957	-0.1957	0.0000	0.00
A2	-0.0382 -0.0016 +	+0.0398	+0.0398	0.0000	0.00
A3	-1.0000 +0.0796 +	+0.9206	+0.9204	0.0002	0.02
A4	+0.3430	-0.3430	-0.3430	0.0000	0.00
A5	-0.3430	+0.3430	+0.3430	0.0000	0.00
A6	-0.2000	+0.2000	+0.2000	0.0000	0.00
A7	+0.5830	-0.5829	-0.5830	-0.0001	0.02
A8	-0.1141 +0.1790 +	-0.0648	-0.0649	-0.0001	0.17
A9	+0.0304	-0.0305	-0.0304	-0.0001	0.33
A10	-0.0305	+0.0305	+0.0305	0.0000	0.00
A11	-0.0390	+0.0390	+0.0390	0.0000	0.00
A12	+0.0390	-0.0391	-0.0390	-0.0001	0.25
M1	+0.1957 +0.1957 x	-0.0382	-0.0383	+0.0001	0.26
M2	+0.1957 +0.5829 x	-0.1141	-0.1141	0.0000	0.00
M3	-0.0878 +0.3430 x	+0.0304	+0.0301	+0.0003	1.00
M4	+0.0390 +0.0390 x	-0.0016	-0.00152	-0.00008	5.25
D1	+0.2000 +0.3430 ÷	+0.5830	+0.5830	0.0000	0.00
D.F.G.	+0.9206	+0.3430	+0.3414	+0.0016	0.47

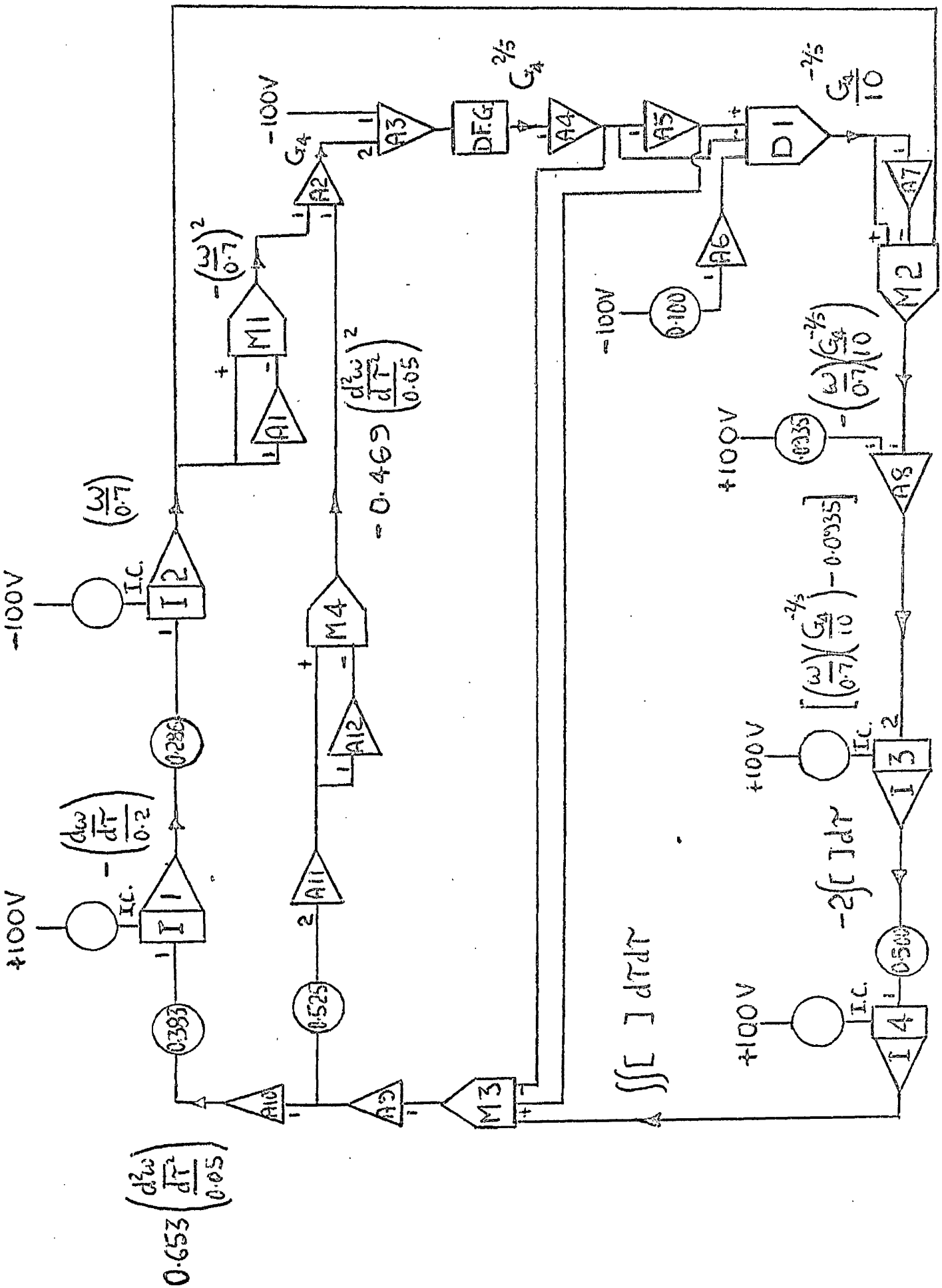
+100V
-100V
I.C.
I 1
I 2
I 3
I 4
0.383
0.286
0.525
0.530
0.653 (d²ω/dT²/0.05)
-(dω/dT/0.2)
(ω/0.7)
-(ω/0.7)²
-0.469 (d²ω/dT²/0.05)
A1
A2
A3
A4
A5
A6
A7
A8
A9
A10
A11
A12
M1
M2
M3
M4
D.F.G
D1
0.100
0.935
G4
2/5 G4
-2/5 G4/10
∫∫∫ dT dT
-2∫∫ dT dT
-0.0935
SCALED COMPUTER CIRCUIT FOR n=5 ; p=2
(ZERO AXIAL LOAD)

FIG. A5.1

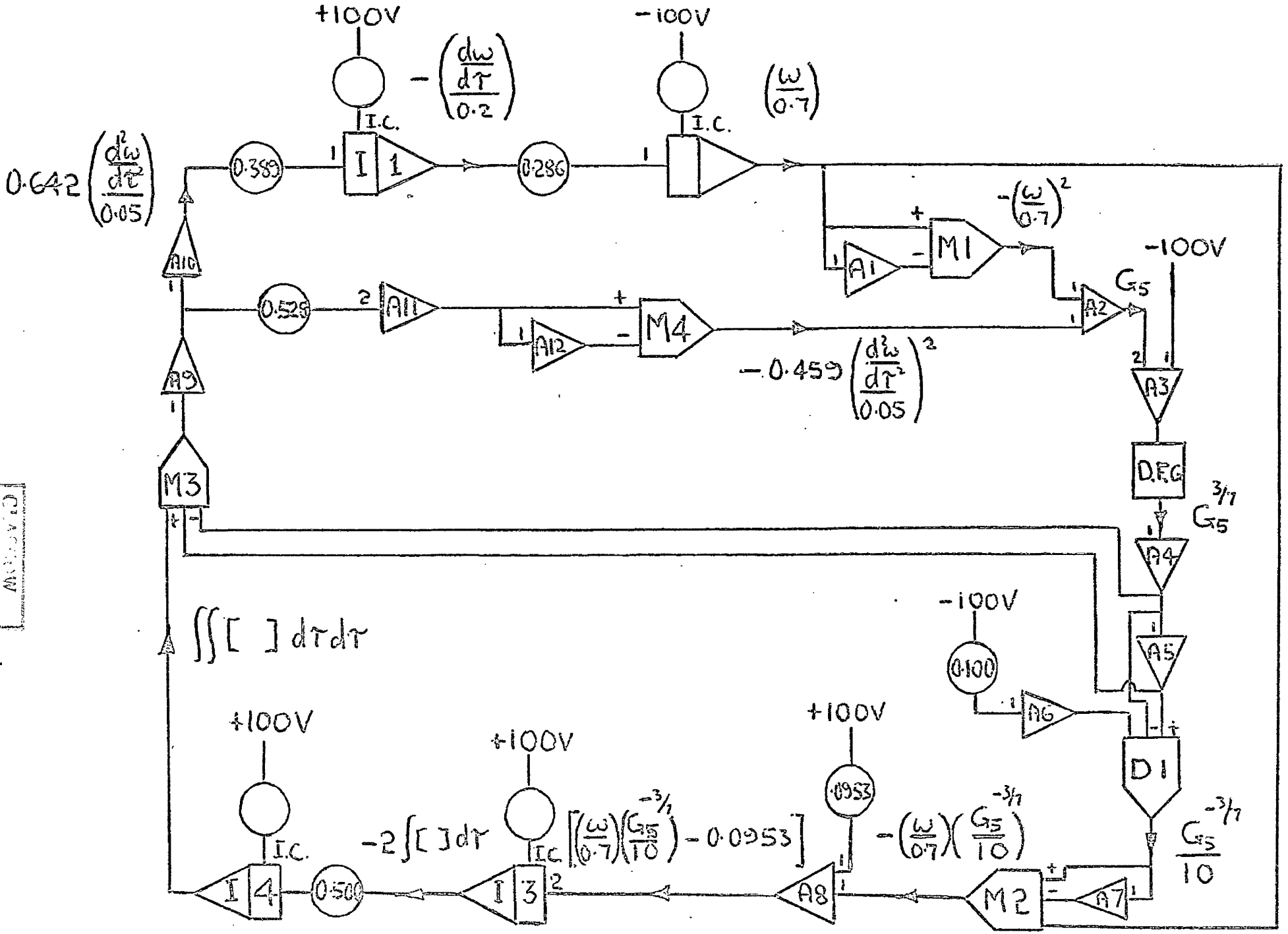

SCALED COMPUTER CIRCUIT FOR $n=7$; $p=2$

(ZERO AXIAL LOAD)

FIG. 852